SOME SPHERICALLY SYMMETRIC ASTROPHYSICAL OBJECTS IN GENERAL RELATIVITY

Kshetrimayum Newton Singh

SOME SPHERICALLY SYMMETRIC ASTROPHYSICAL OBJECTS IN GENERAL RELATIVITY

Thesis submitted for the award
of the degree of

Doctor of Philosophy
(Science)

by

KSHETRIMAYUM NEWTON SINGH

Under the guidance of

Prof. Farook Rahaman

Department of Mathematics
Jadavpur University
Kolkata-700032, India

2022

Dedicated to

My beloved Family

&

mostly to my wife

Ksh. Ushalata Devi

Prof. Dr. Farook Rahaman
Fellow of Royal Astronomical Society
(F R A S, London)

Department of Mathematics
JADAVPUR UNIVERSITY
KOLKATA- 700032, India.

Ref. ....

Date ....

CERTIFICATE FROM THE SUPERVISOR

This is to certify that the thesis entitled "**Some Spherically Symmetric Astrophysical Objects in General Relativity**" submitted by **Kshetrimayum Newton Singh**, who got his name registered on **04.04.2018** for the award of Ph.D. (Science) degree of Jadavpur University, is absolutely based upon his own work under the supervision of **Prof. Farook Rahaman** and that neither this thesis nor any part of it has been submitted for either any degree / diploma or any other academic award anywhere before.

.... *Faran Rahan* 18.04.22 ....

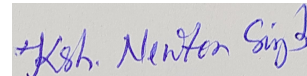(Signature of the Supervisor and date with official seal)

DR. FAROOK RAHAMAN
Professor
Department of Mathematics
JADAVPUR UNIVERSITY
Kolkata-700032, W.B., INDIA

Corresponds at : KHODAR BAZAR, BARUIPUR, KOLKATA-700144 WEST BENGAL, INDIA
WAP+Mob. No.- 9831907279 (Residence), (+91) (033) 24572716
E-mail : farook_rahaman@yahoo.com, rahaman@associates.iucaa.in, farookrahaman@gmail.com

Declaration

I, **Kshetrimayum Newton Singh**, research scholar hereby declare that the thesis titled **"Some Spherically Symmetric Astrophysical Objects in General Relativity"** which is submitted by me to the Jadavpur University in partial fulfillment of the requirement for the award of the degree of Doctor of Philosophy in Science is my own work and complete in all parts under the supervision of Prof. Farook Rahaman, Department of Mathematics, Jadavpur University, Kolkata, West Bengal, India. Also I declare that the thesis fulfilled all the guidelines regarding PhD degree.

Finally, I declare that any part of it has not been submitted for any degree/diploma at any other institute/university.

(Kshetrimayum Newton Singh)

Date: 20.04.2022

Acknowledgments

Place - Kolkata,   **(Kshetrimayum Newton Singh)**
Date - 20.04.2022

List of Publications in Journals

The work of this thesis has been carried out at the Department of Mathematics, Jadavpur University, Kolkata - 700032, West Bengal, India. The thesis is based on the following published papers:

1. Minimally deformed anisotropic model of class one space-time by gravitational decoupling.
Ksh. Newton Singh, S. K. Maurya, M. K. Jasim and Farook Rahaman.
The European Physical Journal C. Vol. 79, Page-851 (2019).

2. Compact stars with exotic matter.
Ksh. Newton Singh, Amna Ali, Farook Rahaman and Salah Nasri.
Physics of the Dark Universe. Vol. 29, Page-100575 (2020).

3. Static fluid spheres admitting Karmarkar condition.
Ksh. Newton Singh, Ravindra K. Bisht, S. K. Maurya and Neeraj Pant.
Chinese Physics C. Vol. 44, Page-035101 (2020).

4. A generalized Finch-Skea class one static solution.
Ksh. Newton Singh, S. K. Maurya, Farook Rahaman and Francisco Tello-Ortiz.
The European Physical Journal C. Vol. 79, Page-381 (2019).

5. Einstein's cluster mimicking compact star in the teleparallel equivalent of general relativity.
Ksh. Newton Singh, Farook Rahaman and Ayan Banerjee.
Physical Review D. Vol. 100, Page-084023 (2019).

6. Physical properties of class I compact star model for linear and Starobinsky$-f(R,T)$ functions.
Ksh. Newton Singh, S.K. Maurya, Abdelghani Errehymy, Farook Rahaman and Mohammed Daoud.
Physics of the Dark Universe. Vol. 30, Page-100620 (2020).

7. Color-flavor locked quark stars in energy-momentum squared gravity.

Ksh. Newton Singh, Ayan Banerjee, S.K. Maurya, Farook Rahaman and Anirudh Pradhan.
Physics of the Dark Universe. Vol. 31, Page-100774 (2021).

8. Conformally symmetric traversable wormholes in modified teleparallel gravity
Ksh. Newton Singh, Ayan Banerjee, Farook Rahaman and M. K. Jasim.
Physical Review D. Vol. 101, Page-084012 (2020).

Conferences Attended

1. Four dimensional relativistic fluid ball embedded in five dimensional space
Ksh. Newton Singh and Farook Rahaman.
National E-Conference on Interdisciplinary Research in Science and Technology (NCIRST-20). (2020).

2. Vacuum solution and Karmarkar condition in General Relativity
Ksh. Newton Singh and Farook Rahaman.
Online International Conference on Mathematical Techniques and Application. (2020).

Abstract

The present thesis is concerned with spherically symmetric astrophysical objects in GR and modified gravity theories. We organize the whole thesis into ten chapters as follow:

The **first chapter** is introductory in which the contents of the certain relevant topics concerning the problems in the subsequent chapters are briefly described. This chapter presents an overview of general relativity (GR), extended theories, supporting evidences of GR, physics of compact stars, basics of wormhole geometry etc.

In the **second chapter**, we have presented a static anisotropic solution of stellar compact objects for self-gravitating system by using minimal geometric deformation techniques in the framework of embedding class one space-time. We deform this system into two separate system through the geometric deformation of radial components for the source function $\lambda(r)$ by mapping: $e^{-\lambda(r)} \rightarrow e^{-\tilde{\lambda}(r)} + \beta\, g(r)$, where $g(r)$ is deformation function. The first corresponds to Einstein's system and other quasi-Einstein system.

The **third chapter** employed Tolman VII solution with exotic matter that may be present in the extremely dense core of compact objects. For our purpose we use generalized non-linear equation of state which may incorporate exotic matter along with dust, radiation and dark energy. The amount of exotic matter contain can be modify by a parameter n which can be linked to adiabatic index. The $M-R$ relation is constructed analytically and the maximum mass and its corresponding radius is determined using the exact solutions and is shown to satisfy various observed stellar compact stars.

In **fourth chapter**, we will explore new relativistic anisotropic solutions of the Einstein field equation for compact stars under embedding class one condition. For this purpose, we use the embedding class one methodology by employing the Karmarkar condition. By using this methodology we obtain a particular differential equation that connects both gravitational potentials e^λ and e^ν. We have also discussed thermodynamical observable like radial and tangential pressures, matter density, etc. Further, we discussed the moment of inertia and $M-R$ curve for rotating and non-rotating stars.

The **fifth chapter** discuss relativistic anisotropic solutions of the Einstein field equation for the spherically symmetric line element under the class one condition. To do so we apply the embedding class one technique using Eisland condition. Once the space-time geometry is specified we obtain the matter density ρ, the radial, and tangential pressures p_r and p_t, respectively. The $M-R$ diagram suggest that the solution yields stiffer EoS as parameter n increases. The $M-I$ graph is in agreement

with the concepts of Bejgar et al. Bejger and Haensel [2002] that the mass at I_{max} is lesser by few percent (for this solution $\sim 3\%$) from M_{max}. This suggest that the EoSs is without any strong high-density softening due to hyperonization or phase transition to an exotic state.

In the **sixth chapter**, we present a physically plausible solution representing Einstein's cluster mimicking the behaviors of compact star in the context of $f(\mathbb{T})-$gravity. We chose both diagonal and off-diagonal tetrads in linear and quadratic functions of $f(\mathbb{T})$. However, we have found that Einstein clusters exist only in the case of Teleparallel Equivalent of General Relativity. The system also gain its stability when a small net electric is introduced.

The aim of the **seventh chapter** is to explore exact solutions in linear and Starobinsky-$f(\mathcal{R}, \mathcal{T})-$gravity theory. Further, we employ embedding class one condition. We then compare the cases when $\xi = \chi = 0$ [GR], $\xi = 0,\ \chi = 0.5$ $[f_L(\mathcal{R}, \mathcal{T})]$, $\xi = 0.5,\ \chi = 0$ $[f_S(\mathcal{R}, \mathcal{T})]$ and $\xi = \chi = 0.5$ $[f_{S+L}(\mathcal{R}, \mathcal{T})]$. The $M - R$ and $M - I$ curves from our solution are well fitted with observational data.

The **eighth chapter** focuses on strange star hydrostatic equilibrium assuming a maximally symmetric phase of homogeneous superconducting quark matter called the *color-flavor-locked* (CFL) phase in the energy-momentum squared gravity (EMSG). We explored the structure of stellar objects in EMSG, which allows a correction term $T_{\mu\nu}T^{\mu\nu}$ in the action. Interestingly, EMSG may be effective to resolve the problems at high energy densities without invoking some new forms of fluid stress. Finally, we solve the complicated field equations numerically to obtain the mass-radius relations for strange stars in CFL equation of state.

In **ninth chapter**, we consider wormhole geometries in the context of teleparallel equivalent of general relativity (TEGR) as well as $f(\mathbb{T})$ gravity. We present the analytical solutions under the assumption of spherical symmetry and the existence of *Conformal Killing Vector*. In addition, a wide variety of solutions are deduced by considering a linear equation of state relating the density and pressure, for the isotropic and anisotropic pressure, independently of the shape functions, and various phantom wormhole geometries are explored.

The summary and future scopes for all the above chapters are presented in the **tenth chapter**.

(Signature of the candidate)

Faran R.... 18.04.22

(Signature of the supervisor with seal)

DR. FAROOK RAHAMAN
Professor
Department of Mathematics
JADAVPUR UNIVERSITY
Kolkata-700032, W.B., INDIA

Contents

Contents

Contents

List of Figures

List of Figures

List of Tables

Chapter 1

Introduction

1.1 Preliminaries of general relativity

The "Universal Law of Gravitation" proposed by Sir Isaac Newton in 1687 in his famous work "*Philosophiae Naturalis Principia Mathematica*" described the motion of planets in the solar system almost perfectly. During this era of Newtonian mechanics, the space and time were separate entities where time is absolute for any observer. This relativity (named as Newtonian or Galilean relativity) explains all the physical phenomena corresponding to low velocity limits. However, the transformation equations from the Galilean relativity was incompatible with the Maxwell's equations of the electromagnetic theory of light. Initially, light needs a hypothetical medium known as "*Ether*" to propagate between two points. To detect this luminiferous medium, Michelson and Morley set up an optical instrument based on Michelson-Morley interferometer. Consequently, the negative results from this experiment put forward to the non existence of the Ether medium. This inspired a young unknown scientist named Albert Einstein to arrived at the postulates of the "Special Theory of Relativity":

1. Laws of physics remain the same in all inertial observers.

2. Speed of light in vacuum is constant and same for all inertial observers.

Using these postulates as foundation Einstein arrived at a relativistic transformations law, which was similar to the one derived by Hendrik Lorentz. These transformations equations are now known as "*Lorentz Transformation*". The concept of space and time as non-separable entities was put forward by Hermann Minkowski as four-dimensional spacetime continuum. This four-dimensional spacetime can be presented by a simple

line element

$$ds^2 = -c^2dt^2 + dx^2 + dy^2 + dz^2 \equiv \eta_{\mu\nu}\, dx^\nu dx^\nu \quad \text{(Einstein convention)} \qquad (1.1)$$

where, $\eta_{\mu\nu}$ is the metric tensor which can be represented by a 4×4 matrix with diagonal elements $(-1, 1, 1, 1)$. Events in Minkowski's spacetime are now represented by four-vectors $x^\mu \equiv (x^0, x^1, x^2, x^3) = (ct, x, y, x)$ in Cartesian coordinates. Now the Lorentz transformation in four-vector form can be written as

$$x^\mu \to x'^\mu = \Lambda^\mu_\nu\, x^\nu, \qquad (1.2)$$

where, Λ^μ_ν is the Lorentz matrix defined as

$$\Lambda^\mu_\nu = \begin{pmatrix} \gamma & \gamma v/c & 0 & 0 \\ \gamma v/c & \gamma & 0 & 0 \\ 0 & 0 & 1 & 0 \\ 0 & 0 & 0 & 1 \end{pmatrix}. \qquad (1.3)$$

Here $\gamma = (1 - v^2/c^2)^{-1/2}$, the Lorentz factor. For inertial frames, equation (1.2) can also be written as

$$dx'^\mu = \Lambda^\mu_\nu\, dx^\nu. \qquad (1.4)$$

The invariance of the four-dimensional line element ds^2 leads to

$$\begin{aligned} \eta_{\mu\nu}dx'^\mu dx'^\nu &= \eta_{\mu\nu}dx^\mu dx^\nu \\ \text{or } \eta_{\mu\nu}\Lambda^\mu_\rho\,\Lambda^\nu_\sigma\, dx^\rho dx^\sigma &= \eta_{\rho\sigma}dx^\rho dx^\sigma \\ \text{or } \eta_{\mu\nu}\Lambda^\mu_\rho\,\Lambda^\nu_\sigma &= \eta_{\rho\sigma}. \end{aligned} \qquad (1.5)$$

The last equation is the Lorentz transformation of the Minkowskian metric tensor. Since the special theory of relativity was confined only to inertial frames, Einstein wanted to generalized to any arbitrary frames (accelerated frames). Soon he realized that accelerating frames can also seen as a source of gravity. This idea led him to the " *Principal of Equivalence*" which states that "*at every space-time point in an arbitrary gravitational field it is possible to choose a locally inertial coordinate system such that, within a sufficiently small region of the point in question, the laws of nature take the same form as in unaccelerated Cartesian coordinate systems in the absence*

of gravitation" (Einstein [1907], Weinberg [1972]). This also further implicates the equivalence of gravitational and inertial masses.

The general theory of relativity was formulated based on the "*Principle of General Covariance* which states that "*a physical equation of general relativity is generally true in all coordinate systems if (a) it preserves its form under general coordinate transformations, and (b) the equation is true in special relativity*" (Weinberg [1972]). In this theory, freely falling massive point-like objects following time-like geodesics of the metric and the equations of motion are independent of their masses given by

$$\frac{d^2 x^\mu}{d\tau^2} + \Gamma^\mu_{\alpha\beta} \frac{dx^\alpha}{d\tau} \frac{dx^\beta}{d\tau} = 0. \tag{1.6}$$

Here τ is the proper time and $\Gamma^\mu_{\alpha\beta}$ the Christoffel symbols of the second kind named as "*affine connection*". Since the equivalence principle implies the equality of inertial and gravitational mass, gravity is nothing to do with force acting on the individual particles but should be related to the structure of the spacetime. In 1915, Einstein finally published the field equation in general relativity as

$$G_{\mu\nu} \equiv R_{\mu\nu} - \frac{1}{2} g_{\mu\nu} \mathcal{R} = -\frac{8\pi G}{c^4} T_{\mu\nu}. \tag{1.7}$$

Here $G_{\mu\nu}$ is named as Einstein tensor, $R_{\mu\nu}$ is the Ricci tensor defined as

$$R_{\mu\nu} = R^\sigma_{\mu\sigma\nu} = \frac{\partial \Gamma^\alpha_{\mu\alpha}}{\partial x_\nu} - \frac{\partial \Gamma^\alpha_{\mu\nu}}{\partial x_\alpha} + \Gamma^\alpha_{\mu\beta} \Gamma^\beta_{\nu\alpha} - \Gamma^\alpha_{\mu\nu} \Gamma^\beta_{\alpha\beta}, \tag{1.8}$$

and $\mathcal{R} = g^{\mu\nu} R_{\mu\nu}$, the Ricci scalar. The left hand side of the field equation (1.7) represents the curvature of the spacetime which is due to the presence of a matter source $T_{\mu\nu}$, defined as

$$T_{\mu\nu} = (p + \rho) v_\mu v_\nu + p g_{\mu\nu}. \tag{1.9}$$

Here, ρ is the energy density of the matter distribution, p the pressure associated and v^ν is the four-velocity satisfying the relation $v_\nu v^\nu = -1$. Further, the conservation of energy and matter requires $\nabla_\mu T^{\mu\nu} \equiv T^{\mu\nu}{}_{;\mu} = 0$.

1.2   Predictions of General Relativity

As consequences of the general relativity, many new phenomena has been predicted theoretically which upon observations can be confirmed. General relativity also predicted the existence of new objects like black holes, compact stars, wormholes etc in astrophysical realm. In cosmological scale, general relativity predicts the origin of universe from a singularity and its evolution. In this thesis, we will only focus on the astrophysical objects.

1.2.1 Perihelion advance of Mercury

In 1859, astronomer Urbain Le Verrier observed an anomalous precessional motion of the perihelion of Mercury about $43''$ arc sec/century that could not accommodated in Newtonian gravity. However, due to perturbations from the other planets the Newtonian gravity predicts a precession of 5557.62 ± 0.20 arc sec/century which was about $43''$ arc sec/century less from the observed value 5600.73 ± 0.41 arc sec/century. Assuming a Schwarzschild exterior around the Sun, the equation of orbit for massive objects following time-like geodesics with relativistic correction is given by

$$\frac{d^2u}{d\phi^2} + u = \frac{GM}{c^2h^2} + \frac{3Gm}{c^2} \, u^2. \tag{1.10}$$

Here $u = 1/r$ and h is the angular momentum. The perihelion shift per revolution was

$$\delta\phi = \frac{6\pi GM}{c^2 a(1 - e^2)}. \tag{1.11}$$

Here a is the semi-major axis and e the eccentricity. For Mercury the observed values was $43.11 \pm 0.45''$ and the prediction was $43.03''$.

1.2.2 Gravitational Lensing

Since gravity is because of the deformation of spacetime due to the presence of massive objects, light paths will also be affected nearby massive objects. In fact the light will bend around near a massive object like in a convex lens. This can be discussed using the relativistic equation of orbit for null geodesics

$$\frac{d^2u}{d\phi^2} + u = \frac{3GM_\odot}{c^2} \, u^2. \tag{1.12}$$

The angle of deflection of light ray at a far away observer was found to be

$$\Delta = \frac{4GM_\odot}{c^2 R_\odot}, \tag{1.13}$$

provided $R_\odot = 6.96 \times 10^{10} cm$ is the radius of the sun. For the sun, the angle of deflection predicted was $1.75''$. The first observational confirmation came from A. Eddington during a solar eclipse in 1919.

1.2.3 Gravitational redshift

When a radiation propagate against a uniform gravitational field, its frequency will be lesser when received (redshift). The amount of frequency shift will depend on mass and radius of the gravitating source. Mathematically, it can be written as

$$z = \left(1 - \frac{2M}{R}\right)^{-1/2} - 1 = (1 - 2U)^{-1/2} - 1. \tag{1.14}$$

The quantity $U = M/R$ is named as compactness factor. Moreover, if the radiation propagates only the direction of the gravity, its frequency will shift towards higher frequencies (blue-shift). This phenomenon was confirmed in 1959 is a famous experiment now kwon as *"Pound-Rebka experiment"*. They have used Fe^{56} $\gamma-$ray source over a verticle height of 22.5 m (Pound and Rebka [1960]). Redshift is one of the important parameter when discussing compact objects.

1.2.4 Existence of black hole

Soon after the publication of the general relativity in 1915, the first solution of the field equations was put forwarded by K. Schwarzschild in 1916. He found the first exact solution of the Einstein field equations describing an exterior of a spherically symmetric object (Schwarzschild [1916b]) given by ($G = c = 1$ unit)

$$ds^2 = -\left(1 - \frac{2m}{r}\right)dt^2 + \left(1 - \frac{2m}{r}\right)^{-1} dr^2 + r^2(d\theta^2 + \sin^2\theta \, d\phi^2). \tag{1.15}$$

This line element has a singularity at $r = 2m$ i.e. $g_{rr} \to \infty$ as $r \to 2m$. This radius $r = 2m$ is named as *"event horizon"*, within which any object not even light can escape and hence the name *"Black Hole"*. The Kretschmann scalar for the Schwarzschild

solution is found to be

$$K = R_{\mu\nu\alpha\beta}R^{\mu\nu\alpha\beta} = \frac{48m^2}{r^6}. \tag{1.16}$$

This scalar blows-up only at $r = 0$ i.e. there exists a physical singularity at $r = 0$. Hence, the singularity at $r = 2m$ is a coordinates singularity and can be avoided e.g. by the following transformation

$$r^* = r + 2m\ln\left(\frac{r}{2m} - 1\right) \quad , \quad \text{Tortoise coordinate} \tag{1.17}$$

and the equation (1.15) reduces to

$$ds^2 = \left(1 - \frac{2m}{r}\right)\left[-dt^2 + dr^{*2}\right] + r^2(d\theta^2 + \sin^2\theta\, d\phi^2), \tag{1.18}$$

where r is now a function of r^*.

Recently, the existence of black hole have been proven by observing the shadow of a black hole at the center of M87* galaxy using the Event Horizon Telescope (Collaboration [2019]).

Figure 1.1: Shadow of black hole at the center of M87* galaxy.

1.2.5 Gravitational waves

Einstein initiated the theory of gravitational waves in 1916 assuming a small perturbation in the Minkowski spacetime, known as *"linearized theory"*. The metric tensor

describing the Lorentzian spacetime expands as

$$g_{\mu\nu} = \eta_{\mu\nu} + \epsilon\, h_{\mu\nu}, \tag{1.19}$$

where $\epsilon << 1$ and $h_{\mu\nu}$ is fluctuation in the spacetime. Under this linearized theory the wave equation is found to be

$$\eta_{\sigma\rho}\partial^\sigma\partial^\rho\bar{h}_{\mu\nu} \equiv \Box\bar{h}_{\mu\nu} = -\frac{16\pi G}{c^4}\, T_{\mu\nu} \tag{1.20}$$

provided,

$$\bar{h}_{\mu\nu} = h_{\mu\nu} - \frac{1}{2}\, \eta_{\mu\nu}h_{\sigma\rho}\eta^{\sigma\rho}. \tag{1.21}$$

The wave equation (1.20) gives a propagating spacetime waves that travel exactly at the speed of light. This first detection of gravitational waves used an indirect method by observing orbital decay of the Hulse-Taylor binary pulsar (a neutron star binary, PSR B1913+16 and PSR J1915+1606 with approximately equal masses of about $1.4 M_\odot$). The rate of orbital decay predicted by general relativity due to the continuous emission of gravitational waves is given by

$$\frac{dr}{dt} = -\frac{64 G^3}{5 c^5}\frac{m_1 m_2(m_1 + m_2)}{r^3}. \tag{1.22}$$
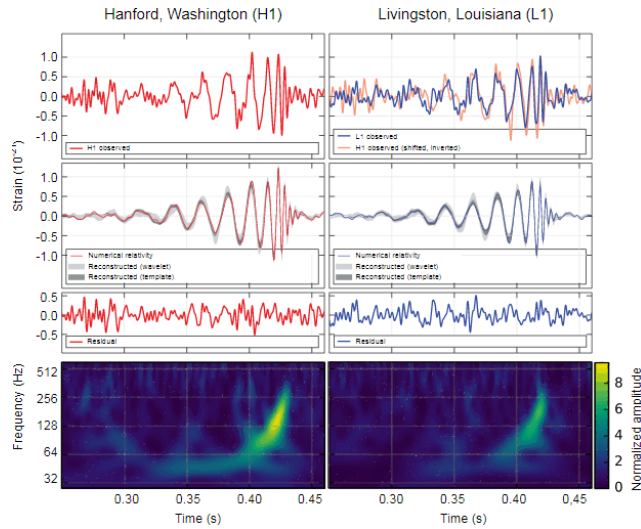
Figure 1.2: LIGO measurement of the gravitational waves at the Livingston (right) and Hanford (left) detectors (Collaboration and Collaboration [2016]).

The ratio of the observed orbital decay rate to the predicted one (1.22) is 0.997 ± 0.002 (Weisberg et al. [2010]). The direct detection for the first time was made in 2015 from a binary black hole merger and was detected by LIGO and VIRGO. This event was named GW150914 and the masses of the two black holes was $36 M_\odot$ and $29 M_\odot$ (Collaboration and Collaboration [2016]). Gravitational waves from first neutron stars merger was also made in the proceeding year and the event was named GW170817 (Collaboration and Collaboration [2017]).

1.2.6 Existence of wormholes

The foundations of wormhole physics dated back to 1916 (Flamm [1916]) when the Schwarzschild exterior solution was just discovered. However, the renaissance on wormhole physics came only after the seminal paper by Morris and Thorne in 1988 (Morris and Thorne [1988]). Wormholes are basically a "bridge" connecting two far away spacetime sheets. This kind of structure can exist by violating classical energy conditions. The spacetime describing such geometry is given by Morrison-Thorne solution given by

$$ds^2 = -e^{2\Phi(r)}dt^2 + \frac{dr^2}{1 - b(r)/r} + r^2(d\theta^2 + \sin^2\theta \, d\phi^2). \tag{1.23}$$

The metric functions $\Phi(r)$ is the "*redshift function*" and $b(r)$, the "*shape function*". The radial coordinate r increases from a minimum value r_0 to $+\infty$. At $r = r_0$, $b(r_0) = r_0$ and this is called "*throat*" of the wormhole. Although the metric potential g_{rr} blows up at the throat $r = r_0$, it is merely a coordinate singularity. The proper radial separation given by

$$\tilde{r} = \pm \int_{r_0}^{r} \frac{dr}{\sqrt{1 - b(r)/r}} \tag{1.24}$$

must be finite everywhere. The two connecting spacetime sheets are represented by $\tilde{r} \in [0, +\infty]$ and $\tilde{r} \in [0, -\infty]$ along with the horizon free condition $g_{tt} \neq 0$.

The wormhole geometry can be visualized via embedding diagram. Considering an equatorial slice $\theta = \pi/2$ for a fixed time $t = constant$, we get

$$ds^2 = \frac{dr^2}{1 - b(r)/r} + r^2 d\phi^2. \tag{1.25}$$

Further, this slice will be embedded in three-dimensional Euclidean space which can

be written in cylindrical coordinate as

$$ds^2 = dz^2 + dr^2 + dr^2 d\phi^2. \tag{1.26}$$

On comparing (1.25) and (1.26) we get

$$\frac{1}{1 - b/r} = 1 + \left(\frac{dz}{dr}\right)^2 \quad \text{or} \quad \frac{dz}{dr} = \pm \left(\frac{r}{b} - 1\right)^{-1/2}. \tag{1.27}$$

Now the embedding surface on the three-dimensional Euclidean space takes the form

$$ds^2 = \left[1 + \left(\frac{dz}{dr}\right)^2\right] dr^2 + r^2 d\phi^2. \tag{1.28}$$

At the throat of the wormhole $r = b(r) = r_0$ and therefore $dz/dr \to \infty$, implying that the embedding surface is vertical at the throat. Also, dz/dr should tends to zero when $r \to \infty$ i.e. the space must be asymptotically flat.

A wormhole solution must satisfy "*flare-out*" condition $d^2r/dz^2 > 0$ at or near the throat. On using (1.27) we get

$$\frac{dr}{dz} = \pm \left(\frac{r}{b} - 1\right)^{1/2} \quad \text{or} \quad \frac{d^2r}{dz^2} = \frac{b - b'r}{2b^2} > 0. \tag{1.29}$$

Satisfying flare-out condition require the violation of few energy conditions. At the throat of the wormhole it is also required to satisfy $b'(r_0) < 1$.
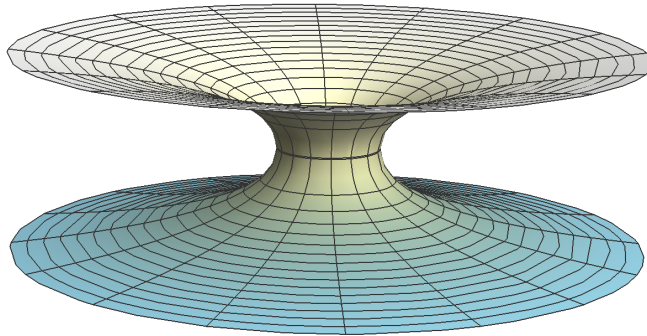
Figure 1.3: Revolution of embedding surface of a wormhole.

1.2.7 Compact stars

The existence of compact stellar system was first conceptualized by K. Schwarzschild as a toy model, which was also the second exact solution of the Einstein's field equation. This solution represents a static stellar system with uniform matter distribution. Due to the assumption of uniform density this solution can't be treated as physical solution. It was the year 1939 Oppenheimer and Volkoff (Oppenheimer and Volkoff [1939]) solved the field equations using an equation of state for degenerate proton (similar to the equation of for degenerate electron used in white dwarf) and found a realistic theoretical model of a neutron star. This compact star can hold a maximum mass up to $0.7 M_\odot$ known as "*Oppenheimer-Volkoff limit*". In the same article they have considered an spherically symmetric spacetime given as

$$ds^2 = -e^\nu c^2 dt^2 + e^\lambda dr^2 + r^2(d\theta^2 + \sin^2\theta \; d\phi^2). \tag{1.30}$$

Now the field equation (1.7) reduces to

$$\frac{8\pi G}{c^4} \; p = \frac{\nu'}{r}e^{-\lambda} - \frac{1-e^{-\lambda}}{r^2} \tag{1.31}$$

$$\frac{8\pi G}{c^4} \; p = e^{-\lambda}\left(\frac{\nu''}{2} - \frac{\lambda'\nu'}{4} + \frac{\nu'^2}{4} + \frac{\nu'-\lambda'}{2r}\right) \tag{1.32}$$

$$\frac{8\pi G}{c^2} \; \rho = \frac{\lambda'}{r}e^{-\lambda} - \frac{1-e^{-\lambda}}{r^2}. \tag{1.33}$$

This reduced field equations can be rearrange in form of hydrostatic equilibrium as (in the unit $G = c = 1$)

$$\frac{dp}{dr} = -\frac{\rho(r)m(r)}{r^2}\left[1 + \frac{p(r)}{\rho(r)}\right]\left[1 + \frac{4\pi r^3 p(r)}{m(r)}\right]\left[1 - \frac{2m(r)}{r}\right]^{-1}, \tag{1.34}$$

where

$$\frac{dm}{dr} = 4\pi r^2 \rho(r). \tag{1.35}$$

Equation (1.34) is now known as "*Tolman-Oppenheimer-Volkoff* (TOV) equation (Oppenheimer and Volkoff [1939]). The equation of state used by Oppenheimer and Volkoff for degenerate neutrons was in the form (in $G = c = h = 1$)(Oppenheimer

and Volkoff [1939])

$$p = \frac{\pi\mu_0^4}{12}\Big(\sinh t - 8\sinh\frac{t}{2} + 3t\Big), \tag{1.36}$$

$$\rho = \frac{\pi\mu_0^4}{4}\Big(\sinh t - t\Big), \tag{1.37}$$

where

$$t = 4\ln\left\{\frac{P_F}{\mu_0} + \sqrt{1 + \Big(\frac{P_F}{\mu_0}\Big)^2}\right\}. \tag{1.38}$$

Here P_F is the Fermi momentum and μ_0 the rest mass of the proton. The Fermi pressure is related to the proper particle density $n = N/V = 8\pi P_F^3/3$. However, this equation of state leads to a maximum mass of about $0.72 M_\odot$.

1.2.8 Einstein cluster

A cluster of stationary gravitating particles moving separately along circular paths about a common center of mass due to their effective gravitational field is named as "*Einstein cluster*". The gravitational field produced by such object can be represented by equation (1.30). For Einstein cluster the stress-energy tensor was chosen as (Einstein [1907])

$$T^{\mu\nu} = \frac{n_0}{m}\, P^\mu P^\nu, \tag{1.39}$$

where $P^\mu = mu^\mu$, m is the rest mass of the particle and n_0, the proper number density. The field equation is given as $(G = c = 1)$

$$\frac{\nu'}{r}e^{-\lambda} - \frac{1 - e^{-\lambda}}{r^2} = 0, \quad \text{(radial)} \tag{1.40}$$

$$e^{-\lambda}\left(\frac{\nu''}{2} - \frac{\lambda'\nu'}{4} + \frac{\nu'^2}{4} + \frac{\nu' - \lambda'}{2r}\right) = 8\pi\, p, \quad \text{(transversal)} \tag{1.41}$$

$$\frac{\lambda'}{r}e^{-\lambda} - \frac{1 - e^{-\lambda}}{r^2} = 8\pi\, \rho. \tag{1.42}$$

Since the radial pressure vanishes, Einstein clusters are highly anisotropic in pressure i.e. the radial pressure is unequal with the transversal pressure. The vanishing radial pressure in (1.40) implies a bridge equation that links the two metric functions as

$$\lambda(r) = \ln\Big(1 + r\nu(r)'\Big) \tag{1.43}$$

Einstein clusters with uniform density are having very large central gravitational redshift. However, one can always see for other types of matter distributions like Burkert or Navarro-Frenk-White type profiles, which are useful in modeling dark matter halos (Geralico et al. [2012]). It has also been reported that instead of circular orbits elliptical orbits are dynamically unstable, which will eventually evolve to circular.

1.3   Physics of compact stars

Compact stars are end products of main sequence stars (MSS) whose masses are generally in the range $\sim 1M_\odot - 25M_\odot$. For the MSS below $8M_\odot$, the compact star remnants are usually white dwarfs. White dwarfs are supported by the electron degeneracy pressure known as *"Fermi pressure"*. Fermi pressure arises due to the Pauli exclusion princple, which states that *"no two fermions can't have the exact same quantum numbers"*. The number of states in a specified volume V in the momentum interval P and $P + dP$ is given by

$$N(P) = \frac{8\pi P^2 V}{h^3}. \tag{1.44}$$

The electron pressure can be calculated as

$$p = \frac{1}{3V} \int_0^\infty N(P) P \, v_P \, dP = \frac{8\pi}{3h^3} \int_0^{P_F} P^3 \frac{\partial E}{\partial P} \, dP. \tag{1.45}$$

Here v_P is the velocity corresponding to the momentum P and E, the kinetic energy. Further, one can also find the internal energy of the electron gas due to their transnational energy as

$$U_k = \int_0^\infty N(P) E \, dP = V \, \frac{8\pi}{h^3} \int_0^{P_F} E P^2 \, dP. \tag{1.46}$$

Now the pressure reduces to

$$p = \frac{8\pi}{3h^3} \, E(P_F) P_F^3 - \frac{U_k}{V}. \tag{1.47}$$

1.3. Physics of compact stars

This is a general expression for any particles. For relativistic particles, we have

$$E = mc^2 \left[\left(1 + \frac{P^2}{m^2 c^2} \right)^{1/2} - 1 \right] \Rightarrow \frac{\partial E}{\partial P} = \frac{1}{m} \left(1 + \frac{P^2}{m^2 c^2} \right)^{-1/2} P. \tag{1.48}$$

Now (1.45) reduces to

$$p = \frac{8\pi}{3mh^3} \int_0^{P_F} \frac{P^4 dP}{\sqrt{1 + P^2/m^2 c^2}} \tag{1.49}$$

which can be integrated with the substitutions

$$\sinh \theta = \frac{P}{mc} \quad \text{and} \quad \sinh \theta_F = \frac{P_F}{mc}$$

we get

$$p = \frac{8\pi m^4 c^5}{3h^3} \left(\frac{\sinh^3 \theta_F \cosh \theta_F}{4} - \frac{3 \sinh(2\theta_F)}{16} + \frac{3\theta_F}{8} \right). \tag{1.50}$$

This is usually kept in the form

$$p = \frac{\pi m^4 c^5}{3h^3} \left[x(2x^2 - 3)\sqrt{x^2 + 1} + 3 \sinh^{-1} x \right] = \frac{\pi m^4 c^5}{3h^3} \, f(x). \tag{1.51}$$

Here $x = P_F/mc$. Similarly, the particle number density can can be found as

$$n = \frac{N}{V} = \frac{8\pi}{h^3} \int_0^{P_F} P^2 dP = \frac{8\pi}{3h^3} \, P_F^3 = \frac{8\pi m^3 c^3}{3h^3} \, x^3. \tag{1.52}$$

Equations (1.51) and (1.52) represents the equation of state of relativistic degenerate electrons in parametric form. Finally, the expression of internal energy takes the form

$$U_k = V \frac{\pi m^4 c^5}{3h^3} \left[8x^3 \{ \sqrt{x^2 + 1} - 1 \} - f(x) \right] = V \frac{\pi m^4 c^5}{3h^3} \, g(x). \tag{1.53}$$

The equation of state for this degenerate electrons reduce to

$$p = \frac{1}{20} \left(\frac{3}{\pi} \right)^{2/3} \frac{h^2}{m} \, n^{5/3} \, , \quad \text{for non-relativistic case } x \to 0, \tag{1.54}$$

$$p = \frac{1}{8} \left(\frac{3}{\pi} \right)^{1/3} hc \, n^{4/3} \, , \quad \text{for relativistic case } x \to \infty. \tag{1.55}$$

Since white dwarf's compactness factor M/R is far less than unity the effects of general relativistic correction is negligible and hence one can use the non-relativistic

hydrostatic equation given by

$$\frac{1}{r^2}\frac{d}{dr}\left(\frac{r^2}{\rho}\frac{dp}{dr}\right) = -4\pi G\rho, \tag{1.56}$$

where $\rho = n\mu_e m_H = 9.82 \times 10^5 \mu_e \ x$. Solving this equation using the equation of state given in (1.51) and (1.52) leads to a maximum mass limit $\frac{5.75}{\mu_e}M_\odot$. For He core, $\mu_e = 2$ and hence the maximum mass limit is $1.44M_\odot$. This limit is known as "*Chandrasekhar limit*" (Chandrasekhar [1931]).

However, if the mass of the MSS is more than $8M_\odot$ the electron degeneracy pressure is not enough to hold the stellar system. This leads to collapsing of the He core generating more gravitational energy producing enough thermal energy to ignite He fusion. The fusion reaction continues until the core He completely converted into Fe^{56} core. Since Fe^{56} is the most stable nucleus, the gravitational energy couldn't produce sufficient thermal energy to ignite it. Hence, the core start collapsing until the atomic nuclei are crushed producing neutrons and protons. At a density of about $10^9 g/cm^3$ the Fermi energy of electrons is high enough to trigger inverse $\beta-$decay i.e. $e^- + p \rightarrow n + \nu$ and hence $_{26}Fe^{56} + e^- \rightarrow {}_{25}Mn^{56} + \nu$ and $_{25}Mn^{56} + e^- \rightarrow {}_{24}Cr^{56} + \nu$. Once the neutron drip density has reached ($\sim 4.3 \times 10^{11} g/cm^3$) the neutrons and protons are no longer bound inside an atomic nucleus leading to electron capture reaction $p + e^- \rightarrow n + \nu$. This process continues during the collapsing of the core until an enough amount of neutrons are generated. Once the neutron degeneracy pressure is sufficient enough to counter-balance the collapse, the collapse will suddenly stop producing an outward shock wave to initial a "*supernova*". Supernova will eject all the matter from outward shells leaving behind the neutron rich compact core along with the release of huge energy and neutrinos. Since the compact core is reach in neutrons, it is named as "*neutron star*". A neutron star consists of many layers (Haensel et al. [2007]):

(i) **Atmosphere** : It is a few cm thick plasma layer. This layer is responsible for the observational evidences like surface temperature, surface gravity, chemical composition, surface magnetic field, mass and radius etc.

(ii) **Outer crust (0.3−0.5 km)**: It is composed of lattice atomic nuclei and relativistic degenerate electron liquid. The pressure in this layer is dominated by the Fermi pressure of electrons. The upper surface is usually solidified.

(iii) **Inner crust ($\sim$ 1 km):** This crust extend from neutron drip density to a transition density $\sim 1.7 \times 10^{14} g/cm^3$. It contain e^-s, free neutrons and neutron-rich nuclei. The the crust-core interface nuclei are disappeared and nucleons are in superfluid states.

(iv) **Outer core**: It is of several km thick that contain protons, electrons, neutron and muons ($npe\mu$). The strong interactions in $n-n$ and $p-p$ makes superfluid neutron liquid and superconducting protons. Electrons and muons acted as ideal fermi gases.

(v) **Inner core**: It may also extend few km thick and the central density may grow in the range $\sim (2.8 - 4.2) \times 10^{15} g/cm^3$. It is also proposed that the following phenomena can also occur:
(a) *Pion condensation.*
(b) *Hyperonization.*
(c) *Koan condensation.*
(d) *Quark matter (u, d, s).*

Since the superfluidity of free neutrons are of Fermi-surface phenomenon, there is negligible effects on the overall equation of state of the neutron star. The neutron superfluids are produced due to the single state pairing ($^1S_0$) in the crust and triple-state pairing ($^3P_2$) at the core (Ruderman [1967], Maekawa and Tamagaki [1968]). The theory of proton superconductivity is given by the Ginzburg-Landau theory where the coherence length $\sim 2-6 fm$ and thereby a type-II superconductivity. The vortices in neutron superfluid was also supported via the Feyman-Onsager quantization which are parallel to the spin axis (Ginzburg and Kirzhnits [1964], Baym et al. [1969]). These vortices may also pinned to the atomic nuclei or the lattice defects within the crust leading to vortex creep. This phenomenon can explain the pulsar glitches. Further, the free quarks at the core may also exist in super-conducting state due to the $color - color$ interactions with a critical temperature of about $50 MeV \equiv 5 \times 10^{11} K$.

The interior compositions of neutron star is highly uncertain due to the presence of many exotic matters which are not familiar with our current knowledge. However, one can propose models with certain matters included. In the composition baryons, mesons (scalar, vector, isovector) and leptons (e^- and muons) the Lagrangian is given

by (Glendenning [1982, 1985])

$$
\begin{aligned}
\mathcal{L} &= \underbrace{\sum_B \bar{\psi}_B \left[i\gamma_\mu \partial^\mu - m_B + g_{\sigma B}\sigma - g_{\omega B}\gamma_\mu \omega^\mu - \frac{1}{2}g_{\rho B}\gamma_\mu \boldsymbol{\tau} \cdot \boldsymbol{\rho^\mu} \right] \psi_B}_{\text{Baryon species: } p,\ n,\ \Lambda,\ \Sigma^+,\ \Sigma^-,\ \Sigma^0,\ \Xi^-,\ \Xi^0 \text{ and interactions with mesons}} \\
&\quad + \underbrace{\frac{1}{2}\left[\partial_\mu \sigma\, \partial^\mu \sigma - m_\sigma^2 \sigma^2 \right] - \frac{1}{4}\,\omega_{\mu\nu}\,\omega^{\mu\nu} + \frac{1}{2}\,m_\omega^2\,\omega_\mu\,\omega^\mu}_{\text{scalar and vector mesons}} \\
&\quad \underbrace{- \frac{1}{4}\,\boldsymbol{\rho}_{\mu\nu} \cdot \boldsymbol{\rho^{\mu\nu}} + \frac{1}{2}\,m_\rho^2\,\boldsymbol{\rho}_\mu \cdot \boldsymbol{\rho^\mu} - \frac{1}{3}\,bm_n \left(g_\sigma \sigma \right)^3 - \frac{1}{4}\,c\left(g_\sigma \sigma \right)^4}_{\text{isovector meson coupled to isospin of baryons}} \\
&\quad + \underbrace{\sum_\lambda \bar{\psi}_\lambda \left(i\gamma_\mu \partial^\mu - m_\lambda \right) \psi_\lambda}_{\text{leptons term}}.
\end{aligned}
\tag{1.57}
$$

Here ψ_B is the baryon spinors and $\bar{\psi}_B \equiv \psi_B^\dagger \gamma_0$. The energy density and pressure can be found as

$$
\begin{aligned}
\epsilon = -\langle \mathcal{L} \rangle + \langle \bar{\psi}\gamma_0 k_0 \psi \rangle &= \frac{1}{3}\,bm_n \big(g_\sigma \sigma \big)^3 + \frac{1}{4}\,c\big(g_\sigma \sigma \big)^4 + \frac{1}{2}\,m_\sigma^2 \sigma^2 + \frac{1}{2}\,m_\omega^2 \omega_0^2 + \frac{1}{2}\,m_\rho^2 \rho_{03}^2 \\
&\quad + \sum_B \frac{2J_B + 1}{2\pi^2} \int_0^{k_B} \sqrt{k^2 + (m_B - g_{\sigma B}\,\sigma)^2}\ k^2 dk \\
&\quad + \sum_\lambda \frac{1}{\pi^2} \int_0^{k_\lambda} \sqrt{k^2 + m_\lambda^2}\ k^2 dk \\
\end{aligned}
\tag{1.58}
$$

$$
\begin{aligned}
p = \langle \mathcal{L} \rangle + \frac{1}{3}\,\langle \bar{\psi}\gamma_i k_i \psi \rangle &= -\frac{1}{3}\,bm_n \big(g_\sigma \sigma \big)^3 - \frac{1}{4}\,c\big(g_\sigma \sigma \big)^4 - \frac{1}{2}\,m_\sigma^2 \sigma^2 + \frac{1}{2}\,m_\omega^2 \omega_0^2 \\
&\quad + \frac{1}{2}\,m_\rho^2 \rho_{03}^2 + \frac{1}{3}\sum_B \frac{2J_B + 1}{2\pi^2} \int_0^{k_B} \frac{k^4 dk}{\sqrt{k^2 + (m_B - g_{\sigma B}\,\sigma)^2}} \\
&\quad + \frac{1}{3}\sum_\lambda \frac{1}{\pi^2} \int_0^{k_\lambda} \frac{k^4 dk}{\sqrt{k^2 + m_\lambda^2}}.
\end{aligned}
\tag{1.59}
$$

Here k_B is the Fermi momenta of baryons species. Now, one can see that the equation of state for the assumed matter contents is very complicated and can only solved by numerical techniques. Further, the above equation of state doesn't include the quark matters, hyperonzation, meson condensation etc and hence for from real physical system.

To include the quark matters the simplest model is given by the MIT-bag model where the quarks are treated as free particles inside a hard spherical bag and the

Lagrangian is given by (Bhaduri [1988])

$$\mathcal{L} = \left[\frac{i}{2}\left\{\overline{\psi}\gamma^\mu\partial_\mu\psi - (\partial_\mu\overline{\psi})\gamma^\mu\psi\right\} - \mathcal{B}\right]\Theta(x) - \frac{1}{2}\overline{\psi}\psi\Delta_s$$

where the symbols have their usual meanings. The Heaviside function and its derivative is defined as

$$\Theta_V(x) = \Theta(\mathcal{R} - r) \quad \text{and} \quad \partial_\mu\Theta = n_\mu\Delta_s. \tag{1.60}$$

The pressure, energy density, baryon number density and entropy at finite temperature for quarks Fermi gas of mass m_f and chemical potential μ_f are

$$p = \sum_f^{u,d,s} \frac{1}{3}\frac{g_f}{2\pi^2}\int_0^\infty \kappa\frac{\partial E_f(\kappa)}{\partial\kappa}\left[n(\kappa,\mu_f) + n(\kappa,-\mu_f)\right]\kappa^2 d\kappa - \mathcal{B}, \tag{1.61}$$

$$\epsilon = \sum_f^{u,d,s} \frac{g_f}{2\pi^2}\int_0^\infty E_f(\kappa)\left[n(\kappa,\mu_f) + n(\kappa,-\mu_f)\right]\kappa^2 d\kappa + \mathcal{B}, \tag{1.62}$$

$$\epsilon_B = \sum_f^{u,d,s} \frac{1}{3}\frac{g_f}{2\pi^2}\int_0^\infty \left[n(\kappa,\mu_f) - n(\kappa,-\mu_f)\right]\kappa^2 d\kappa, \tag{1.63}$$

$$S = \left.\frac{\partial p}{\partial T}\right|_{V,\mu_f}, \tag{1.64}$$

where the kinetic energy of the quarks are

$$E_f(\kappa) = \sqrt{m_f^2 + \kappa^2} \tag{1.65}$$

and $n(\kappa,\mu_f)$ the Fermi distribution function

$$n(\kappa,\pm\mu_f) = \frac{1}{\exp\left[\{E_f(\kappa) \pm \mu_f\}/T\right] + 1} \tag{1.66}$$

with T the temperature and $g_f = 2_{spin} \otimes 3_{color}$. Under the massless quarks approximation i.e. $m_f = 0$, the pressure p and the energy density ρ are link by a linear equation of state (EoS)

$$p = \frac{1}{3}\left(\epsilon - 4\mathcal{B}\right), \tag{1.67}$$

which is the famous MIT-Bag EoS. However, with the inclusion of color-superconductivity the equation of state is modified as (Lugones and Horvath [2002])

$$p = \frac{1}{3} \left(\epsilon - 4\mathcal{B} \right) + \frac{3\xi}{\pi^2} \left[\sqrt{\frac{4\pi^2}{9} \left(\epsilon - \mathcal{B} \right) + \xi^2} - \xi \right] \tag{1.68}$$

where $\xi = 2\delta^2/3 - m_s^2/6$, δ is the color-superconducting gap and m_s mass of the strange quark. However, this is just a simplified model and the actual physical quark matters would be far more complicated. There is also very strong evidences that a new category of compact star named *"quark star "* may also exist next to neutron star. It is believed that if the mass of a neutron star increases beyond a maximum limit, it will start collapsing again until Fermi pressure due to unconfined quarks counter balance the system. The conversion of excess down (d) to strange (s) quark via weak interaction is given by the reactions (Alcock et al. [1986])

$$d \to u + e^- + \bar{\nu}_e \;\; ; \;\; s \to u + e^- + \bar{\nu}_e \;\; ; \;\; d + u \to s + u.$$

Witten [1984] have proposed that *strange matter* as the most stable substance known and *"strange star "* may be the ultimate end product of a dying star.

The matter compositions considered directly link with the resulting equation of state (EOS), which eventually affects the observable quantities, mainly mass and radius of the compact star. A matter compositions of free n, p and leptons ($Ne\mu$) yields a very soft EOS allowing a maximum mass of about $0.7M_\odot$ which is very close to the Oppenheimer-Volkoff Limit i.e. $M_{max} \sim 0.72M_\odot$ in case only free neutron gas is considered. However, with the inclusion of nucleon-nucleon interaction the maximum mass ($M_{max}(Ne\mu)$) can be lift up to $(1.8 - 2.2)M_\odot$. At a density of about $5.6 \times 10^{14} g/cm^3$, hyperonization occurs that convert baryons to hyperons leading to the softening of the EOS and therefore the maximum mass reduces to $M_{max}(NHe\mu) \sim (1.5 - 1.8)M_\odot$. Nishizaki et al. [2002] have shown that by including three-body interactions involving hyperons increases the stiffness of the EOS leading to $M_{max}(NHe\mu) \sim (1.52 - 1.82)M_\odot$. Poin condensation with the presence of pure neutron matter soften the EOS and therefore the maximum mass reduces to $1.32M\odot$ [10.1086/160080]. Further, condensation of kaon in the background of nuclear matter leads to soft EOS with a maximum mass $< 2M_\odot$ (Lim et al. [2014]). The possible maximum mass limit predicted by the general relativity can be found by considering an incompressible fluid i.e. $\rho_{inc} = constant$. For this case the maximum is found to

be

$$M_{max}(inc) \approx 5.09 \left(\frac{5 \times 10^{14} g/cm^3}{\rho_{inc}} \right)^{1/2} M_\odot. \tag{1.69}$$

For $\rho_{inc} = 10^{15} g/cm^3$, $M_{max}(inc) \approx 2.545 M_\odot$. Based on the satisfaction of causality condition and Le Chatelier's principle, the maximum mass limit cannot exceeds $3.2 M_\odot$ (*Ruffini mass limit*) (Rhoades and Ruffini [1974]). As per the recent observations, the maximum mass recorded is about $2.14^{+0.20}_{-0.18} M_\odot$ (Cromartie et al. [2020b]) for a binary pulsar named PSR J0740+6620. To explain such observational evidences, one must seek for more realistic EOSs to incorporate such high mass neutron stars. The recent gravitational waves observation from a binary neutron star merger GW170817 put a strong constraint on the acceptability of an EOS. Any EOSs must yield for a neutron star of mass $1.6 M_\odot$ and $1.4 M_\odot$ a radius above $10.68^{+0.15}_{-0.03} km$ (Bauswein et al. [2017]) and $11.00^{+0.9}_{-0.06} km$ (Capano et al. [2020]) respectively.

1.4 Theories of Modified gravity

There is no doubt that general relativity is one of the greatest achievement in the history of human endeavor in science. It predicted/explained almost perfectly many phenomena starting from the perihelion shifting of Mercury to the detection of gravitational waves recently. General relativity also describe in the most elegant way how the universe began and how it is evolving, which was also supported by observational data from PLANCK (Collaboration [2014]) and WMAP (Bennett et al. [2013]). Despite of huge success, there are some phenomena where the gravitational interaction based on general relativity can't accommodate satisfactory answers. Some these are given below:

(i) Its inability to explain the rotational curve of galaxies and the existence of "*dark matter*" (Aguilar et al. [2013], Collaboration [2013]).

(ii) The accelerating expansion of the Universe with and the hypothetical "*dark energy*".

(iii) General relativity predicted and even confirmed the existence of spacetime singularity or black hole, however has no answer what is happening inside a black hole.

(iv) General relativity still can't reconcile with the quantum theory (or quantum

theory of gravity is still in its infancy).

(v) Some of the massive compact stars can't be accommodated in the realm of general relativity.

1.4.1 Minimal Geometric Decoupling (MGD)

The simplest method of extending the Einstein's gravity is by adding an additional term in the Einstein-Hilbert action i.e. (Ovalle [2010])

$$S = \int \left(\underbrace{\frac{1}{16\pi} \, \mathcal{R} + \mathcal{L}_M}_{EH \ term} + \beta \mathcal{L}_{add} \right) \sqrt{-g} \, dx^4. \tag{1.70}$$

The strength of the $\mathcal{L}_{EH} - \mathcal{L}_{add}$ coupling is decided by the coupling constant β. This additional term modifies the energy-momentum tensor as $T_{\mu\nu} = \tilde{T}_{\mu\nu} + \beta \, \bar{T}_{\mu\nu}$, where

$$\tilde{T}_{\mu\nu} = -\frac{2}{\sqrt{-g}} \frac{\delta(\sqrt{-g} \, \mathcal{L}_M)}{\delta g^{\mu\nu}} = -2 \frac{\partial \mathcal{L}_M}{\partial g^{\mu\nu}} + g_{\mu\nu} \mathcal{L}_M, \tag{1.71}$$

$$\bar{T}_{\mu\nu} = -\frac{2}{\sqrt{-g}} \frac{\delta(\sqrt{-g} \, \mathcal{L}_{add})}{\delta g^{\mu\nu}} = -2 \frac{\partial \mathcal{L}_{add}}{\partial g^{\mu\nu}} + g_{\mu\nu} \mathcal{L}_{add}. \tag{1.72}$$

The field equation now becomes

$$R_{\mu\nu} - \frac{1}{2} \, \mathcal{R} \, g_{\mu\nu} = -8\pi T_{\mu\nu} = -8\pi \left[\tilde{T}_{\mu\nu} + \beta \, \bar{T}_{\mu\nu} \right]. \tag{1.73}$$

Now the density, radial and tangential pressures modify as

$$\rho = \tilde{\rho} + \beta \, \bar{T}_0^0 \ , \ \ p_r = \tilde{p}_r - \beta \, \bar{T}_1^1 \ , \ \ p_t = \tilde{p}_t - \beta \, \bar{T}_2^2. \tag{1.74}$$

The anisotropy in pressure is defined as

$$\Delta = p_t - p_r = \tilde{p}_t - \tilde{p}_r + \beta(\bar{T}_1^1 - \bar{T}_2^2). \tag{1.75}$$

If one consider the unperturbed energy-stress tensor $\tilde{T}_{\mu\nu}$ as perfect fluid i.e. $\tilde{p}_r = \tilde{p}_t$, there is still anisotropy in pressure $\Delta = \beta(\bar{T}_1^1 - \bar{T}_2^2)$. This is the advantage of MGD approach i.e. one can generate anisotropic fluid from isotropic fluid without changing the unperturbed energy-stress. The additional source $\bar{T}_{\mu\nu}$ will generate the anisotropy

and thus an isotropic seed solution can be generalized. It has been suggested that the highly dense interior of compact stars need not to consider isotropic fluid always as many physical phenomena ultimately generate anisotropy. The beauty of this gravity is that the extra source term $\bar{T}_{\mu\nu}$ may arises from the curvature of the spacetime. If one consider a spherically symmetric spacetime of the form,

$$ds^2 = e^\nu dt^2 - e^\lambda dr^2 - r^2(d\theta^2 + \sin^2\theta \, d\phi^2) \tag{1.76}$$

the metric potentials will be modified as

$$e^\nu \rightarrow e^{\tilde{\nu}} + \beta f(r) \quad , \quad e^{-\lambda} \rightarrow e^{-\tilde{\lambda}} + \beta g(r), \tag{1.77}$$

where $f(r)$ and $g(r)$ are deformations functions. If both the g_{00} and g_{11} metric potentials are modified as above, we called it the *Complete Geometric Decoupling (CGD)"* (Ovalle [2019]) and if one of these metric potential is modified, it is the MGD approach. The modification in metric potentials in (1.77) leads to two decoupled field equations, one the unperturbed Einstein field equations and other the *"Quasi-Einstein field equations"*. Further, both the sources satisfy separate the Tolman-Oppenheimer-Volkoff (TOV) equations i.e. $\nabla_\mu \tilde{T}^{\mu\nu} = 0$ and $\nabla_\mu \bar{T}^{\mu\nu} = 0$, which eventually implies $\nabla_\mu T^{\mu\nu} = 0$. The Einstein field equation are given by

$$\frac{1 - e^{-\tilde{\lambda}}}{r^2} + \frac{e^{-\tilde{\lambda}}\tilde{\lambda}'}{r} = 8\pi\tilde{\rho} \tag{1.78}$$

$$\frac{e^{-\tilde{\lambda}} - 1}{r^2} + \frac{e^{-\tilde{\lambda}}\tilde{\nu}'}{r} = 8\pi\tilde{p}_r \tag{1.79}$$

$$e^{-\tilde{\lambda}}\left(\frac{\tilde{\nu}''}{2} + \frac{\tilde{\nu}'^2}{4} - \frac{\tilde{\nu}'\tilde{\lambda}'}{4} + \frac{\tilde{\nu}' - \tilde{\lambda}'}{2r}\right) = 8\pi\tilde{p}_t. \tag{1.80}$$

and the quasi-Einstein field equations (for $f(r) = 0$) are

$$-\frac{g'}{r} - \frac{g}{r^2} = 8\pi\bar{T}_0^0 \tag{1.81}$$

$$-g\left(\frac{\tilde{\nu}'}{r} + \frac{1}{r}\right) = 8\pi\bar{T}_1^1 \tag{1.82}$$

$$-\frac{g}{2}\left(\tilde{\nu}'' + \frac{\tilde{\nu}'^2}{2} + \frac{\tilde{\nu}'}{r}\right) - \frac{g'}{2}\left(\frac{\tilde{\nu}'}{2} + \frac{1}{r}\right) = 8\pi\bar{T}_2^2. \tag{1.83}$$

The methods of solving the field equations can be done in two way:

(a) By choosing a seed solution and the deformation functions, one can find the complete solution. The deformation functions must be chosen so that $0 < g_{00}(r = 0) < 1$ and $g_{11}(r = 0) = 1$ are satisfied.

(b) By choosing a seed solution and solving the quasi-Einstein field equations with a constraint on $\bar{T}_{\mu\nu}$ i.e. $\bar{T}_0^0 = \rho(r)$ (mimic density) or $\bar{T}_1^1 = p(r)$ (mimic pressure) etc.

This modified gravity is very useful in generating compact star solutions. It has the ability to generate high mass compact structures via the coupling parameter β, to incorporate the observational evidences (las Heras and León [2018], Tello-Ortiz et al. [2020], Maurya et al. [2020]).

1.4.2   Embedding class one and Karmarkar condition

This is in fact not a modified gravity since the action is exactly the Einstein-Hilbert action. However, the 4-dimensional Riemannian spacetime will be transformed in to 5-dimensional pseudo-Euclidean spacetime. Hence, the 4-dimensional spacetime is embedded into 5-dimensional flat spacetime. The spherically symmetric configuration given by the spacetime (1.30) with the transformations (Gupta and Goel [1975])

$$z_1 = ke^{\nu/2} \cosh\left(\frac{t}{k}\right), \ z_2 = ke^{\nu/2} \sinh\left(\frac{t}{k}\right), \ z_3 = f(r),$$
$$z^4 = r\sin\theta\cos\phi, \ z_5 = r\sin\theta\sin\phi, \ z_6 = r\cos\theta,$$

takes the form

$$ds^2 = (dz_1)^2 - (dz_2)^2 \mp (dz_3)^2 - (dz_4)^2 - (dz_5)^2 - (dz_6)^2, \tag{1.84}$$

with $[f'(r)]^2 = \mp\left[-\left(e^\lambda - 1\right) + k^2 e^\nu \nu'^2/4\right]$. This means that the 4-dimensional spacetime (1.30) is embedded in 6-dimensional pseudo-Euclidean space (1.84). This kind of solution is called "*embedding class two solution*". One example of class two solution is the Schwarzschild exterior solution. Without the lost of generality, there may exists a function $f(r)$ such that $f'(r) = 0$, then the 6-dimensional pseudo-Euclidean space (1.84) reduces to 5-dimensional pseudo-Euclidean space as

$$ds^2 = (dz_1)^2 - (dz_2)^2 - (dz_4)^2 - (dz_5)^2 - (dz_6)^2. \tag{1.85}$$

1.4. Theories of Modified gravity

Now, the 4-dimensional spacetime (1.30) is embedded in 5-dimensional pseudo-Euclidean space (1.85) i.e. an "*embedding class one solution*". For this case, the two metric potentials g_{00} and g_{rr} are linked

$$e^\lambda = 1 + \frac{k^2}{4}\,\nu'^2 e^\nu. \tag{1.86}$$

This condition was generalized by Karmarkar [1948] as

$$R_{1010}R_{2323} = R_{1212}R_{3030} + R_{1220}R_{1330}. \tag{1.87}$$

An additional condition was proposed by Pandey and Sharma [1982] for spacetime to become class as $R_{2323} \neq 0$ or equivalently $e^\lambda \neq 1$. The advantage of class one method is that only one degree of freedom can determine the entire physical nature of the system. However, there is no physically acceptable solution in isotropic pressure. Using (1.31) and (1.32) the anisotropy $\Delta(r) = p_t(t) - p_r(r)$ in class one condition (1.87) is found to be (Maurya et al. [2015b])

$$\Delta(r) = \frac{\nu'}{4e^\lambda}\left[\frac{2}{r} - \frac{\lambda'}{e^\lambda - 1}\right]\left[\frac{\nu' e^\nu}{2rB^2} - 1\right], \quad B = \frac{1}{k^2}. \tag{1.88}$$

For isotropic case $\Delta(r) = 0$ hence, we get

$$\text{(i) } \nu' = 0 \quad \text{or} \quad \text{(ii) } \left[\frac{2}{r} - \frac{\lambda'}{e^\lambda - 1}\right] = 0 \quad \text{or} \quad \text{(iii) } \left[\frac{\nu' e^\nu}{2rB^2} - 1\right] = 0. \tag{1.89}$$

The case (i) leads to $\nu = C$ implies $e^\lambda = 1$, which is not a class one solution, case (ii) gives

$$e^{-\lambda} = 1 - cr^2, \quad e^\nu = \left(A - \frac{B}{\sqrt{c}}\sqrt{1 - cr^2}\right)^2, \tag{1.90}$$

the Schwarzschild interior solution (Schwarzschild [1916a]) (uniform density model) and case (iii) gives

$$e^\nu = A + Br^2, \quad e^\lambda = \frac{A + 2Br^2}{A + Br^2} \tag{1.91}$$

an asymptotically bounded Kohler and Chao [1965] solution. However, by introducing anisotropy and electric charge many solutions has be explored and even many more can be found. An interesting fact is that embedding class one solutions are usually well-behaved and hence can model physically acceptable astrophysical models.

1.4.3 $f(\mathbb{T})-$**gravity**

This theory was firstly proposed by Albert Einstein himself attempting to unify the gravity and electromagnetism (Einstein [1928, 1930]). The action in $f(\mathbb{T})-$gravity is given by

$$S = \frac{1}{16\pi} \int ef(\mathbb{T}) \ d^4x + \int e\mathcal{L} \ d^4x, \tag{1.92}$$

where, $e = |e_\mu^i|$ and $\mathbb{T}$ is the torsion scalar. The tetrads are defined as

$$e_\mu^i e_i^\nu = \delta_\mu^\nu \quad \text{and} \quad e_\mu^i e_j^\mu = \delta_j^i. \tag{1.93}$$

Here indices $i, j, ...$ runs over tangent spacetime and $\mu, \nu, ...$ runs of coordinate spacetime. The spacetime metric tensor links with the tetrads as

$$g_{\mu\nu}(x) = \eta_{ij} e_\mu^i(x) \, e_\nu^j(x), \tag{1.94}$$

with η_{ij} is the Miskowski metric of the tangent space.

The distinct feature of $f(\mathbb{T})-$gravity is the use of Weintzenböck connection

$$\hat{T}_{\mu\nu}^\sigma = e_i^\sigma \ \partial_\nu e_\mu^i = -e_\mu^i \ \partial_\nu e_i^\sigma \tag{1.95}$$

instead of the Levi-Civita connection (i.e. $\Gamma_{\mu\nu}^\sigma$). Here, the Weintzenböck covariant derivative of the tetrads field is defined as

$$D_\mu e_\nu^i \equiv \partial_\mu e_\nu^i - \hat{T}_{\mu\nu}^\sigma e_\sigma^i. \tag{1.96}$$

Weintzenböck connection associated with a vanishing scalar curvature $\mathcal{R} = 0$ but non-null torsion i.e. $\mathbb{T} \neq 0$. The Weintzenböck and Levi-Civita connections are linked through the torsion and contorsion tensors as

$$\mathbb{T}_{\mu\nu}^\sigma \quad \equiv \quad \hat{T}_{\nu\mu}^\sigma - \hat{T}_{\mu\nu}^\sigma = e_i^\sigma (\partial_\nu e_\mu^i - \partial_\mu e_\nu^i) \tag{1.97}$$

$$\mathbb{K}_\sigma^{\mu\nu} \quad \equiv \quad \mathbb{T}_{\mu\nu}^\sigma - \hat{T}_{\mu\nu}^\sigma = \frac{1}{2}\Big(\mathbb{T}^{\mu\nu}{}_\sigma + \mathbb{T}^{\nu\mu}{}_\sigma - \mathbb{T}_\sigma{}^{\mu\nu} \Big). \tag{1.98}$$

Further, a superpotential tensor can be found as

$$\mathbb{S}_\sigma^{\mu\nu} = \mathbb{K}_\sigma^{\mu\nu} - \delta_\sigma^\nu \mathbb{T}_\alpha^{\alpha\mu} + \delta_\sigma^\mu \mathbb{T}_\alpha^{\alpha\nu}, \tag{1.99}$$

which defines the torsion scalar $\mathbb{T}$ as $\mathbb{T} \equiv \mathbb{T}^\sigma_{\mu\nu} \mathbb{S}^{\mu\nu}_\sigma$.

By variation of (1.92) with respect to e^i_μ leads to the field equation as

$$\mathbb{S}^{\mu\nu}_i f_{\mathbb{TT}} \partial_\mu \mathbb{T} + e^{-1} \partial(e\, \mathbb{S}^{\mu\nu}_i)\, f_{\mathbb{T}} - \mathbb{T}^\sigma_{\mu i} \mathbb{S}^{\nu\mu}_\sigma f_{\mathbb{T}} - \frac{1}{4}\, e^\nu_i f(\mathbb{T}) = -4\pi \mathcal{T}^\nu_i, \qquad (1.100)$$

with $f_{\mathbb{T}} = df(\mathbb{T})/d\mathbb{T}$, $f_{\mathbb{TT}} = d^2 f(\mathbb{T})/d\mathbb{T}^2$ and $\mathcal{T}^\nu_i$, the energy-momentum tensor of the source. The Teleparallel Equivalent of General Relativity (TEGR) (de Andrade et al. [2000]) has the function $f(\mathbb{T}) = \mathbb{T}$ and $f(\mathbb{T}) = \mathbb{T} - 2\Lambda$, with the cosmological constant, which are dynamically identical to the GR.

In the Born-Infeld modification to teleparallel gravity, the Lagrangian is given by

$$\mathcal{L}_{BI} = \frac{\lambda}{16\pi}\, e\, \left(\sqrt{1 + \frac{2\mathbb{S}^{\nu\rho}_\mu \mathbb{T}^\mu_{\nu\rho}}{\lambda}} - 1 \right) \qquad (1.101)$$

which can explain the inflation without an inflation (Ferraro and Fiorini [2007]).

1.4.4 $f(\mathcal{R}, \mathcal{T})-$gravity

The action in $f(\mathcal{R}, \mathcal{T})-$gravity is given by (Harko et al. [2011])

$$S = \frac{1}{16\pi}\, \int f(\mathcal{R}, \mathcal{T})\sqrt{-g}\, d^4x + \int \mathcal{L}_m\, \sqrt{-g}\, d^4x, \qquad (1.102)$$

where $f(\mathcal{R}, \mathcal{T})$ is an arbitrary function of the Riemann curvature $\mathcal{R}$ and trace of energy-momentum tensor $\mathcal{T} = g^{\mu\nu}T_{\mu\nu}$, and $\mathcal{L}_m$, the matter field Lagrangian that relates with the energy-stress tensor as

$$T_{\mu\nu} = -\frac{2}{\sqrt{-g}} \frac{\delta(\sqrt{-g}\, \mathcal{L}_m)}{\delta g^{\mu\nu}} = g_{\mu\nu}\, \mathcal{L}_m - 2\, \frac{\partial \mathcal{L}_m}{\partial g^{\mu\nu}}. \qquad (1.103)$$

By varying the action (1.102) with respect to $g^{\mu\nu}$ we get the field equation as

$$(R_{\mu\nu} - \nabla_\mu \nabla_\nu)f_{\mathcal{R}}(\mathcal{R}, \mathcal{T}) + g_{\mu\nu} \,\Box\, f_{\mathcal{R}}(\mathcal{R}, \mathcal{T}) - \frac{1}{2}\, f(\mathcal{R}, \mathcal{T})g_{\mu\nu} = 8\pi T_{\mu\nu} - f_{\mathcal{T}}(\mathcal{R}, \mathcal{T})$$
$$\left(T_{\mu\nu} + \Theta_{\mu\nu} \right). \quad (1.104)$$

Here, $f_{\mathcal{R}}(\mathcal{R}, \mathcal{T}) = \partial f(\mathcal{R}, \mathcal{T})/\partial \mathcal{R}$, $f_{\mathcal{T}}(\mathcal{R}, \mathcal{T}) = \partial f(\mathcal{R}, \mathcal{T})/\partial \mathcal{T}$ and

$$\Box \equiv \frac{1}{\sqrt{-g}} \frac{\partial}{\partial x^{\mu}} \left(\sqrt{-g} \; g^{\mu\nu} \frac{\partial}{\partial x^{\nu}} \right) \quad \text{and} \quad \Theta_{\mu\nu} = g^{\alpha\beta} \frac{\delta T_{\alpha\beta}}{\delta g^{\mu\nu}}. \tag{1.105}$$

The covariant derivative of the energy-stress tensor gives

$$\nabla^{\mu} T_{\mu\nu} = \frac{f_{\mathcal{T}}}{8\pi - f_{\mathcal{T}}} \Big[(T_{\mu\nu} + \Theta_{\mu\nu}) \nabla^{\mu} \ln f_{\mathcal{T}} + \nabla^{\mu} \Theta_{\mu\nu} - \frac{1}{2} \; g_{\mu\nu} \nabla^{\mu} \mathcal{T}, \tag{1.106}$$

which is non-vanishing. Hence, theory is non-conservative. Choosing $\mathcal{L}_m = -\mathcal{P} = (p_r + 2p_t)/3$ (Harko et al. [2011]) and using (1.105), we get

$$\Theta_{\mu\nu} = -2T_{\mu\nu} + g_{\mu\nu}\mathcal{L}_m - 2g^{\alpha\beta} \frac{\partial^2 \mathcal{L}_m}{\partial g^{\mu\nu} \; \partial g^{\alpha\beta}} = -2T_{\mu\nu} - \mathcal{P} \; g_{\mu\nu}. \tag{1.107}$$

For a linear function $f(\mathcal{R}, \mathcal{T}) = \mathcal{R} + 2\chi\mathcal{T}$, the field equation (1.104) takes the form

$$G_{\mu\nu} = 8\pi T_{\mu\nu} + \chi\mathcal{T}g_{\mu\nu} + 2\chi(T_{\mu\nu} + \mathcal{P} \; g_{\mu\nu}) \tag{1.108}$$

and the corresponding covariant derivative of stress-energy tensor reduced to

$$\nabla^{\mu} T_{\mu\nu} = -\frac{\chi}{2(4\pi + \chi)} \Big[g_{\mu\nu} \nabla^{\mu} \mathcal{T} + 2\nabla^{\mu}(\mathcal{P} \; g_{\mu\nu}) \Big]. \tag{1.109}$$

The field equation (1.104) for Starobinsky-$f(\mathcal{R}, \mathcal{T})$ function i.e. $f(\mathcal{R}, \mathcal{T}) = \mathcal{R} + \xi\mathcal{R}^2 + 2\chi\mathcal{T}$ reduced to

$$(1 + 2\xi\mathcal{R})G_{\mu\nu} + \frac{\xi}{2} \; \mathcal{R}^2 g_{\mu\nu} + 2\xi(g_{\mu\nu}\Box - \nabla_{\mu}\nabla_{\nu})\mathcal{R} = 8\pi T_{\mu\nu} + \chi\mathcal{T} \; g_{\mu\nu}$$
$$+ 2\chi(T_{\mu\nu} + \mathcal{P} \; g_{\mu\nu}). \tag{1.110}$$

This extension of Einstein-Hilbert action with higher order curvature and the matter-geometry coupling can explain the origin of the mysterious dark energy with $f(\mathcal{R}, \mathcal{T}) = f_1(\mathcal{R}) + f_2(\mathcal{R})f(\mathcal{T})$ form (Moraes and Sahoo [2017a]). Further, the non-conservative nature of the $f(\mathcal{R}, \mathcal{T})$ gravity was also considered as a possible source of dark energy (Josset et al. [2017]) and accelerated expansion of the universe (Riess et al. [1998b]).

1.4.5   Energy-momentum squared gravity (EMSG)

The EMSG modifies the Einstein-Hilbert action by adding a non-linear term of energy-momentum tensor to embrace non-minimal matter-geometry coupling. The action is given by (Katirci and Kavuk [2014], Roshan and Shojai [2016])

$$
S = \int \left(\frac{1}{8\pi} \, \mathcal{R} + \alpha \, T_{\mu\nu} T^{\mu\nu} + \mathcal{L}_m \right) \sqrt{-g} \, d^4x. \tag{1.111}
$$

The variation of (1.111) with respect to $g^{\mu\nu}$ leads to the field equation

$$
R_{\mu\nu} - \frac{1}{2} \, \mathcal{R} \, g_{\mu\nu} = 8\pi T_{\mu\nu} + 8\pi\alpha (g_{\mu\nu} T_{\beta\gamma} T^{\beta\gamma} - 2\Theta_{\mu\nu}), \tag{1.112}
$$

where

$$
\begin{aligned}
T_{\mu\nu} &= -\frac{2}{\sqrt{-g}} \frac{\delta(\sqrt{-g} \, \mathcal{L}_m)}{\delta g^{\mu\nu}} = \mathcal{L}_m g_{\mu\nu} - 2 \frac{\partial \mathcal{L}_m}{\partial g^{\mu\nu}}, \tag{1.113} \\
\Theta_{\mu\nu} &= T^{\beta\gamma} \frac{\delta T^{\beta\gamma}}{\delta g^{\mu\nu}} + T_{\beta\gamma} \frac{\delta T^{\beta\gamma}}{\delta g^{\mu\nu}} \\
&= -2\mathcal{L}_m \left(T_{\mu\nu} - \frac{1}{2} \, g_{\mu\nu} \mathcal{T} \right) - \mathcal{T} T_{\mu\nu} + 2T_\mu^\gamma T_{\nu\gamma} - 4T^{\beta\gamma} \frac{\partial^2 \mathcal{L}_m}{\partial g^{\mu\nu} \partial g^{\beta\gamma}} \tag{1.114}
\end{aligned}
$$

and $\mathcal{T} = g^{\mu\nu} T_{\mu\nu}$. This formalism has a non-conservative gravity since

$$
\nabla^\mu T_{\mu\nu} = -\alpha g_{\mu\nu} \nabla^\mu (T_{\beta\gamma} T^{\beta\gamma}) + 2\alpha \nabla^\mu \Theta_{\mu\nu} \tag{1.115}
$$

which is non vanishing. The field equation (1.112) has the same geometrical form as in GR, however the matter field has been modified. This gravity can become a conservative theory if one defines an effective energy-momentum tensor as

$$
T_{\mu\nu}^{eff} = T_{\mu\nu} + \alpha (g_{\mu\nu} T_{\beta\gamma} T^{\beta\gamma} - 2\Theta_{\mu\nu}) \tag{1.116}
$$

so that $\nabla^\mu T_{\mu\nu}^{eff} = 0$.

Faraji et al. [2021] have used the EMSG gravity in the context of cosmology. They found that this gravity have bouncing solution and a observably viable inflation for the coupling strength in the range $0 < \alpha < 2.1 \times 10^{-5}$. Another group (Nazari et al. [2020]) has shown that the field equation in Palatini-EMSG i.e. $\mathcal{L} = \mathcal{R} + \beta \mathcal{R}^2 + \alpha T_{\mu\nu} T^{\mu\nu}$ reduces to Poisson equation on weak field limit and also there exist a bouncing solution in $\alpha > 0$.

1.5   Killing vectors and conformal motion

The conformal motion is a mapping of manifold $\mathcal{M} \to \tilde{\mathcal{M}}$ such that the metric g transforms as

$$g \to \tilde{g} = 2e^{\psi}g \ , \quad \text{with} \ \ \psi \equiv \psi(x^{\mu}). \tag{1.117}$$

This can also be expressed as (Radinschi et al. [2010], Moopanar and Maharaj [2010])

$$\mathbb{L}_{\xi} \ g_{\mu\nu} = \xi_{\mu;\nu} + \xi_{\nu;\mu} = \psi \ g_{\mu\nu}. \tag{1.118}$$

Here $\mathbb{L}_{\xi}$ is the Lie derivative along ξ^{μ} and $\psi(x^{\mu})$, the conformal factor. In GR, the vector field that generates conformal symmetry with static and spherically symmetric spacetime is found as (Herrera et al. [1984], Herrera and de León [1985])

$$\xi = \xi^t r \ \frac{\partial}{\partial t} + \xi^r r \ \frac{\partial}{\partial r}. \tag{1.119}$$

On using (1.119) in (1.118) we get

$$\xi^r \frac{d \ln g_{tt}}{dr} = \psi(r) \ , \ \ \xi^t = \text{const.} \ , \ \ \xi^r = \frac{\psi(r) \, r}{2} \ , \ \ \xi^r \frac{d \ln g_{rr}}{dr} + 2 \ \frac{d\xi^r}{dr} = \psi(r) \tag{1.120}$$

which further reduces to

$$g_{tt} = c_1^2 r^2 \ , \ \ g_{rr} = \left(\frac{\psi}{c_2} \right)^{-2} \ , \ \ \xi^i = c_3 \delta_0^i + \frac{1}{2} \ \psi \ r \ \delta_r^i \tag{1.121}$$

with c_1, c_2 and c_3 are the constants of integration. The vectors in (1.120) are physically acceptable since $\psi = 0$ gives Killing vector, a homothetic vector if $\psi = 0$ and conformal motion when $\psi = \psi(x^{\mu})$.

    The method of solving the field equations with conformal symmetry simplifies the mathematical structures without neutralizing the physics behind it Herrera et al. [1984], Maartens and Maharaj [1990].

Chapter 2

Minimally deformed anisotropic model of class one space-time by gravitational decoupling [1]

2.1 Introduction

General Relativity (GR) theory of gravitation has been established by Einstein in 1916 in which gravitational properties spread with the speed of light and the law of physics articulated to be invariant with respect to accelerated observers (Einstein [1915a,d,b,c], Will [2006]). The main assumptions of Einstein's theory of gravitation are based on the (i) all events in the universe as a 4-dimensional Riemannian manifold, which is called space-time, (ii) the curvature related with the metric is related to the matter by Einstein's field equations (EFE). There will be various fields on the space-time which describe the matter content the space-time through energy-momentum tensor $T_{\mu\nu}$. The field equation of GR is non-linear 2nd order partial differential equation of hyperbolic type, which permits clear freedom of change of coordinates. The first solution of EFE describing a self-gravitating, bounded object was obtained by Schwarzschild [1916a]. This interior solution represents a constant density model with the outer space-time being empty. However, the velocity of sound within the sphere exceeds the velocity of light thus such a model is not realistic. Therefore, this encouraged us to search for physically viable solutions to the Einstein field equations

---

[1]Content of this chapter has been published in *European Physical Journal C* (Springer), 79 (2019) 851.

2. Minimally deformed anisotropic model of class one space-time by gravitational decoupling

which describe the realistic models. The space-time of Schwarzschild's exterior solution (Schwarzschild [1916b]) was obtained in 1916 which describes the gravitational field outside a spherical mass by imposing spherical symmetry on the space-time manifold. The theory of spherical symmetric space-time has been investigated by Takeno (1966) from the point of view of invariant classification, group of motion, conformal transformation and embedding classes, etc.

The method of gravitational decoupling by Minimal Geometric Deformation (MGD) is a great and powerful technique that extends known solutions into more difficult situations. By using this MGD technique, Gabbanelli et al. [2018] have extended isotropic Durgapal-Fuloria solution in the anisotropic domain while Ovalle et al. [2018b] have shown that how a spherically symmetric fluid modifies the Schwarzschild vacuum solution and necessity of anisotropy in the fluid. In this connection, several other authors have used the MGD approach to discover the more complex solution which can be seen in the following Refs. Sharif and Sadiq [2018b], Contreras [2018], Sharif and Sadiq [2018a], Contreras and Bargueño [2018], Morales and Tello-Ortiz [2018a], las Heras and León [2018], Panotopoulos and Rincón [2018], Sharif and Saba [2018], Contreras et al. [2019], Maurya and Tello-Ortiz [2019], Contreras [2019], Ovalle et al. [2018a], Sharif and Waseem [2019], Gabbanelli et al. [2019]. The GD was developed by Ovalle as a consequence of the Minimal Geometric Deformation (MGD) Ovalle [2017, 2019] (see also Ref. Casadio et al. [2015]) in the framework of Randall-Sundrum gravity (Randall and Sundrum [1999b,a]). In Ref. Casadio et al. [2015], the author extended the Minimal Geometric Deformation approach to investigate a new black hole solution.

The key features of this approach for new solutions to EFE are available in literature as Ovalle et al. [2018c]:

I. Considering the energy-momentum tensor $\tilde{T}_{\mu\nu}$ for known metric as a source and extend known solutions of EFE into more complex situations. The new source is coupled with the $\tilde{T}_{\mu\nu}$ associated with the seed solution through a non-dimensional coupling constant β which can be written as:

$$\tilde{T}_{\mu\nu} \mapsto \hat{T}_{\mu\nu}^{(1)} = \tilde{T}_{\mu\nu} + \beta^{(1)} T_{\mu\nu}^{(1)} \tag{2.1}$$

and then continue to same the process with more sources, like

$$\hat{T}_{\mu\nu}^{(1)} \mapsto \hat{T}_{\mu\nu}^{(2)} = \hat{T}_{\mu\nu}^{(1)} + \beta^{(2)} T_{\mu\nu}^{(2)} \tag{2.2}$$

and so on. In this approach, we can spread direct solutions of the Einstein equations related with the simplest gravitational source $\tilde{T}_{\mu\nu}$ into the province of more complex forms of gravitational sources $\tilde{T}_{\mu\nu} = \hat{T}_{\mu\nu}^{(n)}$.

II. It is noted that we can also use the reverse of the above methodology in order to find an exact solution to Einstein's field equation. In this procedure, we can split a more difficult energy-momentum tensor $\hat{T}_{\mu\nu}$ into simpler components, say $\tilde{T}_{\mu\nu}^{(i)}$, and then Einstein's equations have to be solved for each one of these components. In this situation, there will be many solutions corresponding to each component of $\tilde{T}_{\mu\nu}^{(i)}$ associated with the original energy-momentum tensor. At last, we can find the solution of Einstein's equations for the original energy-momentum tensor $\hat{T}_{\mu\nu}$ by combining all the above individual solution. However, we would like to mention that this procedure works very well as each source satisfies the conservation equation identically, which can be written as

$$\nabla_\mu \hat{T}^{\mu\nu} = \nabla_\mu \tilde{T}^{(1)\mu\nu} = \nabla_\mu \tilde{T}^{(2)\mu\nu} = \cdots = \nabla_\mu \tilde{T}^{(n)\mu\nu} = 0. \qquad (2.3)$$

Now we explain the procedure to explore MGD-decoupling methodology which is as follows: Suppose we have two gravitational sources namely S_1 and S_2 where we will first solve the standard Einstein's equations corresponding to the source S_1 and then the other set of quasi-Einstein equations are solved for the source S_2. At last, we combine these two solutions to determine the complete solution for the total system of $S_1 \cup S_2$. As we know that Einstein's field equations are non-linear, therefore the above procedure leads a powerful technique to find the solutions and their analysis, especially during the situations that away form trivial cases.

Many analytical solutions were created by Tolman [1939], which describe the structure of the interior stellar geometry for the perfect fluid models. However, the anisotropic models where the tangential and radial pressures are unequal, allows a better understanding of the highly-dense matter. Ruderman [1972] and Bowers and Liang [1974] have been studied the anisotropic fluid distribution that has explored the most updated research. In this continuation Mak and Harko [2003] has suggested that anisotropy plays an important role to understand the variation of properties of the dense nuclear matter for a strange star. On the other hand, the presence of anisotropy could be identified through the existence of a solid core or type 3A superfluid (Kippenhahn et al. [1990]), pion condensed phase (Sawyer [1972]), and different kinds of phase transitions (Sokolov [1980]). The positive anisotropy inside

2. Minimally deformed anisotropic model of class one space-time by gravitational decoupling

star provides a realistic star which have been studied by several authors. If we have the anisotropy factor $\Delta(r) = p_t - p_r > 0$, then anisotropic force inside the stellar system outward-directed which improve the stability and equilibrium criteria, and if the anisotropy factor $\Delta(r) = p_t - p_r < 0$, then anisotropic force inside the stellar system is directed inward that introduce instability in the system.

Now the finding of the solutions to EFE is a great challenge to meet the requirements of physical acceptability (Ovalle [2016], Delgaty and Lake [1998], Gokhroo and Mehra [1994]). Recently Jasim et al. [2016] have constructed an anisotropic fluid sphere model by supposing a specific form of the potential metric functions e^λ and e^ν to EFE with MIT bag EOS in presence of cosmological constant. This model yields a realistic fluid sphere such as PSR 1937 +21. In this connection, an extensive study has been conducted by several authors to understand the role of anisotropy of the interior of stellar objects (Maurya et al. [2017a], Ivanov [2002b], Schunck and Mielke [2003], Usov [2004], Deb et al. [2018], Panahi et al. [2016], Shee et al. [2016], Rahaman et al. [2012a], Kalam et al. [2012], Rahaman et al. [2011], Varela et al. [2010], Negreiros et al. [2009]).

The purpose of this chapter is to the study of minimally deformed solution for class one space-time by using gravitational decoupling method that gives a generalised solution for ansitropic compact star models. The chapter is organized as follows. In sections 2.2 and 2.3, MGD have been used to scrutinize the interior space-time and field equation to find new embedding class one solution. The non-singularity of the solution has been discussed in section 2.4 while, in section 2.5, the boundary condition and determination of constraints have been analyzed. The section 2.6 is devoted for analysis of the slow rotation approximation, moment of inertia and Kepler frequency. The elastic property of compact stars in section 2.7 has been studied to focus and determine K_e on compression modulus K_e while, in section 2.8 the energy conditions have been considered and confirmed at all points in the interior of a star. In section 2.9, we analyzed the physical features as well as stability of the resulting solution with the help of graphical illustrations considering the equilibrium under various forces, causality, adiabatic index, and Harrison-Zeldovich-Novikov static. We also compared the solution for different values of β and analyzed for a well-behaved solution. Finally, we summarize the results in the last section.

2.2 Interior space-time and field equations with MGD

2.2.1 Einstein equations for two sources:

The action of this modified matter distribution for MGD defined as (Ovalle [2019])

$$S = S_{EH} + \beta\, S_1 = \int \left[\frac{\mathcal{R}}{16\pi} + \mathcal{L}_M + \beta\, \mathcal{L}_1 \right] \sqrt{-g}\, d^4 x \tag{2.4}$$

provided $\mathcal{L}_M$ and $\mathcal{L}_1$ are matter fields and additional Lagrangian density due to the extra source respectively. However $\mathcal{R}$ denotes the Ricci scalar, g is the determinant of the metric tensor $g_{\mu\nu}$ and β is a coupling constant. Now we define the energy-momentum tensor for both Lagrangian matter which are given by

$$\tilde{T}_{\mu\nu} = -\frac{2}{\sqrt{-g}} \frac{\delta(\sqrt{-g}\, \mathcal{L}_M)}{\delta g^{\mu\nu}} = -\frac{2\, \partial(\mathcal{L}_M)}{\partial g^{\mu\nu}} + g_{\mu\nu}\mathcal{L}_M \tag{2.5}$$

$$\Theta_{\mu\nu} = -\frac{2}{\sqrt{-g}} \frac{\delta(\sqrt{-g}\mathcal{L}_1)}{\delta g^{\mu\nu}} = -2\frac{\delta \mathcal{L}_1}{\delta g^{\mu\nu}} + g_{\mu\nu}\mathcal{L}_1. \tag{2.6}$$

By Varying the action, (2.4) with respect to the metric tensor $g^{\mu\nu}$, we get the general equations of motion

$$R_{\mu\nu} - \frac{1}{2}g_{\mu\nu}\mathcal{R} = -8\pi\, T_{\mu\nu} \tag{2.7}$$

where,

$$T_{\mu\nu} = \tilde{T}_{\mu\nu} + \beta\, \Theta_{\mu\nu}. \tag{2.8}$$

The symbols used in above equations have their usual meanings. Let us consider the inside of spherical body is filled of an anisotropic fluid matter, therefore in the current situation the stress-energy tensor $\tilde{T}_{\mu\nu}$ takes the following form

$$\tilde{T}_{\mu\nu} = (\tilde{\rho} + \tilde{p}_t)u_\mu u_\nu - \tilde{p}_t g_{\mu\nu} + (\tilde{p}_r - \tilde{p}_t)\, v_\mu v_\nu, \tag{2.9}$$

where the covariant component u_ν denote the 4-velocity, fulfilling $u_\mu u^\mu = -1$ and $u_\nu \nabla^\mu u_\mu = 0$. Here, $\tilde{\rho}$, $\tilde{p}_r$ and $\tilde{p}_t$ represent the matter density and pressures (radial and tangential) for anisotropic matter. It is noted that the presence of this extra

2. Minimally deformed anisotropic model of class one space-time by gravitational decoupling

source $\Theta_{\mu\nu}$ in Eq. (2.8) produce an ansitropies in self gravitating system that can be a scalar, vector or tensor field. We would like to mention here that the Einstein tensor is always divergence free, therefore the stress tensor $T_{\mu\nu}$ in Eq. (2.7) must satisfy the conservation law,

$$\nabla^{\mu}T_{\mu\nu} = 0, \tag{2.10}$$

To describe the space-time geometry inside the body for complete system we assume a spherically symmetric line element of the form,

$$ds^2 = e^{\nu(r)}dt^2 - e^{\lambda(r)}dr^2 - r^2\left(d\theta^2 + \sin^2\theta d\phi^2\right) \tag{2.11}$$

where ν and λ are functions of the radial coordinate 'r' only. Then the Einstein field equations (2.7) together with the eqs. (2.8), (2.9) and line element (2.11) give the following set of the equations,

$$8\pi(\tilde{\rho} + \beta\Theta_t^t) = e^{-\lambda}\left(\frac{\lambda'}{r} - \frac{1}{r^2}\right) + \frac{1}{r^2}, \tag{2.12}$$

$$8\pi(\tilde{p}_r - \beta\Theta_r^r) = e^{-\lambda}\left(\frac{\nu'}{r} + \frac{1}{r^2}\right) - \frac{1}{r^2}, \tag{2.13}$$

$$8\pi(\tilde{p}_t - \beta\Theta_\varphi^\varphi) = \frac{e^{-\lambda}}{4}\left(2\nu'' + \nu'^2 + 2\frac{\nu' - \lambda'}{r} - \nu'\lambda'\right). \tag{2.14}$$

where the effective density (ρ), effective radial pressure (p_r), effective tangential pressure (p_t) and effective anisotropy corresponding to the energy momentum tensor $T_{\mu\nu}$ can be defined as,

$$\rho = \tilde{\rho} + \beta\Theta_t^t, \tag{2.15}$$

$$p_r = \tilde{p}_r - \beta\Theta_r^r, \tag{2.16}$$

$$p_t = \tilde{p}_t - \beta\Theta_\varphi^\varphi, \tag{2.17}$$

$$\Delta = \tilde{p}_t - \tilde{p}_r + \beta(\Theta_r^r - \Theta_\varphi^\varphi). \tag{2.18}$$

Further, We would like to mention that the linear combination of equations (2.12)-(2.14) satisfy the conservation equation for the energy-momentum tensor $T_\nu^\mu = \tilde{T}_\nu^\mu + \beta\Theta_\nu^\mu$ with coupling parameter β as

$$-\frac{d\tilde{p}_r}{dr} - \beta\left[\frac{\nu'}{2}\left(\Theta_t^t - \Theta_r^r\right) - \frac{d\Theta_r^r}{dr} + \frac{2}{r}\left(\Theta_\varphi^\varphi - \Theta_r^r\right)\right] - \frac{\nu'}{2}\left(\tilde{\rho} + \tilde{p}_r\right) + \frac{2(\tilde{p}_t - \tilde{p}_r)}{r} = 0. \tag{2.19}$$

2.2.2   Gravitational decoupling by MGD approach:

Since the system of equations (2.12) - (2.14) contains seven unknown functions which are namely $p(r)$, $\rho(r)$, $\nu(r)$, $\lambda(r)$ and three independent components of Θ. Therefore, this system has infinitely many solutions. Now we will apply the MGD approach to solve this system of equations. In this approach, the system will be converted in the such way that the field equations connected with the source $\Theta_{\mu\nu}$ will satisfy "effective quasi-Einstein". Now we can start by taking a solution of the Eq. (2.7) for the stress-tensor $\tilde{T}_{\mu\nu}$ which correspond to GR perfect fluid solution [that will be same as the equations (2.12)-(2.14) when $\beta \to 0$] with the line element,

$$d\tilde{s}^2 = e^{\tilde{\nu}(r)}dt^2 - e^{\tilde{\lambda}(r)}dr^2 - r^2(d\theta^2 + \sin^2\theta d\phi^2), \tag{2.20}$$

where the gravitational potential $e^{\tilde{\lambda}(r)}$ can be defined as,

$$e^{-\tilde{\lambda}(r)} = 1 - \frac{8\pi}{r}\int_0^r r^2\,\rho(r)dr = 1 - \frac{2m(r)}{r} \tag{2.21}$$

here the $m(r)$ represents the Misner-Sharp mass function for the standard general relativity. The influence of the extra source $\Theta_{\mu\nu}$ on the energy-momentum tensor $\tilde{T}_{\mu\nu}$ can be determined by the geometric deformation via perfect fluid geometry $\{\tilde{\nu}(r), \tilde{\lambda}(r)\}$ in Eq. (2.20) as

$$e^{\tilde{\nu}} \to e^{\nu} = e^{\tilde{\nu}} + \beta f(r) \tag{2.22}$$

$$e^{-\tilde{\lambda}} \to e^{-\lambda} = e^{-\tilde{\lambda}} + \beta g(r). \tag{2.23}$$

where $f(r)$ and $g(r)$ are the deformation functions associated with the temporal and radial components of line elements, respectively. It is noted that these deformation functions depend only on radial coordinate while constant β is a free parameter. The considered MGD method allows to set $g = 0$ or $f = 0$, then for this situation the deformation will be performed only on the radial component and other temporal one unaltered (it corresponds to $f = 0$). By setting $f = 0$ we get

$$e^{-\tilde{\lambda}} \to e^{-\lambda} = e^{-\tilde{\lambda}} + \beta\,g(r) \tag{2.24}$$

2. Minimally deformed anisotropic model of class one space-time by gravitational decoupling

This is called as the Minimal Geometric Deformation (MGD) along the radial component of the line element. After plugging the eqs. (2.24) into field equations (2.12) -(2.14), we get two sets of equations as first set corresponding to the standard Einstein field equations for an energy-momentum tensor $\tilde{T}_{\mu\nu}$ which is given as,

$$\frac{1 - e^{-\tilde{\lambda}}}{r^2} + \frac{e^{-\tilde{\lambda}}\tilde{\lambda}'}{r} = 8\pi\tilde{\rho} \tag{2.25}$$

$$\frac{e^{-\tilde{\lambda}} - 1}{r^2} + \frac{e^{-\tilde{\lambda}}\tilde{\nu}'}{r} = 8\pi\tilde{p}_r \tag{2.26}$$

$$e^{-\tilde{\lambda}}\left(\frac{\tilde{\nu}''}{2} + \frac{\tilde{\nu}'^2}{4} - \frac{\tilde{\nu}'\tilde{\lambda}'}{4} + \frac{\tilde{\nu}' - \tilde{\lambda}'}{2r}\right) = 8\pi\tilde{p}_t. \tag{2.27}$$

along with the conservation equation,

$$-\frac{d\tilde{p}_r}{dr} - \frac{\nu'}{2}\left(\tilde{\rho} + \tilde{p}_r\right) + \frac{2(\tilde{p}_t - \tilde{p}_r)}{r} = 0. \tag{2.28}$$

while second set of equations for the source $\Theta_{\mu\nu}$, called as quasi-Einstein equations, is given as

$$-\frac{g'}{r} - \frac{g}{r^2} = 8\pi\Theta_t^t \tag{2.29}$$

$$-g\left(\frac{\tilde{\nu}'}{r} + \frac{1}{r}\right) = 8\pi\Theta_r^r \tag{2.30}$$

$$-\frac{g}{2}\left(\tilde{\nu}'' + \frac{\tilde{\nu}'^2}{2} + \frac{\tilde{\nu}'}{r}\right) - \frac{g'}{2}\left(\frac{\tilde{\nu}'}{2} + \frac{1}{r}\right) = 8\pi\Theta_\phi^\phi. \tag{2.31}$$

The corresponding conservation equation $\nabla^\nu\Theta_{\mu\nu} = 0$ gives,

$$\frac{\nu'}{2}\left(\Theta_t^t - \Theta_r^r\right) - \frac{d\Theta_r^r}{dr} + \frac{2}{r}\left(\Theta_\varphi^\varphi - \Theta_r^r\right) = 0. \tag{2.32}$$

The above expression is a linear combination of the quasi-Einstein equations. At this stage it is noted that both sources $\tilde{T}_{\mu\nu}$ and $\Theta_{\mu\nu}$ are individually conserved, which implies that both systems interact only gravitationally.

2.2.3 Embedding class one condition associated with line element (2.20):

If the space-time (2.20) satisfies the Karmarkar [1948] condition

$$R_{1414}R_{2323} = R_{1212}R_{3434} + R_{1224}R_{1334} \tag{2.33}$$

then the two metric functions $\tilde{\lambda}$ and $\tilde{\nu}$ can be link via

$$\frac{\tilde{\lambda}' \, \tilde{\nu}'}{1 - e^{\tilde{\lambda}}} = \tilde{\lambda}' \, \tilde{\nu}' - 2\tilde{\nu}'' - \tilde{\nu}'^2 \tag{2.34}$$

The above condition implies that the four dimensional space-time (2.20) is embedded into five dimensional pseudo-Euclidean space i.e. embedding class one solutions. The Karmarkar condition must satisfy the Pandey and Sharma condition (Pandey and Sharma [1982]) $R_{2323} \neq 0$ to describe a class one solution. On integrating (2.34) we get

$$e^{\tilde{\nu}} = \left(A + B \int \sqrt{e^{\tilde{\lambda}} - 1} \, dr \right)^2 \tag{2.35}$$

where A and B are constants of integration.

Using the definition of ansitropy in Eqs. (2.26) and (2.27) together with Eq. (2.35) we express the anisotropic factor, $\tilde{\Delta}(r)$, corresponding to energy-momentum tensor $\tilde{T}_{\mu\nu}$ by some manipulation (Maurya et al. [2015b]) as

$$\tilde{\Delta}(r) = \tilde{p}_t - \tilde{p}_r = \frac{\tilde{\nu}'}{32\pi e^{\tilde{\lambda}}} \left[\frac{2}{r} - \frac{\tilde{\lambda}'}{e^{\tilde{\lambda}} - 1} \right] \left[\frac{\tilde{\nu}' e^{\tilde{\nu}}}{2 \, r \, B^2} - 1 \right]. \tag{2.36}$$

Here some comments are in order: i) In this paper, we want to determine a new solution for the field equations (2.25)-(2.27) using embedding class one condition. However, it is well known that we can achieve only two kinds of perfect fluid solutions, namely Schwarzschild interior solution (by vanishing of first factor in Eq. (2.36)) and Kohlar-Chao solution (by vanishing of second factor in Eq. (2.36)), for embedding class one space-time which have been already discussed in the literature. Therefore, we choose anisotropic matter distribution corresponding to energy momentum tensor $\tilde{T}_{\mu\nu}$ for determining a new solution of embedding class one space-time. ii.) After solving the system (2.25)-(2.27), we will solve the quasi-Einstein equations (2.29)-(2.31) by taking a suitable form of the deformation function $g(r)$ which we are going

to discuss in next section.

2.3   New embedding class one solution by MGD

Here the field equations (2.25)-(2.27) corresponding to energy momentum tensor $\tilde{T}_{ij}$ depends upon two unknown source functions, namely $\tilde{\lambda}$ and $\tilde{\nu}$. Once these source functions are determined then immediately we can obtain the thermodynamical observable like $\tilde{\rho}$, $\tilde{p}_r$ and $\tilde{p}_t$ to describe the complete structure of the proposed model. In this connection, the physical validity of this source function $\tilde{\nu}(r)$ has been proposed by Lake, in which the function should be monotonic increasing function with a regular minimum at $r = 0$ that gives a physically viable static spherically symmetric perfect fluid solution of Einstein's equations which is regular at $r = 0$ (Delgaty and Lake [1998]). On the other hand, the form of another source function $\tilde{\lambda}(r)$ must ensure that $e^{\tilde{\lambda}(r))} = 1 + O(r^2)$. This form of $\tilde{\lambda}$ gives a sufficient condition for a static perfect fluid solution to be regular at the centre. Therefore in view of above points we consider a new source function $\tilde{\lambda}(r)$, to generate the physical viable solution, of the form as,

$$e^{\tilde{\lambda}} \;=\; 1 + cr^2 e^{nar^2}. \tag{2.37}$$

where c and a are arbitrary parameters with the dimension of $length^{-2}$ while n is a positive constant. Now form Eq. (2.37) we observe that $e^{\tilde{\lambda}} \to 1 + O(r^2)$ and regular at centre as $e^{\tilde{\lambda}(0)} = 1$. On inserting eq.(2.37) into (2.35) and integrate we obtain,

$$e^{\tilde{\nu}} \;=\; \left(A + \frac{B\sqrt{c}}{an}\; e^{anr^2/2}\right)^2. \tag{2.38}$$

We observe that $\tilde{\nu}(r)$ is regular at centre $r = 0$ and positive increasing throughout within the stellar compact object which provides a realistic compact star model. Therefore, the solution of the field equations (2.25)-(2.27) can be given by following line element,

$$d\tilde{s}^2 = \left(A + \frac{B\sqrt{c}}{an}\; e^{anr^2/2}\right)^2 dt^2 - \left(1 + cr^2 e^{nar^2}\right)^{-1} dr^2 + r^2(d\theta^2 + \sin^2\theta\; d\phi^2). \tag{2.39}$$

Now our next task to find all the components of Θ^{μ}_{ν} to describe the complete struc-

2.3. New embedding class one solution by MGD

ture of the model. As we see that all these components depend on the deformation function $g(r)$ that requires some restrictions to lead the well-behaved solutions i.e. free of undesired mathematical and physical singularities, and non-decreasing nature, etc. These choices of deformation functions $g(r)$ have been widely considered by authors (Maurya and Tello-Ortiz [2019], Morales and Tello-Ortiz [2018b], Estrada and Prado [2019]). However, we can also be considered other options like as radial pressure associated with Θ_r^r to the mimic radial pressure i.e. $\Theta_r^r = p_r$ and density associated with Θ_t^t to mimic energy density i.e. $\Theta_t^t = \rho$, or relate only Θ-sector components through a polytropic, barotropic, or linear equation of state. It is worth mentioning that both later cases are too complicated for determining the deformation function $f(r)$. Therefore, we adopt the first procedure to construct the physically acceptable model then deformation function $g(r)$ has the following form,

$$g(r) = \frac{ncr^2}{cr^2 + 1}. \tag{2.40}$$

This form was inspired by the property of e^λ that it tends to unity if $r \to 0$ and increasing outward to describe the well-behaved solutions. Then the explicit form of the complete space-time associated with the energy momentum tensor $T_{\mu\nu}$ can be written as

$$\begin{aligned}
ds^2 &= \left(A + \frac{B\sqrt{c}}{an} \ e^{anr^2/2}\right)^2 dt^2 - r^2(d\theta^2 + \sin^2\theta \ d\phi^2) \\
&\quad - \left[\frac{(1 + cr^2 e^{nar^2})(cr^2 + 1)}{(cr^2 + 1) + \beta ncr^2 \left(1 + cr^2 e^{nar^2}\right)}\right] dr^2.
\end{aligned} \tag{2.41}$$

where,

$$e^{\lambda(r)} = \frac{(1 + cr^2 e^{nar^2})(cr^2 + 1)}{(cr^2 + 1) + \beta ncr^2 \left(1 + cr^2 e^{nar^2}\right)}, \tag{2.42}$$

$$e^{\nu(r)} = \left(A + \frac{B\sqrt{c}}{an} \ e^{anr^2/2}\right)^2 = e^{\tilde{\nu}(r)}. \tag{2.43}$$

The variation of both gravitational functions are shown in Fig. 2.1.

Now the density, pressures (radial & transverse), and anisotropy for complete

2. Minimally deformed anisotropic model of class one space-time by gravitational decoupling

system are givn as,

$$8\pi\rho(r) = \frac{1}{r^2}\left[\frac{2anr^2+1}{cr^2e^{anr^2}+1} - \frac{2\left(anr^2+1\right)}{\left(cr^2e^{anr^2}+1\right)^2} - \frac{\beta cnr^2\left(cr^2+3\right)}{\left(cr^2+1\right)^2} + 1\right], \tag{2.44}$$

$$8\pi p_r(r) = \frac{c\left(cr^2+1\right)^{-1}\left(cr^2e^{anr^2}+1\right)^{-1}}{aAn\sqrt{cr^2e^{anr^2}} + Bcre^{anr^2}}\left[arAn\sqrt{ce^{anr^2}}\left\{e^{anr^2}\left(cr^2(\beta n-1)-1\right)\right.\right.$$
$$\left.+\beta n\right\} + Bre^{anr^2}\left\{cn\left[2ar^2(\beta n+1)+\beta\right] + c\,e^{anr^2}\right.$$
$$\left.\left[cr^2\left\{\beta n\left(2anr^2+1\right)-1\right\}-1\right] + 2an\right\}\right], \tag{2.45}$$

$$\Delta = \frac{cr^2\left(cr^2+1\right)^{-2}\left(cr^2e^{anr^2}+1\right)^{-2}}{aAn\sqrt{cr^2e^{anr^2}} + Bcre^{anr^2}}\left[Br\left\{f_2(r)+f_3(r)\right\}e^{anr^2} - aAnf_1(r)\right.$$
$$\left.\sqrt{cr^2e^{anr^2}}\right] \tag{2.46}$$

$$8\pi p_t(r) = 8\pi p_r + \Delta \tag{2.47}$$

where,

$$f_1(r) = ne^{anr^2}\left[a\left(cr^2+1\right)^2 + 2\beta c^2r^2\right] + ce^{2anr^2}\left[\beta c^2nr^4 - \left(cr^2+1\right)^2\right]$$
$$+\beta cn \tag{2.48}$$

$$f_2(r) = 2cne^{anr^2}\left[\beta cr^2\left(anr^2+1\right)\left\{c\left(anr^2-1\right)+an\right\} - a\left(cr^2+1\right)^2\right] \tag{2.49}$$

$$f_3(r) = c^2e^{2anr^2}\left[\beta cnr^4\left(anr^2+1\right)\left\{c\left(anr^2-1\right)+an\right\} + \left(cr^2+1\right)^2\right]$$
$$+n\left[a^2n(cr^2+1)\left\{cr^2(\beta n+1)+1\right\} + a\beta cn - \beta c^2\right] \tag{2.50}$$

The variations of density, pressure and anisotropy are shown in Figs. 2.2-2.4.

As we see that the central density is decreasing when n moves from 0.5 to 3.5 while the surface density increases for same n. This implies that the core will be more denser if n increases. However, it will have reverse situation for surface density. On the other hand, the pressure has totally opposite behavior than density. From Fig. 3, it can be observed that central pressure increases with increasing value of n. In this connection, we would like to mention that local anisotropies play an important role in the study of the compact objects. Since positive anisotropy leads the repulsive force which allows to more compact objects while negative anisotropy gives inward force that encourage the compact in collapsing direction. The Fig. 2.4 shows that the local anisotropy is increasing towards the boundary for each value of n.

2.3. New embedding class one solution by MGD

Figure 2.1: Variation of metric functions with radial coordinate r for 4U 1608-52 ($M = 1.74M_\odot$, $R = 9.528km$) by taking $a = 0.001\ km^{-2}$ and $\beta = 0.01$.
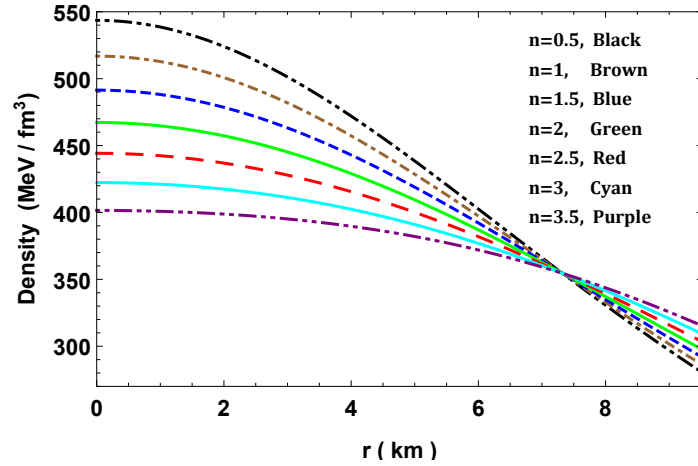
Figure 2.2: Variation of density with radial coordinate r for 4U 1608-52 ($M = 1.74M_\odot$, $R = 9.528km$) by taking $a = 0.001\ km^{-2}$ and $\beta = 0.01$.
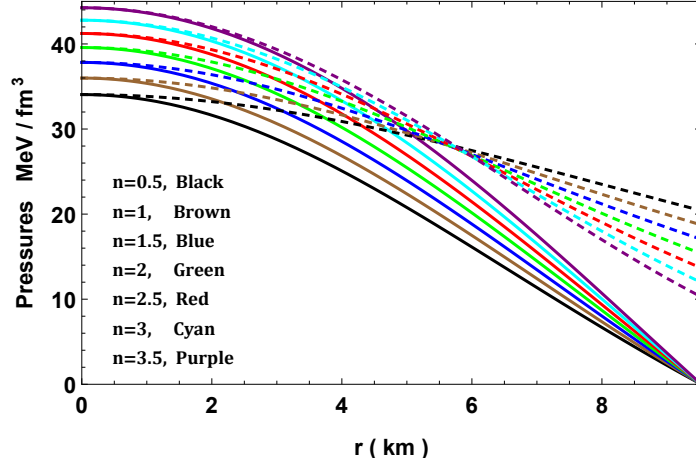
Figure 2.3: Variation of pressure with radial coordinate r for 4U 1608-52 ($M = 1.74M_\odot$, $R = 9.528km$) by taking $a = 0.001$ km^{-2} and $\beta = 0.01$.
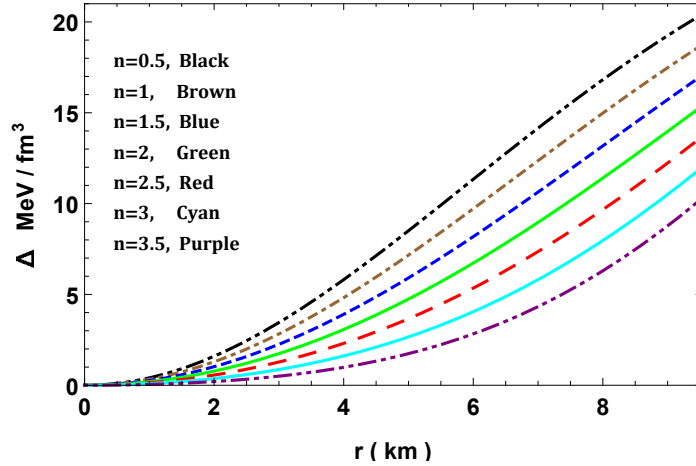
Figure 2.4: Variation of anisotropy with radial coordinate r for 4U 1608-52 ($M = 1.74M_\odot$, $R = 9.528km$) by taking $a = 0.001$ km^{-2} and $\beta = 0.01$.

2.3. New embedding class one solution by MGD

The mass, compactness parameter, equation of state parameter and red-shift can be evaluated from

$$m(r) = 4\pi \int r^2 \rho(r)\, dr = \frac{r}{2}\left[1 - \frac{1}{cr^2 e^{anr^2} + 1} + \beta n\left(\frac{1}{cr^2 + 1} - 1\right)\right] \quad (2.51)$$

$$u(r) = \frac{2m(r)}{r} \quad (2.52)$$

$$\omega_r = \frac{p_r}{\rho} \; ; \; \omega_t = \frac{p_t}{\rho} \quad (2.53)$$

$$z(r) = e^{-\nu/2} - 1. \quad (2.54)$$
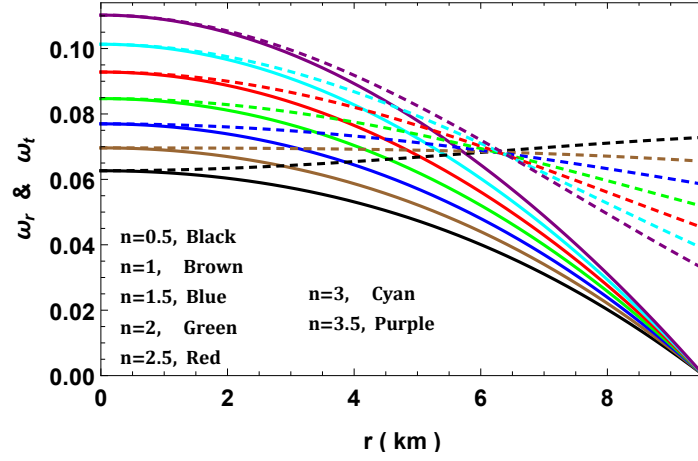
Figure 2.5: Variation of pressure to density ratio with radial coordinate r for 4U 1608-52 ($M = 1.74M_\odot$, $R = 9.528km$) by taking $a = 0.001\ km^{-2}$ and $\beta = 0.01$.
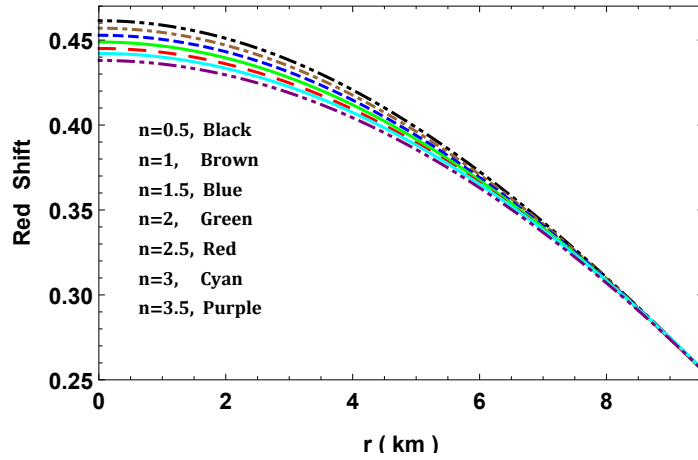
Figure 2.6: Variation of red-shift with radial coordinate r for 4U 1608-52 ($M = 1.74M_\odot$, $R = 9.528km$) by taking $a = 0.001\ km^{-2}$ and $\beta = 0.01$.

For a realistic equation of state, the equation state parameters must be less than unity. The variations of equation state parameter and red-shift are shown in Figs. 2.5 and 2.6.
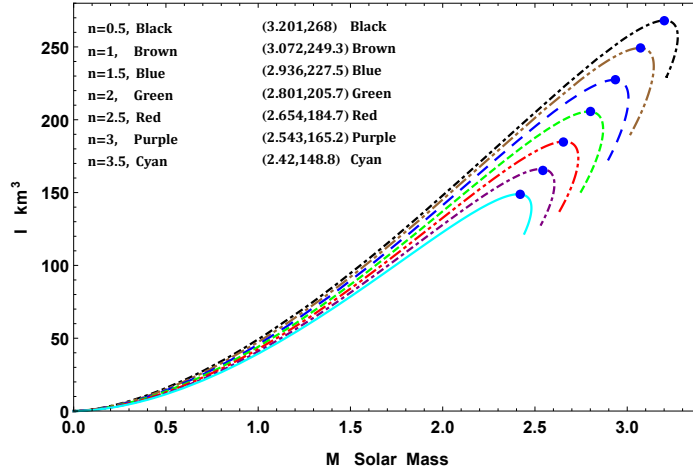
Figure 2.7: $M - I$ graphs for $a = 0.001\ km^{-2}$ and $\beta = 0.2$.
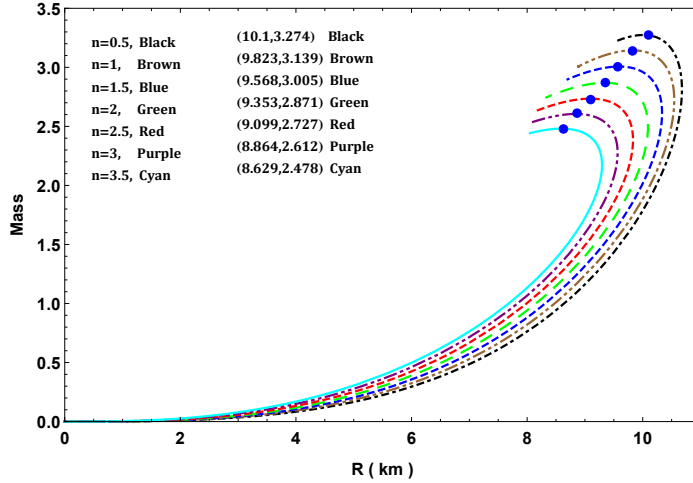
Figure 2.8: $M - R$ graphs for non-rotating case with $a = 0.001\ km^{-2}$ and $\beta = 0.2$.

2.4   Non-singularity of the solution

The physical cogency of the solution confirm that the central values of pressure

and density must be finite i.e.

$$\rho_c = \frac{3c(\beta n - 1)}{8\pi} > 0, \quad \forall \quad \beta n < 1 \quad \& \quad c < 0, \tag{2.55}$$

$$p_{rc} = p_{tc} = \frac{aAcn(\beta n - 1) + B\sqrt{c}\,[2an + c(\beta n - 1)]}{8\pi(aAn + B\sqrt{c})}. \tag{2.56}$$

Also, it needs to ensure that any physical fluid fulfills the Zeldovich's criterion i.e. $p_{rc}/\rho_c \leq 1$ which implies

$$\frac{p_{rc}}{\rho_c} = \frac{aAcn(\beta n - 1) + B\sqrt{c}\,[2an + c(\beta n - 1)]}{3c(\beta n - 1)(aAn + B\sqrt{c})} \leq 1. \tag{2.57}$$

Now a limitations on B/A arises due to (2.56) and (2.57) as

$$\frac{-2acn(\beta n - 1)}{3c^{3/2}(\beta n - 1) - \sqrt{c}\{2an + c(\beta n - 1)\}} \leq \frac{B}{A} < \frac{-acn(\beta n - 1)}{\sqrt{c}[2an + c(\beta n - 1)]}. \tag{2.58}$$

2.5 Boundary Conditions and determination of constants

The line element (2.11) which describes the interior of the star should join continuously with the exterior *Schwarzschild* metric, and can be written as

$$ds^2 = -\left(1 - \frac{2m}{r}\right)dt^2 + \left(1 - \frac{2m}{r}\right)^{-1}dr^2 + r^2\big(d\theta^2 + \sin^2\theta\,d\phi^2\big) \tag{2.59}$$

with the radial coordinate r must be greater than $2m$.

At the pressure free interface $(r = R)$, which needs the equality of corresponding potential functions e^ν and e^λ across the boundary $(r = R)$, to get the following equations (Israel [1966a])

$$1 - \frac{2M}{R} = e^{\nu_s} = e^{-\lambda_s}. \tag{2.60}$$

Whereas the extrinsic curvature or the 2nd fundamental form of stars $K_{\mu\nu} = \nabla_\mu r_\nu$, where the unit radial vector r_μ is normal to any surface of radius r which is also continuous at the interface $(r = R)$. This can be stated in terms of Einstein's tensorial

form as (Santos [1985])

$$[G_{\mu\nu}r^\nu]_\Sigma = \lim_{r \to R^+} (G_{\mu\nu}r^\nu) - \lim_{r \to R^-} (G_{\mu\nu}r^\nu) = 0. \tag{2.61}$$

By using the field equations and (2.61) we get

$$\left[8\pi T_{\mu\nu}r^\nu\right]_\Sigma = 0, \tag{2.62}$$

which implies

$$\left[8\pi\left(p_r - \beta\,\Theta_1^1\right)\right]_\Sigma = 0$$

$$\text{Or}\quad p_r(R) - \beta\,\Theta_1^1(r \to R^-) = 0. \tag{2.63}$$

On using the boundary conditions (2.60) and (2.63) we get

$$c = \frac{e^{-anR^2}}{2R^4[2M + R(\beta n - 1)]}\Big[R^3 e^{anR^2} - 2MR^2 e^{anR^2} - 2MR^2 - \beta nR^3 + R^2\Big\{$$

$$\Big[2M\left(e^{anR^2} + 1\right) - Re^{anR^2} + \beta nR\Big]^2 - 8Me^{anR^2}[2M + R(\beta n - 1)]\Big\}^{\frac{1}{2}}\Big] \tag{2.64}$$

$$A = \sqrt{1 - \frac{2M}{R}} - \frac{B\sqrt{c}\,e^{anR^2/2}}{an} \tag{2.65}$$

$$B = an\sqrt{1 - \frac{2M}{R}}\sqrt{cR^2 e^{anR^2}}\Big[e^{anR^2}\left\{cR^2(\beta n - 1) - 1\right\} + \beta n\Big]\Big[cR\,e^{anR^2}$$

$$\left\{e^{anR^2}\left[cR^2(\beta n - 1) - 1\right] + \beta n\right\}Re^{anR^2}\Big\{cn\left[2aR^2(\beta n + 1) + \beta\right] + ce^{anR^2}$$

$$\left[cR^2\left\{\beta n\left(2anR^2 + 1\right) - 1\right\} - 1\right] + 2an\Big\}\Big]^{-1}. \tag{2.66}$$

The observed values of compact stars are providing us the values of M and R, where a, n, β as free constraints.

2.6 Slow rotation approximation, moment of inertia and Kepler frequency

The moment of inertia for a uniformly rotating star with angular velocity $\bar{\omega}$ is assumed by Lattimer and Prakash [2000]

$$I = \frac{8\pi}{3}\int_0^R r^4(\rho + p_r)e^{(\lambda-\nu)/2}\,\frac{\bar{\omega}}{\Omega}\,dr \tag{2.67}$$

2.6. Slow rotation approximation, moment of inertia and Kepler frequency
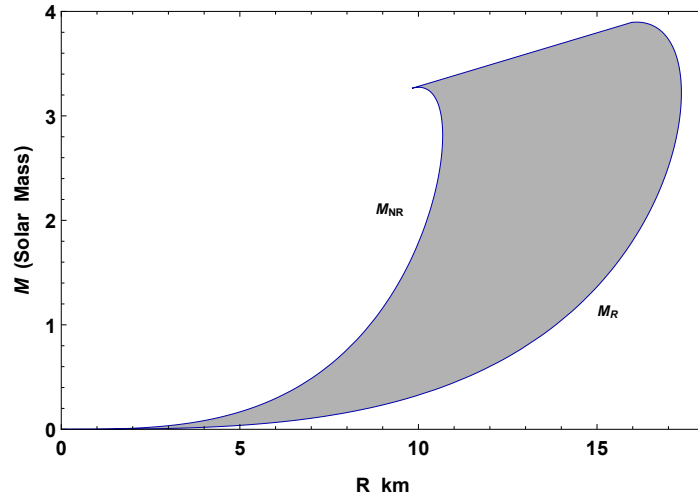
Figure 2.9: $M - R$ graphs for rotating (R) and non-rotating (NR) cases with $a = 0.001\ km^{-2}$ and $\beta = 0.2$.
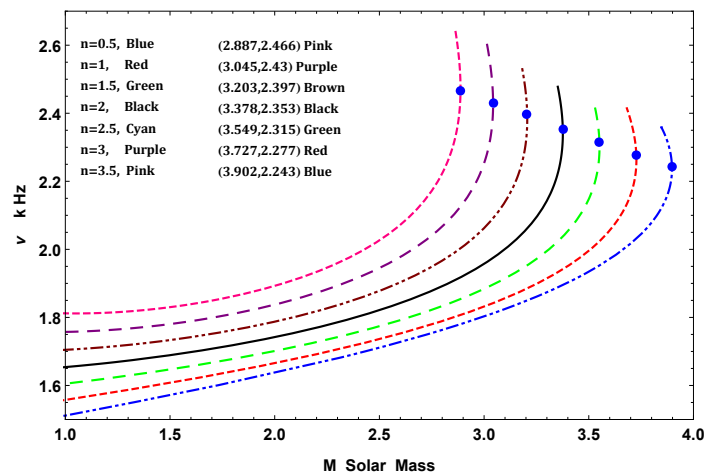
Figure 2.10: $\nu - M$ graphs for $a = 0.001\ km^{-2}$ and $\beta = 0.2$.

where, the Hartle's equation has been satisfied for the rotational drag $\bar{\omega}$ (Hartle [1978])

$$\frac{d}{dr}\left(r^4 j \frac{d\bar{\omega}}{dr}\right) = -4r^3\bar{\omega}\,\frac{dj}{dr}.\tag{2.68}$$

with $j = e^{-(\lambda+\nu)/2}$ at boundary value $j(R) = 1$. The moment of inertia solutions I up to the maximum mass M_{max} have been provided by Bejger and Haensel [2002] as

$$I = \frac{2}{5}\left(1+x\right)M_{NR}R_{NR}^2,\tag{2.69}$$

where $x = (M_{NR}/R_{NR})\cdot km/M_\odot$. The solution so obtained have been plotted mass vs I in Fig. 2.7 that demonstrated as n increases, the mass and moment of inertia are increasing till up to convinced value of mass and then decreases. From $M-R$ diagram and by comparing Figs. 2.7 and 2.8, we have noticed that the mass corresponding to I_{max} and M_{max} are not equal. Actually, the mass corresponding to I_{max} is lesser by $\sim 1.46\%$ from the M_{max}. This occurs to the EoSs due to hyperonization or phase transition to an unusual state without any strong high-density softening (Bejger et al. [2005]). Using this graph we can estimate the maximum moment of inertia for a particular compact star or by matching the observed I with the $I_{\max}$ we can determine the validity of a model.

A rotating compact star can hold higher M_{max} than non-rotating one. The mass relationship between non-rotating and rotating is given by (in the unit $G = C = 1$) can be written as (Ghosh [2007])

$$M_R = M_{NR} + \frac{1}{2}I\Omega_K^2.\tag{2.70}$$

Due to centrifugal force, the radius at the equator increases as some factor as compare to the static one. Cheng and Harko [2000] find out the approximate radius formulas for static and rotating stars as $R_R/R_{NR} \approx 1.626$. Assuming the compact star is rotating in Kepler frequency $\Omega_K = (GM_{NR}/R_{NR}^3)^{1/2}$ and on using the Cheng-Harko formula we have plotted the $M-R$ for rotating and non-rotating (Fig. 2.9). The corresponding frequency of rotating can be determined as (Haensel et al. [2007, 1995])

$$\nu \approx 1.22 \left(\frac{R_{NR}}{10km}\right)^{-3/2} \left(\frac{M_{NR}}{M_\odot}\right)^{1/2} \text{ kHz}.\tag{2.71}$$

The variation of frequency with mass is shown in Fig. 2.10.

2.7 Energy Conditions

The energy conditions null energy condition (NEC), dominant energy condition (DEC), weak energy condition(WEC) and strong energy condition (SEC) have to be confirmed at all points in the interior of a star. Therefore, if the following inequalities hold, then the energy conditions will be satisfied simultaneously:

$$\text{WEC} \quad : \quad T_{\mu\nu}t^\mu t^\nu \geq 0 \text{ or } \rho \geq 0, \ \rho + p_i \geq 0 \tag{2.72}$$

$$\text{NEC} \quad : \quad T_{\mu\nu}l^\mu l^\nu \geq 0 \text{ or } \rho + p_i \geq 0 \tag{2.73}$$

$$\text{DEC} \quad : \quad T_{\mu\nu}t^\mu t^\nu \geq 0 \text{ or } \rho \geq |p_i| \ \text{ where } \ T^{\mu\nu}t_\mu \in \text{nonspace-like vector} \tag{2.74}$$

$$\text{SEC} \quad : \quad T_{\mu\nu}t^\mu t^\nu - \frac{1}{2}T_\lambda^\lambda t^\sigma t_\sigma \geq 0 \text{ or } \rho + \sum_i p_i \geq 0. \tag{2.75}$$

where $i \equiv (radial \ r, transverse \ t)$, t^μ and l^μ are time-like vector and null vector respectively.

With the help of graphical illustrations, the energy conditions have been checked. In Fig. 2.11, the above inequalities have been plotted which confirms that all the energy conditions are fulfilled at the interior of stellar object.

2.8 Stability of the model and equilibrium

2.8.1 Equilibrium under various forces

The conservation of stress tensor $\nabla_\mu T_\nu^\mu = \nabla_\mu \tilde{T}_\nu^\mu + \beta\nabla_\mu \Theta_\nu^\mu = 0$ leads to Tolman-Oppenheimer-Volkoff equations due to fluid and extra sources Ovalle [2017] as

$$-\frac{\tilde{\nu}}{2}(\tilde{\rho} + \tilde{p}_r) - \frac{d\tilde{p}_r}{dr} + \frac{2}{r}(\tilde{p}_t - \tilde{p}_r) = 0 \tag{2.76}$$

$$-\frac{\tilde{\nu}'}{2}\left[\Theta_t^t - \Theta_r^r\right] + \frac{d\Theta_r^r}{dr} + \frac{2}{r}\left[\Theta_r^r - \Theta_\phi^\phi\right] = 0. \tag{2.77}$$

Now the overall TOV-equation becomes

$$-\frac{\tilde{\nu}}{2}(\tilde{\rho} + \tilde{p}_r) - \frac{d\tilde{p}_r}{dr} + \frac{2}{r}(\tilde{p}_t - \tilde{p}_r) - \beta\left[\frac{\tilde{\nu}'}{2}\left(\Theta_t^t - \Theta_r^r\right) - \frac{d\Theta_r^r}{dr}\right.$$
$$\left. - \frac{2}{r}\left(\Theta_r^r - \Theta_\phi^\phi\right)\right] = 0. \tag{2.78}$$

The components for different effective forces due to MGD gravitational decoupling namely gravitational force (F_g), hydrostatic force (F_h) and anisotropic force (F_a) can be defined as,

$$F_g = -\frac{\nu'}{2}\left[\tilde{\rho} + \tilde{p} + \beta(\Theta_t^t - \Theta_r^r)\right], \tag{2.79}$$

$$F_h = -\left(\frac{d\tilde{p}_r}{dr} + \beta\frac{d\Theta_r^r}{dr}\right), \tag{2.80}$$

$$F_a = \frac{2}{r}\left[(\tilde{p}_t - \tilde{p}_r) + \beta\left(\Theta_t^t - \Theta_r^r\right)\right]. \tag{2.81}$$

The profile of three different forces are plotted in Fig. 2.12. From this figure we can observe that the system is in equilibrium position. Moreover, the gravitational force F_g is balanced the system by joint action of anisotropic force F_a and hydrostatic force F_h. However, the parameter n plays an important effects on different forces as gravitational force and anisotropic force decreases in magnitude when $n \rightarrow 0.5$ to 3.5 while hydrostatic force F_h is increasing when n moves from 0.5 to 3.5.
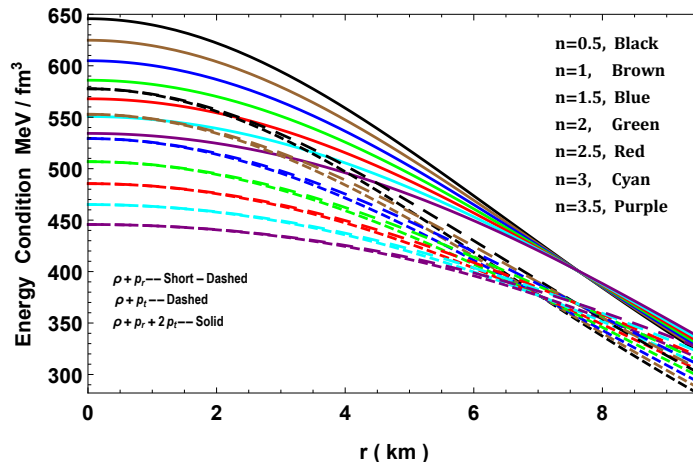
Figure 2.11: Variation of energy conditions (EC) with radial coordinate r for 4U 1608-52 ($M = 1.74M_\odot$, $R = 9.528km$) by taking $a = 0.001\ km^{-2}$ and $\beta = 0.01$.

2.8.2 Causality and stability condition

With the help of Causality condition, the stability situation have been analyzed. The causality condition will occurs when the sound velocities (radial (v_r^2) and transverse (v_t^2) are greater than zero and less than 1. The radial velocity and transverse velocity
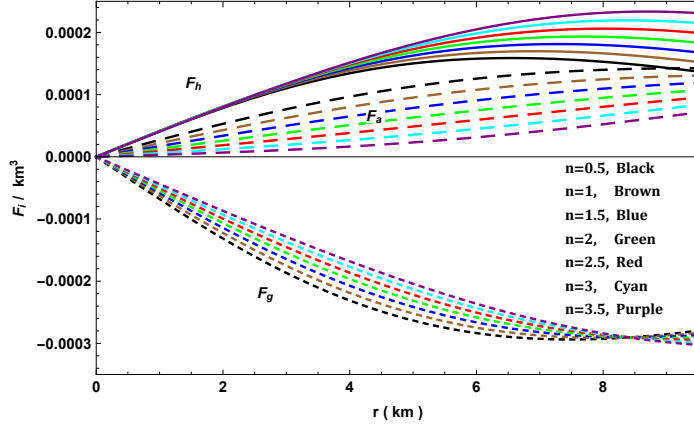
Figure 2.12: Variation of forces in TOV-equation with radial coordinate r for 4U 1608-52 ($M = 1.74 M_\odot$, $R = 9.528 km$) by taking $a = 0.001\ km^{-2}$ and $\beta = 0.01$.

of sound can be achieved as

$$v_r^2 = \frac{dp_r}{d\rho} \quad , \quad v_t^2 = \frac{dp_r}{d\rho}. \tag{2.82}$$

Fig. 2.13, shows the profile of radial and transverse velocities of sound, which indicates that our model fulfills the causality condition. While (Fig. 2.14) shows the stability condition that proposed by Abreu et al. [2007], Herrera [1992]. i.e. $-1 \leq v_t^2 - v_r^2 \leq 0$.

2.8.3   Adiabatic index and stability condition

The adiabatic index syndicates the basic features of the EoS on the randomness formulae and consequently contains the link between the relativistic structure of the anisotropic spheres and the EoS of the interior fluid. The stability is linked to the adiabatic index Γ, which can be written as (Chan et al. [1993]),

$$\Gamma_r = \frac{\rho + p_r}{p_r}\ \frac{dp_r}{d\rho}. \tag{2.83}$$

The stability of a Newtonian sphere condition is $\Gamma_r > 4/3$ while, for $\Gamma = 4/3$ is the condition for a neutral equilibrium (Bondi [1964]). Due to the regenerative effect of pressure, this condition changes for a relativistic isotropic sphere, which is unstable. For the anisotropic fluid sphere, if the stability depends on the type of anisotropy then the situation becomes more complicated (Herrera [1992], Chan et al. [1993]).

2. Minimally deformed anisotropic model of class one space-time by gravitational decoupling

A recent work by Moustakidis Moustakidis [2017] reveals that the critical value of adiabatic index strongly depends on the M/R. The critical value was found to be

$$\Gamma_{crit} = \frac{4}{3} + \frac{19}{42}\frac{2M}{R}. \tag{2.84}$$

Fig. 2.15, confirms that the model under consideration is stable, due to the adiabatic index is greater than $4/3$.
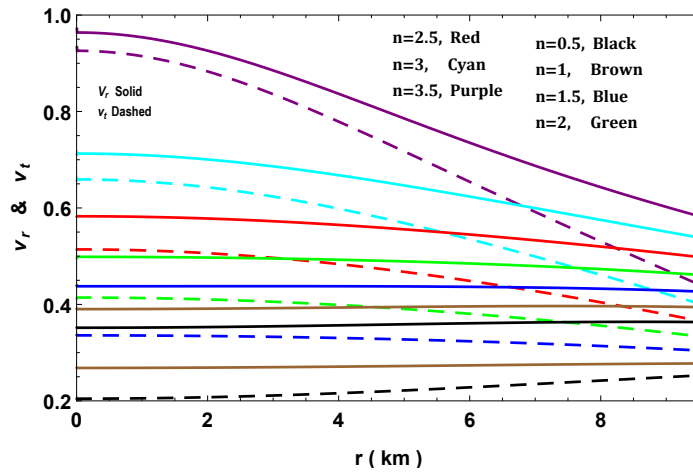
Figure 2.13: Variation of sound speed with radial coordinate r for 4U 1608-52 ($M = 1.74M_\odot$, $R = 9.528km$) by taking $a = 0.001\ km^{-2}$ and $\beta = 0.01$.
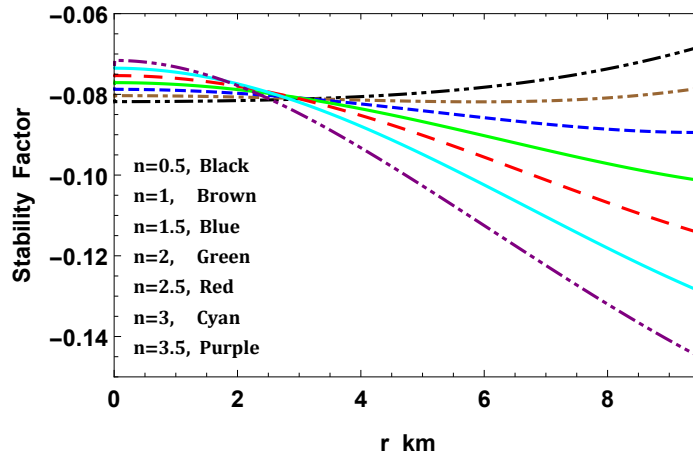
Figure 2.14: Variation of stability factor with radial coordinate r for 4U 1608-52 ($M = 1.74M_\odot$, $R = 9.528km$) by taking $a = 0.001\ km^{-2}$ and $\beta = 0.01$.

Figure 2.15: Variation of adiabatic index with radial coordinate r for 4U 1608-52 ($M = 1.74 M_\odot$, $R = 9.528 km$) by taking $a = 0.001\ km^{-2}$ and $\beta = 0.01$.

2.9 Elastic property of compact stars

Assuming neutron stars exhibits isotropic bcc polycrystal structure one can defined the elastic properties via equation of deformation energy as (Haensel et al. [2007])

$$\mathcal{E} = \frac{1}{2} K_e (\nabla \cdot \mathbf{u})^2 + \mu \left(u_{ik} - \frac{1}{3} \delta_{ik}\ \nabla \cdot \mathbf{u} \right)^2 \tag{2.85}$$

where K_e and μ represents compression and shear modulus respectively. The stress tensor is given by

$$\sigma_{ik} = \frac{\partial \mathcal{E}}{\partial u_{ik}} = K_e \delta_{ik} \nabla \cdot \mathbf{u} + 2\mu \left(u_{ik} - \frac{1}{3} \delta_{ik}\ \nabla \cdot \mathbf{u} \right) \tag{2.86}$$

In this work we will focus on compression modulus K_e which can be determine as $K_e = n_b (\partial p_r / \partial n_b) = \Gamma_r p_r$ (Haensel et al. [2007]). The variation of compression modulus w.r.t. radius and mass are shown in Figs. 2.16 and 2.17 respectively.

2.9.1 Harrison-Zeldovich-Novikov static stability criterion

Harrison et al. [1965] and Zeldovich and Novikov [1971] have revealed that the adiabatic index are the same of pulsating star and in slowly deformed matter, which leads to be stable if the mass of the star is increasing with central density i.e. $\partial m / \partial \rho_c > 0$ and unstable if $\partial m / \partial \rho_c < 0$.

Therefore, the mass can be furnished as a function of central density and can be
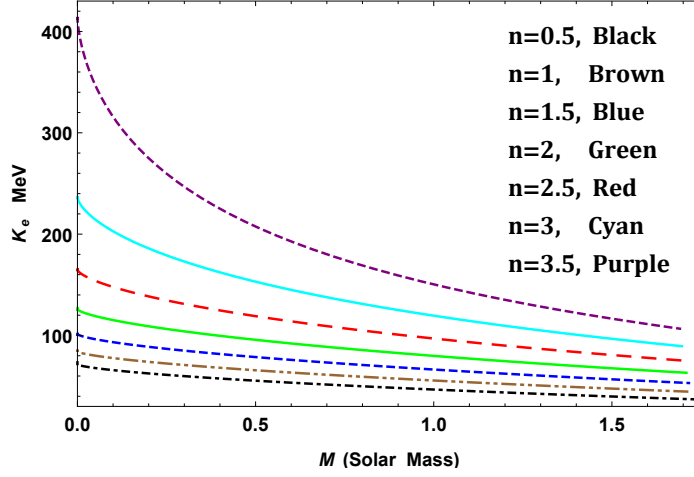
Figure 2.16: $K_e - M$ graph r for 4U 1608-52 ($M = 1.74 M_\odot$, $R = 9.528 km$) by taking $a = 0.001 \ km^{-2}$ and $\beta = 0.01$.
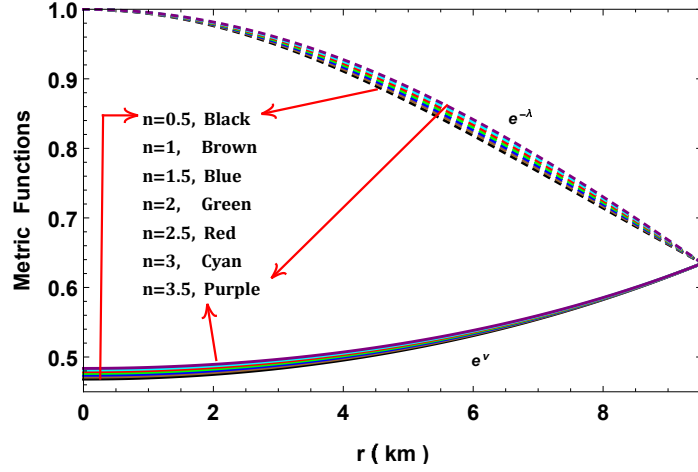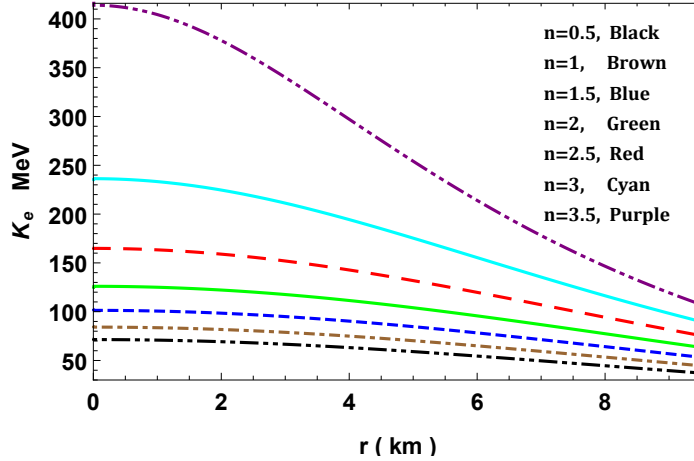

Figure 2.17: Variation of K_e with radial coordinate r for 4U 1608-52 ($M = 1.74 M_\odot$, $R = 9.528 km$) by taking $a = 0.001 \ km^{-2}$ and $\beta = 0.01$.

Figure 2.18: Variation of total mass with central density for $R = 9.528\ km$, $a = 0.001\ km^{-2}$ and $\beta = 0.01$.

defined as

$$m(\rho_c) = \frac{R}{2}\left[\frac{3 - 3\beta n}{3\beta n - 8\pi\rho_c R^2 e^{anR^2} - 3} - \beta n + \frac{\beta n}{\frac{8\pi\rho_c R^2}{3 - 3\beta n} + 1} + 1\right] \tag{2.87}$$

$$\frac{\partial m(\rho_c)}{\partial \rho_c} = \frac{4\pi R^3}{3 - 3\beta n}\left[\frac{9(\beta n - 1)^2 e^{anR^2}}{(8\pi\rho R^2 e^{anR^2} - 3\beta n + 3)^2} - \frac{\beta n}{\left(\frac{8\pi\rho R^2}{3 - 3\beta n} + 1\right)^2}\right] \tag{2.88}$$

Its can be verified using the $M - \rho_c$ graph in Fig. 2.18.

2.9.2 Effect of coupling parameter β on the models

To complete the analysis in detail, we need to observe the effects of β on the nature of the solution. To proceed, we are needed to assume a particular value of n and then see the behavior by changing β. For $n = 3$ we have analyzed thoroughly and found that the physically acceptable range of β is limited with a range between 0 and 0.7. As β increases, the central density and pressure decrease while the anisotropy changes very little. However, the central values of the adiabatic index and sound speed increase with an increase of β. Therefore, the corresponding equation of state gains its stiffness along with β i.e. as the MGD+GR coupling gets stronger we can obtain a very stiff equation of states, which may explain the current observations of very massive neutron stars (i.e. $M > 2M_\odot$). Although, the range of β for a physically acceptable solution depends on the assumed values of n.
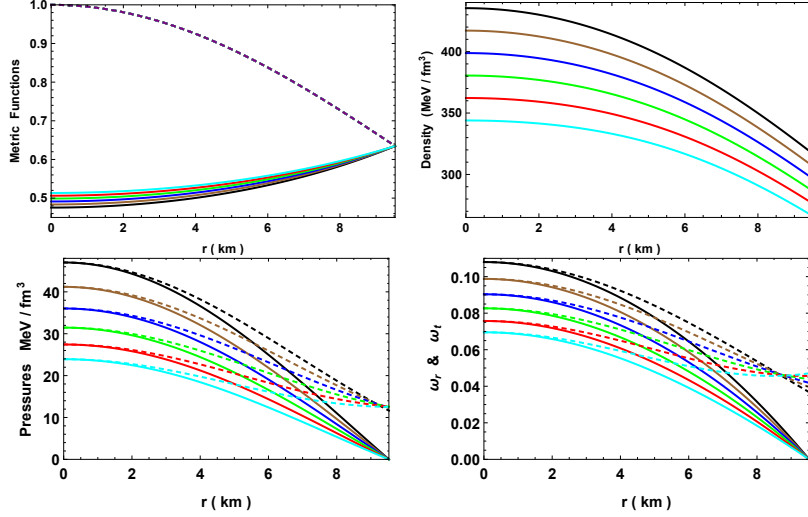
Figure 2.19: Variation of mertric fuctions ($e^\nu-$solid, $e^{-\lambda}-$dashed), density, pressrues (p_r-solid, p_t-dashed) and equation of state parameters (ω_r-solid, ω_t-dashed) with radial coordinate r for 4U 1608-52 ($M = 1.74 M_\odot$, $R = 9.528 km$) by taking $a = 0.001\ km^{-2}$ and $n = 3$. We are using the same color notation in all the graphs from Fig. 2.19 to Fig. 2.21 as $\beta = 0$ (black), 0.014 (brown), 0.028 (blue), 0.042 (green), 0.056 (red) and 0.07 (cyan).
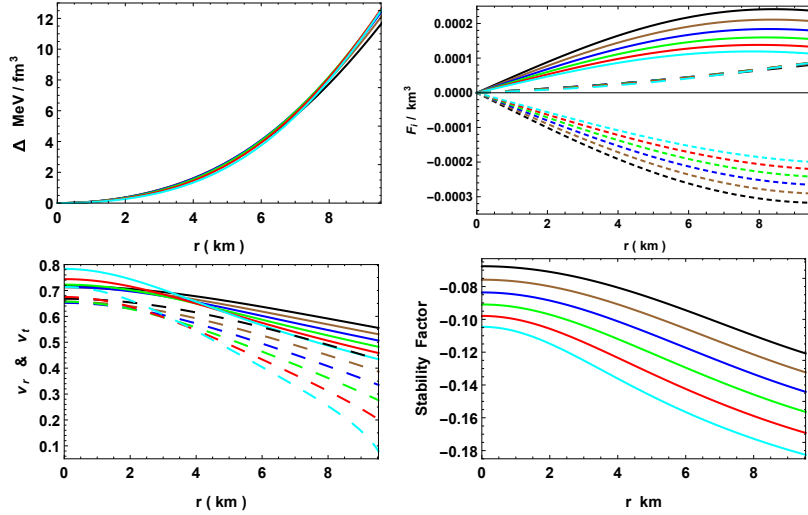
Figure 2.20: Variation of anisotropy, TOV-equation (F_a-dashed, F_g-small dashed, F_h-solid), sound speed (v_r-solid, v_t-dashed) and stability factor with radial coordinate r for 4U 1608-52 ($M = 1.74 M_\odot$, $R = 9.528 km$) by taking $a = 0.001\ km^{-2}$ and $n = 3$. We are using the same color notation in all the graphs from Fig. 2.19 to Fig. 2.21 as $\beta = 0$ (black), 0.014 (brown), 0.028 (blue), 0.042 (green), 0.056 (red) and 0.07 (cyan).
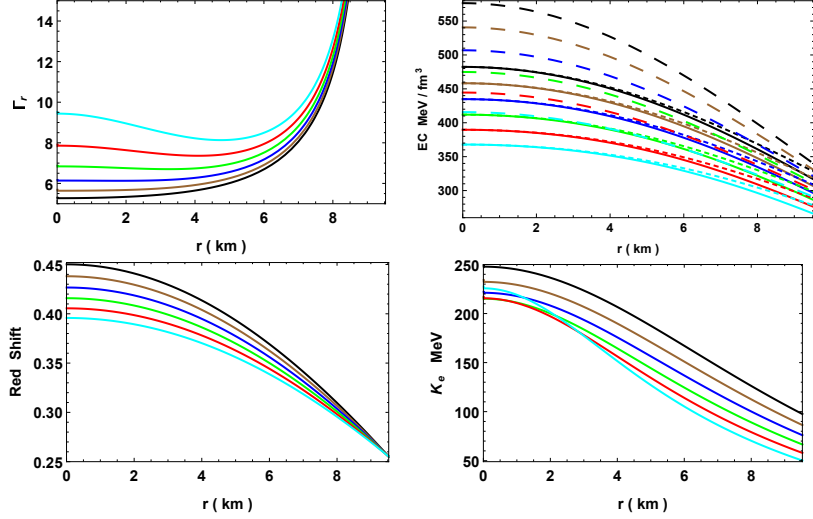
Figure 2.21: Variation of Γ_r, energy conditon (EC) ($p_r + \rho$−solid, $p_t + \rho$−small dashed, $p_r + 2p_t + \rho$−dashed), redshift and compression modulus with radial coordinate r for 4U 1608-52 ($M = 1.74M_\odot$, $R = 9.528km$) by taking $a = 0.001\ km^{-2}$ and $n = 3$. We are using the same color notation in all the graphs from Fig. 2.19 to Fig. 2.21 as $\beta = 0$ (black), 0.014 (brown), 0.028 (blue), 0.042 (green), 0.056 (red) and 0.07 (cyan).

Table 2.1: Few interior parameters for 4U 1608-52 ($M = 1.74M_\odot$, $R = 9.528km$) by taking $a = 0.001\ km^{-2}$ and $\beta = 0.01$.

n	$\rho_c \times 10^{14}$ (g/cc)	$\rho_s \times 10^{14}$ (g/cc)	$p_c \times 10^{34}$ (dyne/cm^2)	Γ_c	M_{max} ($M_\odot$)	R (km)	ν_{max} kHz	$I \times 10^{45}$ (g-cm^2)
0.5	9.69	4.06	5.44	2.07	3.27	10.1	2.47	3.45
1.0	9.22	5.09	5.76	2.35	3.14	9.83	2.43	3.21
1.5	8.76	5.19	6.06	2.69	3.01	9.57	2.4	2.93
2.0	8.33	5.30	6.34	3.14	2.87	9.35	2.35	2.65
2.5	7.92	5.39	6.60	3.99	2.73	9.1	2.32	2.38
3.0	7.54	5.50	6.86	5.52	2.61	8.86	2.28	2.12
3.5	7.15	5.61	7.09	9.49	2.48	8.63	2.24	1.91

2.10   Discussion and conclusion

In this chapter, we have successfully incorporated the concepts of embedding class one in the gravitational decoupling formalism for the first time. This method makes a simple way of exploring new solutions in MGD, which leads to the new window of re-investigating all the existed embedding class one solutions in MGD formalism and their responses due to the additional source. The chapter presents a new embedding class one solution which is deformed minimally by the gravitation decoupling technique. The MGD methodology demonstrated its adaptability in this area, making it an important and acceptable solution for EFE. It is reproduced through the graphical analysis, where the variation of the metric functions with the radial coordinate r, (see Fig. 2.1) for $M = 1.74 M_\odot$ and $R = 9.528$ km considering $a = 0.001 \ km^{-2}$ and $\beta = 0.01$, and the deformation function $g(r)$ as in Eq. (2.40). The deformation function will be vanished at $r = 0$, while $g(r) = n$ as r approaches to infinity. Thus, the metric potential functions are well-behaved at the center and finite and regular throughout of stars. Therefore they are proper to produce new models for anisotropic compact stars.

Figs. 2.2 and 2.3, shows the behavior of density, pressures(radial and transverse) with respect to $M = 1.74 M_\odot$ and $R = 9.528 \ km$ considering $a = 0.001 \ km^{-2}$ and $\beta = 0.01$, which detected that the model is non- singular, furthermore the model is positively finite, and monotone decreasing functions throughout the interior of the star, and achieve their maximum value at the center. Also, radial pressure vanishes at the boundary. The anisotropy factor, which is given in (Fig. 2.4) with radial coordinate r. However, $\Delta(0) = 0$ at the center and it is positively increasing away from the center. From Fig. 2.5, it is clear that the EoS is characterized by the parameters ω_r and ω_t relating to radial coordinate r, in which, the EoS factors of the model are less than unity i.e. within the region and demonstrated as a well-behaved model. Fig. 2.6 shows the variations of surface red-shift with radial coordinate r. Thus, the surface of redshift $z(r) \to 0$ as $r \to 0$ and subsequently monotonically increasing onto the boundary. For $n = 2$ yields larger moment of inertia M_{max} and K_e (Figs. 2.7, 2.16). Also, we have noticed that from Figs 2.7 and 2.8 the $M - I$ graph is more sensitive and/or sharp in the stiffness of equation of states than $M - R$ graph. By using the concepts of Ghosh and Cheng-Harko i.e. Eq. (2.70) and $R_R/R_{NR} \equiv 1.626$ one can compare the $M - R$ graphs of rotating and non-rotating limits in one frame (Fig. 2.9), while the variation of frequency with mass for different

2.10. Discussion and conclusion

values of n is shown in Fig. 2.10. The EC with radial coordinate r for 4U 1608-52 ($M = 1.74 M_\odot, R = 9.528 \; km$) by taking $a = 0.001 \; km^2$ and $\beta = 0.01$ are shown in Fig. 2.11, which confirms that all EC are fulfilled at the interior of the stellar object. While Fig. 2.12, shows the profile of three different forces to observe that the system is equilibrium i.e variation of forces in TOV-equation with radial coordinate for 4U 1608-52 ($M = 1.74 M_\odot, R = 9.528 \; km$) by taking $a = 0.001 \; km^{-2}$ and $\beta = 0.01$. In the Table 2.1, we have presented the values of physical parameters for different values of n. The profile of radial and transverse velocities of sound has been motivated in Fig. 2.13, which indicates that our model fulfills the causality condition. While (Fig. 2.14) shows the stability condition proposed by Abreu et al. [2007].

The satisfactions of static stability criterion, modified TOV-equation and Herrera's cracking method also ensures that the solution is static, equilibrium and stable. Also, we noticed that the system is stable due to the adiabatic index Γ_r is greater than 4/3 as shown in (Fig. 2.15), and is also increasing monotonically outward. The $K_e - M$ graphs (Fig. 2.16) signifies that as the mass of compact star increases, the compression modulus decreases while the K_e with radial coordinate r graph implies an increasing trend of K_e as r approaches the center i.e .the parameter n increases the stiffness of the corresponding equation of states increases. While in Fig. 2.17 a variation of K_e with radial coordinate r for 4U 1608-52 ($M = 1.74 M_\odot, R = 9.528 \; km$) by taking $a = 0.001 \; km^{-2}$ and $\beta = 0.01$ are motivated for different n. Also, the static stability criterion can be confirmed by the Figs. 2.18.

The former tendency can be explained as the mass increases the central density also increases which may leads to generation of many interesting particles that unstiffen the equation of state and the compression modulus. The later one is due to the central density is highly dense as compare to the surface that leads to more compression modulus at the core than its surface. As the maximum mass M_{max} increases when n increases, the spinning rate ν_{max} also increases. We have also compared the nature and behavior of the solution by assuming a particular value of n with different values of β. For this case, we have found that the central values of density and pressure decreases with increase in β (Fig. 2.19). However, other physical behaviors of solution for different β are given in Figs. 2.20 and 2.21. On the other hand, the stiffness increases with increase in β as the adiabatic index increases and the speed of sound approaches the speed of light. Although, the anisotropy changes in a very small amount when changing the coupling constant β. The acceptable range of β depends upon the chosen value of n. For $n = 3$ the possible range lies in $0 \leq \beta \leq 0.7$.

If $\beta > 0.7$, the trend of the density start increase slightly and decreasing near the surface, and the solution start violating causality condition.

Summing up, we can conclude that our models are physically acceptable to describe minimally deformed class one space-time by gravitational decoupling based on the results so obtained.

Chapter 3

Compact stars with exotic matter [1]

3.1 Introduction

The advances in astrophysical observations has lead to great interest in the study of composition of the astrophysical compact object. Moreover these objects contains compressed ultra-dense nuclear matter in their interiors which make them superb astrophysical laboratories for a wide range of intriguing physical studies. Traditionally the term compact objects or compact stars refers collectively to white dwarfs, neutron stars, and black holes. Compact stars are also called the stellar remnants as they are often the endpoints of catastrophic astrophysical events such as supernova explosions and binary stellar collisions. The state and type of a stellar remnant depends primarily on the composition and properties of the dense matter of the star. However, due to lack of knowledge of the extreme condition and its complex composition it is a difficult task to determine the exact equation of state(EoS) to represent compact stars. Various astrophysical observations measure masses and radii of compact stars (Pons et al. [2002], Drake et al. [2002], Walter and Lattimer [2002], Cottam et al. [2002], Miller [2002]), which in turn, constrain the EoS of dense matter in compact stars. For example the observation of 2-solar mass neutron stars (Demorest et al. [2010], Antoniadis et al. [2013]) suggests that the EoS for compact stars needs to be sufficiently stiffer than the normal nuclear matter to accommodate the large mass. This enables one to think of a stable mass configurations with exotic matter in their interiors. In case of low mass compact stars too, the core matter density is much larger

---

than the normal matter. Due to extreme density, nuclear matter may consist not only of nucleons and leptons but also several exotic components in their different forms and phases such as Bose-Einstein condensates of strange mesons (Kaplan and Nelson [1986], Nelson and Kaplan [1987], Schaffner-Bielich et al. [2002], Glendenning and Schaffner-Bielich [1998], Banik and Bandyopadhyay [2003]), hyperons, and baryon resonances (Glendenning [1985]), as well as strange quark matter (Prakash et al. [1997], Farhi and Jaffe [1984], Schertler et al. [2000]).

Constructing the EoS of matter above the nuclear saturation density, relevant for the description of compact stars, is a vast arena for research. For a proposed EoS, the study of physical features of relativistic spheres like compact objects in general relativity is done by finding the exact analytic solutions for static Einstein field equations and imposing conditions for physical acceptability. However, it is a daunting task to obtain explicit analytical solutions of Einstein's field equation on account of their complicated and non-linear nature. Karl Schwarzschild obtained the first exact solution of Einstein's field equations (Schwarzschild [1916b]). The number of valid, exact solutions has been growing since then and are extensively used in the studies of neutron stars and black hole formation (Ray et al. [2003], de Felice et al. [1999]). Exact solutions for modelling more realistic relativistic fluids include Buchdahl [1967] and Tolman VII (Tolman [1939], Raghoonundun and Hobill [2015]) solutions. In pirticular, Tolman VII solution is stable for a large range of compactness (ratio of mass over the radius) (Negi and Durgapal [1999, 2001]) and is used to study various problems related to very compact object (Neary et al. [2001]).For better understanding of the compact objects these analytical solutions with various EoS are considered in the literature. In particular the linear EoS is considered to model charged or neutral anisotropic relativistic fluid with strange quark matter (Mak et al. [2002], Sharma and Maharaj [2007], Esculpi and Aloma [2010], Komathiraj and Maharaj [2007], Mafa Takisa and Maharaj [2013], Takisa and Maharaj [2013], Rahaman et al. [2012b], Kalam et al. [2013], Maharaj et al. [2014]).

Usually EoS of dense matter including exotic phases are constructed using relativistic field theoretical models and chiral models. It was noted that the appearance of exotic forms of matter in the high density regime resulted in kinks in the EoS (Dai et al. [2010]), which resulted discontinuity in the speed of sound. This has a great implication on determining the stability of the star. Using fundamental particle physics, quark matter at high density is studied which leads to the MIT-bag model for strange stars (Chodos et al. [1974]). This model added a correction term to the usual

classical barotropic EoS called the Bag constant and assumes that the free quarks in stellar configuration is confined in a bag characterized by a vacuum energy density equal to the bag constant. As it is well established from cosmological observations that around 70% of the energy budget of universe is invisible dark energy, there is a growing interest to understand whether a stable configuration of compact can be made up of dark energy. For this various dark energy EoS has been employed to model compact objects ranging from quark stars through to neutron stars (Rahaman et al. [2012a]).

The phenomenon of late time cosmic acceleration (Perlmutter et al. [1999], Riess et al. [1998a]) can be understood by incorporating dark energy as an exotic relativistic fluid with large negative pressure fills the whole universe. There is also an alternative view according to which current cosmic acceleration is an artifact of modification of gravity at large scale rather than the consequence of dark energy. Tons of theoretical approaches have been employed to explain the evolution of universe in the light of cosmological observations. More recently the theory of ever exiting or emergent universe (Ellis et al. [2003]) was formulated under which it may be possible to build models which avoid the quantum regime for space-time, nevertheless share the novel features of the standard big-bang model. This scenario can be treated as alternative inflationary model within the standard big bang framework which incorporates an asymptotically Einstein static universe in the past and evolves to an accelerating universe subsequently. The emergent universe scenario and has been studied recently in different theories of modified gravity (Chen et al. [2009], Parisi et al. [2012], Zhang et al. [2013]), Brane world models (Banerjee et al. [2007]), Brans-Dicke (Paul and Ghose [2010]). In the framework of $f(\mathcal{R})$ gravity, Mukherjee et al. [2005] pointed out that the Starobinsky model, the original as well as the modified version, permits solutions portraying an emergent universe. Subsequently, a general framework for such a scenario in general relativity was proposed Mukherjee et al. [2006] with a different constituents of matter that are prescribed by an non linear EoS : $p = A\rho - B\rho^{1/n}$, where n, A and B are constants. For $B > 0$ and $n = 2$ the possible primordial compositions of universe has been suggested that are permitted by the EoS. It admits existence of exotic matter such as cosmic strings, domain wall, quark matter and dark energy in addition to radiation and dust.

The purpose of the chapter is to model the stellar Compact star, with aforesaid EoS and determine the physical stability by studying its exact solutions. The chapter is organized as follows. In Sec 3.2 we consider a spherical symmetric metric and present

the Einstein's equations for anisotropic fluid distributions. In Sec. 3.3 we employ the Tolman VII equation with above EoS and obtain the expressions for density and pressures. Next, in Sec 3.4 we investigate non-Singular nature of the solutions. In Sec. 3.5, from the Boundary conditions we determine the constant parameters of the model. In Secs. 3.6 and 3.7 we discuss the energy conditions and stability of the model. Finally, Sec. 3.8 is devoted to concluding remarks of the study.

3.2 Interior space-time and field equations

The interior space-time line element for an uncharged, static and spherically symmetric fluid is given by:

$$ds^2 = e^{\nu(r)}dt^2 - e^{\lambda(r)}dr^2 - r^2\left(d\theta^2 + \sin^2\theta\ d\phi^2\right) \tag{3.1}$$

where ν and λ are functions of the radial coordinate 'r' only.

The interior of a star is often modelled as a perfect fluid, which requires the pressure to be isotropic. However, theoretical studies indicate that, at extremely high densities, deviations from local isotropy may play an important role (Dev and Gleiser [2002]). It was argued (Ruderman [1972]) that at high density regimes ($\rho > 10^{15}\ g/cm^3$) the nuclear matter interacts relativistically as a result of which nuclear matter may have anisotropic features. The numerical calculations of Barreto and Rojas [1992] suggests that the exotic phase transitions that occurs during the process of gravitational collapse (Collins and Perry [1975], Itoh [1970]) such as pion condensed state (Hartle et al. [1975]), anisotropic stress tensor associated type II superconductor (Jones [1975], Easson and Pethick [1977]), solid core (Ruderman [1972]), type P superfluid (Ruffini and Bonazzola [1969]) etc. may also induce anisotropy. Therefore, assuming an anisotropic fluid distribution the Einstein's field equations can be written as

$$R^\mu_\nu - \frac{1}{2}g^\mu_\nu \mathcal{R} = -8\pi\left[(p_t + \rho c^2)v^\mu v_\nu - p_t g^\mu_\nu + (p_r - p_t)\chi_\nu\chi^\mu\right] \tag{3.2}$$

where the symbols have their usual meanings.

3.2. Interior space-time and field equations

For the space-time (3.1), the field equations reduces to

$$\frac{1 - e^{-\lambda}}{r^2} + \frac{e^{-\lambda}\lambda'}{r} = 8\pi\rho \tag{3.3}$$

$$\frac{e^{-\lambda} - 1}{r^2} + \frac{e^{-\lambda}\nu'}{r} = 8\pi p_r \tag{3.4}$$

$$e^{-\lambda}\left(\frac{\nu''}{2} + \frac{\nu'^2}{4} - \frac{\nu'\lambda'}{4} + \frac{\nu' - \lambda'}{2r}\right) = 8\pi p_t \tag{3.5}$$

where $(')$ denotes derivative with respect to radial coordinate r. We define that the measure of anisotropy: $\Delta = p_t - p_r$.

To study the static spherically symmetric configurations with anisotropic matter distribution we adopt the following variable transformations:

$$x = r^2, \qquad Z(x) = e^{-\lambda(r)} \quad \text{and} \quad y^2(x) = e^{\nu(r)}, \tag{3.6}$$

the field equations (3.3)-(3.5)then takes the form

$$8\pi\rho = \frac{1 - Z}{x} - 2\dot{Z} \tag{3.7}$$

$$8\pi p_r = 4Z\frac{\dot{y}}{y} + \frac{Z - 1}{x} \tag{3.8}$$

$$8\pi\Delta = 4xZ\frac{\ddot{y}}{y} + \dot{Z}\left(1 + 2x\frac{\dot{y}}{y}\right) + \frac{1 - Z}{x} \tag{3.9}$$

$$p_t = p_r + \Delta \tag{3.10}$$

where $\dot{Z} = dZ/dx$ and $\ddot{Z} = d^2Z/dx^2$.

To proceed further, we assume $Z(x)$ as Tolman VII and a nonlinear equation of state as

$$Z(x) = 1 - ax + bx^2 \quad \text{and} \quad p_r = A\rho - B\rho^{1/n}. \tag{3.11}$$

Here a, b, A, B and n are arbitrary constants.

These constants are not restricted to specific values. For $A = 0$, $\gamma = 1/n$, $B = -K$ gets $p = K\rho^\gamma$ (polytropic EoS); $A = 1/3$, $B = 4\mathcal{B}/3$, gives $p = (\rho - 4\mathcal{B})/3$ (the MIT model); $B = 0$, $A = 1$ gets $p = \rho$ (Zeldovich's stiff fluid); $A = 1/3$, $B = 0$ yields radiation ($p = \rho/3$) etc. Hence, for $0 < A \leq 1$, the first term of the EoS

represents normal/stiff matter/relativistic matter depending on the values of A. The second term is the non-linear extension and by choosing $B > 0$, we ensure that it is the source of dark energy and exotic matter. Since we have chosen $n > 1$, the quantity p_r/ρ given below

$$\frac{p_r}{\rho} = A - \frac{B}{\rho^{1-1/n}} \tag{3.12}$$

tends to A as $\rho \to \infty$. This means that the contribution of dark energy component is minimum at the center. Therefore, the dense core is populated with exotic and stiff fluid. The density at which the second term in the above equation vanishes depends on parameter n thereby determining the amount of exotic matter in the stellar configuration. For large n the exotic component is more than for low n. As exotic contribution stiffens the EoS therefore, the parameter n is directly linked with the stiffness of EoS. For $n = 2$, $B > 0$ and $-1 \leq A \leq 1$, it is shown that the EoS satisfies various constituents of universe (Mukherjee et al. [2006]), which includes exotic matter, cosmic strings, dark energy, dust, radiation and stiff matter. We intend to analyze the EoS for a variable n and deduce the other constants using the boundary condition to fit for observed compact stars i.e. the X-ray pulsar LMC X-4.
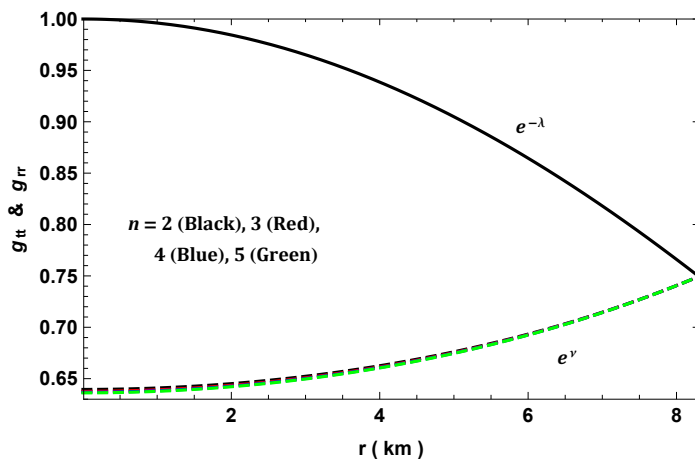
Figure 3.1: Variation of metric functions with r for LMC X-4 assuming $M = 1.04 M_\odot$, $R = 8.301\ km$, $a = 0.0039$ and $A = 0.7$.

3.3 A generalized solution

Solution of the field equations depend on the metric function ν and λ. As discussed above we choose Tolman VII g_{rr} satisfying a nonlinear EoS. Using these in eqn. (3.6)
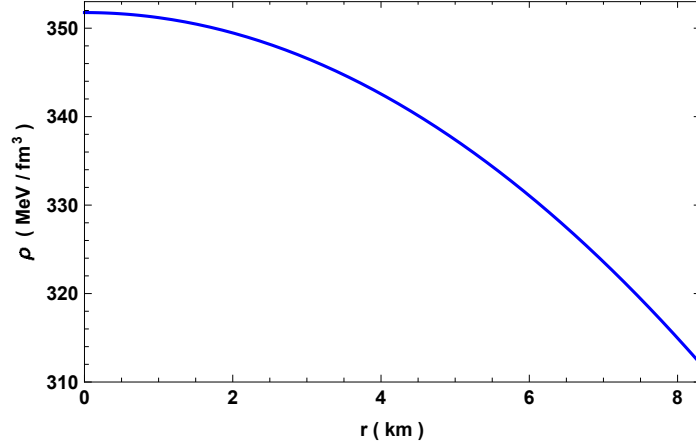
Figure 3.2: Variation of energy density with r for LMC X-4 assuming $M = 1.04M_\odot$, $R = 8.301$ km, $a = 0.0039$ and $A = 0.7$.
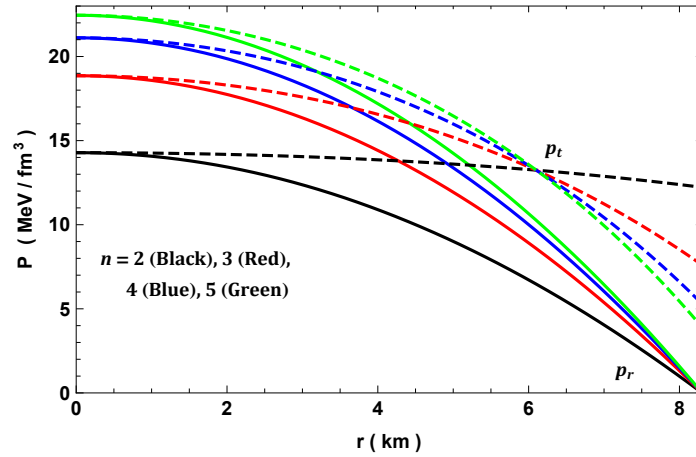
Figure 3.3: Variation of pressure with r for LMC X-4 assuming $M = 1.04M_\odot$, $R = 8.301$ km, $a = 0.0039$ and $A = 0.7$.
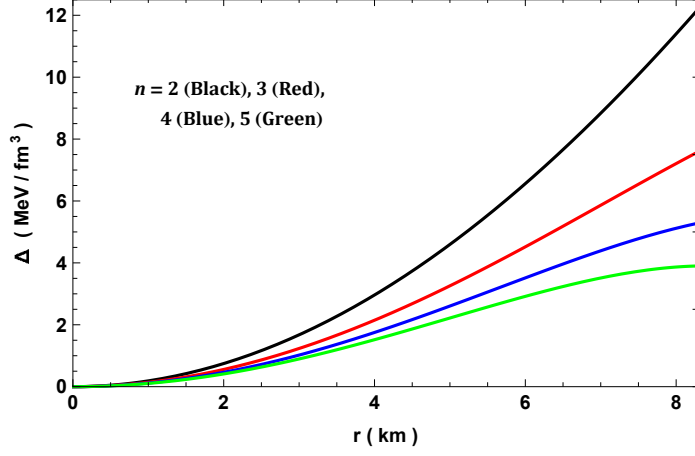
Figure 3.4: Variation of anisotropy with r for LMC X-4 assuming $M = 1.04 M_\odot$, $R = 8.301\ km$, $a = 0.0039$ and $A = 0.7$.

we get

$$
\begin{aligned}
y(x) &= F\left(1 - ax + bx^2\right)^{-\frac{5A}{8} - \frac{1}{8}} \exp\left[\frac{a(A+1)}{4\sqrt{4b - a^2}} \tan^{-1}\left(\frac{2bx - a}{\sqrt{4b - a^2}}\right)\right.\\
&\quad \left. + \frac{2^{\frac{n-4}{n}} 5^{1/n} Bn\pi^{\frac{n-1}{n}} \tau(x)}{\sqrt{a^2 - 4b}} (3a - 5bx)^{1/n}\right],
\end{aligned}
\tag{3.13}
$$

where F is constant of integration and

$$
\begin{aligned}
\tau(x) &= \chi(x)\left(\frac{3a - 5bx}{a - \sqrt{a^2 - 4b} - 2bx}\right)^{-1/n} - \xi(x)\left(\frac{3a - 5bx}{\sqrt{a^2 - 4b} + a - 2bx}\right)^{-1/n}\\
\chi(x) &= {}_2F_1\left[-\frac{1}{n}, -\frac{1}{n}; \frac{n-1}{n}; \frac{5\sqrt{a^2 - 4b} - a}{5\left(\sqrt{a^2 - 4b} + a - 2bx\right)}\right]\\
\xi(x) &= {}_2F_1\left[-\frac{1}{n}, -\frac{1}{n}; \frac{n-1}{n}; \frac{5\sqrt{a^2 - 4b} + a}{5\left(\sqrt{a^2 - 4b} - a + 2bx\right)}\right].
\end{aligned}
$$

Using the above equations we deduce the physical properties of the compact star such as density, radial and transverse pressure and anisotropic factor from eqns. (3.7), (3.8)

and (3.9) which leads us to,

$$\rho(x) = \frac{3a - 5bx}{8\pi} \tag{3.14}$$

$$p_r(x) = A\rho - B\rho^{1/n} \tag{3.15}$$

$$\Delta(x) = \frac{2^{-\frac{6}{n}-5}\pi^{-\frac{n+2}{n}}x}{n(3a - 5bx)(ax - bx^2 - 1)}\left[3a^2 n(8\pi)^{1/n}f_1(x) - 9a^3\left(3A^2 + 4A + 1\right)\right.$$
$$\left.64^{1/n}n\pi^{2/n} - a\left\{f_2(x) + f_3(x)\right\} + 5b\left\{f_4(x) + f_5(x) + f_6(x)\right\}\right] \tag{3.16}$$

$$p_t(x) = p_r(x) + \Delta(x) \,, \tag{3.17}$$

where,

$$f_1(x) = 2A\left[24\pi B(3a - 5bx)^{1/n} + 19b(8\pi)^{1/n}x\right] + 32\pi B$$
$$(3a - 5bx)^{1/n} + 45A^2 b(8\pi)^{1/n}x + 13b(8\pi)^{1/n}x$$

$$f_2(x) = 192\pi^2 B^2 n(3a - 5bx)^{2/n} + bB2^{\frac{3}{n}+4}(19n - 10)\pi^{\frac{1}{n}+1}x(3a - 5bx)^{1/n}$$
$$+225A^2 b^2 64^{1/n}n\pi^{2/n}x^2 + 55b^2 64^{1/n}n\pi^{2/n}x^2$$

$$f_3(x) = 15Ab2^{\frac{3}{n}+2}n\pi^{1/n}\left[8\pi Bx(3a - 5bx)^{1/n} + 2^{\frac{n+3}{n}}b\pi^{1/n}x^2 - (8\pi)^{1/n}\right] \tag{3.18}$$

$$f_4(x) = bB2^{\frac{3}{n}+4}(3n - 2)\pi^{\frac{1}{n}+1}x^2(3a - 5bx)^{1/n} + 25A^2$$
$$b^2 64^{1/n}n\pi^{2/n}x^3 + 5b^2 64^{1/n}n\pi^{2/n}x^3$$

$$f_5(x) = 5Ab\, 2^{\frac{n+3}{n}}n\pi^{1/n}x\left[8\pi Bx(3a - 5bx)^{1/n} + b(8\pi)^{1/n}x^2 - 2^{\frac{n+3}{n}}\pi^{1/n}\right]$$

$$f_6(x) = 32\pi B(3a - 5bx)^{1/n}\left[2\pi Bnx(3a - 5bx)^{1/n} - (8\pi)^{1/n}\right].$$

The variation of interior metric function of the chosen compact star: X-ray pulsar LMC X-4 with distance r is shown in Fig. 3.1 and the trends of the above physical quantities are depicted in Figs. 3.2-3.4.

The mass, compactness parameter, equation of state parameter and red-shift can be determined as:

$$m(r) = 4\pi\int r^2\rho(r)\,dr = \frac{1}{2}\left(ar^3 - br^5\right) \tag{3.19}$$

$$u(r) = \frac{2m(r)}{r} \tag{3.20}$$

$$\omega_r \quad = \quad \frac{p_r}{\rho} \quad ; \quad \omega_t = \frac{p_t}{\rho} \tag{3.21}$$

$$z(r) \quad = \quad e^{-\nu/2} - 1 = \frac{1}{y(r)} - 1. \tag{3.22}$$

It is to be noted that for a realistic physical system, the EoS parameters must be less than unity, which is depicted in Fig. 3.5. The redshift profile is shown in Fig. 3.6.
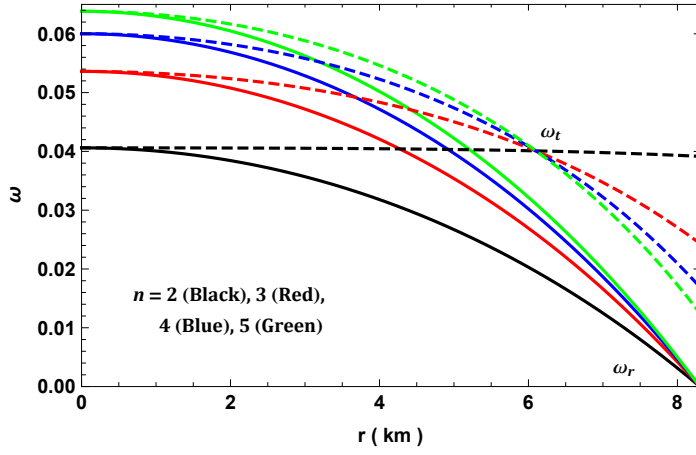
Figure 3.5: Variation of equation of state parameters with r for LMC X-4 assuming $M = 1.04 M_\odot$, $R = 8.301 \; km$, $a = 0.0039$ and $A = 0.7$.
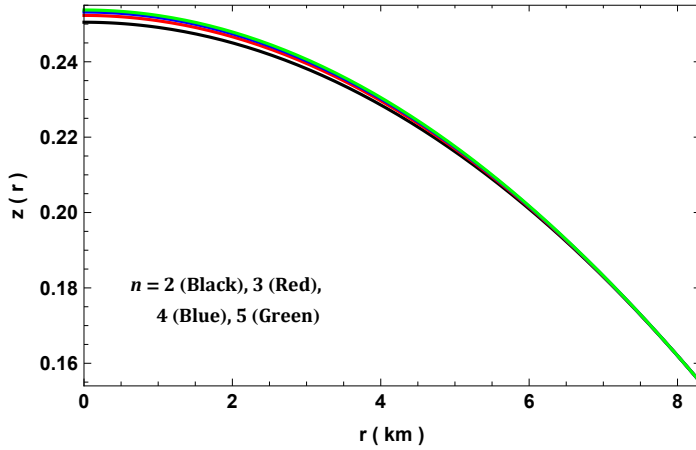
Figure 3.6: Variation of redshift with r for LMC X-4 assuming $M = 1.04 M_\odot$, $R = 8.301 \; km$, $a = 0.0039$ and $A = 0.7$.

3.4   Non-singular nature of the solution

For a physical viable solution for an astrophysical compact object we must ensure that the central values of density, pressure etc.are finite i.e.

$$\rho_c = \frac{3a}{8\pi} > 0, \tag{3.23}$$

$$p_{rc} = p_{tc} = A\rho_c - B\rho_c^{1/n} > 0 \tag{3.24}$$

provided $a > 0$ and $A > B\rho_c^{1/n-1}$. These inequalities provide a bound on the constant parameters and also implies that the solution is free from singularities.
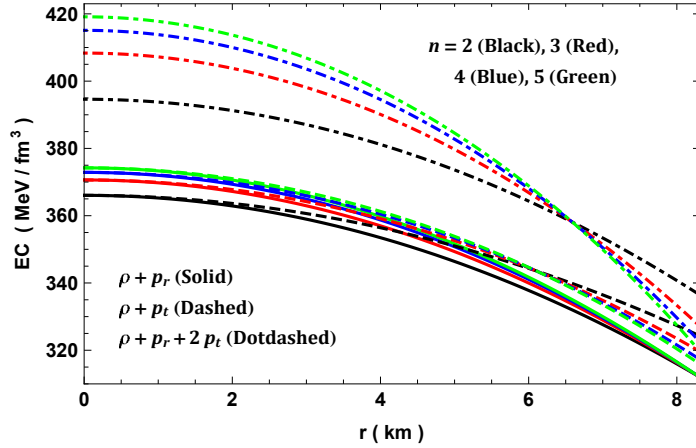
Figure 3.7:   Variation of energy conditions with r for LMC X-4 assuming $M = 1.04 M_\odot$, $R = 8.301\ km$, $a = 0.0039$ and $A = 0.7$.

3.5   Boundary Conditions and determination of constants

Assuming the exterior space-time to be *Schwarzschild*'s which is given as

$$ds^2 = \left(1 - \frac{2M}{r}\right) dt^2 - \left(1 - \frac{2M}{r}\right)^{-1} dr^2 - r^2\left(d\theta^2 + \sin^2\theta\ d\phi^2\right). \tag{3.25}$$

The continuity of the metric coefficients e^ν and $e^{-\lambda}$ across the boundary $r = R$,

also imposing that the radial pressure vanishes at the boundary yields:

$$1 - \frac{2M}{R} = e^{\nu_s} = e^{-\lambda_s} \tag{3.26}$$

$$p_r(r = R) = 0 \tag{3.27}$$

that leads to

$$b = \frac{aR^3 - 2M}{R^5} \tag{3.28}$$

$$B = A(8\pi)^{\frac{1}{n}-1} \left(3a - 5bR^2\right)^{1-\frac{1}{n}} \tag{3.29}$$

$$F = \sqrt{1 - \frac{2M}{R}} \left(1 - aR^2 + bR^4\right)^{\frac{5A}{8}+\frac{1}{8}} \exp\left[\frac{-a(A+1)}{4\sqrt{4b-a^2}} \tan^{-1}\left(\frac{2bR^2 - a}{\sqrt{4b-a^2}}\right) - \right.$$
$$\left. \frac{2^{\frac{n-4}{n}} \, 5^{1/n} B \, n \, \pi^{\frac{n-1}{n}} \, \tau(R) \, \left(3a - 5bR^2\right)^{1/n}}{\sqrt{a^2 - 4b}}\right] \tag{3.30}$$

where M and R denotes the mass and radius of the chosen compact star respectively, while a and A are kept as free parameter.

3.6   Energy Conditions

Our next goal is to examine the condition under which static stellar configurations, satisfies all the energy conditions namely, weak energy condition (WEC), null energy condition (NEC), dominant energy condition (DEC) and strong energy condition (SEC) at all points inside the star. The above energy conditions are determined by the following inequalities:

$$\text{WEC} \quad : \quad T_{\mu\nu}t^\mu t^\nu \geq 0 \text{ or } \rho \geq 0, \ \rho + p_i \geq 0 \tag{3.31}$$

$$\text{NEC} \quad : \quad T_{\mu\nu}l^\mu l^\nu \geq 0 \text{ or } \rho + p_i \geq 0 \tag{3.32}$$

$$\text{DEC} \quad : \quad T_{\mu\nu}t^\mu t^\nu \geq 0 \text{ or } \rho \geq |p_i| \ \text{ where } \ T^{\mu\nu}t_\mu \in \text{nonspace-like vector}$$

$$\text{SEC} \quad : \quad T_{\mu\nu}t^\mu t^\nu - \frac{1}{2}T_\lambda^\lambda t^\sigma t_\sigma \geq 0 \text{ or } \ \rho + \sum_i p_i \geq 0 \quad \rho + p_i \geq 0 \tag{3.33}$$

where $i \equiv (radial \ r, transverse \ t)$, t^μ and l^μ are time-like vector and null vector
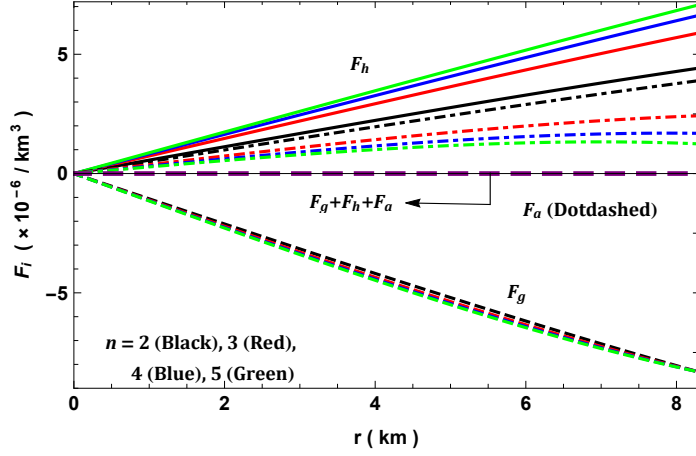
Figure 3.8: Variation of forces in TOV-equation with r for LMC X-4 assuming $M = 1.04 M_{\odot}$, $R = 8.301\ km$, $a = 0.0039$ and $A = 0.7$.

respectively. The verification of the energy conditions are shown in Fig. 3.7.

3.7 Stability of the model and equilibrium

3.7.1 Equilibrium under various forces

The generalized Tolman-Oppenheimer-Volkoff (TOV) equation determine whether a relativistic stellar system is in equilibrium or not. Mathematically, it is given by

$$-\frac{M_g(r)(\rho + p_r)}{r}\ e^{(\nu - \lambda)/2} - \frac{dp_r}{dr} + \frac{2}{r}(p_t - p_r) = 0, \tag{3.34}$$

where $M_g(r)$ is the gravitational mass and is calculated using the Tolman-Whittaker formula and the Einstein field equations. The expression is given as

$$M_g(r) \;=\; 4\pi \int_0^r \left(T_t^t - T_r^r - T_\theta^\theta - T_\phi^\phi\right)\ r^2 e^{(\nu + \lambda)/2} dr. \tag{3.35}$$

For the Eqs. (3.3)-(3.5), the above Eqn. (3.35) reduces to

$$M_g(r) = \frac{r}{2}\ e^{(\lambda - \nu)/2}\ \nu'. \tag{3.36}$$

Using the above expression of $M_g(r)$ in Eq. (3.34), we get

$$-\frac{\nu'}{2}(\rho + p_r) - \frac{dp_r}{dr} + \frac{2}{r}(p_t - p_r) = 0 \tag{3.37}$$

which can also be expressed as:

$$F_g + F_h + F_a = 0, \tag{3.38}$$

where F_g, F_h and F_a are the gravitational, hydrostatics and anisotropic forces respectively i.e.

$$F_g = -\frac{\nu'}{2}(\rho + p_r) , \quad F_h = -\frac{dp_r}{dr} , \quad F_a = \frac{2\Delta}{r}. \tag{3.39}$$

Variation of the above forces with distance r is shown in Fig. 3.8 which clearly convinces that the solution is in equilibrium.
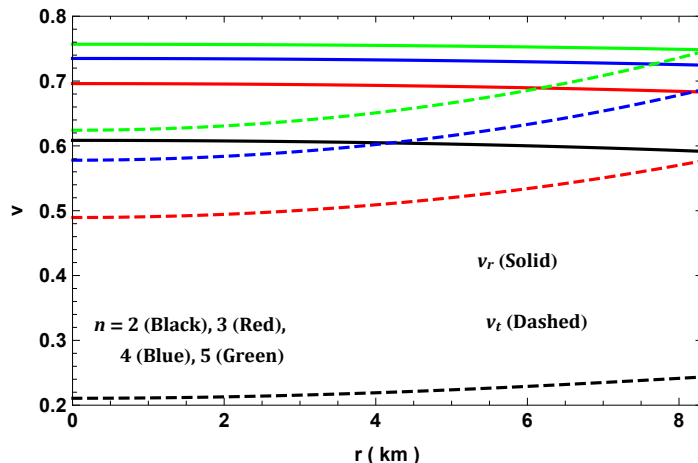
Figure 3.9: Variation of speed of sound with r for LMC X-4 assuming $M = 1.04M_\odot$, $R = 8.301$ km, $a = 0.0039$ and $A = 0.7$.

3.7.2 Causality and stability condition

The sound speed is an important parameter to check the causality condition, which implies that the radial velocity (v_r^2) and tangential velocity (v_t^2) of sound should be less than unity everywhere within the compact object, i.e., $0 < v_r^2 \le 1$ and $0 < v_t^2 \le 1$, where

$$v_r^2 = \frac{dp_r}{d\rho}, \quad v_t^2 = \frac{dp_t}{d\rho}. \tag{3.40}$$

Figure 3.9 verify the subliminal sound speed at the interior. The solution also satisfy the Abreu's stability criterion (Abreu et al. [2007]), which states: $-1 \le v_t^2 - v_r^2 \le 0$,

which is depicted in Fig. 3.10.

3.7.3 Adiabatic index and stability condition

For an anisotropic matter distribution adiabatic index also determine the stability of the fluid distribution which is defined as (Chan et al. [1993]),

$$\Gamma_r = \frac{\rho + p_r}{p_r} \frac{dp_r}{d\rho}. \tag{3.41}$$

According to Bondi condition (Bondi [1964]) $\Gamma_r > 4/3$ gives a stable Newtonian system whereas $\Gamma = 4/3$ is the condition for a neutral equilibrium. This condition is partially valid for anisotropic case as it depends on nature of anisotropy. For an anisotropic fluid sphere the adiabatic index modify to (Chan et al. [1993]),

$$\Gamma > \frac{4}{3} + \left[\frac{4}{3} \frac{(p_{ti} - p_{ri})}{|p'_{ri}|r} + \frac{8\pi}{3} \frac{\rho_i p_{ri}}{|p'_{ri}|} r \right]_{max}, \tag{3.42}$$

where, p_{ri}, p_{ti}, and ρ_i are the initial radial, tangential pressures and energy density respectively in static equilibrium. Within the square bracket, first term gives the anisotropic modification and the last term is relativistic correction to Γ (Chan et al. [1993], Herrera [1992]). If the anisotropy is positive, then a system with $\Gamma_r > 4/3$ may not be in stable and vice versa. For such case the adiabatic index is more than $4/3$ including the extra correcting terms (see Fig. 3.11) and therefore is stable.
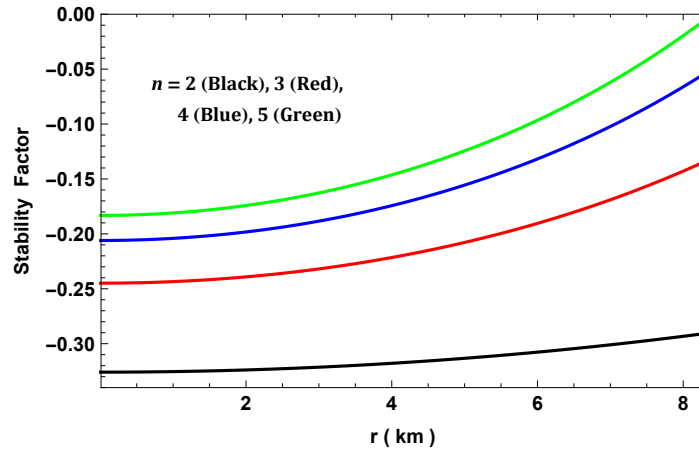
Figure 3.10: Variation of stability factor with r for LMC X-4 assuming $M = 1.04M_\odot$, $R = 8.301\ km$, $a = 0.0039$ and $A = 0.7$.
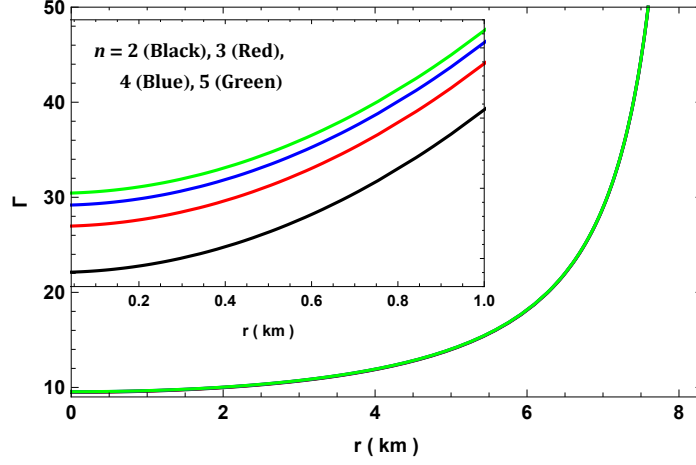
Figure 3.11: Variation of adiabatic index with r for LMC X-4 assuming $M = 1.04 M_\odot$, $R = 8.301\ km$, $a = 0.0039$ and $A = 0.7$.
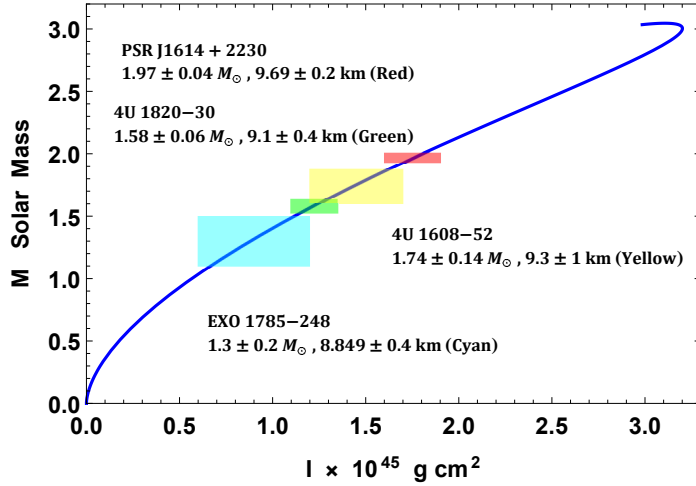
Figure 3.12: Variation of moment of inertia with M ($A = 0.72$, $B = 0.01025$, $n = 2$, $b = 8 \times 10^{-7}$).

3.7.4 Harrison-Zeldovich-Novikov static stability criterion
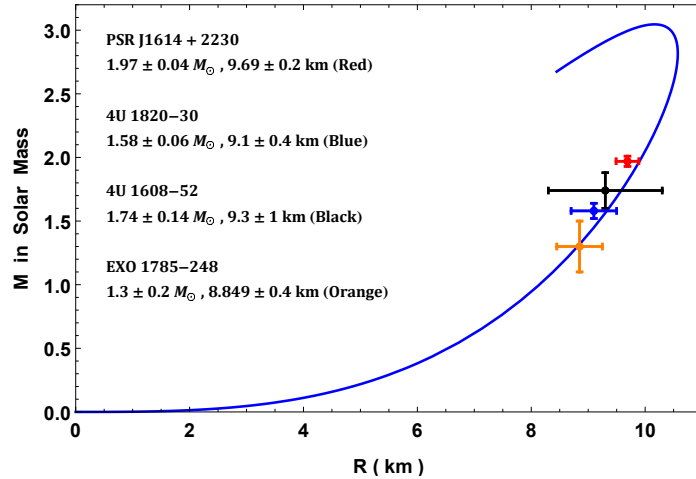
Figure 3.13: $M - R$ curve fitted for few compact stars ($A = 0.72$, $B = 0.01025$, $n = 2$, $b = 8 \times 10^{-7}$).

The static stability criterion proposed by Harrison et al. [1965] and Zeldovich and Novikov [1971] are much simpler than the Chandrasekhar's criterion (Chandrasekhar [1964]). It states that any stellar model is a stable configuration only if its mass increases with growing central density i.e. $d\mu/d\rho_c > 0$. The opposite inequality i.e., $d\mu/d\rho_c < 0$ always implies instability of stellar models. Mass as a function of central density is given below:

$$\mu(\rho_c) \;=\; \frac{1}{6}\left(8\pi R^3 \rho_c - 3bR^5\right) \tag{3.43}$$

One can clearly see the mass is a linear function of its central density which straight ways yields $\partial\mu(\rho_c)/\partial\rho_c > 0$ at constant R since b is of the order of 10^{-5}. Therefore, the static stability criterion is fulfilled.

3.7.5 Determination of moment of inertia under slow rotation approximation

Bejger and Haensel [2002] defined an approximate expression for the moment of inertia of compact stars under slow rotation which is within 5% accuracy given by

$$I = \frac{2}{5}\left(1 + \frac{M}{R} \cdot \frac{km}{M_\odot}\right) MR^2. \tag{3.44}$$

The $M - I$ curve in Fig. 3.12 can be generated using the above expression incorporating the variations of mass and radius from $M - R$ curve in Fig. 3.13. As per Fig. 3.12, the estimated values of I are $1.75 \times 10^{45} g\ cm^2$ (PSR J1614 + 2230), $1.42 \times 10^{45} g\ cm^2$ (4U 1608-52), $1.23 \times 10^{45} g\ cm^2$ (4U 1820-30) and $8.92 \times 10^{44} g\ cm^2$ (EXO 1785-248).

3.8 Discussion and conclusion

We have studied the effects of exotic matter on the astrophysical compact objects. Owing to the high density in the interior of the compact objects, it is quite possible that many exotic form of matter may exist. To explore this idea we employ Tolman VII solutions to a generalized non-linear EoS. of the form mentioned in Eq. (3.12). A special form of such EoS has been studied widely in case ever existing universe (Mukherjee et al. [2006]), where the values of parameter determine the primordial constitutes of universe. We have modeled such constituents in a stellar compact star configuration, namely an X-ray pulsar i.e., LMC X-4, having the observed mass as $M = 1.04 M \odot$. In order to solve Einstein's equation and derive different thermodynamic properties from it we first need to constraint the parameters of the model. The constraint equations of the parameters are deduced from the boundary conditions which are shown in Eqs. (3.29) and (3.30). Here parameters b and B are related to parameters n, A and a, which are treated as free parameters. We explore several physical aspects of the model analytically along with graphical display in order to verify that the model can depict a viable astrophysical compact object. Our analysis show that model is free from all singularities and is stable for the parameter A ranging from $0.58 - 1$ for all n. Therefore, we choose the value of A in this range and investigate all the physical aspects of the model for different values of n, which are discussed below:

The metric potentials as a function of r is displayed in Fig. 3.1. We notice that both the potentials are finite at the stellar center. The metric potential e^ν at center($r = 0$) is constant and is monotonically increases towards the boundary whereas $e^{-\lambda}$ at $r = 0$ is one and is monotonically decreasing towards the boundary of the star. They are free from singularities inside the star and values of both the potential is identical at the surface of the star.

The thermodynamic properties of the interior of the star is shown in Fig. 3.2 and Fig. 3.3. From the plots we notice that the density ρ and pressures p_r and p_t are
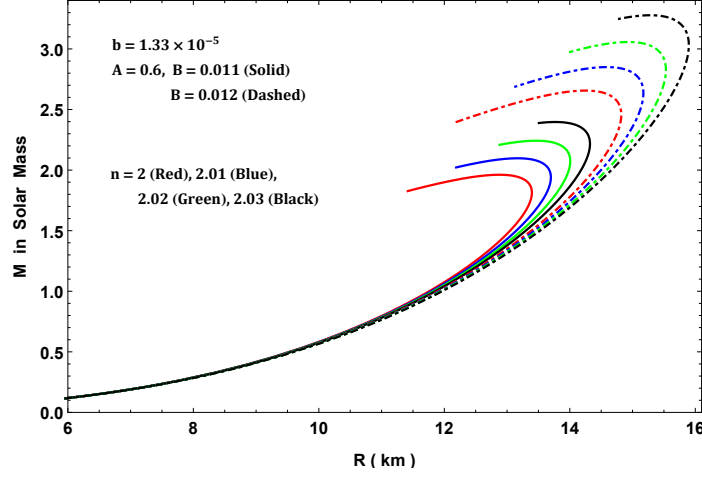
Figure 3.14: Effects on $M - R$ curve due to B and n parameter.

positive and maximum at the core of the star. They decreases towards the surface of the star and are free from any central singularity. The radial pressure p_r drops to zero at the boundary of the star but the tangential pressure p_t remains finite both at the core and at the boundary. However the values of both p_r and p_t are equal at the center of the star which implies that the pressure anisotropy factor vanishes at the center, $\Delta(r = 0) = 0$ as is evident from the profile of anisotropy Δ in Fig. 3.4. Also one can note from it that anisotropy increases with distance r and is maximum at the surface of the star. Moreover the anisotropy decreases for increasing values of n. $\Delta > 0$ inside the star causes the anisotropic force to be repulsive in nature. One important information extracted from these graphs is that as the parameter n increases the central values of pressure increases and anisotropy reduces. This means that the EoS is getting stiffer as n increase i.e. by increasing dark energy/exotic contribution $(B\rho^{1/n})$ makes the EoS stiffer.

This can also be confirms from the variation of both radial (ω_r) and transverse (ω_t) EoS parameters with radial distance r (Fig. 3.5). As n increases the $\omega-$parameters increases. The variation of gravitational redshift with radial distance is shown in Fig. 3.6, which shows it is monotone decreasing. All the energy conditions mentioned in Section 3.6 are fulfilled by the stellar configuration which is depicted in Fig. 3.7. This suggests that the model is viable in nature with no instability or presence of ghost (negative mass or energy).

Equilibrium of a stellar system is determined by different forces that generate inside the system. These forces can be estimated from the TOV Eqs. (3.37)-(3.39).The

variation of these forces, namely gravitational force (F_g), hydrodynamic force (F_h), and anisotropic force (F_a) are shown in Fig. (3.8). From the figure we conclude that the system is in equilibrium. Another important criterion to test the stability is the causality condition which is valid when the sound is less than one. Fig. 3.9 confirms not only the fulfillment of the causality condition but also the increase in stiffness as n increases. It also follows the Abereu's stability criterion viz: $-1 \leq v_t^2 - v_r^2 \leq 0$ as can be seen from Fig. 3.10.

Stability of anisotropic matter distribution is also determined by the adiabatic index of the constituents of the stellar configuration, which is verified in Fig. 3.11. For the values of n considered the anisotropic stellar configuration is steady as $\Gamma > 4/3$ in the interior of the system. Lastly the Harrison-Zeldovich-Novikov static stability criterion is also checked for the model. Figure depicts the fulfillment of the criteria as we see the mass increases with growing central density which is the necessary condition for a stable stellar configuration.

To verify whether the stellar configuration can depict more varieties of observed compact objects we construct the $M - R$ plot in Fig. 3.13. From this curve we notice that many observed compact objects can be modeled considering exotic matter as their constituents. Particularly, it is well fitted within the observation errors for EXO 1785-248 (Gangopadhyay et al. [2013]), PSR J1614 + 2230 (Demorest et al. [2010]), 4U 1608-52 (Güver et al. [2010a]) and 4U 1820-30 (Güver et al. [2010b]). The approximate moment of inertia I for these fitted compact objects can be estimated from Fig. 3.13 within 5% accuracy. The $M - R$ curve in Fig. 3.14 demonstrates the effect of B and n parameters. As n increase the stiffness increases resulting into increase in M_{max} significantly. In the similar fashion, a small change in B increases M_{max} significantly. It means as n and B increases the dark energy contribution increases resulting into more stiffer EoS. We therefore conclude that the theoretical prediction of stellar configuration with non-linear EoS which incorporates the dark energy/exotic matter follows all the stability criterion as well as goes well with the observational data.

Chapter 4

Static fluid spheres admitting Karmarkar condition [1]

4.1 Introduction

The existence of anisotropy inside the compact star plays an essential role in the modeling of relativistic stellar configuration. The well-known work on anisotropy has been done by Bowers and Liang [1974], Herrera and Santos [1997] in which they showed the effect of anisotropy on the self-gravitating system. Dev and Gleiser [2002, 2003] have shown that the pressure anisotropy introduces an effect on the mass, structure and other physical phenomena of highly dense compact stars. It is also observed that the anisotropy influences the red-shift of the compact objects. In view of Ruderman [1972], the compact objects having a high density of order $> 10^{15} gm/cm^3$ pressure anisotropy is the underlying nature of the atomic substance and their interactions are relativistic. In this connection, some other important work on the anisotropic stellar models can be seen in Refs. Mak and Harko [2003], Cosenza et al. [1981], Herrera et al. [1984], Herrera and de León [1985], Herrera and Ponce de Leon [1985], Esculpi and Herrera [1986], Herrera et al. [2001, 2002], Rahaman et al. [2010b]. Normally anisotropy arises due to the occurrence of different types, viz., a mixture of fluids, rotation, the survival of superfluid, phase transitions, the existence of magnetic field or external field, etc. Recently, significant efforts have been done by the researchers in the modeling of observed astrophysical objects for the anisotropic matter configuration. Also, some important physical features of the anisotropic star have been

---

[1] Content of this chapter has been published in *Chinese Physics C* (IOP), 244 (2020) 035101.

discussed in some recent works of Maurya et al. [2019, 2018, 2017b], Sharma and Ratanpal [2013], Ngubelanga et al. [2015], Murad and Fatema [2015b], and the references therein. The physical analyses contained in these works shows that the presence of nonzero anisotropy plays an important role in modeling astrophysical stellar models. Also, de la Fuente [2009], Malaver [2014] have discussed compact star models for strange quark matter in GR by taking linear and quadratic equation of state. The conformal symmetry relativistic compact star objects have been proposed by many authors (Rahaman et al. [2017, 2010a], Esculpi and Aloma [2010], Manjonjo et al. [2018], Maharaj et al. [1995], Maartens et al. [1995, 1996, 1995]). Therefore, for discussing any astrophysical relativistic compact objects, it is important to find an exact solution of the system of the Einstein field equations. Delgaty and Lake [1998] have given a complete detail of many exact solutions of the Einstein field equations which have been obtained over the last century. They argued that only a few of them satisfy the physical and mathematical requirements for a realistic stellar object in general relativity. It is well-known that the solution of the Einstein field equation is not an easy task due to its nonlinear nature. Therefore, in order to develop a physically realistic consistent stellar model, either we restrict the space-time geometry by classifying an equation of state or another different approach. In this connection, we have employed an embedding approach to tackle this field equation. From the past of many years, the embedding approach keep continues a great interest among the researchers (Singh et al. [2017c,b,a], Bhar et al. [2016a], Maurya and Govender [2017]). By employing this embedding theory, we may link the classical general theory of relativity to the higher dimensional flat space-time that describes the inner symmetry group characteristic of the particles. Romero and his collaborators (Rippl et al. [1995], Romero et al. [1996]) have linked the different manifolds like vacuum 5D manifold to 4D manifold, 4D field equation in vacuum to 3D field equation, and the 4D Einstein equations are embedded in a 5D Ricci-flat space-time by using the Campbell's theorem (Campbell [1926]). This theory gives the algebraic explanations of the membrane theory and convinced matter theory. It is worth mentioning that m dimensional manifold V_m can always be embedded into $n-$dimensional pseudo-Euclidian space E_n, where $n = m(m+1)/2$. This least additional dimension p of the pseudo-Euclidian space is called the embedding class of the manifold V_m that must be less than or equal to the value $(n - m) = m(m - 1)/2$. For example, 4 dimensional relativistic space V_4 time can be embedded in flat space-time of dimension 10. In this case, the embedding class of V_4 is 6. On the other hand, the class of plane

symmetric is 3 while the spherically symmetric space-time and Schwarzschild's exterior solution (Schwarzschild [1916b]) both are of class 2. Moreover, the well-known Friedman-Robertson-Lemaitre (Friedman [1922], Lemaître [1933], Robertson [1933]) space-time and Schwarzschild's interior solution of class one (Schwarzschild [1916a]).

In this chapter, we have used Karmarkar condition to obtain relativistic anisotropic stellar models of the Einstein field equation for spherically symmetric line element. We derive a particular differential equation (known as class one condition) by using the Karmarkar condition that connects both gravitational potential ν and λ. We solve this equation by taking a particular form of ansatz for the gravitational potential λ. After that, we perform physical analysis of the solution which describes realistic anisotropic stellar compact objects. The chapter is organized as follows: We begin with Sec. 4.2 that include the spherically symmetric interior space-time and the Einstein field equations for anisotropic matter distribution. We also mention the non-vanishing components for Riemannian tensor along with embedding class one condition for spherically symmetric metric line element. In Sec. 4.3, We have obtained a generalized solution for anisotropic compact star model by solving of class one condition. The expressions for pressures, density and anisotropy are also given in Sec. 4.3. In Sect. 4.4, we have determined all necessary constant parameters by matching of our interior space-time to the exterior space-time (Schwarzscild metric). The non-singular nature of pressures, density, and bounds of the constant are given in Sect. 4.5. We have also included the most important features of the compact star models like the velocity of sound, adiabatic index, Tolman-Oppenheimer-Volkoff equation equilibrium condition, stability through Harrison-Zeldovich-Novikov criterion and Herrera cracking concept in same Sec. 4.5. In Sec. 4.6, we have discussed Slow rotation approximation, the moment of inertia and Kepler frequency and energy conditions. The final remark has been given in Sec. 4.7.

4.2 The Einstein Field Equations

The interior of the super-dense star is assumed to be described by the line element

$$ds^2 = e^{\nu(r)}dt^2 - e^{\lambda(r)}dr^2 - r^2(d\theta^2 + \sin^2\theta \ d\phi^2). \tag{4.1}$$

For our model the energy-momentum tensor for the stellar fluid is

$$T_{\alpha\beta} = (\rho + p_t)v_\alpha v_\beta - p_t g_{\alpha\beta} + (p_r - p_t)\chi_\alpha\chi_\beta. \tag{4.2}$$

Here all the symbols are having usual meanings with $v_\alpha v^\alpha = -1 = -\chi_\alpha\chi^\alpha$ and $v_\alpha\chi^\alpha = 0$.

The Einstein field equations for the line element (4.1) are

$$8\pi\rho = \frac{1 - e^{-\lambda}}{r^2} + \frac{\lambda' e^{-\lambda}}{r} \tag{4.3}$$

$$8\pi p_r = \frac{\nu' e^{-\lambda}}{r} - \frac{1 - e^{-\lambda}}{r^2} \tag{4.4}$$

$$8\pi p_t = \frac{e^{-\lambda}}{4}\left[2\nu'' + \nu'^2 - \nu'\lambda' + \frac{2(\nu' - \lambda')}{r}\right] \tag{4.5}$$

where primes denotes the derivative w.r.t. radial coordinate r. We use the geometrized units $G = c = 1$ throughout the study. Using Eqs. (4.4) and (4.5) we get

$$\Delta = 8\pi(p_t - p_r) = e^{-\lambda}\left[\frac{\nu''}{2} - \frac{\lambda'\nu'}{4} + \frac{\nu'^2}{4} - \frac{\nu' + \lambda'}{2r} + \frac{e^\lambda - 1}{r^2}\right]. \tag{4.6}$$

To solve (4.3)-4.5 we have adopted the method of embedding class one where e^ν and e^λ are linked via the Karmarkar condition (Karmarkar [1948]) as

$$\frac{\lambda'\nu'}{1 - e^\lambda} = \lambda'\nu' - 2(\nu'' + \nu'^2) + \nu'^2. \tag{4.7}$$

The solutions of (4.7) are class I so long as they satisfy the Pandey-Sharma condition (Pandey and Sharma [1982]).

4.3 A new physical solution

In this model, we assume the following metric potential g_{rr} consisting of hyperbolic function

$$e^\lambda = 1 + ar^2\left\{1 + \cosh\left(br^2 + c\right)\right\}^n. \tag{4.8}$$

In the above equation the constant parameters a, b, c and n are positive and we coose $e^{\lambda(r)}$ such that $e^{\lambda(0)} = 1$ which infers that the tangent 3 space is flat at the center and the Einstein field equations can be solved for physically acceptable solution.

The metric potential g_{tt} is found using (4.7) and given by

$$e^{\nu} = \left(A - \frac{f(r)B\sqrt{a\left[\cosh\left(br^2 + c\right) + 1\right)\right]^n}}{b(n+1)\sqrt{2 - 2\cosh\left(br^2 + c\right)}} \right)^2, \qquad (4.9)$$

where A and B are constants of integration and

$$f(r) = {}_2F_1\left[\frac{1}{2}, \frac{n+1}{2}; \frac{n+3}{2}; \cosh^2\left(\frac{1}{2}\left(br^2 + c\right)\right)\right]\sinh\left(br^2 + c\right). \qquad (4.10)$$

The variations of the two metric functions are shown in Fig. 4.1. For $n = -2$ to $n = -18$ the behavior of metric function changes slightly.

Using metric potentials given in Eqns (4.8) and (4.9), the expressions of ρ, p_r, Δ and p_t are given as

Figure 4.1: Variation of metric functions for the neutron star in Vela X-1 with parameters $n = -2$ to -18, $b = 0.001/km^2$, $c = 0.0001$, $M = 1.77M_{\odot}$ and $R = 9.56km$.

Figure 4.2: Variation of pressure for the neutron star in Vela X-1 with parameters $n = -2$ to -18, $b = 0.001/km^2$, $c = 0.0001$, $M = 1.77M_\odot$ and $R = 9.56km$. Here δn is the increment in n while ploting the graph.

Figure 4.3: Variation of density for the neutron star in Vela X-1 with parameters $n = -2$ to -18, $b = 0.001/km^2$, $c = 0.0001$, $M = 1.77M_\odot$ and $R = 9.56km$.

Figure 4.4: Variation of pressure anisotropy for the neutron star in Vela X-1 with parameters $n = -2$ to -18, $b = 0.001/km^2$, $c = 0.0001$, $M = 1.77M_\odot$ and $R = 9.56km$.

Figure 4.5: Variation of pressure and density gradients for the neutron star in Vela X-1 with parameters $n = -2$ to -18, $b = 0.001/km^2$, $c = 0.0001$, $M = 1.77M_\odot$ and $R = 9.56km$.

$$p_r = \frac{f_2(r)\sqrt{a\left[\cosh\left(br^2+c\right)+1\right]^n}}{8\pi f_1(r)\left(ar^2\left(\cosh\left(br^2+c\right)+1\right)^n+1\right)} \tag{4.11}$$

$$\rho = \frac{a\left[\cosh\left(br^2+c\right)+1\right]^{n-1}}{8\pi\left[ar^2\left\{\cosh\left(br^2+c\right)+1\right\}^n+1\right]^2} \times \left[ar^2\left\{\cosh\left(br^2+c\right)+1\right\}^{n+1}+2bnr^2\right.$$
$$\left.\sinh\left(br^2+c\right)+3\cosh\left(br^2+c\right)+3\right] \tag{4.12}$$

$$\Delta = \frac{rf_3(r)\sqrt{ar^2\left[\cosh\left(br^2+c\right)+1\right]^n}}{f_4(r)\left[\cosh\left(br^2+c\right)+1\right]} \times$$
$$\frac{bn\sinh\left(br^2+c\right)-a\left[\cosh\left(br^2+c\right)+1\right]^{n+1}}{\left[ar^2\left\{\cosh\left(br^2+c\right)+1\right\}^n+1\right]^2} \tag{4.13}$$

$$p_t = p_r + \frac{\Delta}{8\pi}. \tag{4.14}$$

The variations of pressures, density, anisotropy, equation of state parameters, $d\rho/dr$, dp_r/dr and dp_t/dr are shown in Figs. 4.2-4.6. As values of n increases the central density, anisotropy, adiabatic index increases, however, the pressures, equation of state parameters and speed of sounds decreases.

Here,

$$f_1(r) = 2Ab(n+1)r\sqrt{1-\cosh\left(br^2+c\right)} - \sqrt{2}B\sinh\left(br^2+c\right)$$
$$\sqrt{ar^2\left[\cosh\left(br^2+c\right)+1\right]^n}\,{}_2F_1\left[\frac{1}{2},\frac{n+1}{2};\frac{n+3}{2};\cosh^2\left(\frac{br^2+c}{2}\right)\right]$$

$$f_2(r) = 2b(n+1)\sqrt{1-\cosh\left(br^2+c\right)}\left(2Br-A\sqrt{ar^2\left[\cosh\left(br^2+c\right)+1\right]^n}\right)+$$
$$\sqrt{2}aBr\sinh\left(br^2+c\right)\left[\cosh\left(br^2+c\right)+1\right]^n$$
$${}_2F_1\left[\frac{1}{2},\frac{n+1}{2};\frac{n+3}{2};\cosh^2\left(\frac{br^2+c}{2}\right)\right]$$

$$f_3(r) = 2b(n+1)\sqrt{1-\cosh\left(br^2+c\right)}\left(Br-A\sqrt{ar^2\left[\cosh\left(br^2+c\right)+1\right]^n}\right)$$
$$+\sqrt{2}aBr\sinh\left(br^2+c\right)\left[\cosh\left(br^2+c\right)+1\right]^n$$
$${}_2F_1\left[\frac{1}{2},\frac{n+1}{2};\frac{n+3}{2};\cosh^2\left(\frac{br^2+c}{2}\right)\right]$$

$$f_4(r) = 2Ab(n+1)r\sqrt{1-\cosh\left(br^2+c\right)} - \sqrt{2}B\sinh\left(br^2+c\right)$$
$$\sqrt{ar^2\left[\cosh\left(br^2+c\right)+1\right]^n}\,{}_2F_1\left[\frac{1}{2},\frac{n+1}{2};\frac{n+3}{2};\cosh^2\left(\frac{br^2+c}{2}\right)\right].$$

4.4   Matching of interior and exterior spacetime

Assuming the exterior spacetime to be the Schwarzschild solution which has to match smoothly with our interior solution and is given by

$$ds^2 = \left(1 - \frac{2M}{r}\right)dt^2 - \left(1 - \frac{2M}{r}\right)^{-1}dr^2 - r^2(d\theta^2 + \sin^2\theta\, d\phi^2). \quad (4.15)$$

By matching the first and second fundamental forms the interior solution (4.1) and exterior solution (4.15) at the boundary $r = R$ (Darmois-Israel condition Darmois [1927], Israel [1966a]) we get

$$e^{\nu_b/2} = 1 - \frac{2M}{R} = A - \frac{f(R)B\sqrt{a^2\left[\cosh\left(bR^2 + c\right) + 1\right]}^n}{b(n+1)\sqrt{2 - 2\cosh\left(bR^2 + c\right)}} \quad (4.16)$$

$$e^{-\lambda_b} = 1 - \frac{2M}{R} = \left[1 + aR^2\left\{1 + \cosh\left(bR^2 + c\right)\right\}^n\right]^{-1} \quad (4.17)$$

$$p_r(R) = 0. \quad (4.18)$$

Using the boundary conditions (4.16-4.18), we get

$$a = \frac{2M\left(\cosh\left(bR^2 + c\right) + 1\right)^{-n}}{R^2(R - 2M)} \quad (4.19)$$

$$A = \frac{B\left[\cosh\left(bR^2 + c\right) + 1\right]^{-n/2}}{2\sqrt{a}b(n+1)\sqrt{1 - \cosh\left(bR^2 + c\right)}} \quad (4.20)$$

$$B = \frac{\sqrt{a}}{2}\sqrt{1 - \frac{2M}{R}}\left[\cosh\left(bR^2 + c\right) + 1\right]^{n/2} \times \left[\sqrt{2}a\sinh\left(bR^2 + c\right)\right.$$
$$\left[\cosh\left(bR^2 + c\right) + 1\right]^n {}_2F_1\left[\frac{1}{2}, \frac{n+1}{2}; \frac{n+3}{2}; \cosh^2\left(\frac{1}{2}\left\{bR^2 + c\right\}\right)\right]$$
$$\left. + 4b(n+1)\sqrt{1 - \cosh\left(bR^2 + c\right)}\right]. \quad (4.21)$$

4.5   Properties of the new solution

The central pressure and density at the interior are given by

$$
8\pi p_r(0) = 8\pi p_t(0) = \left\{ \sqrt{2}aB\sinh c\,(\cosh c + 1)^n\,{}_2F_1\left[\frac{1}{2}, \frac{n+1}{2}; \frac{n+3}{2}; \cosh^2\left(\frac{c}{2}\right)\right] \right\}
$$

$$
\left\{ 8\pi\left(\sqrt{2}B\sinh c\sqrt{a\,(\cosh c + 1)^n}\,{}_2F_1\left[\frac{1}{2}, \frac{n+1}{2}; \frac{n+3}{2}; \cosh^2\left(\frac{c}{2}\right)\right]\right.\right.
$$

$$
\left.\left. -2Ab(n+1)\sqrt{1-\cosh c}\right)\right\}^{-1} > 0 \tag{4.22}
$$

$$
\rho(0) = \frac{3a\,(\cosh c + 1)^n}{8\pi} > 0. \tag{4.23}
$$

The finite central values of the above parameters ensure that the solution is non-singular. The Zeldovich's condition i.e. p_r/ρ at center is ≤ 1, which is a must for physical matters.
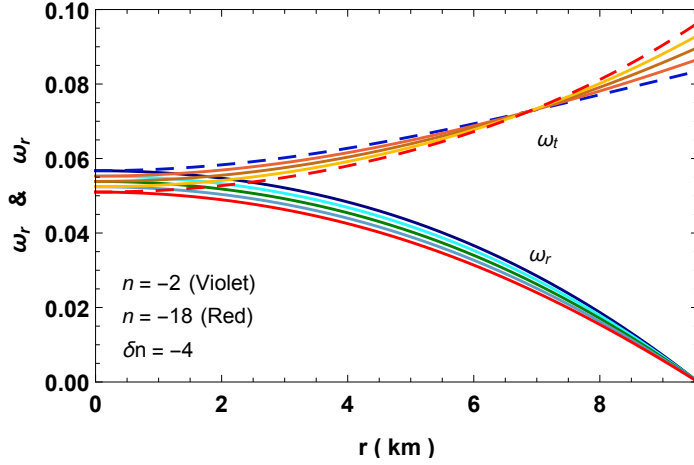
Figure 4.6: Variation of equation of state parameters for the neutron star in Vela X-1 with parameters $n = -2$ to -18, $b = 0.001/km^2$, $c = 0.0001$, $M = 1.77M_\odot$ and $R = 9.56km$.

4.5.1 Velocity of Sound and adiabatic index

The velocity of sound inside the stellar interior can be determined by using

$$
v_r^2 = \frac{dp_r/dr}{d\rho/dr}, \quad v_t^2 = \frac{dp_t/dr}{d\rho/dr}. \tag{4.24}
$$

4.5. Properties of the new solution

For a stable configuration the stability factor $v_t^2 - v_r^2$ should lie between 0 and -1 (Abreu et al. [2007], Herrera [1992]). Variations of sound speed and stability factor are shown in Figs. 4.7 and 4.8. The figures show that the solution satisfy the causality condition and stability criterion. If $n = 0$, some part of the stability factor become positive and therefore not stable, however, n can go beyond -18 and are still stable.

The relativistic adiabatic index is given by

$$\Gamma = \frac{\rho + p_r}{p_r} \frac{dp_r}{d\rho}. \tag{4.25}$$

For a static configuration at equilibrium Γ has to be more than $4/3$ (Bondi [1964]). The figure in Fig. 4.9 shows that the adiabatic index is $> 4/3$.

4.5.2 Equilibrium via modified Tolman-Oppenheimer-Volkoff (TOV) equation

The modified Tolman-Oppenheimer-Volkoff (TOV) equation for anisotropic fluid distribution was given by Ponce de Leon [1987] as

$$-\frac{M_g(\rho + p_r)}{r^2} e^{(\lambda - \nu)/2} - \frac{dp_r}{dr} + \frac{2\Delta}{r} = 0 \tag{4.26}$$

provided

$$M_g(r) = \frac{1}{2} r^2 \nu' e^{(\nu - \lambda)/2}. \tag{4.27}$$

The above equation (4.26) can be written in terms of balanced force equation due to anisotropy (F_a), gravity (F_g) and hydrostatic (F_h) i.e.

$$F_g + F_h + F_a = 0. \tag{4.28}$$

Here

$$F_g = -\frac{M_g(\rho + p_r)}{r^2} e^{(\lambda - \nu)/2} \tag{4.29}$$

$$F_h = -\frac{dp_r}{dr} \tag{4.30}$$

$$F_a = \frac{2\Delta}{r}. \tag{4.31}$$

The TOV equation (4.28) can be represented by the figure showing that the forces are counter balanced to each other Fig. 4.10. As n increases from -2 to -18 the peak of the F_g increases, F_h is almost same from center upto about 4 km and show significant increment till the surface, however, F_a decreases as n approaches -18.
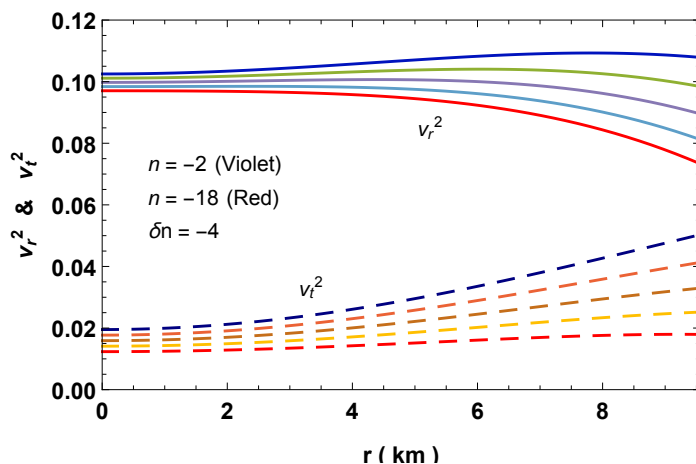
Figure 4.7: Variation of velocity of sound for the neutron star in Vela X-1 with parameters $n = -2$ to -18, $b = 0.001/km^2$, $c = 0.0001$, $M = 1.77M_\odot$ and $R = 9.56km$.
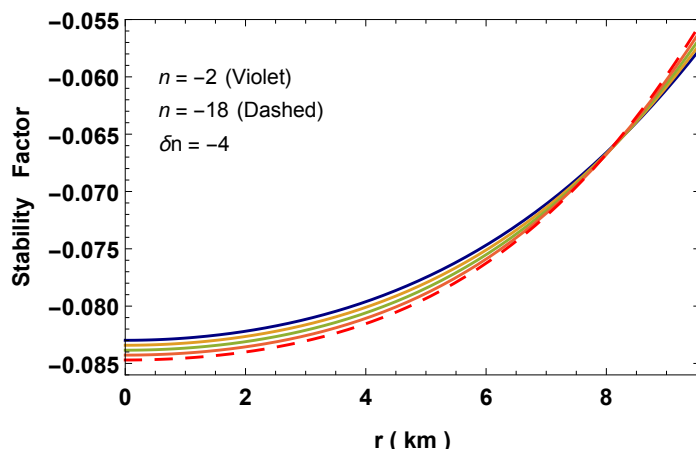
Figure 4.8: Variation of stability factor for the neutron star in Vela X-1 with parameters $n = -2$ to -18, $b = 0.001/km^2$, $c = 0.0001$, $M = 1.77M_\odot$ and $R = 9.56km$.

4.5.3 Stability Harrison-Zeldovich-Novikov criterion

The satisfaction of static stability criterion ensures that the solution is static and stable. It was proposed independently by Harrison et al. [1965] and Zeldovich and
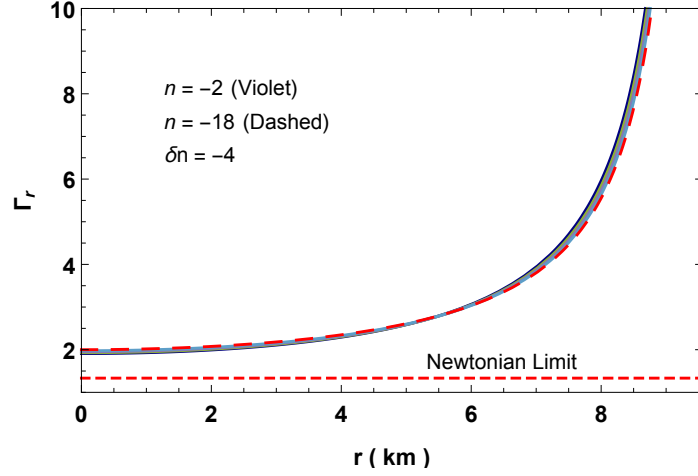
Figure 4.9: Variation of adiabatic index for the neutron star in Vela X-1 with parameters $n = -2$ to -18, $b = 0.001/km^2$, $c = 0.0001$, $M = 1.77M_\odot$ and $R = 9.56km$.
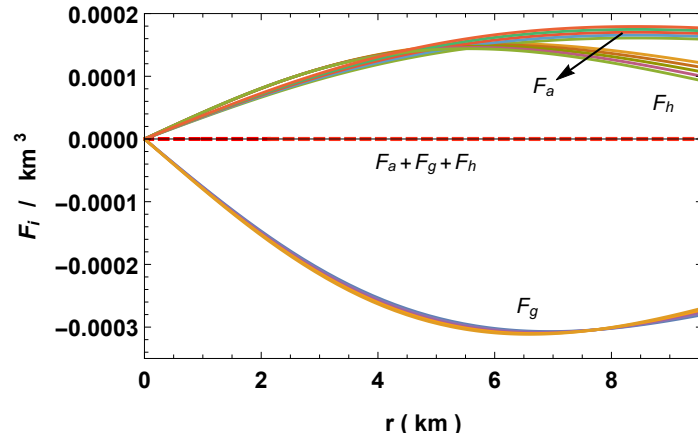
Figure 4.10: Variation of forces acting on the system via TOV-quation for the neutron star in Vela X-1 with parameters $n = -2$ to -18, $b = 0.001/km^2$, $c = 0.0001$, $M = 1.77M_\odot$ and $R = 9.56km$.

Novikov [1971]. According to this criterion mass of compact stars must be an increasing function of its central density i.e. $dM/d\rho_c > 0$.
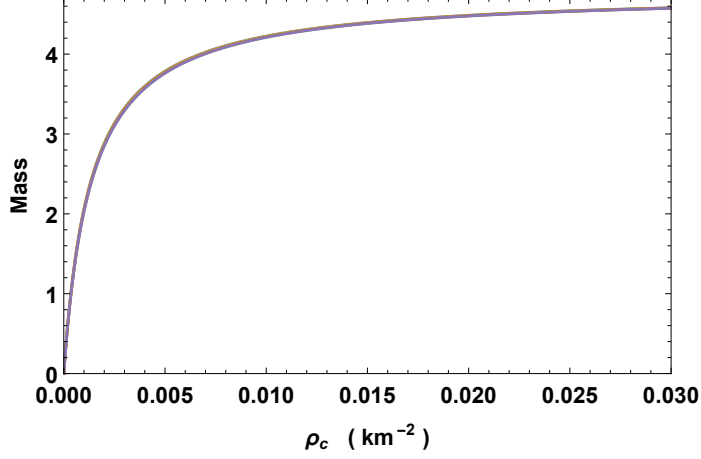
Figure 4.11: Variation of mass with central density for the neutron star in Vela X-1 with parameters $n = -2$ to -18, $b = 0.001/km^2$ and $R = 9.56km$.

For the solutions the mass as function of central density can be written as

$$M(\rho_c) = \frac{4\pi r^3 \rho_c \left[\cosh\left(bR^2 + c\right) + 1\right]^n}{8\pi R^2 \rho_c \left[\cosh\left(bR^2 + c\right) + 1\right]^n + 3(\cosh c + 1)^n}$$

(4.32)

$$\frac{\partial M}{\partial \rho_c} = \frac{12\pi R^3 \left[\cosh\left(bR^2 + c\right) + 1\right]^n}{(\cosh c + 1)^{-n}} \left[3(\cosh c + 1)^n\right.$$

$$\left. + 8\pi R^2 \rho_c \left\{\cosh\left(bR^2 + c\right) + 1\right\}^n\right]^{-2} > 0.$$

(4.33)

Referring to Fig. 4.11 we see that the solution fulfills this criterion.

Now the gravitational red-shift is given by

$$z(r) = e^{-\nu/2} - 1 = \left[-\frac{f(r)B\sqrt{ar^2\left(\cosh\left(br^2 + c\right) + 1\right)^n}}{b(n+1)r\sqrt{2 - 2\cosh\left(br^2 + c\right)}} + A\right]^{-1} - 1. (4.34)$$

The variation of red-shift is shown in Fig. 4.12.
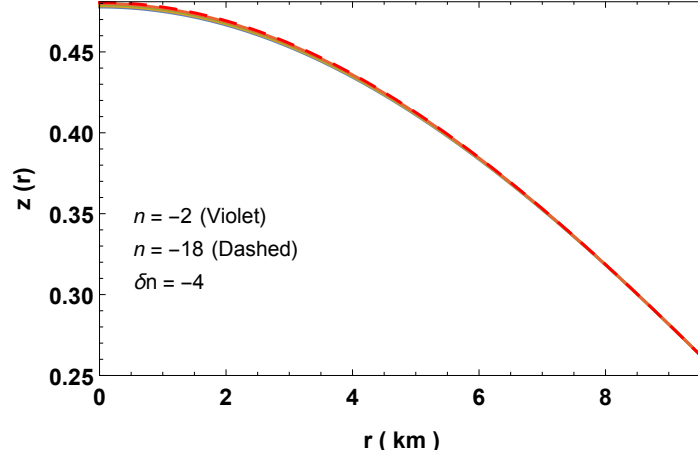
Figure 4.12: Variation of red-shift for the neutron star in Vela X-1 with parameters $n = -2$ to -18, $b = 0.001/km^2$, $c = 0.0001$, $M = 1.77M_\odot$ and $R = 9.56km$.

4.5.4 Maximum allowable mass and compactness factor

The mass function and compactness factor of the solution can be determined using the equations given below:

$$
m(r) = \int_0^r 4\pi\rho(r) \ r^2 \ dr = \frac{ar^3 \left[\cosh\left(br^2 + c\right) + 1\right]^n}{2ar^2 \left[\cosh\left(br^2 + c\right) + 1\right]^n + 2} \tag{4.35}
$$

$$
u(r) = \frac{2m(r)}{r} = \frac{ar^2 \left[\cosh\left(br^2 + c\right) + 1\right]^n}{ar^2 \left[\cosh\left(br^2 + c\right) + 1\right]^n + 1}. \tag{4.36}
$$
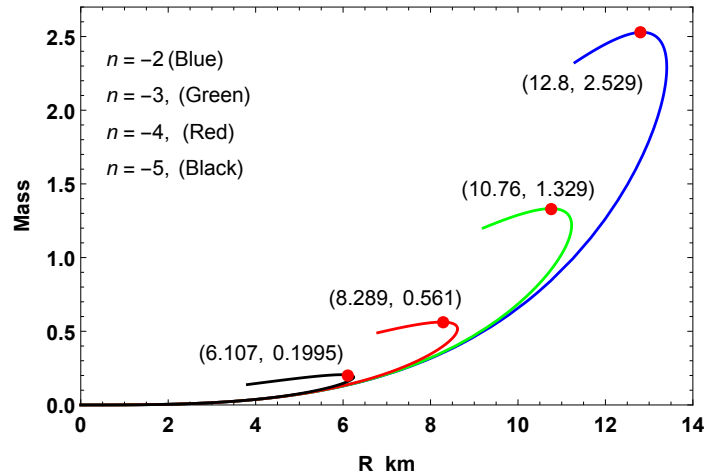
Figure 4.13: Variation of mass with radius for $a = 0.01$, $b = 0.001$ and $c = 0.0001$.

The surface redshift can be found as

$$z_s = e^{\lambda_b/2} - 1 = (1 - u_b)^{-1/2} - 1. \tag{4.37}$$

Using the Buchdahl limit i.e. $u = 8/9$, we get the maximum surface redshift $z_s(max) = 2$. When the compactness parameter is zero, the surface redshift is also zero. As the compactness parameter reaches the Buchdahl limit i.e. $u = 8/9$ the surface redshift will be exactly 2, however, if the compactness parameter is beyond the Buchdahl limit the surface redshift blow-up. This is because of the formation of singularity. However, Ivanov [2002a] has derived that that for a realistic anisotropic star models the surface redshift z_s cannot go beyoond to 5.211 (this value corresponds to a model without cosmological constant).

4.6 Slow rotation approximation, moment of inertia and Kepler frequency

For a uniformly rotating star with angular velocity Ω, the moment of inertia is given by

$$I = \frac{8\pi}{3} \int_0^R r^4 (\rho + p_r) e^{(\lambda - \nu)/2} \, \frac{\omega}{\Omega} \, dr \tag{4.38}$$

where, the rotational drag ω satisfy the Hartle's equation

$$\frac{d}{dr} \left(r^4 j \, \frac{d\omega}{dr} \right) = -4r^3 \omega \, \frac{dj}{dr}. \tag{4.39}$$

with $j = e^{-(\lambda+\nu)/2}$ which has boundary value $j(R) = 1$. The approximate solution of moment of inertia I up to the maximum mass M_{max} was given by Bejger and Haensel [2002] as

$$I = \frac{2}{5} \Big(1 + x \Big) MR^2, \tag{4.40}$$

where parameter $x = (M/R) \cdot km/M_\odot$. For the solution we have plotted mass vs I in Fig. 4.14 that shows as n increases, the mass also increase and the moment of inertia increases till up to certain value of mass and then decreases. Comparing Figs. 4.13 and 4.14 we can see that the mass corresponding to I_{max} is not equal to M_{max} from $M - R$ diagram. In fact the mass corresponding to I_{max} is lower by $\sim 1.46\%$ from

96

4.6. Slow rotation approximation, moment of inertia and Kepler frequency

the M_{max}. This happens to the EoSs without any strong high-density softening due to hyperonization or phase transition to an exotic state (Bejger et al. [2005]). Using this graph we can estimate the maximum moment of inertia for a particular compact star or by matching the observed I with the $I_{\max}$ we can determine the validity of a model.

A rotating compact star can hold higher M_{max} than non-rotating one. The mass relationship between non-rotating and rotating is given by (in the unit $G = C = 1$) can be written as (Ghosh [2007])

$$M_{rot} = M_{non-rot} + \frac{1}{2} I \Omega^2. \tag{4.41}$$

Due to centrifugal force, the radius at the equator increases as some factor as compare to the static one. Cheng and Harko [2000] find out the approximate radius formulas for static and rotating stars as $R_{rot}/R_{non-rot} \approx 1.626$. Assuming the compact star is rotating in Kepler frequency $\Omega_K = (GM_{non-rot}/R^3_{non-rot})^{1/2}$ and on using the Cheng-Harko formula we have plotted the $M - R$ for rotating and non-rotating (Fig. 4.15). The corresponding frequency of rotating can be determined as (Haensel et al. [1995])

$$\nu \approx 1.22 \left(\frac{R_{non-rot}}{10km} \right)^{-3/2} \left(\frac{M_{non-rot}}{M_\odot} \right)^{1/2} \ kHz. \tag{4.42}$$

The variation of frequency with mass is shown in Fig. 4.16. It shows that the frequency of rotation corresponding to maximum mass. On the other hand, we would like to mention that recently, the direct detection of the gravitational wave (GW) signal $GW170817$ has been reported by the LIGO-Virgo collaboration from a binary compact star system (Abbott et al. [2017]). New constraints for the tidal deformability of the 1.4 solar mass compact stars ($\Lambda_{1.4}$) have been estimated as $\Lambda_{1.4} < 800$ (Zhou et al. [2019]), which can also put constraints on the equation of state (EOS) for the star matter and constrain the parameter sets for phenomenological models. In the works Zhou et al. [2018], Chu et al. [2019], Rhoades and Ruffini [1974], the researchers have used different phenomenological models to calculate the properties of the tidal deformability and the maximum mass of neutron stars or quark stars with the constraints of $GW170817$, which can provide another alternative methods
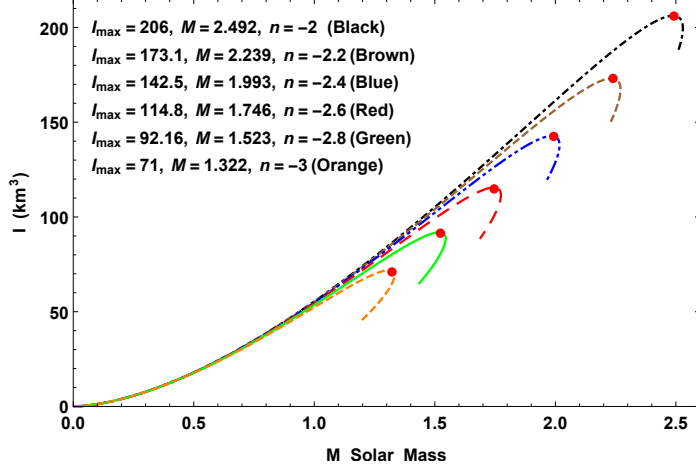
Figure 4.14: Variation of moment of inertia with mass for $n = -2$ to $n = -3$ taking $a = 0.01/km^2$, $b = 0.001/km^2$, $c = 0.0001$.
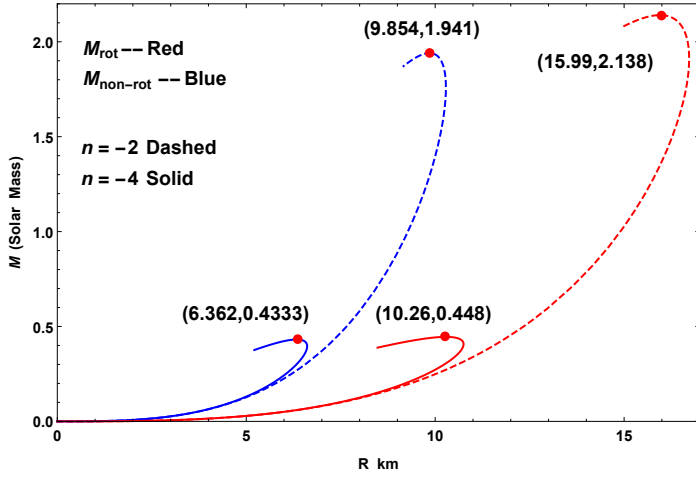
Figure 4.15: Variation of mas with radius for $n = -2$ & $n = -4$ taking $a = 0.01/km^2$, $b = 0.001/km^2$, $c = 0.0001$ for rotating and non-rotating star.

Table 4.1: Central and surface values of some parameters for different values of n.

n	a	A	B	M $M_\odot$	R km	z_c	$\rho_c \times 10^{14}$ g/cc	$\rho_s \times 10^{14}$ g/cc	$p_c \times 10^{34}$ $dyne/cm^2$	Γ_{rc}
-2	0.0259	0.6766	0.03183	1.77	9.56	0.477	10.44	4.89	5.31	1.91
-6	0.4170	0.6763	0.03183	1.77	9.56	0.478	10.50	4.85	5.22	1.93
-10	6.7279	0.6759	0.03183	1.77	9.56	0.479	10.59	4.81	5.13	1.95
-14	108.55	0.6756	0.03183	1.77	9.56	0.480	10.68	4.76	5.04	1.98
-18	1751.4	0.6753	0.03183	1.77	9.56	0.481	10.77	4.71	4.94	2.00
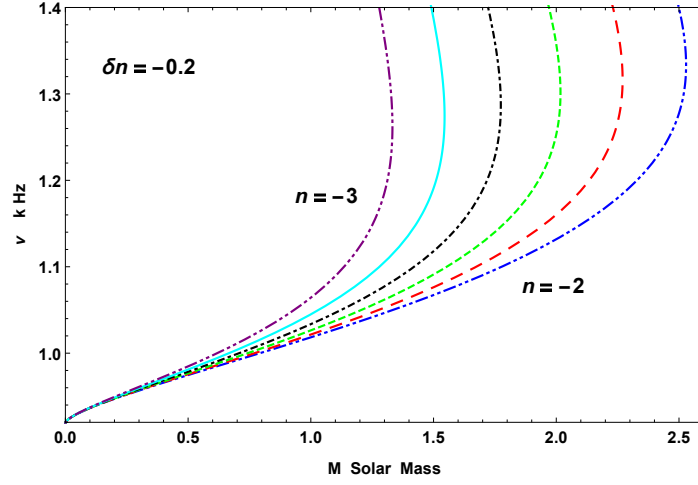
Figure 4.16: Variation of rotational frequency with mass for $n = -2$ to $n = -3$ taking $a = 0.01/km^2$, $b = 0.001/km^2$, $c = 0.0001$ for rotating and non-rotating star.

to constrain the parameter sets in the models.

4.6.1 Energy conditions

Any physical solutions other than those represent exotic matters, must fulfills the energy conditions i.e. strong, weak, null and dominant energy conditions which can be stated as,

$$\text{NEC} \quad : \quad T_{\mu\nu}l^{\mu}l^{\nu} \geq 0 \text{ or } \rho + p_i \geq 0 \tag{4.43}$$

$$\text{WEC} \quad : \quad T_{\mu\nu}t^{\mu}t^{\nu} \geq 0 \text{ or } \rho \geq 0, \ \rho + p_i \geq 0 \tag{4.44}$$

$$\text{SEC} \quad : \quad T_{\mu\nu}t^{\mu}t^{\nu} - \frac{1}{2}T_{\lambda}^{\lambda}t^{\sigma}t_{\sigma} \geq 0 \text{ or } \rho + \sum_{i} p_i \geq 0. \tag{4.45}$$

$$\text{DEC} \quad : \quad T_{\mu\nu}t^{\mu}t^{\nu} \geq 0 \text{ or } \rho \geq |p_i| \ \text{ where } \ T^{\mu\nu}t_{\mu} \in \text{nonspace-like vector.} \tag{4.46}$$

where $i \equiv (radial\ r, transverse\ t)$, t^{μ} and l^{μ} are time-like vector and null vector respectively.

Since the pressures and density are positive throughout within the stellar objects. Then it is obvious that the energy conditions NEC, WEC and SEC will automatically satisfy. We have shown the graphical representation for dominant energy conditions in Figs. 4.17-4.19 where it can be observed that our solutions also hold good for dominant energy conditions.
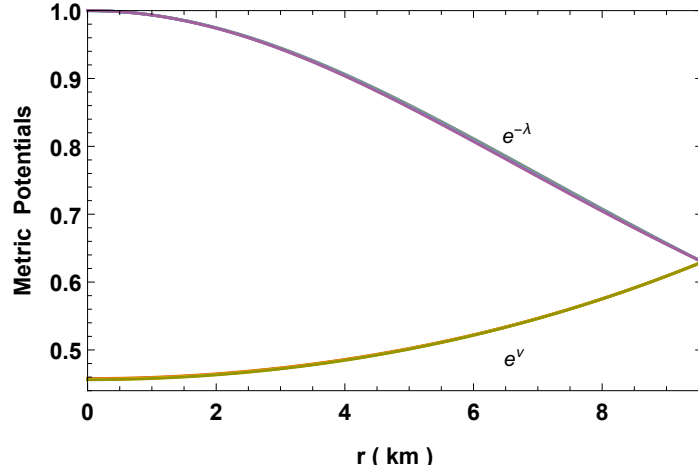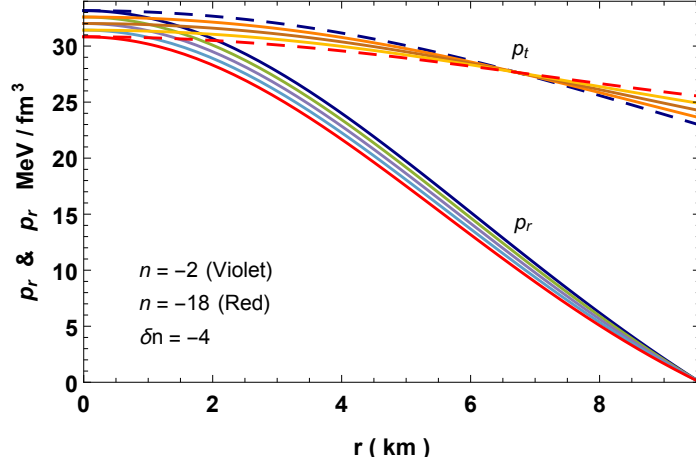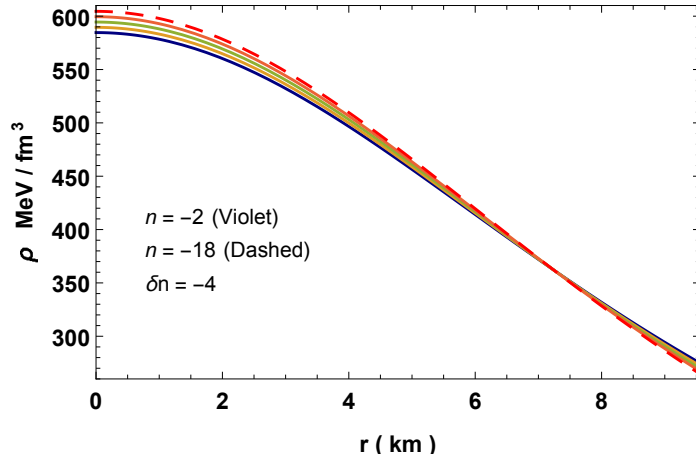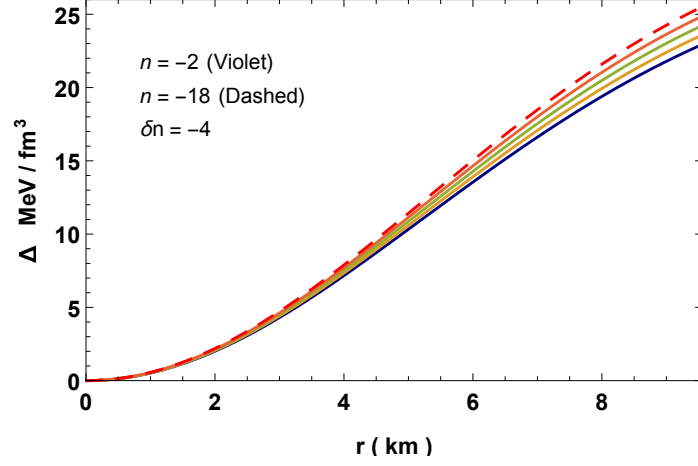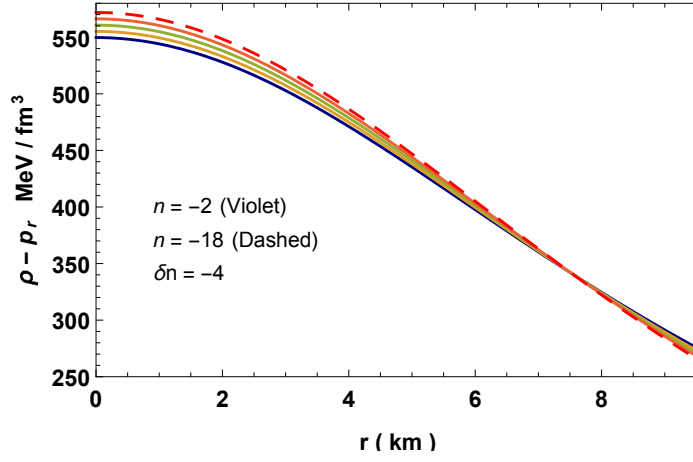
Figure 4.17: Variation of $\rho - p_r$ for the neutron star in Vela X-1 with parameters $n = -2$ to -18, $b = 0.001/km^2$, $c = 0.0001$, $M = 1.77M_\odot$ and $R = 9.56km$.
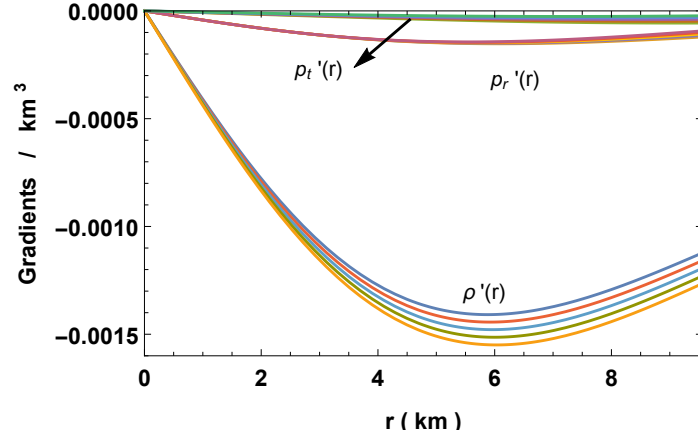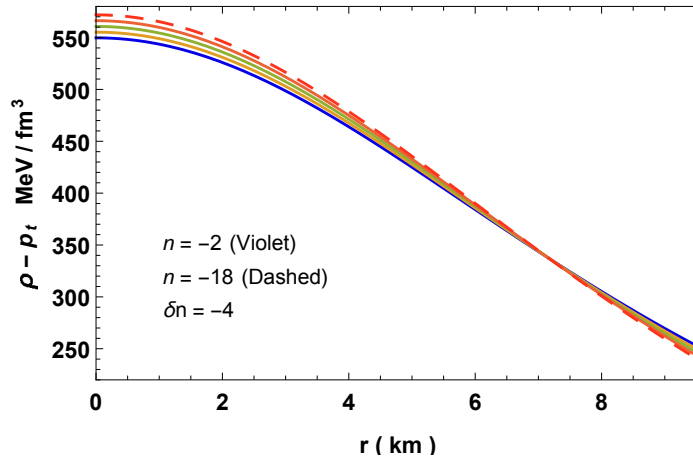

Figure 4.18: Variation of $\rho - p_r$ for the neutron star in Vela X-1 with parameters $n = -2$ to -18, $b = 0.001/km^2$, $c = 0.0001$, $M = 1.77M_\odot$ and $R = 9.56km$.

Figure 4.19: Variation of $\rho - p_r$ for the neutron star in Vela X-1 with parameters $n = -2$ to -18, $b = 0.001/km^2$, $c = 0.0001$, $M = 1.77 M_{\odot}$ and $R = 9.56 km$.

4.7 Results and conclusion

A new family of non-singular solutions of the Einstein field equations for compact stars under embedding class one condition is presented. The thermodynamical quantities for stellar matter like anisotropic pressures, baryon density, red-shift and the velocity of sound have been investigated using the Karmarkar condition of embedding class one spacetime.

Based on various physical analysis such as equilibrium condition (TOV-equation), static stability criterion ($\partial M/\partial \rho_c > 0$), Bondi condition ($\Gamma_r > 4/3$), singularity free ($\rho_c$, $p_{rc} = p_{tc} > 0$), Zeldovich condition ($p_{rc}/\rho_c < 1$) and satisfaction of energy conditions imply that the new family of solutions is possible to represent realistic matter. Therefore, these solutions are suitable to model physical compact stars.

For $n = 0$, some parts of the stability factor becomes positive, resulting instability in the model. However, beyond $n = -18$, the stability factor turns out to be stable. From Fig. 4.10, one can observe that as n decreases from -2 to -18, the peak of the F_g increases, F_h is almost same from center upto about 4 km and show significant increment till the surface. However, F_a decreases as n approaches to -18. Using the Buchdahl limit, we get the maximum surface red-shift $z_s(max) = 2$. For zero value of the compactness parameter, the surface red-shift is also zero. As the compactness parameter reaches the Buchdahl limit, the surface red-shift becomes exactly 2. However, if the compactness parameter is beyond the Buchdahl limit, then because of the formation of singularity the surface red-shift blows up. The unique

character of these solutions can be observed from the fact that for large range of parameter n, the profiles of density, pressures, equation of state parameters and speed of sounds seem to be different, however, the profiles of adiabatic index, mass with central density and red-shift are not very different. This signifies the fact that for modeling compacts various choices of equation of state (EoS) can be made for a single compact star. These choices of EoS lead to various structure of interior space-times, however, look the same physical properties like mass, radius, luminosity etc. to an external observer. It is to be noted form Fig. 4.13 that for larger values of parameter n leads to smaller M_{max} and R_{max}. From Fig. 4.13, we can see that for $n = -2$ the values of $(M_{max},\ R_{max})$ are (12.8 km, $2.529 M_\odot$) which is under the theoretical limit proposed by Rhoades and Ruffini [1974], while for $n = -5$, the values are (6.107 km, $0.1995 M_\odot$). But in recent studies, the heavy pulsars such as PSR J1614-2230, PSR J0348+0432 and MSR J0740+6620 were discovered in the works of Demorest et al. [2010], Antoniadis et al. [2013], Cromartie et al. [2020a], which has set the new record of the maximum mass of the pulsars. Further, from Fig. 4.7, it is also clear that the values of v_r^2 and v_t^2 are maximum for $n = -2$. Therefore, we can conclude that the stiffness of the equation of state reduces as n increases. The sensitivity to EoS is sharper in $M - I$ graph than $M - R$ because the peak points in these graphs are more sharper in the former graph than the later. After the complete analysis of the solutions with various mathematical and graphical representation, we can conclude that the solution is physically reasonable. With the inclusion of small rotation, we have also shown that the maximum mass that can hold by the system increases and the corresponding radius also increases due to the centrifugal force. For smaller values of n yields more M_{max}. The corresponding frequency of rotation can also be determined using Haensel et al. formula (Haensel et al. [1995]).

4.8   Generating functions

Herrera et al. [2008] proposed an algorithm for generating all types of spherically symmetric static solutions using two physical quantities namely anisotropy and function related to redshift function. These two generator are defined as

$$\zeta(r) = \frac{\nu'}{2} + \frac{1}{r} \quad \text{and} \quad \Pi(r) = 8\pi(p_r - p_t). \tag{4.47}$$

4.8. Generating functions

For this solution, they are found to be

$$
\begin{aligned}
\zeta(r) &= \frac{1}{r} + 4bB(n+1)r^2 \sinh^2\left[\frac{1}{2}\left(br^2 + c\right)\right] \\
&\quad \sqrt{a\left(\cosh\left(br^2 + c\right) + 1\right)^n}\left[B\sinh\left(br^2 + c\right)\right. \\
&\quad \overline{\sqrt{2 - 2\cosh\left(br^2 + c\right)}\sqrt{ar^2\left(\cosh\left(br^2 + c\right) + 1\right)^n}} \\
&\quad {}_2F_1\left[\frac{1}{2}, \frac{n+1}{2}; \frac{n+3}{2}; \cosh^2\left(\frac{1}{2}\left\{br^2 + c\right\}\right)\right] + \\
&\quad \left. 4Ab(n+1)r \sinh^2\left(\frac{1}{2}\left\{br^2 + c\right\}\right)\right]^{-1} \\
\Pi(r) &= -\Delta(r).
\end{aligned}
$$

$$(4.48)$$

$$(4.49)$$

Chapter 5

A generalized Finch-Skea class one static solution [1]

5.1 Introduction

It is well known that Einsteins general theory of relativity has fruitfully explained about several observations or cosmological measures including astrophysical backgrounds (Tipler et al. [1980], Shapiro and Teukolsky [2008]). The golden age of cosmology saw the theory of Hubble, the material, the biological structure, the nuclear synthesis, as well as the higher level of precision in explaining the potential origin of the universe and its subsequent evolution. Basically Einstein general theory of relativity is generalization of Newtonian gravity which is mainly suitable to describe the structure of compact star in the strong gravitational fields. Few of these compact objects like pulsars, black holes and neutron stars have densities of the order greater than or equal $10^{14} gm/cm^3$. The Schwarzschild has discovered the first precise solution of Einstein field equations for the gravitational field in the inner part of a non-circular spherical body consisting of a non-compressible fluid. This is also known as constant density solution with outer being empty and has zero pressure at the surface. Now a days, the researcher are busy on the study of relativistic compact stars. For object modeling, we study the solutions of Einstein's equations of static spherically symmetric with different physical causes. These solution may be stated as perfect fluid, anisotropic fluid, and dust. However, there are strong theoretical evidence that steep excessive dense celestial bodies are not made of perfect fluids.

---

[1]Content of this chapter has been published in *European Physics C* (Springer), 79 (2019) 381.

In some cases, the objects with different physical phenomena are found, for example anisotropy. The first theoretical attempt to look at the effect of variance was seen in about 1922 when Jeans [1922] looked anisotropic pressure on the self-gravitating bodies of Newtonian configurations.

After this, Ruderman [1972] has studied the effect of the anisotropy. He said that the stars may have anisotropic characteristics at very high density of the order $10^{15}gm/cm^3$ where the nuclear interaction becomes relativistic. Sudden after, Bowers and Liang [1974] studied about confined properties of relativistic anisotropic matter distribution for static spherically symmetric configurations, which is comprehensively populated. Recently, An extensive research was conducted in the study of physics related to anisotropic pressures.In this connection, Dev and Gleiser [2002, 2003] have shown that pressure variation affects the physical properties of mass, structure and excessive pressure areas. Also there are other several analytical static solutions have been already discovered by several authors (Herrera and de León [1985], Maurya et al. [2016b,a,c], Deb et al. [2017], Gupta and Maurya [2011], Mak and Harko [2003]). Most pioneering work by Herrera and Santos [1997] where they have specified about effect of local anisotropy in self gravitating systems. More remarkably, the algorithm for all possible static isotropic, anisotropic as well as charged anisotropic solutions of Einstein's equation for the spherically symmetric line element can be attractively determined by a general procedure which are given in Refs. Lake [2003], Herrera et al. [2008].

It is essential to note that the redshift and mass of the stellar model both varies with the anisotropy. Recently, an extensive efforts have been made in the modeling of physical observed astronomical objects in the existence of anisotropy which can be seen in recent research papers Sharma and Ratanpal [2013], Ngubelanga et al. [2015], Murad and Fatema [2015b,a] and the references therein. In these recent papers, the physical analysis reaffirms the significance of the presence of a non-zero anisotropy in the modeling of astrophysical objects. In order to create a substantially reliable object, it is necessary to find an analytical solution of Einstein field equations for relativistic matter distribution which can be solved by restricting the space-time geometry or stating an equation of state (EOS) of the matter distribution. On the other hand, we can generate the exact solution of relativistic field equation using another different approach known as embedding class one condition. In this connection, Riemann has presented the idea, known as Riemannian geometry, to study the essential geometric properties of the objects. Immediately after this, Schlaefli [1871] estimated

that a Riemannian manifold of metric which is analytic with positively defined signature can be embedded locally and isometrically into the higher dimensional flat Euclidean space.

The idea of embedding locally and isometrically an n-dimensional Riemannian manifold V_n into an $N = n(n+1)/2$ dimensional pseudo-Euclidean space was proved in the past by authors Janet [1927], Cartan [1927], Burstin [1931]. The embedding class p of V_n is the minimum number of extra dimensions required by the pseudo-Euclidean space, which is obviously equal to $p = N - n = n(n-1)/2$. As we know, general theory of relativity deals only with four dimensional spacetime, however embedding class solution may provide new characteristics to gravitational field, as well to physics. In case of relativistic space time V_n, the embedding class p turns out to be $p = 6$. In particular the classes of spherical and plane symmetric space-time are $p = 2$ and $p = 3$ respectively. The famous Friedman-Robertson-Lemaitre spacetime, is of class $p = 1$, while the Schwarzschilds exterior and interior solutions are of class $p = 2$ and class $p = 1$ respectively, moreover Kerr metric is class 5. In the literature Barnes [1974], Kumar et al. [2010], Barnes [2011], de Leon [2015], Akbar [2017], Abbas et al. [2018], Kuhfittig [2018], Kuhfittig and Gladney [2018], there are many interesting work concerning the effects of the technique of embedding of lower dimensional Riemannian space into the higher dimensional pseudo-Euclidean space in the framework of GR. The main consequence of embedding a Riemannian variety corresponding to a spherically symmetric and static spacetime into a pseudo Euclidean space is the so-called Eisland condition. This condition links both metric potentials e^ν and e^λ into a single differential equation. It is a mathematical simplification which reduces the problem of obtaining exact solutions to a single-generating function. The approach is to choose one of the gravitational potentials on physical grounds and to then integrate the Eisland condition to fully specify the gravitational behavior of the model. In this paper we utilize Eisland condition to derive solutions which describe compact objects in general relativity. We subject our solutions to rigorous physical tests which ensure that they do describe physically observable objects in the universe.

This chapter is organized as follows: In Sec. 5.2 we have specified the interior space time and Einstein field equations for anisotropic matter distribution. This section also includes the embedding class one condition along with non-vanishing Riemannian tensor for interior space time. In the next section 5.3, we have presented a generalized Finch-Skea solution for anisotropic matter distribution using the class one condition. The nonsingular nature of pressures, density and bounds of the constant are given

in Sec. 5.4. In Sec. 5.5, we presents the necessary and sufficient conditions to determine all possible constant parameters that describe the anisotropic solution. For this purpose, we match our interior space-time to the exterior space-time (Schwarzscild metric). The section 5.6 includes the energy conditions. In Sec. 5.7, we have discussed the most important features of the objects like equilibrium condition via. Tolman-Oppenhimer-Volkoff equation, Causality and stability condition through Herrera Aberu criterion, adiabatic index and Harrison-Zeldovich-Novikov static stability criterion.

5.2 Interior space-time and field equations

The interior space-time for spherically symmetric space-time is chosen as,

$$ds^2 = e^{\nu(r)}dt^2 - e^{\lambda(r)}dr^2 - r^2\left(d\theta^2 + \sin^2\theta\ d\phi^2\right) \tag{5.1}$$

where ν and λ are functions of the radial coordinate 'r' only.

The Einstein's field equations corresponding an anisotropic fluid distribution becomes

$$R^\mu_\nu - \frac{1}{2}g^\mu_\nu\mathcal{R} = -8\pi\left[(p_t + \rho c^2)v^\mu v_\nu - p_t g^\mu_\nu + (p_r - p_t)\chi_\nu\chi^\mu\right] \tag{5.2}$$

where the symbols have their usual meanings.

For the space-time (5.1), the field equations can be written as

$$\frac{1 - e^{-\lambda}}{r^2} + \frac{e^{-\lambda}\lambda'}{r} = 8\pi\rho \tag{5.3}$$

$$\frac{e^{-\lambda} - 1}{r^2} + \frac{e^{-\lambda}\nu'}{r} = 8\pi p_r \tag{5.4}$$

$$e^{-\lambda}\left(\frac{\nu''}{2} + \frac{\nu'^2}{4} - \frac{\nu'\lambda'}{4} + \frac{\nu' - \lambda'}{2r}\right) = 8\pi p_t. \tag{5.5}$$

The measure of anisotropy is defined as $\Delta = 8\pi(p_t - p_r)$.

On the other hand, It was proved by Eisenhart [1966] that an embedding class 1 space (A $(n+1)$ dimensional space V^{n+1} can be embedded into a $(n+2)$ dimensional pseudo-Euclidean space E^{n+2}) can be described by a $(n+1)$ dimensional space V^{n+1} if there exists a symmetric tensor a_{mn} which satisfies the following Gauss- Codazzi

equations:

$$R_{mnpq} = 2 \, e \, a_{m\,[p}a_{q]n}$$

$$\text{and} \quad a_{m[n;p]} - \Gamma^q_{[n\,p]} \, a_{mq} + \Gamma^q_{m\,[n} \, a_{p]q} = 0, \tag{5.6}$$

where $e = \pm 1$, R_{mnpq} denotes the curvature tensor and square brackets represent antisymmetrization. Here, a_{mn} are the coefficients of the second differential form. Moerover, A necessary and sufficient condition for the embedding class I of Eq. (5.6) in a suitable convenient form was given by Karmarkar [1948] as

$$R_{0101}R_{2323} = R_{0202}R_{1313} - R_{1202}R_{1303}. \tag{5.7}$$

The non-vanishing components of Riemannian tensor for the spherically symmetric interior space-time (5.1) are given as

$$R_{0101} = -\frac{1}{4}\,\mathrm{e}^{\nu}\left(-\nu'\lambda' + \nu'^2 + 2\,\nu''\right),$$

$$R_{2323} = -r^2\sin^2\theta\left(1 - \mathrm{e}^{-\lambda}\right), \quad R_{0202} = -\frac{1}{2}\,r\nu'\mathrm{e}^{\nu-\lambda},$$

$$R_{1313} = -\frac{1}{2}\,\lambda' r\sin^2\theta, \quad R_{1202} = 0, \quad R_{1303} = 0 \tag{5.8}$$

By plugging the values of above Riemannian components into Eq. (5.7) we obtain a differential equation in ν and λ of the form

$$(\lambda' - \nu')\,\nu'\,\mathrm{e}^{\lambda} + 2\,(1 - \mathrm{e}^{\lambda})\nu'' + \nu'^2 = 0. \tag{5.9}$$

The solutions Eq. (5.9) of are named as 'embedding class one solution" and they can be embedded in five dimensional pseudo-Euclidean space.

On integration of Eq. (5.9) we get

$$e^{\nu} = \left(A + B\int\sqrt{e^{\lambda} - 1}\,dr\right)^2 \tag{5.10}$$

where A and B are constants of integration.

By using (5.10) we can express the anisotropy as (Maurya et al. [2015b])

$$\Delta = \frac{\nu'}{4e^{\lambda}}\left[\frac{2}{r} - \frac{\lambda'}{e^{\lambda} - 1}\right]\left[\frac{\nu'e^{\nu}}{2rB^2} - 1\right]. \tag{5.11}$$

For isotropic case $\Delta = 0$ and there are three possible solutions when (a) $e^\nu = C$ and $e^\lambda = 1$ (not physical), (b) Schwarzschild interior solution (not physical) and (c) Kohler-Chao solution (cosmological solution as the pressure vanishes at $r \to \infty$).

5.3   A generalized solution for compact star model

Since the field equations depend on metric functions ν and λ. To construct a viable anisotropic model, we have assumed the generalized form of Finch-Skea metric (Finch and Skea [1989]) function g_{rr} as

$$\lambda \;\; = \;\; \ln(1 + ar^2 + b^{n-1}r^n) \tag{5.12}$$

where a and b are non-zero positive constants and n is a positive integer. It is note that Finch and Skea [1989] have used above metric function g_{rr} corresponding $b = 0$ to solve Einstein field equations. The choice of this gravitational potential g_{rr} is well motivated particularly they have shown that the solution is regular and physically realistic for the some range of parameters as well as a good approximation to a neutron star model (specially in terms of predicting central densities of neutron stars) based on the relativistic mean field theory of Walecka [1975]. So, considering it we have generalized this gravitational potential g_{rr} by introducing another parameter b with the radial coordinate r which will provide a class of solution for compact stars, along this the energy density, radial and tangential pressure are decreasing outward.

By substituting the value of λ from Eq. (5.12) into Eq. (5.10) we get

$$
e^\nu \;\; = \;\; \left(A - \left\{ 2B \left[ab(n-2)r^2 f(r)\sqrt{ab^{1-n}r^{2-n} + 1} + \right. \right. \right.
$$
$$
\left. \left. \left. (6-n)\left(abr^2 + b^n r^n\right) \right] \right\} \frac{(a + b^{n-1}r^{n-2})^{-1/2}}{b(n-6)(n+2)} \right)^2 \tag{5.13}
$$

where $f(r) = {}_2F_1\left(\frac{1}{2}, \frac{n-6}{2(n-2)}; \frac{10-3n}{4-2n}; -ab^{1-n}r^{2-n}\right)$ is known as Gauss hypergeometric function. The behaviour of the metric potentials are plotted in Fig. 5.1.

By using the metric potentials ν and λ, we directly obtain the expression for thermodynamic variables like density, radial and transverse pressure and anisotropy

5.3. A generalized solution for compact star model

as

$$
8\pi\rho(r) = \frac{1}{\left(ar^2 + b^{n-1}r^n + 1\right)^2}\left[a^2r^2 + a\left(2b^{n-1}r^n + 3\right) + b^{n-1}r^{n-2}\right.
$$
$$
\left.\left(b^{n-1}r^n + n + 1\right)\right] \tag{5.14}
$$

$$
8\pi p_r(r) = \left[(n-6)b^n k(r)r^n\left\{b\left[2Br\left(ar^2 - n - 2\right) + A(n+2)j(r)\right] + 2Bb^n r^{n+1}\right\}\right.
$$
$$
\left. -2abB(n-2)r^3 f(r)(abr^2 + b^n r^n)\right]\left[(6-n)\left\{2abBr^3 + Ab(n+2)j(r) + \right.\right.
$$
$$
\left.\left. 2Bb^n r^{n+1}\right\} + 2abB(n-2)r^3 f(r)k(r)\right]^{-1}\frac{b^{-n}r^{-n-2}\left(abr^2 + b^n r^n\right)}{k(r)\left(abr^2 + b^n r^n + b\right)} \tag{5.15}
$$

$$
\Delta(r) = \frac{k(r)l(r)q(r)}{2r^2 p(r)\left(abr^2 + b^n r^n\right)\left(abr^2 + b^n r^n + b\right)^2} \tag{5.16}
$$

$$
8\pi p_t(r) = 8\pi p_r + \Delta. \tag{5.17}
$$

where,

$$
j(r) = \sqrt{ar^2 + b^{n-1}r^n} \tag{5.18}
$$
$$
k(r) = \sqrt{ab^{1-n}r^{2-n} + 1} \tag{5.19}
$$
$$
l(r) = 2a^2 b^2 r^4 + 4ab^{n+1}r^{n+2} + b^n r^n\left[2b^n r^n + b(2-n)\right] \tag{5.20}
$$
$$
n(r) = b\left[Br(2ar^2 - n - 2) + A(n+2)j(r)\right] + 2Bb^n r^{n+1} \tag{5.21}
$$
$$
q(r) = 2abB(2-n)r^3 f(r)\left[abr^2 + b^n r^n\right] + (n-6)b^n k(r)n(r)r^n \tag{5.22}
$$
$$
p(r) = (n-6)\left[2abBr^3 + Ab(n+2)j(r) + 2Bb^n r^{n+1}\right] + 2abB(2-n)
$$
$$
r^3 f(r)k(r). \tag{5.23}
$$

There variations of the above physical quantities are given in Figs. 5.2-5.4. We should ensure that values of p_r/ρ and p_t/ρ at the interior must be less than unity for a physical system (Fig. 5.5).

The other physical parameters mass, compactness factor and red-shift can be determine as

$$
m(r) = 4\pi\int r^2\rho\ dr = \frac{r}{2}\left(1 - \frac{b}{abr^2 + b^n r^n + b}\right) \tag{5.24}
$$
$$
u(r) = \frac{2m(r)}{r} = 1 - \frac{b}{abr^2 + b^n r^n + b} \tag{5.25}
$$
$$
z(r) = e^{-\nu/2} - 1. \tag{5.26}
$$

We have plotted the $M - R$ diagram in Fig. 5.6. Here we have determined the radius from surface density and determine the mass using this radius using the boundary condition. The trend of red-shift is plotted in Fig. 5.7.

5.4 Non-singular nature of the solution

To check the physical validity of the solution, we ensure that the central values of pressure and density must be finite i.e.

$$\rho_c \;=\; \frac{3a}{8\pi} > 0, \tag{5.27}$$

$$p_{rc} \;=\; p_{tc} = \frac{\sqrt{a}\,(2B - \sqrt{a}A)}{8\pi A} > 0. \tag{5.28}$$

It is also require to ensure that any physical fluid satisfies the Zeldovich's criterion i.e. $p_{rc}/\rho_c \leq 1$ which implies

$$\frac{p_{rc}}{\rho_c} = \frac{2B - \sqrt{a}A}{3\sqrt{a}A} \leq 1. \tag{5.29}$$

Now a physical constraint on B/A arises due to (5.28) and (5.29) as

$$\frac{\sqrt{2}}{a} < \frac{B}{A} \leq 2\sqrt{a}. \tag{5.30}$$

5.5 Boundary Conditions and determination of constants

It is necessary that we should match our interior space-time to the exterior Schwarzschild [1916b] line element

$$ds^2 \;=\; \left(1 - \frac{2m}{r}\right)dt^2 - \left(1 - \frac{2m}{r}\right)^{-1}dr^2 - r^2\big(d\theta^2 + \sin^2\theta\; d\phi^2\big) \tag{5.31}$$

at the boundary $r = R$. Also, the radial coordinate r must be greater than $2m$ so that it doesn't form a black hole.

Using the continuity of the metric coefficients e^ν and e^λ across the boundary $(r = R)$ and vanishing of radial pressure at the boundary $(r = R)$ we get the following

5.5. Boundary Conditions and determination of constants

equations

$$1 - \frac{2M}{R} = e^{\nu_s} = e^{-\lambda_s} \tag{5.32}$$

$$p_r(r = R) = 0. \tag{5.33}$$

On using the boundary conditions (5.32) and (5.33) we obtain the value of arbitrary constants as,

$$a = \frac{b^n(R - 2M)R^n - 2bM}{bR^2(2M - R)} \tag{5.34}$$

$$A = \sqrt{1 - \frac{2M}{R} + \frac{2BR^2}{b(n-6)(n+2)}} \Big[b(6-n) \sqrt{a + b^{n-1}R^{n-2}}$$

$$+ a(n-2)b^{\frac{3-n}{2}} f(R)R^{\frac{2-n}{2}} \Big] \tag{5.35}$$

$$B = \sqrt{1 - \frac{2M}{R}} \frac{b(6-n)(n+2)\sqrt{a + b^{n-1}R^{n-2}}}{2} \Big[2(n-6)b^n R^n + b(n-6)$$

$$\left(aR^2 - n - 2\right) - \frac{a(n-2)b^{1-n} f(R)R^{2-n} \left(abR^2 + b^n R^n\right)}{\sqrt{ab^{1-n}R^{2-n} + 1}} + ab(n-2)R^2$$

$$f(R)\sqrt{ab^{1-n}R^{2-n} + 1} + (6-n) \left(abR^2 + b^n R^n\right) \Big]^{-1} \tag{5.36}$$

Here M and R are chosen from observed values of compact stars and b as free parameter.
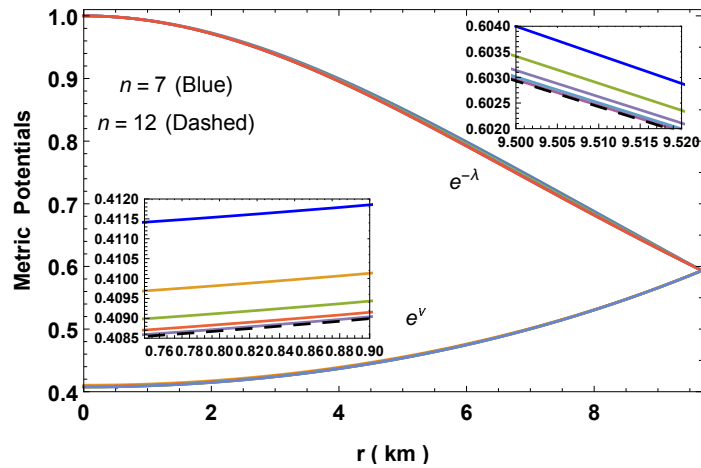
Figure 5.1: Variation of metric potentials w.r.t radial coordinate r for $M = 1.97M_\odot$, $R = 9.69km$ and $b = 0.04$.
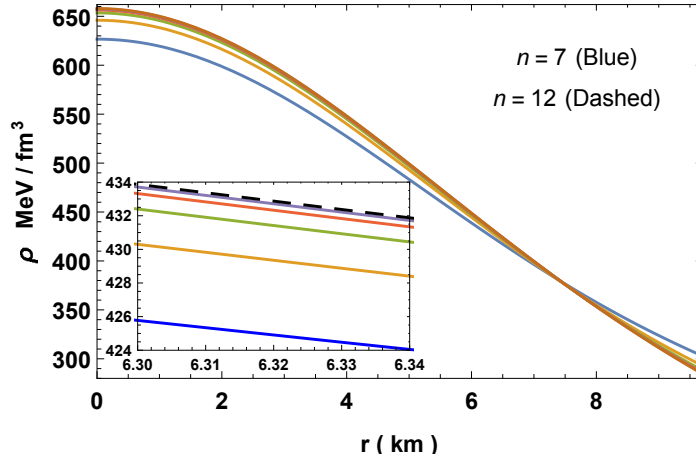
Figure 5.2: Density profile of PSR J1614-2230 for $M = 1.97 M_{\odot}, R = 9.69 km$ and $b = 0.04$.
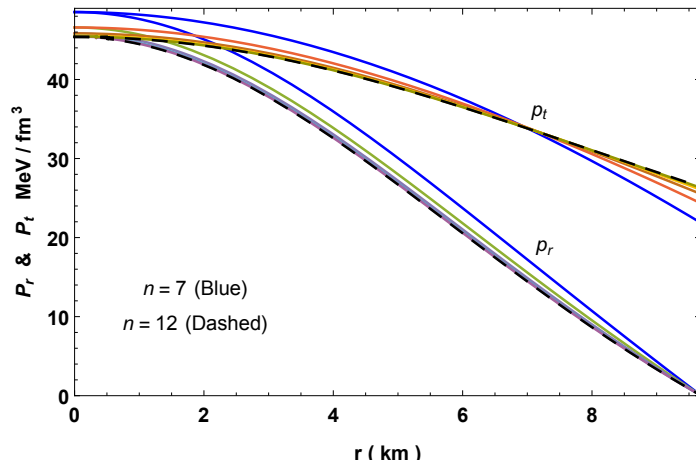
Figure 5.3: Radial and transverse pressure profile of PSR J1614-2230 for $M = 1.97 M_{\odot}, R = 9.69 km$ and $b = 0.04$.

5.6 Energy Conditions

In this section we are willing to verify the energy conditions namely null energy condition (NEC), dominant energy condition (DEC) and weak energy condition(WEC) at all points in the interior of a star which will be satisfied if the following inequalities hold simultaneously:

$$\text{WEC} \quad : \quad T_{\mu\nu}t^{\mu}t^{\nu} \geq 0 \text{ or } \rho \geq 0, \ \rho + p_i \geq 0 \tag{5.37}$$

$$\text{NEC} \quad : \quad T_{\mu\nu}l^{\mu}l^{\nu} \geq 0 \text{ or } \rho + p_i \geq 0 \tag{5.38}$$

$$\text{DEC} \quad : \quad T_{\mu\nu}t^{\mu}t^{\nu} \geq 0 \text{ or } \rho \geq |p_i| \ \text{ where } \ T^{\mu\nu}t_{\mu} \in \text{nonspace-like vector} \tag{5.39}$$

$$\text{SEC} \quad : \quad T_{\mu\nu}t^{\mu}t^{\nu} - \frac{1}{2}T_{\lambda}^{\lambda}t^{\sigma}t_{\sigma} \geq 0 \text{ or } \rho + \sum_i p_i \geq 0 \tag{5.40}$$

where $i \equiv (radial \ r, transverse \ t)$, t^{μ} and l^{μ} are time-like vector and null vector respectively.

We will check the energy conditions with the help of graphical representation. In Fig. 5.8, we have plotted the L.H.S of the above inequalities which verifies that all the energy conditions are satisfied at the stellar interior.
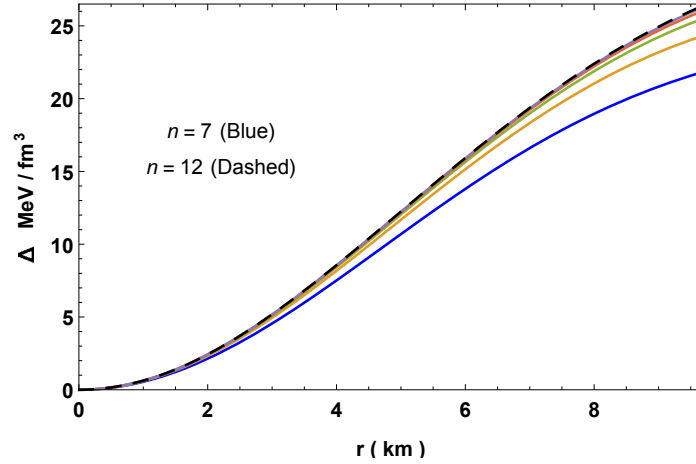
Figure 5.4: Anisotropy profile of PSR J1614-2230 for $M = 1.97M_{\odot}, R = 9.69km$ and $b = 0.04$.
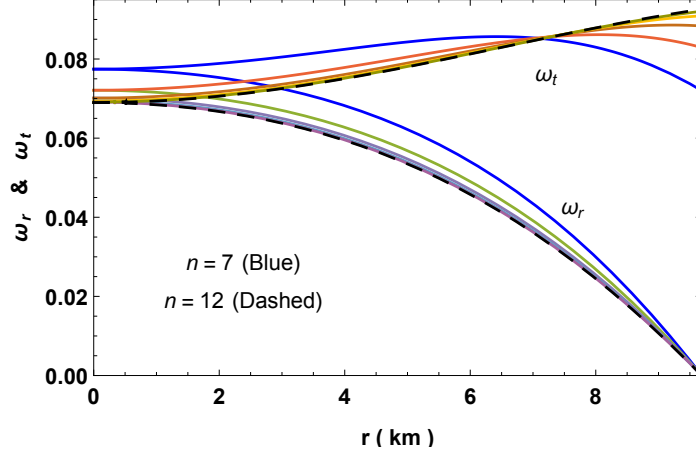
Figure 5.5: Equation of state parameter profiles of PSR J1614-2230 for $M = 1.97M_\odot, R = 9.69km$ and $b = 0.04$.

5.7 Stability and equilibrium of the model

5.7.1 Equilibrium under various forces

Equilibrium state under three forces *viz* gravitational, hydrostatics and anisotropic forces can be analyze whether they satisfy the generalized Tolman-Oppenheimer-Volkoff (TOV) equation or not and it is given by

$$-\frac{M_g(r)(\rho + p_r)}{r}e^{\frac{\nu-\lambda}{2}} - \frac{dp_r}{dr} + \frac{2}{r}(p_t - p_r) = 0, \tag{5.41}$$

where $M_g(r)$ represents the gravitational mass within the radius r, which can derived from the Tolman-Whittaker formula and the Einstein field equations and is defined by

$$M_g(r) = 4\pi \int_0^r \left(T_t^t - T_r^r - T_\theta^\theta - T_\phi^\phi\right) r^2 e^{\frac{\nu+\lambda}{2}} dr. \tag{5.42}$$

For the Eqs. (5.3)-(5.5), the above Eq. (5.42) reduced to

$$M_g(r) = \frac{1}{2}re^{(\lambda-\nu)/2}\,\nu'. \tag{5.43}$$

Plugging the value of $M_g(r)$ in equation (5.41), we get

$$-\frac{\nu'}{2}(\rho + p_r) - \frac{dp_r}{dr} + \frac{2}{r}(p_t - p_r) = 0. \tag{5.44}$$

5.7. Stability and equilibrium of the model
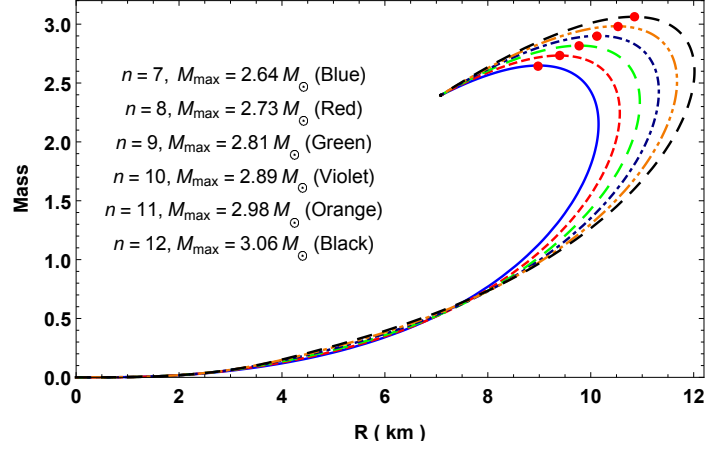
Figure 5.6: $M - R$ diagram for $a = 0.001$ and $b = 0.04$.
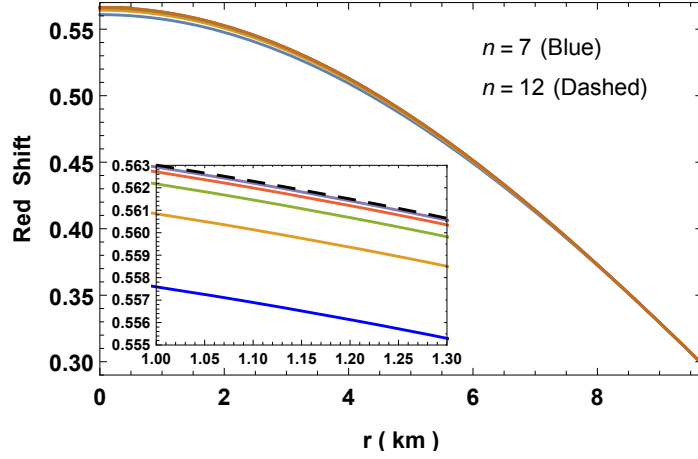
Figure 5.7: Red-shift profiles of PSR J1614-2230 for $M = 1.97 M_{\odot}, R = 9.69 km$ and $b = 0.04$.

The above expression may also be written as

$$F_g + F_h + F_a = 0, \tag{5.45}$$

where F_g, F_h and F_a represents the gravitational, hydrostatics and anisotropic forces respectively and can be written as,

$$F_g = -\frac{\nu'}{2}(\rho + p_r) \tag{5.46}$$

$$F_h = -\frac{dp_r}{dr} \tag{5.47}$$

$$F_a = \frac{2\Delta}{r}. \tag{5.48}$$

117
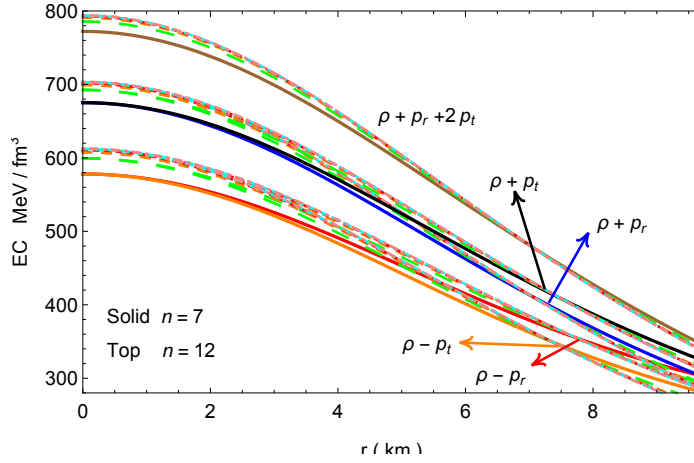
Figure 5.8: Energy Consitions of PSR J1614-2230 for $M = 1.97 M_{\odot}, R = 9.69 km$ and $b = 0.04$.
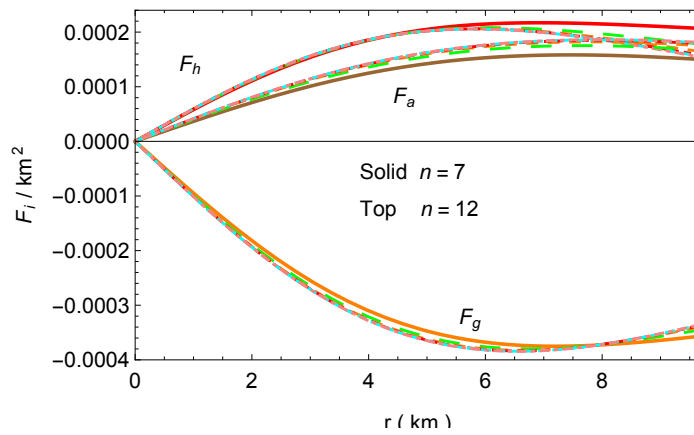
Figure 5.9: TOV-equation profile of PSR J1614-2230 for $M = 1.97 M_{\odot}, R = 9.69 km$ and $b = 0.04$.

5.7. Stability and equilibrium of the model

The profile of three different forces are plotted in Fig. 5.9 and we can see that the system is in equilibrium state.

5.7.2 Causality and stability condition

In this section we are going to find the subliminal velocity of sound and stability condition. For a physically acceptable model of anisotropic fluid sphere the radial and transverse velocities of sound should be less than 1, which is known as the causality condition. The radial velocity (v_{sr}^2) and transverse velocity (v_{st}^2) of sound can be obtained as

$$v_r^2 = \frac{dp_r}{d\rho} = \alpha \quad , \quad v_t^2 = \frac{dp_t}{d\rho}. \tag{5.49}$$

The profile of radial and transverse velocities of sound have been plotted in Fig. 5.10, the figure indicates that our model satisfies the causality condition. Now the stability condition proposed by Abreu et al. [2007] i.e. $-1 \leq v_t^2 - v_r^2 \leq 0$ (Fig. 5.11).
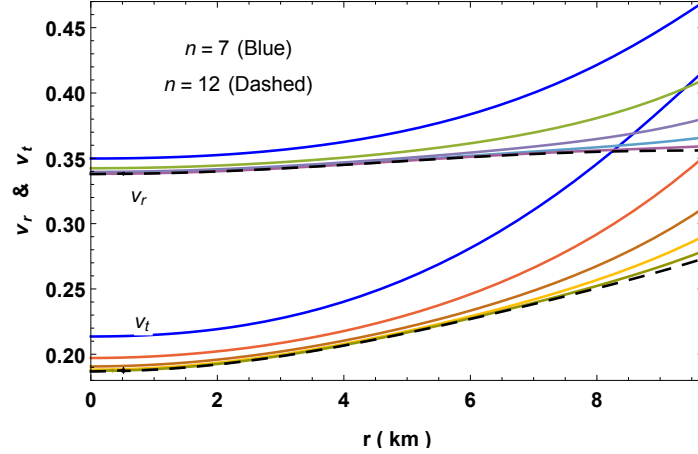
Figure 5.10: Velocity of sound profiles of PSR J1614-2230 for $M = 1.97 M_\odot, R = 9.69 km$ and $b = 0.04$.

5.7.3 Adiabatic index and stability condition

For a relativistic anisotropic sphere the stability is related to the adiabatic index Γ, the ratio of two specific heats, defined by (Chan et al. [1993]),

$$\Gamma_r = \frac{\rho + p_r}{p_r} \frac{dp_r}{d\rho}. \tag{5.50}$$
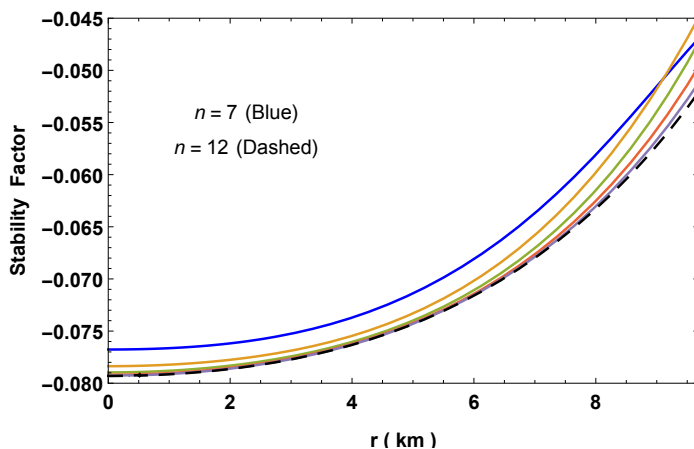
Figure 5.11: Stability factor $(v_t^2 - v_r^2)$ profiles of PSR J1614-2230 for $M = 1.97 M_\odot, R = 9.69 km$ and $b = 0.04$.

Now $\Gamma_r > 4/3$ gives the condition for the stability of a Newtonian sphere and $\Gamma = 4/3$ being the condition for a neutral equilibrium proposed by Bondi [1964]. This condition changes for a relativistic isotropic sphere due to the regenerative effect of pressure, which renders the sphere more unstable. For an anisotropic general relativistic sphere the situation becomes more complicated, because the stability will depend on the type of anisotropy. For an anisotropic relativistic sphere the stability condition is given by (Chan et al. [1993]),

$$\Gamma > \frac{4}{3} + \left[\frac{4}{3} \frac{(p_{ti} - p_{ri})}{|p'_{ri}|r} + \frac{8\pi}{3} \frac{\rho_i p_{ri}}{|p'_{ri}|} r \right]_{max}, \tag{5.51}$$

where, p_{ri}, p_{ti}, and ρ_i are the initial radial, tangential pressures and energy density in static equilibrium satisfying (5.41). The first and last term inside the square bracket represent the anisotropic and relativistic corrections respectively and both the quantities are positive that increase the unstable range of Γ (Herrera [1992], Chan et al. [1993]). For this solution the adiabatic index is more than $4/3$ and hence stable, Fig. 5.12.

5.7.4 Harrison-Zeldovich-Novikov static stability criterion

The stability analysis of Harrison et al. [1965] and Zeldovich and Novikov [1971] have shown that the adiabatic index of a pulsating star is same as in a slowly deformed matter. This leads to a stable configuration only if the mass of the star is increasing with central density i.e. $\partial m/\partial \rho_c > 0$ and unstable if $\partial m/\partial \rho_c < 0$.
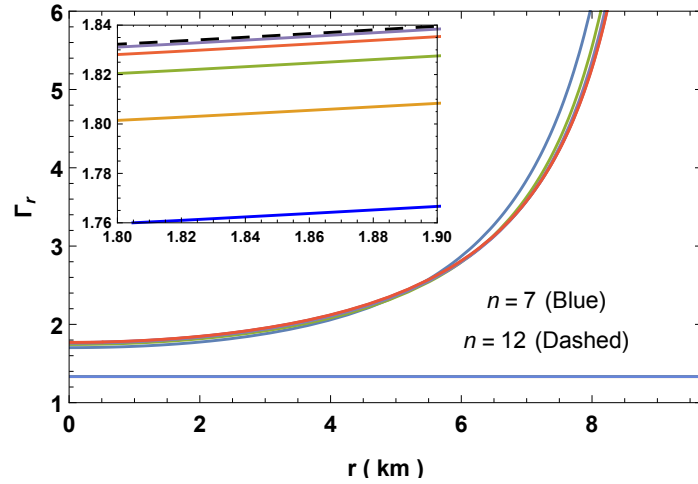
Figure 5.12: Adiabatic index profiles of PSR J1614-2230 for $M = 1.97M_\odot, R = 9.69km$ and $b = 0.04$.
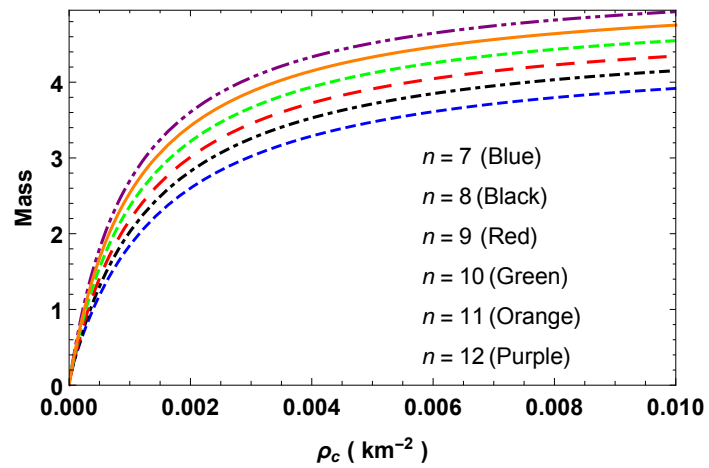
Figure 5.13: $M - \rho_c$ profiles with $R = 10.86km$ and $b = 0.04$.

In our solution, the mass as a function of central density can be written as

$$m(\rho_c) \;=\; \frac{R}{2}\left(1 - \frac{3b}{3b^n R^n + 8\pi b\rho_c R^2 + 3b}\right) \tag{5.52}$$

$$\frac{\partial m(\rho_c)}{\partial \rho_c} \;=\; \frac{12\pi b^2 R^3}{\left[3b^n R^n + b\left(8\pi\rho R^2 + 3\right)\right]^2} > 0. \tag{5.53}$$

$$\tag{5.54}$$

The satisfaction of the above condition is shown as a plot in Fig. 5.13.
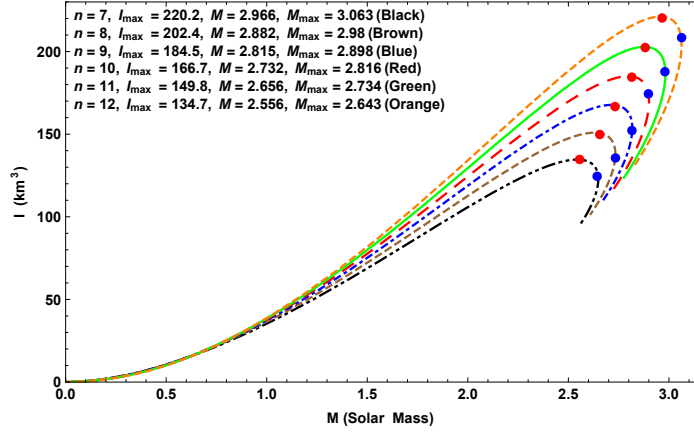
Figure 5.14: Variation of moment of inertia w.r.t. mass for $a = 0.001$ and $b = 0.04$. The red dots represents $\left(M, I_{max}\right)$ and blue dots $\left(M_{max}, I\right)$

5.8   Discussion and conclusion

The solution of Einstein's field equation with $e^{-\lambda} = 1 + ar^2$ was presented by Duorah and Ray [1987], however, Finch and Skea [1989] pointed out that the Duorah-Ray (DR) solution doesn't satisfy the field equations. Therefore, Finch-Skea (FS) corrected the solution and hence known as FS solution. FS not only corrected the DR solution but also performed extensive works to describe physically realistic neutron stars. The resulting equation of state from FS solution was also compared with Walecka's relativistic mean-field theory description and found to be quite in good agreement.

An interesting result was presented by Bhar et al. [2017] showing that with the assumption of electric charge and Adler g_{tt} metric potential in the Karmarkar condition, one leads to FS g_{rr} metric potential which is a well behaved solution while its

5.8. Discussion and conclusion

neutral counterpart isn't.

The current chapter generalized the FS g_{rr} with the higher order term $b^{n-1}r^n$. We also successfully analysed the behaviour of the solution showing its well behaved range w.r.t. the parameter n. It is found that the solution exist and satisfy causality condition for $n = 4$, 5 and within the range $7 \leq n \leq 12$. All the solutions correspond to other values are not well-behaved. The fulfillment of the stable static criterion signifies that the solution is static and stable. The satisfaction of TOV-equation also implies the solution is in equilibrium. We have also plotted the $M - R$ diagram for the range $7 \leq n \leq 12$ and it shows that the maximum mass increases with n. For $n = 7$ the maximum mass is $2.643 M_\odot$ with radius 8.976 km and for $n = 12$, $M_{max} = 3.063 M_\odot$ with radius 10.85 km. The profile of adiabatic index (see Fig. 5.12) shows that the equation of state gets stiffer for larger values of n since the central values of Γ_r are larger. This increases the stiffness of the equation of state leading to increase the maximum mass.

The stiffness of an EoS is also link with moment of inertia of the compact star. For a uniformly rotating star with angular velocity Ω the moment of inertia is given by (Lattimer and Prakash [2000])

$$I = \frac{8\pi}{3} \int_0^R r^4 (\rho + p_r) e^{(\lambda - \nu)/2} \; \frac{\omega}{\Omega} \; dr \tag{5.55}$$

where, the rotational drag ω satisfy the Hartle's equation (Hartle [1978])

$$\frac{d}{dr} \left(r^4 j \frac{d\omega}{dr} \right) = -4r^3 \omega \frac{dj}{dr}. \tag{5.56}$$

with $j = e^{-(\lambda + \nu)/2}$ which has boundary value $j(R) = 1$. The approximate moment of inertia I up to the maximum mass M_{max} was given by Bejger and Haensel [2002] as

$$I = \frac{2}{5} \left(1 + x \right) MR^2, \tag{5.57}$$

where parameter $x = (M/R) \cdot km/M_\odot$. For the solution we have plotted mass vs I in Fig. 5.14 that shows as n increases, the mass also increase and the moment of inertia increases till up to certain value of mass and then decreases. Therefore, we can say that as moment of inertia increases, the stiffness of the corresponding EoS also increases. Comparing Figs. 5.6 and 5.14 we can see that the mass corresponding to I_{max} is not equal to M_{max} from $M - R$ diagram. In fact the mass corresponding

to I_{max} is lower by $\sim 3\%$ from the M_{max}. This happens to the EoSs without any strong high-density softening due to hyperonization or phase transition to an exotic state (Bejger and Haensel [2002]).

Chapter 6

Einsteins cluster mimicking compact star in the teleparallel equivalent of general relativity ¹

6.1 Introduction

The concepts of Einstein's cluster (Einstein [1939]) was introduced in 1939 to under-stand the system of stationary gravitating particles each moving along circular path about a common center under the influence of their combine gravitational field. If these particles are orbiting in same path with different phases or a similar orbit but inclined at a different angle, it can construct a shell named as "Einstein's Shell". By constructing layers of Einstein's shell a *Einstein's Cluster* is formed. All these particles are distributed spherically symmetric in sufficient continuous, random and collisionless geodesics. Such systems are static and in equilibrium where the grav-itational force is balanced by the centrifugal force. Therefore, in this way a thick spherical shell of matter is composed without pressure in the radial direction, but only tangential stresses.

Einstein clusters have been extensively studied in different literature (Florides [1974], Zapolsky [1968], Gilhert [1954], Comer and Katz [1993]). Specially, the com-ponents of energy momentum tensor for the cluster have been obtained in several representations. Due to the spherical symmetry nature, the only non-vanishing com-ponents of T^μ_ν are $T^t_t = \rho^{\text{eff}}$, $T^r_r = -p^{\text{eff}}_r$ and $T^\theta_\theta = T^\varphi_\varphi = -p^{\text{eff}}_t$, with ρ^{eff} is the effective

---

energy density and p_r^{eff} and p_t^{eff} are the effective radial and tangential pressures of the cluster, respectively. In principle, the junction conditions require p_r^{eff} to be continuous across the boundary of each layer of the shell, which follows that for the Einstein cluster $p_r^{\text{eff}} = 0$. Therefore, Einstein's clusters are known for their highly anisotropic in nature, for which the radial pressure is different from the tangential one, $p_r^{\text{eff}} \neq p_t^{\text{eff}}$.

Interesting features of relativistic anisotropic matter distributions have been extensively pointed out as early as 1933 by Lemaître [1933], Lemaître [1997]. Though in ref. Bowers and Liang [1974], they build up anisotropic models as the beginning of the epoch of more active research. In the latter, anisotropic model has widely been studied in many astrophysical objects such as stars, gravastars, wormholes etc. Not surprisingly, in the last few decades there has been renewed interest in structure and evolution of compact objects with interior anisotropic fluids (see for instance Mak and Harko [2003], Herrera et al. [2004], Chaisi and Maharaj [2005], Abreu et al. [2007], Thirukkanesh and Maharaj [2008], Maurya et al. [2017a], Folomeev and Dzhunushaliev [2015]). In Böhmer and Harko [2006], Andréasson and Böhmer [2009], upper and lower bounds for spherically-symmetric static solutions of the Einstein-fluid equations in presence of a positive cosmological constant.

Within the context of GR, Florides [1974] had tried to understand why a spherically symmetric distribution of pressure-less dust at rest cannot maintain itself in equilibrium. Since this attempt had opened up a new interior uniform density (Schwarzschildlike) solution. Specifically, the obtained interior solution process a positive tangential pressure which is increasing function of the radial coordinate and having constant density. In next, it has been found that Florides interior solution describes the interior field of an *Einstein cluster*. In this spirit, a modified approach to the problem of relativistic clusters was proposed by Zel'Dovich and Polnarev [1974]. Further, Zapolsky [1968] discussed the stability of such clusters by adopting the same methods which is used to study the stability of compact stars. Gilhert [1954] investigated the stability of Einstein clusters, leading to an upper limit to the velocities of the particles in the cluster. In this same context, Cocco and Ruffini [1997] introduced the concept of metastable clusters by considering explicit examples.

In the 1970's, Hogan [1973] who suggested that neutrinos can be emitted from Einstein's cluster at a very specific angle ranges from 0 to $\pi/2$ with the radial direction. If the cluster is made up of charged particles than it can't be in stationary equilibrium so long as the total charge is greater than or equal to the total mass (Banerjee and Som [1981]). Interestingly, Einstein's cluster is also considered as a spin fluid with

zero pressure where the spin density vanishes at the boundary of the fluid sphere (Bedran and Som [1982]). In a sense, elliptical Einstein shells by means of "elliptical" orbits was studied (Comer et al. [1993]), however, such configurations were not stable and eventually reduces to spherical shells (see Comer et al. [1993] for review).

Number of modified gravity theories have been proposed which may describe the accelerated expansion of the universe in an effective level. This endeavor arises from unifying gravitation and quantum mechanics, and addressing some cosmological problems which include the dark energy problem (non-standard cosmic fluid with negative pressure) in the late Universe and singularity problem in the early Universe. In addition to theoretical considerations modified gravity also could give adequate description of cosmological observations (Bahcall et al. [1999], Bamba et al. [2012], Joyce et al. [2015], Perrotta et al. [1999]). A systematic review on recent progress in the construction of modified gravity models has been done (see Nojiri et al. [2017]) in cosmology, emphasizing on inflation, bouncing cosmology and late-time acceleration era.

Among the modified theories of gravity, recently $f(\mathbb{T})$ gravity has attracted much attention in the community. Inspired by the formulation of $f(\mathcal{R})$-gravity (Sotiriou and Faraoni [2010], Santos et al. [2008], Harko [2008], Capozziello et al. [2018b], Astashenok et al. [2015, 2013], Goswami et al. [2014]), where $f(\mathcal{R})$ is a generic function of the Ricci scalar $\mathcal{R}$ of the underlying geometry, $f(\mathbb{T})$ gravity is a similar generalization. This theory is based on the old definition of the "Teleparallel equivalent to General Relativity" (TEGR) (Hayashi [1977], Hayashi and Shirafuji [1979, 1981]), where the Lagrangian is an analytic function of the torsion scalar $\mathbb{T}$ (Ferraro and Fiorini [2008], Fiorini and Ferraro [2009]). The basic equations of GR and its teleparallel equivalent is $\mathcal{R} = -\mathbb{T} + B$, where $\mathcal{R}$ and $\mathbb{T}$ are the Ricci scalar and torsion scalar with $B = \frac{2}{e}\partial_\mu(eT^\mu)$ is a total derivative term which only depends on torsion. Thus, Einstein-Hilbert action can now be represented in two distinct ways, either using the Ricci scalar or the torsion scalar, and consequently these two theories have the same equations of motion (Bahamonde and Wright [2015, 2016], Bahamonde et al. [2015]). However, the theoretical framework of $f(\mathbb{T})$ gravity depends on an appropriate ansatz for the tetrad field. It is interesting to mention that this theory is not invariant under local Lorentz transformations, and therefore the choice of tetrad plays an important role in determining such model. However TEGR, as a torsion theory, is equivalent to GR, but $f(\mathbb{T})$ theory is not equivalent to GR.

Although, $f(\mathbb{T})$ gravity does not coincide with $f(\mathcal{R})$ gravity. The main catch point is that for a nonlinear $f(\mathcal{R})$ function, gravity is a fourth-order theory, whereas $f(\mathbb{T})$-

gravity field equations are always second-order. At this point one should have noted that $f(\mathcal{R})$ modified gravity, in the Palatini version, can also be viewed as a second order system of equations (Ruiz-Lapuente [2010], De Felice and Tsujikawa [2010]). Compare to $f(\mathcal{R})$ gravity, the action of $f(\mathbb{T})$ theory and the field equations are not invariant under local Lorentz transformations (Li et al. [2011]), which relates to the fact that $f(\mathbb{T})$ theories appear to have extra degrees of freedom with respect to the teleparallel equivalent of GR (Sotiriou et al. [2011]), although their physical nature is not yet well understood. Though, there has been a growing interest in this kind of theories due to its ability to explain both early (Bamba et al. [2017], Jamil et al. [2015], Qiu et al. [2019]), as well as at late times accelerating phases of the Universe (Paliathanasis et al. [2016], Hohmann et al. [2017], Cai et al. [2016], Capozziello et al. [2018a]) without the inclusion of a dark energy fluid.

In recent years attentions have been focused on the gravitational waves from compact binary (Nunes et al. [2019, 2018]) in $f(\mathbb{T})$ gravity. In Bamba et al. [2014], the effects of the trace anomaly on inflation in $\mathbb{T}^2$ gravity has been examined. On the other hand, this model has been used for studying wormhole solution (see ?Rani et al. [2016b,a] and references therein). The structure of compact stars in $f(\mathbb{T})$ gravity was investigated recently in refs. Ilijić and Sossich [2018]. This method is examined for $f(\mathbb{T})$ theory where a special form of $f(\mathbb{T}) = \mathbb{T} + \frac{\alpha}{2}\mathbb{T}^2$ is selected. Similar studies have also concluded that due to presence of anisotropic fluid affects the value of luminosities, redshifts, and maximum mass of a compact relativistic object in Abbas et al. [2015a], Momeni et al. [2018], Abbas et al. [2015b].

Recently, Lake [2006] and Boehmer and Harko [2007] considered Einstein's cluster of WIMPs dark matter generating spherically symmetric gravitational field of a galactic halo that can fit the rotational curve of any galaxy by adjusting two parameters (i) angular momentum distribution and (ii) number distribution of the WIMPs. Also it was shown that Einstein's clusters were dynamically stable under radial and non-radial perturbations Boehmer and Harko [2007]. The gravitation lensing due to such Einstein's cluster is slightly smaller as compare to isothermal sphere of dark matter Boehmer and Harko [2007].

Inspired by the above applications of teleparallel and $f(\mathbb{T})$ theories of gravity, we are interested to investigate solution representing Einstein's cluster. The chapter is organized as follows: in Sec. 6.1 we briefly review the foundations of teleparallel and $f(\mathbb{T})$ theories. We find the corresponding field equations for general spherically symmetric spacetime with diagonal and off-diagonal tetrad, and by assuming different

$f(\mathbb{T})$ function. In Sec. 6.2, we derive charged and uncharged solutions for Einstein cluster and compare them with standard GR model. In Sec. 6.3, we presented the Einstein clusters for charged and uncharged solutions. The metric exterior to the sphere is given by Reissner-Nordström metric in Sec. 6.4. Secs. 6.5, 6.6 and 6.7 are devoted to discuss the stability of the Einstein cluster model. The modified Oppenheimer-Volkoff limit is analyzed as well as other properties of the spheres, such as causality condition, adiabatic index. Moment of inertia and time period of the cluster are obtained in Sec. 6.8. Finally, in Sec. 6.9 we summarized the results.

6.2 Field equation and spherically symmetric solutions in $f(\mathbb{T})$ gravity

In this section we briefly present the main points of the $f(\mathbb{T})$ gravity. We get the field equations by varying the action

$$S = \int d^4x \, \left[\frac{f(\mathbb{T})}{16\pi} + \mathcal{L}\right], \tag{6.1}$$

where $\mathcal{L}$ is the matter Lagrangian with $G = c = 1$, and $\mathbb{T}$ is the torsion scalar constructed from the torsion tensor:

$$T^\sigma_{\mu\nu} \;\; = \;\; \Gamma^\sigma_{\mu\nu} - \Gamma^\sigma_{\nu\mu} = e^\sigma_i\left(\delta_\mu e^i_\nu - \delta_\nu e^i_\mu\right). \tag{6.2}$$

Notably, the difference of Weitzenböck connection and the Levi-Civita connection $\widetilde{T}^\sigma_{\mu\nu}$ widely used in GR is defined as the contorsion tensor $K^{\mu\nu}_\sigma$ as follows

$$K^{\mu\nu}_\sigma \;\; \equiv \;\; T^\sigma_{\mu\nu} - \widetilde{T}^\sigma_{\mu\nu} = \frac{1}{2}\left(T^{\mu\nu}_\sigma + T^{\nu\mu}_\sigma - T^{\mu\nu}_\sigma\right). \tag{6.3}$$

In $f(\mathbb{T})$ geometry, we introduce for convenience, the "superpotential", namely

$$S^{\mu\nu}_\sigma \;\; = \;\; K^{\mu\nu}_\sigma - \delta^\nu_\sigma \, T^{\alpha\mu}_\alpha + \delta^\mu_\sigma \, T^{\alpha\nu}_\alpha, \tag{6.4}$$

and then the torsion scalar $\mathbb{T}$ is given by

$$\mathbb{T} \equiv T^\sigma_{\mu\nu}S^{\mu\nu}_\sigma, \tag{6.5}$$

which is equivalent to the Ricci scalar R up to a total derivative term. Actually, with the existence of torsion tensor, in particular, if $f(\mathbb{T}) = \mathbb{T}$, the resulting equations of motion are equivalent to GR, and $T^\sigma_{\mu\nu}$ no longer be expressed in terms of metric, but act as an independent variable (see reviews Hehl et al. [1976], Cai et al. [2016]).

In torsional formulations of gravity ones uses the tetrad fields e^i_μ are related to the metric tensor $g_{\mu\nu}$ by $g_{\mu\nu}(x) = \eta_{ij}e^i_\mu(x)e^j_\nu(x)$, where η_{ij} is the Minkowski metric of the tangent space with the form of $\eta_{ij} = \text{diag}\,(1, -1, -1, -1)$.

Additionally, we define the co-tetrad e^i_μ through

$$e^\mu_i e^i_\nu = \delta^\mu_\nu \quad \text{and} \quad e^\mu_i e^j_\mu = \delta^j_i, \qquad (6.6)$$

with $e = \sqrt{-g} = det(e^i_\mu)$. Variation of the action (6.1) with respect to the tetrad field gives the field equations

$$S_i^{\mu\nu} f_{,\mathbb{T}\mathbb{T}}\ \mathbb{T}_{,\mu} + e^{-1}(eS_i^{\mu\nu})_{,\mu}\ f_{,\mathbb{T}} - T^\sigma_{\mu i}S^{\nu\mu}_\sigma f_{,\mathbb{T}} \frac{1}{4}e^\nu_i f = 4\pi T_i^\nu. \qquad (6.7)$$

where $f_{,\mathbb{T}}$ and $f_{,\mathbb{T}\mathbb{T}}$ denote the first and second derivatives of the function $f(\mathbb{T})$ with respect to $\mathbb{T}$, and the tensor T_i^ν represents the energy-momentum tensor of the matter source $\mathcal{L}$. Considering the description of energy momentum tensor, which, in the present study is written as $T_i^\nu = M_i^\nu + E_i^\nu$. Since, M_i^ν stands for the energy-momentum tensor of an anisotropic fluid distribution and E_i^ν is the electromagnetic energy-momentum tensor. So, the complete form of Einstein-Maxwell field equations is

$$M_i^\nu = (p_t + \rho)u^\nu u_i - p_t g_i^\nu + (p_r - p_t)\chi_i\chi^\nu, \qquad (6.8)$$

$$E_i^\nu = \frac{1}{4\pi}\left(\frac{1}{4\pi}\ g_i^\nu F_{\alpha\beta}F^{\alpha\beta} - g^{\alpha\beta}F^\nu_\alpha F_{i\beta}\right), \qquad (6.9)$$

where u_ν is the four-velocity and χ_ν is the unit spacelike vector in the radial direction. Moreover, the electromagnetic tensor F_{ij} satisfies Mexwells equations

$$F_{\alpha\gamma,\beta} + F_{\gamma\beta,\alpha} + F_{\alpha\beta,\gamma} = 0,$$
$$\left[\sqrt{-g}F^{\alpha\beta}\right]_{,\beta} = 4\pi J^\alpha\sqrt{-g}\ , \qquad (6.10)$$

where $J^\alpha = \sigma u^\alpha$ is the electric current density and $F_{\alpha\beta}$ denotes the skew symmetric electromagnetic field tensor, with the parameter σ is the charge density.

6.2. Field equation and spherically symmetric solutions in $f(\mathbb{T})$ gravity

Since we are interested in spherically symmetric solutions that can be used to describe a dense compact relativistic star. To this end, we write the space-time metric in the following form

$$ds^2 = e^{\nu(r)}dt^2 - e^{\lambda(r)}dr^2 - r^2\left(d\theta^2 + \sin^2\theta \ d\phi^2\right), \tag{6.11}$$

where (t, r, θ, ϕ) are the usual Schwarzschild-like coordinates, with ν and λ are the functions of the radial coordinate r, are yet to be determined. Now, by considering diagonal and off-diagonal tetrad with different functional forms, we derive different field equations, as $f(\mathbb{T})$ theory is not invariant under local Lorentz transformations.

6.2.1 Diagonal tetrad and $f(\mathbb{T}) = a\mathbb{T} + b$

Here, we start with the simplest possible diagonal tetrad (T1) giving this metric (6.11) as follows (Abbas et al. [2015a], Momeni et al. [2018]):

$$[e^i_\mu] = \mathrm{diag}(e^{\nu/2}, \ e^{\lambda/2}, \ r, \ r\sin\theta), \tag{6.12}$$

and its determinant is $|e^i_\mu| = r^2\sin\theta \ e^{(\nu+\lambda)/2}$. The corresponding torsion scalar and its derivative is given by

$$\mathbb{T}(r) = \frac{2e^{-\lambda}}{r}\left(\nu' + \frac{1}{r}\right), \tag{6.13}$$

$$\mathbb{T}'(r) = \frac{2e^{-\lambda}}{r}\left[\nu'' + \frac{1}{r^2} - \mathbb{T}\left(\lambda' + \frac{1}{r}\right)\right], \tag{6.14}$$

where the prime denotes the derivative with respect to r. Thus, the general field Eq. (6.7) give rise to the explicit equations of motion:

$$4\pi\rho + E^2 = \frac{f}{4} - \frac{f,_{\mathbb{T}}}{2}\left[\mathbb{T} - \frac{1}{r^2} - \frac{e^{-\lambda}(\lambda' + \nu')}{r}\right], \tag{6.15}$$

$$4\pi p_r - E^2 = \frac{f,_{\mathbb{T}}}{2}\left(\mathbb{T} - \frac{1}{r^2}\right) - \frac{f}{4}, \tag{6.16}$$

$$4\pi p_t + E^2 = \left[\frac{\mathbb{T}}{2} + e^{-\lambda}\left\{\frac{\nu''}{2} + \left(\frac{\nu'}{4} + \frac{1}{2r}\right)(\nu' - \lambda')\right\}\right]\frac{f,_{\mathbb{T}}}{2} - \frac{f}{4}, \tag{6.17}$$

$$\frac{\cot\theta}{2r^2}\ \mathbb{T}'\ f,_{\mathbb{T}\mathbb{T}} = 0, \tag{6.18}$$

$$\sigma(r) = \frac{e^{-\lambda/2}}{4\pi r^2}\left(r^2 E\right)'. \tag{6.19}$$

The Eq. (6.18) puts a strict constraint on the possible $f(\mathbb{T})$ functions. We immediately observe few interesting facts. The Eq. (6.18) implies here that all solutions satisfy either $f_{,\mathbb{T}\mathbb{T}} = 0$ or $\mathbb{T}' = 0$, where the former reduces the theory to TEGR (see Ref. Boehmer et al. [2011]). As a result, the choice of $f_{,\mathbb{T}\mathbb{T}} = 0$ leads to the following linear model (Abbas et al. [2015a]):

$$f(\mathbb{T}) = a\mathbb{T} + b, \tag{6.20}$$

where a and b are integration constants. Inserting Eq. (6.20) into the field Eqs. (6.15)-(6.17), one can obtain the modified field equations in Teleparallel gravity as,

$$4\pi\rho + E^2 = \frac{2a\left(re^{-\lambda}\lambda' - e^{-\lambda} + 1\right) + br^2}{4r^2}, \tag{6.21}$$

$$4\pi p_r - E^2 = \frac{2ae^{-\lambda}\left(r\nu' + 1\right) - 2a - br^2}{4r^2}, \tag{6.22}$$

$$4\pi p_t + E^2 = \frac{e^{-\lambda}}{8r}\left[2a\nu' - a\lambda'\left(r\nu' + 2\right) + ar\left(2\nu'' + \nu'^2\right) - 2bre^{\lambda}\right]. \tag{6.23}$$

where ρ is the energy density with p_r and p_t are the radial and tangential pressure of the matter sector, considered correspond to a anisotropic fluid.
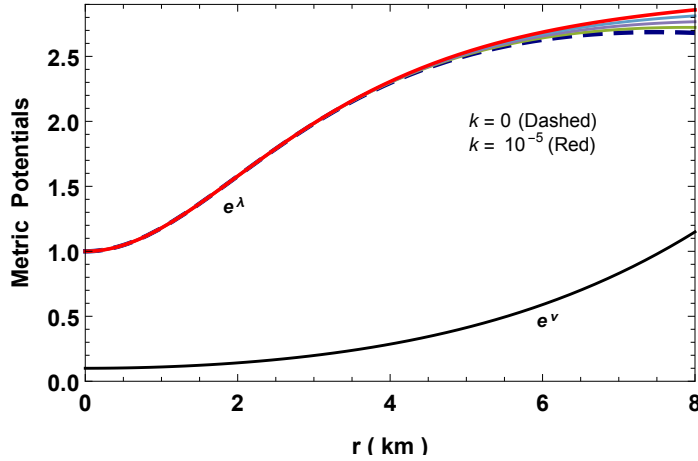
Figure 6.1: Variation of metric potentials with radial coordinate for $a = 1$, $b = 0.01$, $c = 0.01$, $d = 0.0001$ and $A = 0.1$ ($f(\mathbb{T}) = a\mathbb{T} + b$ and T1).

6.2.2   Off-diagonal tetrad and $f(\mathbb{T}) = a\mathbb{T} + b$

Proceeding forward the above discussed linear model of $f(\mathbb{T})$ function, we consider another possible tetrad field which is off-diagonal (T2), given by Boehmer et al. [2012]
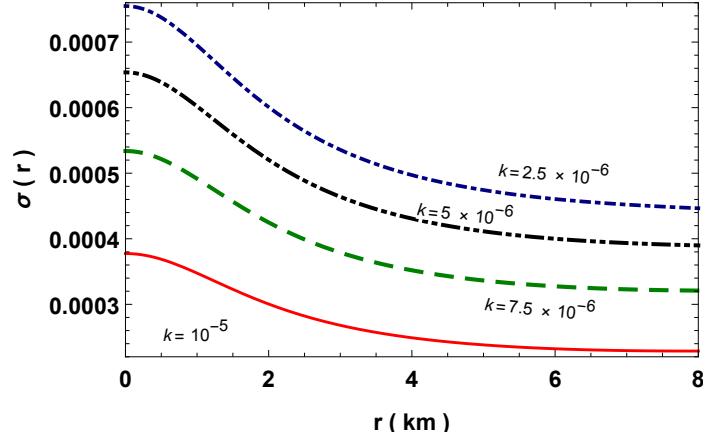
Figure 6.2: Variation of charge density with radial coordinates ($f(\mathbb{T}) = a\mathbb{T} + b$ and T1).

$$
e^i_\mu = \begin{bmatrix}
e^{\nu/2} & 0 & 0 & 0 \\
0 & e^{\lambda/2}\sin\theta\cos\phi & r\cos\theta\cos\phi & -r\sin\theta\sin\phi \\
0 & e^{\lambda/2}\sin\theta\sin\phi & r\cos\theta\sin\phi & r\sin\theta\cos\phi \\
0 & e^{\lambda/2}\cos\theta & -r\sin\theta & 0
\end{bmatrix}.
$$
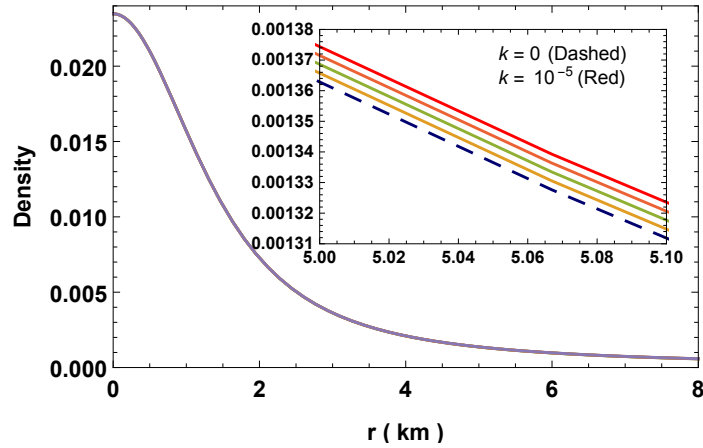
Figure 6.3: Variation of density with radial coordinate ($f(\mathbb{T}) = a\mathbb{T} + b$ and T1).

By doing a rotation, the off-diagonal basis tetrad is related to its diagonal form. One can obtain $e = |e^i_\mu| = r^2\sin\theta\ e^{(\nu+\lambda)/2}$, and we determine the torsion scalar as

$$
\mathbb{T}(r) = \frac{2e^{-\lambda}}{r^2}\left(e^{\lambda/2} - 1\right)\left(e^{\lambda/2} - 1 - 2\nu'\right). \tag{6.24}
$$
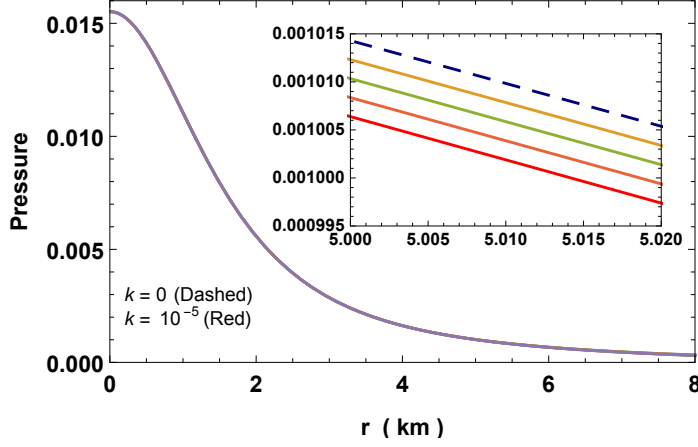
Figure 6.4: Variation of pressure with radial coordinate ($f(\mathbb{T}) = a\mathbb{T} + b$ and T1).

Inserting this and the components of the tensors S and $\mathbb{T}$ into the equation (6.7), we obtain the modified field equations

$$4\pi\rho = \frac{e^{-\lambda}}{4r^2}\left[2ar\lambda' + 2ae^{\lambda/2}\left(r\nu' + 2\right) - 2a + be^{\lambda}r^2\right] - E^2 \tag{6.25}$$

$$4\pi p_r = \frac{e^{-\lambda}}{4r^2}\left[a\left(2 - 4e^{\lambda/2}\right) - 2a\left(e^{\lambda/2} - 1\right)r\nu' - be^{\lambda}r^2\right] + E^2, \tag{6.26}$$

$$4\pi p_t = \frac{e^{-\lambda}}{8r}\left[2a\nu' - a\lambda'\left(r\nu' + 2\right) + 2ar\nu'' + ar\nu'^2 - 2be^{\lambda}r\right] - E^2. \tag{6.27}$$

We would like to mention that gravitational sector of TEGR is Lorentz invariant in the sense that any choice of the tetrad fields leads to the same equations of motion. Here, we would like to emphasize that the claim made above concerned solely with the argument.

6.2.3 Diagonal tetrad and $f(\mathbb{T}) = a\mathbb{T}^2$

Proceeding forward and using the T1 tetrad with $f(\mathbb{T}) = a\mathbb{T}^2$, one can get the following field equations:

$$4\pi\rho = \frac{ae^{-2\lambda}}{r^4}\left(r\nu' + 1\right)\left(2e^{\lambda} + 2r\lambda' - r\nu' - 3\right) - E^2, \tag{6.28}$$

$$4\pi p_r = \frac{ae^{-2\lambda}}{r^4}\left(r\nu' + 1\right)\left(-2e^{\lambda} + 3r\nu' + 3\right) + E^2, \tag{6.29}$$

$$4\pi p_t = \frac{ae^{-2\lambda}}{2r^4}\left(r\nu' + 1\right)\left[r\{\nu' - \lambda'(r\nu' + 2) + 2r\nu''\}(r\nu' + 4)\} + 2\right] - E^2 \tag{6.30}$$

134
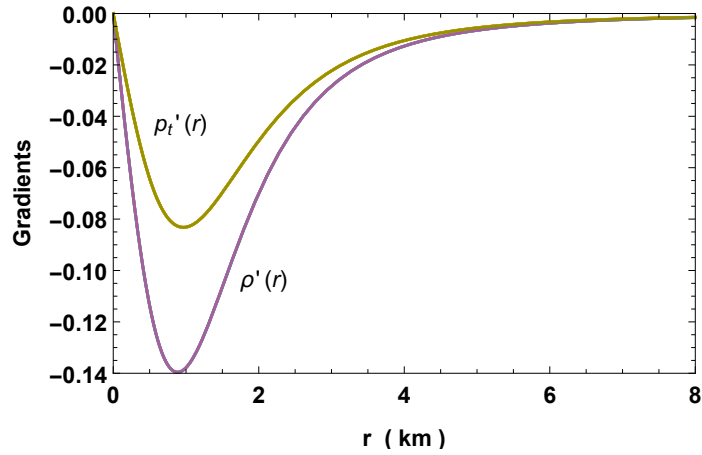
Figure 6.5: Variation of density and pressire gradients with radial coordinate ($f(\mathbb{T}) = a\mathbb{T} + b$ and T1).
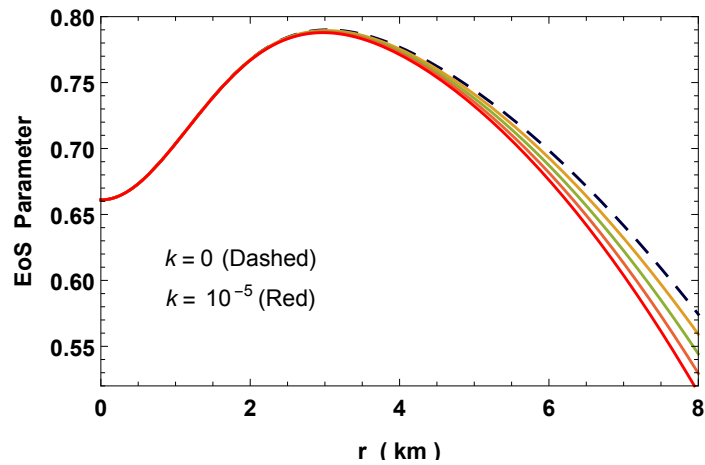
Figure 6.6: Variation of equation of state (EoS) parameter with radial coordinate ($f(\mathbb{T}) = a\mathbb{T} + b$ and T1).

Additional information are required to solve the above field equations.

6.2.4 Off-diagonal tetrad and $f(\mathbb{T}) = a\mathbb{T}^2$

Taking into account the off-diagonal tetrad and viable power-law form of the $f(\mathbb{T}) = a\mathbb{T}^2$ model, the field equations reduce to

$$
\begin{aligned}
4\pi\rho &= \frac{ae^{-2\lambda}}{r^4} \left(1 - e^{\lambda/2}\right) \left(e^{\lambda/2} - r\nu' - 1\right) \left[3 - 2r\lambda\{r\nu' + 2\} + e^\lambda \right. \\
&\quad \left. + r\nu' - 3e^{\lambda/2}\right] - E^2,
\end{aligned}
\tag{6.31}
$$

$$
\begin{aligned}
4\pi p_r &= \frac{ae^{-2\lambda}}{r^4} \left(e^{\lambda/2} - 1\right) \left(e^{\lambda/2} - r\nu' - 1\right) \left[e^\lambda - 6e^{\lambda/2} - 3\left\{e^{\lambda/2} - 1\right\} \right. \\
&\quad \left. r\nu' + 3\right] + E^2,
\end{aligned}
\tag{6.32}
$$

$$
\begin{aligned}
4\pi p_t &= \frac{ae^{-2\lambda}}{2r^4} \left(e^{\lambda/2} - 1\right) \left(e^{\lambda/2} - r\nu' - 1\right) \left[2\left\{\left(e^{\lambda/2} - 1\right)^2 + r^2\nu''\right\} \right. \\
&\quad \left. + r^2\nu'^2 - r\lambda'(r\nu' + 2) - 2\left(e^{\lambda/2} - 2\right)r\nu'\right] - E^2.
\end{aligned}
\tag{6.33}
$$

To proceed further, we will assume $p_r = 0$ and a specific form of electric field E in the proceeding section.

6.2.5 Field equations in pure GR

The well known field equation in the framework of GR with anisotropic stress-energy tensor profile is given by

$$
\rho = \frac{1}{8\pi} \left\{\frac{1 - e^{-\lambda}}{r^2} + \frac{\lambda'e^{-\lambda}}{r}\right\},
\tag{6.34}
$$

$$
p_r = \frac{1}{8\pi} \left\{\frac{\nu'e^{-\lambda}}{r} - \frac{1 - e^{-\lambda}}{r^2}\right\},
\tag{6.35}
$$

$$
p_t = \frac{e^{-\lambda}}{32\pi} \left\{2\nu'' + \nu'^2 - \nu'\lambda' + \frac{2\nu'}{r} - \frac{2\lambda'}{r}\right\}.
\tag{6.36}
$$

6.3 Einstein's cluster in $f(\mathbb{T})-$gravity and pure GR

Now, we want to show how it is possible to obtain an Einstein's cluster solution starting from a spherically symmetric metric in the absence and presence of electric
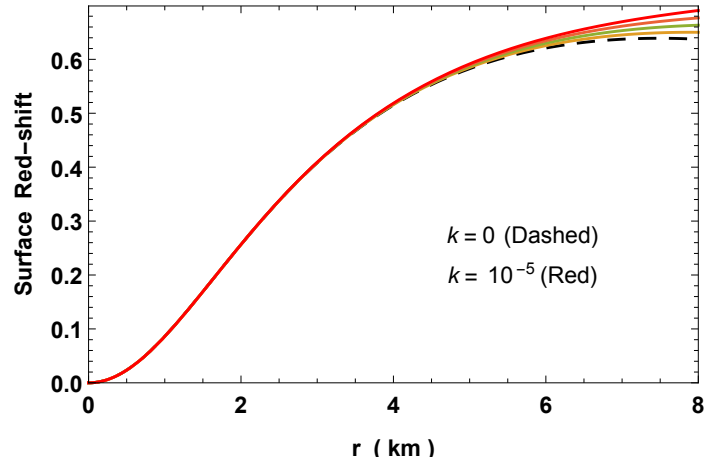
Figure 6.7: Variation of surface red-shit with radial coordinate ($f(\mathbb{T}) = a\mathbb{T} + b$ and T1).
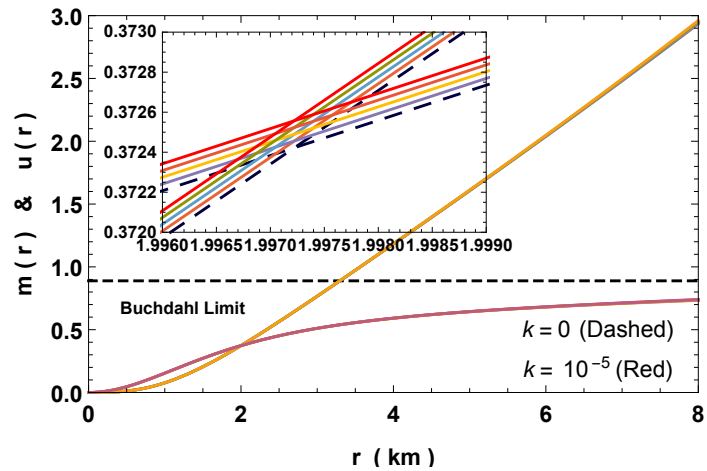
Figure 6.8: Variation of mass and radius with radial coordinate ($f(\mathbb{T}) = a\mathbb{T} + b$ and T1).

charge by considering diagonal/off-diagonal tetrad with Specific $f(\mathbb{T})$ function. More interestingly, we compare these results with the results from pure GR.

6.3.1 Neutral solution with T1 and $f(\mathbb{T}) = a\mathbb{T} + b$:

In the case of neutral anisotropic system with vanishing radial pressure (Boehmer and Harko [2007]), Eq. (6.22), gives

$$2ae^{-\lambda}\left(r\nu' + 1\right) - 2a - br^2 = 0. \tag{6.37}$$

Seeking solutions to the Eq. (6.37) is extremely difficult due to the presence of two unknown variables. We need at least one additional information. Hence, the simplest conception is to introduce the metric potential of form

$$e^{\nu} = A + cr^2 + dr^4, \tag{6.38}$$

and solving the Eq. (6.37) using (6.38), we get

$$e^{\lambda} = \frac{2a\left(A + 3cr^2 + 5dr^4\right)}{\left(2a + br^2\right)\left(A + cr^2 + dr^4\right)}. \tag{6.39}$$

Accordingly we obtained solution, the energy density and transverse pressure in the following form

$$\rho(r) = \frac{\left(A + cr^2 + dr^4\right)\left(6ac + 20adr^2 - Ab + 5bdr^4\right)}{8\pi\left(A + 3cr^2 + 5dr^4\right)^2}, \tag{6.40}$$

$$
\begin{aligned}
p_t(r) = {} & \frac{1}{16\pi\left(A + cr^2 + dr^4\right)\left(A + 3cr^2 + 5dr^4\right)^2}\left[A^2\Big\{8a\left(c + 4dr^2\right)\right. \\
& \left. - br^2\left(9c + 4dr^2\right)\Big\} + A\Big\{2a\left(11c^2r^2 + 64cdr^4 + 68d^2r^6\right) + br^4 \right. \\
& \left(10d^2r^4 - 15c^2 - 14cdr^2\right)\Big\} + r^4\Big\{a\left(6c^3 + 54c^2dr^2 + 96cd^2r^4 + 40d^3r^6\right) \\
& \left. - br^2\left(12c^3 + 37c^2dr^2 + 41cd^2r^4 + 20d^3r^6\right)\Big\} - 2A^3b\right]. \tag{6.41}
\end{aligned}
$$

To examine the system more closely we find the density and pressure gradients

takes the form

$$\frac{d\rho}{dr} = -\frac{r\big[Af_1(r) - f_2(r) + f_3(r)\big]}{\left(A + 3cr^2 + 5dr^4\right)^3}, \tag{6.42}$$

$$\frac{dp_t}{dr} = -\frac{r}{2\left(A + cr^2 + dr^4\right)^2\left(A + 3cr^2 + 5dr^4\right)^3} \Big[A^3 f_5(r) - A^4\left(32ad + 5bc + 36bdr^2\right)$$
$$+ A^2 r^2 f_4(r) + Ar^4\left\{f_6(r) + f_7(r)\right\} + r^6 f_8(r)\Big], \tag{6.43}$$

where

$$\begin{aligned}
f_1(r) &= 2a\big(15c^2 + 64cdr^2 + 120d^2r^4\big) + br^2\big(20d^2r^4 - 3c^2 - 30cdr^2\big),\\
f_2(r) &= A^2\left(20ad + 5bc + 28bdr^2\right) + 5bcdr^6\left(3c + dr^2\right),\\
f_3(r) &= 2a\left(9c^3r^2 + 45c^2dr^4 + 100cd^2r^6 + 50d^3r^8\right),\\
f_4(r) &= 2a\big(63c^3 + 275c^2dr^2 + 692cd^2r^4 + 572d^3r^6\big) + br^2\big(20d^3r^6 - 3c^3\\
&\quad - 205c^2dr^2 - 250cd^2r^4\big)\\
f_5(r) &= 2a\big(17c^2 + 8cdr^2 + 52d^2r^4\big) - br^2\big(15c^2 + 172cdr^2 + 140d^2r^4\big),\\
f_6(r) &= br^2\big(15c^4 - 30c^3dr^2 + 95c^2d^2r^4 + 508cd^3r^6 + 380d^4r^8\big),\\
f_7(r) &= 2a\big(63c^4 + 406c^3dr^2 + 1295c^2d^2r^4 + 1808cd^3r^6 + 860d^4r^8\big),\\
f_8(r) &= 2a\big(9c^5 + 63c^4dr^2 + 267c^3d^2r^4 + 525c^2d^3r^6 + 420cd^4r^8 + 100d^5r^{10}\big)\\
&\quad - bcdr^4\big(45c^3 + 119c^2dr^2 + 67cd^2r^4 - 15d^3r^6\big).
\end{aligned}$$

Now, the EoS parameter and surface red-shift can be found as

$$\omega = \frac{p_t}{\rho} \leq 1, \qquad z_s = e^{\lambda_s} - 1. \tag{6.44}$$

To conclude this section, we report the gravitational mass and compactness parameter by a spherically symmetric source with radius r, we get

$$m(r) = 4\pi\int_0^r \rho(\zeta)\,\zeta^2\,d\zeta = \frac{r^3\big[6a\left(c + 2dr^2\right) - Ab + bdr^4\big]}{6\left(A + 3cr^2 + 5dr^4\right)}, \tag{6.45}$$

$$u(r) = \frac{2m(r)}{r} = \frac{r^2\big[6a\left(c + 2dr^2\right) - Ab + bdr^4\big]}{3\left(A + 3cr^2 + 5dr^4\right)}. \tag{6.46}$$

6.3.2 Charged solution with T1 and $f(\mathbb{T}) = a\mathbb{T} + b$:

Using Eq. (6.22), we have

$$\frac{2ae^{-\lambda}\left(r\nu' + 1\right) - 2a - br^2}{4r^2} + E^2 = 0. \tag{6.47}$$

Follow the assumption (6.38) along with $E^2 = kr^2$ and the solution is easily found as

$$e^\lambda = \frac{2a\left(A + 3cr^2 + 5dr^4\right)}{\left(2a + br^2 - 4kr^4\right)\left(A + cr^2 + dr^4\right)}, \tag{6.48}$$

and the proper charge density is given by

$$\sigma(r) = \frac{3\sqrt{k}}{4\sqrt{2\pi}}\sqrt{\frac{\left(2a + br^2 - 4kr^4\right)\left(A + cr^2 + dr^4\right)}{a\left(A + 3cr^2 + 5dr^4\right)}}. \tag{6.49}$$

Hence, at $k = 0$ the charge solution reduces to the neutral solution. The variations of metric functions and charge density are shown in Figs. 6.1 and 6.2. The next step is to determine the energy density and pressure which are given by

$$8\pi\rho = \frac{A + cr^2 + dr^4}{2\left(A + 3cr^2 + 5dr^4\right)^2}\left[6ac + 20adr^2 - Ab + 8Akr^2 + 5bdr^4 + 12ckr^4\right], \tag{6.50}$$

$$8\pi p_t = \frac{2A^3\left(2kr^2 - b\right) + A^2 g_1(r) + Ar^2 g_2(r) - r^4 g_3(r)}{4\left(A + cr^2 + dr^4\right)\left(A + 3cr^2 + 5dr^4\right)^2}. \tag{6.51}$$

where

$$\begin{aligned}
g_1(r) &= 8a\left(c + 4dr^2\right) - 9bcr^2 - 4bdr^4 + 4ckr^4 - 36dkr^6, \\
g_2(r) &= 2a\left(11c^2 + 64cdr^2 + 68d^2r^4\right) - r^2\left[b\left(15c^2 + 14cdr^2 - 10d^2r^4\right)\right. \\
&\quad \left. + 4kr^2\left(4c^2 + 46cdr^2 + 57d^2r^4\right)\right], \\
g_3(r) &= r^2\left[b\left(12c^3 + 37c^2dr^2 + 41cd^2r^4 + 20d^3r^6\right) + 4dkr^4\left(16c^2\right.\right. \\
&\quad \left.\left. + 35cdr^2 + 15d^2r^4\right)\right] - 2a\left(3c^3 + 27c^2dr^2 + 48cd^2r^4 + 20d^3r^6\right).
\end{aligned}$$

The trends of density and pressure are shown in Figs. 6.3 and 6.4.

The mass function, compactness parameter and surface red-shift can be calculated

as

$$
\begin{aligned}
m(r) &= \frac{1}{2}\int_0^r \left(8\pi\rho x^2 + E^2 x^2\right)dx + \frac{q^2}{2r} = \frac{r^3}{12\left(A + 3cr^2 + 5dr^4\right)}\Big[6a\left(c + 2dr^2\right) - A \\
&\quad \left(b - 12kr^2\right) + r^4\left(bd + 24ck + 36dkr^2\right)\Big],
\end{aligned}
\tag{6.52}
$$

$$
u(r) = \frac{2m(r)}{r}
\tag{6.53}
$$

$$
z_s = e^{\lambda_R} - 1.
\tag{6.54}
$$

The variations in gradients, equation of state parameter, surface red-shift, mass function and compactness parameter are shown in Figs. 6.5, 6.6, 6.7 and 6.8.

6.3.3 Charged solution with T2 and $f(\mathbb{T}) = a\mathbb{T} + b$:

Proceeding the same as in previous section with vanishing radial pressure and assuming $E^2 = kr^2$ for Eq. (6.26), our model provides that

$$
a(2 - 4e^{\frac{\lambda}{2}}) - 2a\nu' r(e^{\frac{\lambda}{2}} - 1) - br^2 e^{\lambda} + kr^2 = 0.
\tag{6.55}
$$
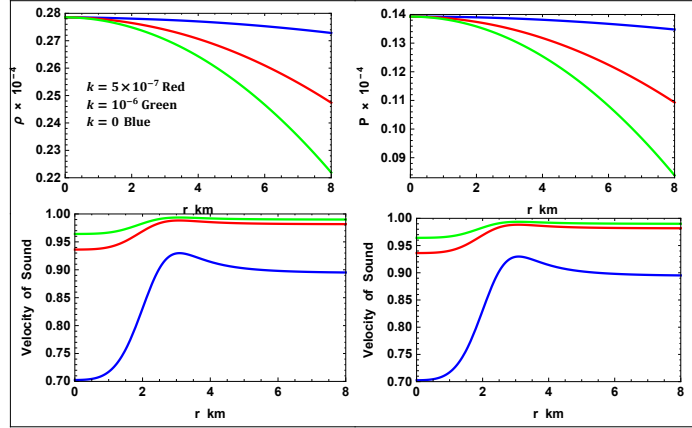
Figure 6.9: Variation of pressure with radial coordinate with for solution in III.3 for $a = 1.5$, $b = 0.0007$, $c = 0.002$, $d = 0.001$ and $A = 0.3$.

However, in order to solve Eq. (6.55) we assume a specific from of g_{tt} as $e^{\nu} = A + cr^2 + dr^4$, and the solution can be written as

$$
e^{\lambda} = \frac{k}{b} + \frac{2a\left(A + 3cr^2 + 5dr^4\right)}{br^2\left(A + cr^2 + dr^4\right)} + \frac{4h_3(r)}{b^2 r^4\left(A + cr^2 + dr^4\right)^2}.
\tag{6.56}
$$

Taking into account the metric potential and plugging those values into the Eqs. (6.25)-(6.27), one can easily obtain the stress-energy tensor profile. However, we avoid to enlist the physical character because of very complicated and lengthy expressions. Alternatively, we could get rid of this complicated expressions through a graphical representation. The qualitative behaviour of the stress-energy tensor components (density, pressure, velocity of sound and adiabatic index) are depicted in Figs. 6.9. Notice, that the pressure and density are decreasing outward, the velocity of sound is also within the causal limit and the adiabatic index is $> 4/3$. Our approach here follows make sense as a cluster solution which is sufficient to mimic as a compact star. Similar to solution in Sect 6.2, one can also see that as charge parameter k increases, the stiffness of the EoS also increases. Therefore, this cluster solution can also mimic properties of compact star.
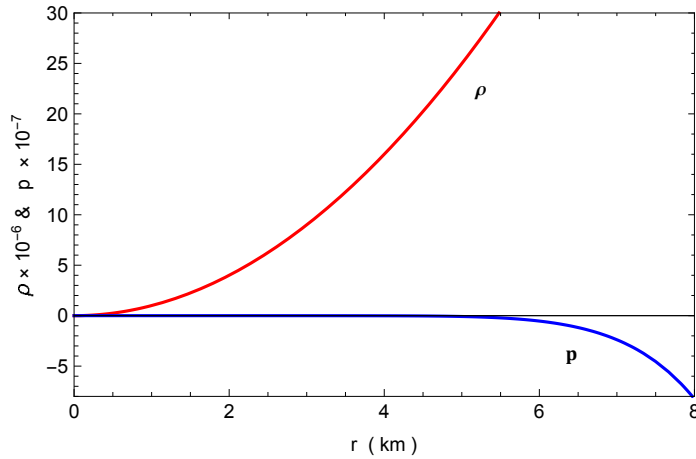
Figure 6.10: Variation of desnity and pressure with radial coordinate for in $f(\mathbb{T}) = a\mathbb{T}^2$ and T1.

6.3.4 Charged solution with T1 and $f(\mathbb{T}) = a\mathbb{T}^2$:

Further, we introduce the T1 tetrad and the function $f(\mathbb{T}) = a\mathbb{T}^2$. For vanishing radial pressure (6.29), we get

$$\frac{ae^{-2\lambda}}{r^4}\left(r\nu' + 1\right)\left(3 - 2e^\lambda + 3r\nu'\right) + E^2 = 0. \tag{6.57}$$

To solve the Eq. (6.57), we need an additional information because of the three unknowns λ, ν and E. Therefore, we have assumed the same $e^\nu = A + cr^2 + dr^4$ and

$E^2 = kr^2$. The resulting solution can be written as

$$e^\lambda = \frac{1}{2k}\sqrt{\frac{a^2[\chi_1(r)]^2}{r^4} - 4ak\chi_2(r)} + \frac{a\chi_1(r)}{r^2}, \qquad (6.58)$$

where,

$$\chi_1(r) = \frac{4c}{r^2\left(A + cr^2 + dr^4\right)} + \frac{8d}{A + cr^2 + dr^4} + \frac{2}{r^4},$$

$$\chi_2(r) = \frac{12c^2}{r^2\left(A + cr^2 + dr^4\right)^2} + \frac{48cd}{\left(A + cr^2 + dr^4\right)^2} + \frac{3}{r^6} + \frac{48d^2r^2}{\left(A + cr^2 + dr^4\right)^2}$$

$$+ \frac{24d}{r^2\left(A + cr^2 + dr^4\right)} + \frac{12c}{r^4\left(A + cr^2 + dr^4\right)}.$$

Again, we avoid to write the expressions for pressure and density because of their lengthy expressions. Interestingly enough, from the Fig. 6.10, that the transverse pressure and density vanishes at the center. In spite of the fact that there is no physical solution exist because of the density vanishes at the center and increasing outward.

A crucial point in this discussion is about the neutral solution i.e. $E^2 = 0$. According to Eq. (6.57) and $E^2 = 0$, the expression is a product of two terms. Investigating solutions for metric potential with the first equality of (6.57) we obtain $\nu(r) = B - \ln r$. Substituting this value we get $e^\lambda = 0$. Therefore, one can immediately conclude that no physical solutions exist in this scenarios.

Furthermore, for T2 tetrad with the same function we found the exactly same situation for neutral case i.e. $\nu = A - \ln r$ and $e^\lambda = 0$. Therefore, the main drawback of the $f(\mathbb{T}) = a\mathbb{T}^2$ gravity model along the T1 and T2 tetrad is that the obtained solutions do not process any physically realistic Einstein's cluster solution.

6.3.5 Charged solution with T2 and $f(\mathbb{T}) = a\mathbb{T}^2$:

For Einstein's cluster, the vanishing radial pressure gives

$$\frac{ae^{-2\lambda}}{r^4}\left(e^{\lambda/2} - 1\right)\left(e^{\lambda/2} - r\nu' - 1\right)\left(e^\lambda - 6e^{\lambda/2} - 3\left\{e^{\lambda/2} - 1\right\}r\nu' + 3\right) + E^2 = 0. \quad (6.59)$$
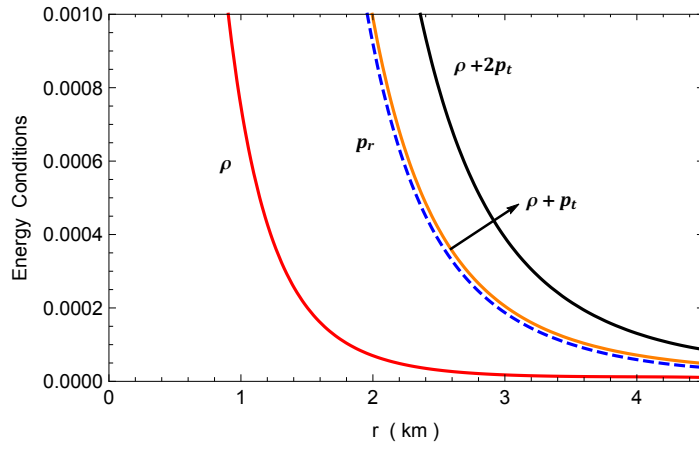
Figure 6.11: Variation of density, pressure and energy conditions with radial coordinate in T2 and $f(\mathbb{T}) = a\mathbb{T}^2$.
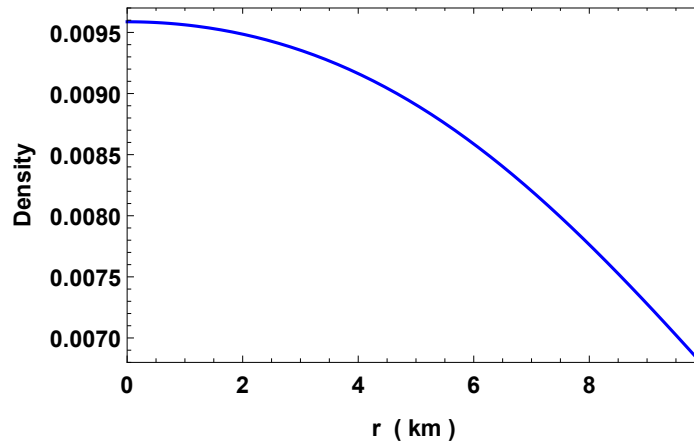
Figure 6.12: Variation of density with radial coordinate in pure GR.
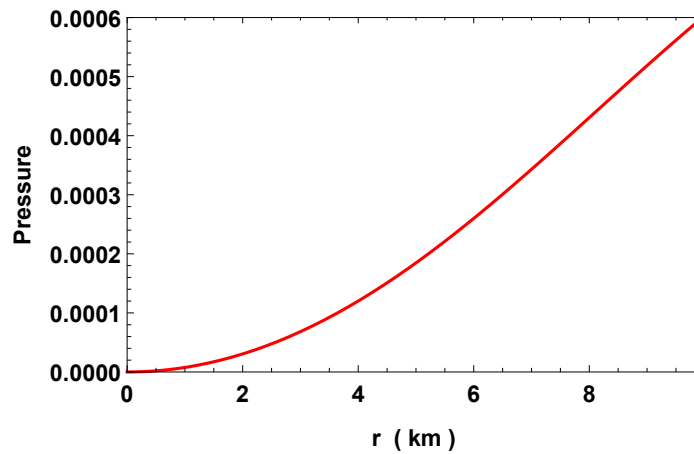
Figure 6.13: Variation of pressure with radial coordinate in pure GR.

Here, to simplify the solution we ansatz $e^\nu = A + cr^2$ and $E^2 = kr^2$, and the solution gives

$$
\begin{aligned}
e^{\lambda/2} &= \frac{2a\tau(r)}{e^\nu \gamma(r)} + \zeta(r)\left[\frac{1}{e^{2\nu}\gamma(r)^2}\left\{8a^2\tau(r)^2 - a\gamma(r)\left(4A^2 + 16Acr^2 + 15c^2r^4\right)\right.\right. \\
&\quad \left. -ae^\nu\gamma(r)(A + 3cr^2) + \frac{e^\nu\gamma(r)\zeta(r)}{\tau(r)}\left[a\left(3A^2 + 12Acr^2 + 13c^2r^4\right)\right.\right. \\
&\quad \left.\left.\left. -kr^6\left(A^2 + 4Acr^2 + 3c^2r^4\right)\right]\right\}\right]^{1/2},
\end{aligned}
\tag{6.60}
$$

where,

$$
\begin{aligned}
\tau(r) &= A + 2cr^2 \;\;,\;\;\; \gamma(r) = a + kr^6 \\
\zeta(r) &= \sqrt{\frac{a\left(a - 3kr^6\right)\left(A + 2cr^2\right)^2}{\left(a + kr^6\right)^2\left(A + cr^2\right)^2}} \;\;.
\end{aligned}
$$

Due to extremely lengthy expressions of density and pressure will exclude their expressions, however, their properties have been obtained by numerically integration for the charged fluid equation of state and by graphical representation. As one can see from Fig. 6.11, that the pressure and density are positive and decreasing outward, however, they blows up at $r = 0$. Such a solution can mimic compact stars which contain a central singularity. Even if such solutions could exist, they do not gravitationally stable.

6.3.6 Neutral Einstein's cluster solution in pure GR

Up to now, we have concentrated our discussion on modified teleparallel gravity or $f(\mathbb{T})$ gravity. We attempt to discuss here the general relativity case. Let us now concentrate on Eq. (6.35), with vanishing radial pressure, we find

$$
\frac{\nu' e^{-\lambda}}{r} - \frac{1 - e^{-\lambda}}{r^2} = 0 \quad \text{or} \quad e^\lambda = 1 + r\nu'.
\tag{6.61}
$$

Our focus is to obtain a complete solution, and for that we use $e^\nu = A + cr^2 + dr^4$ as previously discussed. Then, we find

$$
e^\lambda = \frac{A + 3cr^2 + 5dr^4}{A + cr^2 + dr^4}.
\tag{6.62}
$$

From Eqs. (6.34)-(6.36), we deduce

$$8\pi\rho = \frac{2\left(3c + 10dr^2\right)\left(A + cr^2 + dr^4\right)}{\left(A + 3cr^2 + 5dr^4\right)^2},\qquad(6.63)$$

$$8\pi p_t = \frac{3c^2r^2 + 16cdr^4 + 20d^2r^6}{\left(A + 3cr^2 + 5dr^4\right)^2}.\qquad(6.64)$$

Since, our goal now is to build a more realistic model of Einstein's cluster. To do so we first fix the values of few unknown parameters by matching the Schwarzschild's vacuum solution at the boundary, which are found to be

$$A = \frac{cR^2(R - 3M) + dR^4(2R - 5M)}{M},\qquad(6.65)$$

$$d = \frac{M - cR^3}{2R^5}.\qquad(6.66)$$

The parameter c will be treated as free parameter for tuning purpose. Moreover, c is directly related with determining cluster solution.

Considering Eq. (6.64), one immediately finds that $p_t = 0$ at the center $r = 0$, which violates the physical condition of a compact star. The qualitative behaviour of the density and pressure are depicted in Figs. 6.12 and 6.13. Note that the energy density is positive throughout the spacetime, but the pressure is zero at the center and increasing outward. In a recent paper, Thirukkanesh et al. [2015] investigated a particular class of stellar solutions which describe spherically symmetric matter distributions with vanishing radial stresses within the framework of GR. However, their model process $p_t > 0$ everywhere inside the star but it decreases monotonically from the center and reaches a minimum at certain radius, and thereafter increasing monotonically toward the boundary of the star. But our pressure is strictly increasing throughout the interior spacetime. Qualitatively, we verify that for increasing nature of the pressure give raise to imaginary sound speed and the negative values of adiabatic index. In general, this scenario does not process a physically valid compact star. Thus, in pure GR the solutions representing Einstein cluster can't mimic compact stars.

6.4 Matching of boundary for charged solution for diagonal tetrad in linear $f(\mathbb{T})$

Having derived the equations that describe charged Einstein cluster, we now pro-

ceed to match the interior solution with an exterior Reissner-Nordström vacuum solution. Moreover, we fix the values of constant a, b, A and B from junction conditions imposed on the internal and external metrics at the hyper-surface. The Reissner-Nordström metric is given by

$$ds^2 = \left(1 - \frac{2m}{r} + \frac{q^2}{r^2}\right) dt^2 - \left(1 - \frac{2m}{r} + \frac{q^2}{r^2}\right)^{-1} dr^2 - r^2(d\theta^2 + \sin^2\theta \ d\phi^2). \quad (6.67)$$

Now, using the continuity of the metric coefficients e^ν and e^λ across the boundary $r = R$, we get the following

$$\left(1 - \frac{2M}{R} + \frac{Q^2}{R^2}\right)^{-1} = \frac{2a\left(A + 3cR^2 + 5dR^4\right)}{(2a + bR^2 - 4kR^4)} \left(A + cR^2 + dR^4\right)^{-1}, \quad (6.68)$$

$$1 - \frac{2M}{R} + \frac{Q^2}{R^2} = A + cR^2 + dR^4. \quad (6.69)$$

Solving Eqs. (6.68) and (6.69), we get

$$a = R^2\left(b - 4kR^2\right)\left(A + cR^2 + dR^4\right)\left[2AkR^4 - 2AU + 6ckR^6 - 6cR^2U\right.$$
$$\left. + 4cR^2 + 10dkR^8 - 10dR^4U + 8dR^4\right]^{-1}, \quad (6.70)$$

$$A = 1 - cR^2 - dR^4 + kR^4 - \frac{2M}{R}. \quad (6.71)$$

Here $U = 2M/R$, c, d, k and b will be treated as fitting parameters while M and R can be chosen from observed values of compact stars.

6.5 Non-singular nature of the solution

The central density and central pressure are surprisingly independent of electric charge and found as

$$8\pi\rho_c = \frac{6ac - Ab}{2A} > 0, \quad (6.72)$$

$$8\pi p_{tc} = \frac{4ac - Ab}{2A} > 0, \quad (6.73)$$

which implies $4ac > Ab$. The solution also satisfies the Zeldovich's (Zeldovich and

Novikov [1971]) condition as

$$\frac{p_{tc}}{\rho_c} = \frac{4ac - Ab}{6ac - Ab} < 1. \tag{6.74}$$

Therefore, the solution doesn't contain any singularity and also can represent physical matters.
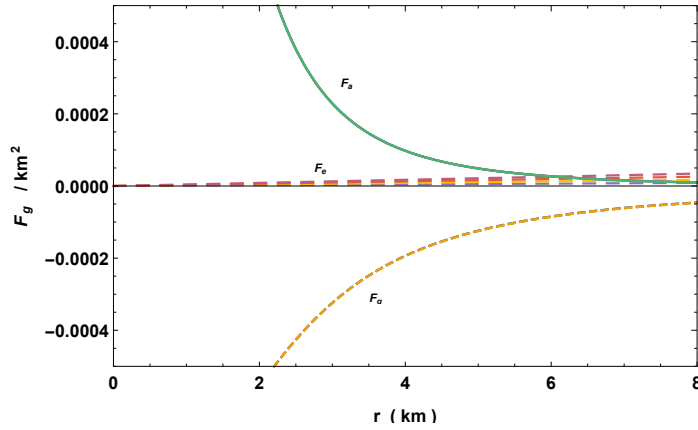
Figure 6.14: Variation of forces acting on TOV-equation with radial coordinate $(f(\mathbb{T}) = a\mathbb{T} + b$ and T1).

6.6   Equilibrium and stability analysis

The task is now to study the stability of self-consistent regular solution. In the present section, we analyse the stability of the Einstein clusters by performing some analytical calculations and plotting several figures.

6.6.1   Equilibrium analysis via TOV-equation

In the spirit of completion we discuss the stability of the Einstein cluster modle. Consider hydrostatic equilibrium via Tolman-Oppenheimer-Volkoff (TOV) equation. Now by employing the generalised-TOV equation (Tolman [1939], Oppenheimer and Volkoff [1939]) in the presence of charge, as prescribed in Ponce de Leon [1993], we have the following form

$$-\frac{M_g(r) \, \rho(r)}{r} e^{(\nu - \lambda)/2} + \frac{2p_t(r)}{r} + \sigma E e^{\lambda/2} = 0, \tag{6.75}$$

where $M_g(r)$ represents the gravitational mass within the radius r. It is defined using the Tolman-Whittaker mass formula through the Einstein's field equations as

$$M_g(r) = 4\pi \int_0^r \left(T_t^t - T_r^r - T_\theta^\theta - T_\phi^\phi\right) r^2 e^{(\nu+\lambda)/2} dr = \frac{1}{2} r e^{(\lambda-\nu)/2} \nu'. \quad (6.76)$$

Now, plugging the value of $M_g(r)$ in equation (6.75), we get

$$-\frac{\nu'}{2} \rho(r) + \frac{2p_t(r)}{r} + \sigma E e^{\lambda/2} = 0 \quad \text{or} \quad F_g + F_a + F_e = 0, \quad (6.77)$$

where F_g, F_e and F_a are the three different forces namely gravitational, anisotropic and electromagnetic forces, respectively. For our system the forces are as follows:

$$F_g = -\frac{\nu'}{2} \rho(r), \quad F_a = \frac{2p_t(r)}{r}, \quad F_e = \sigma E e^{\lambda/2}. \quad (6.78)$$

The variation of forces in TOV-equation w.r.t. the radial coordinate r is given in Fig. 6.14.

6.6.2 Causality condition and stability criterion

For static spherically symmetric spacetime solution one has to check also the behavior of speed of sound propagation v^2, which is given by the expression $dp/d\rho$. Normally it is believed that the velocity of sound is less than the velocity of light. For that the speed of sound should be ≤ 1 and it can be determined as
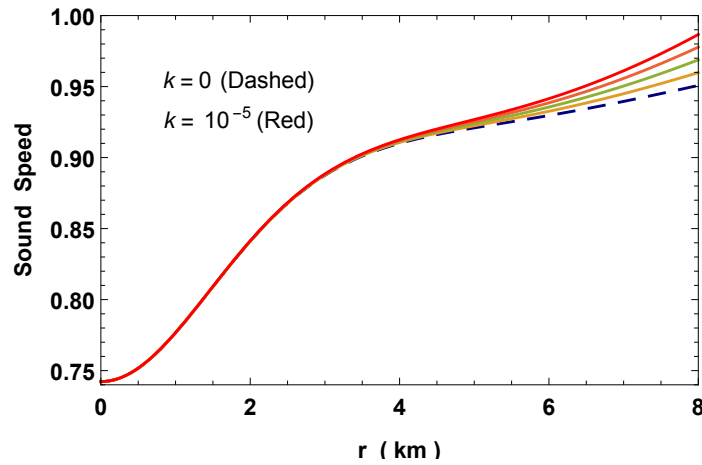
Figure 6.15: Variation of sound speed with radial coordinate ($f(\mathbb{T}) = a\mathbb{T}+b$ and T1).

$$v_t^2 = \frac{dp_t}{d\rho} = \frac{1}{2\chi_6(r)\,(A + cr^2 + dr^4)^2} \times \Big[4A^5k + A^4\chi_1(r) - A^3\chi_2(r) - A^2r^2\chi_3(r)$$
$$- Ar^4\chi_4(r) + r^6\chi_5(r) \Big], \tag{6.79}$$

where,

$$\chi_1(r) = 32ad + b\left(5c + 36dr^2\right) - 4kr^2\left(c + 43dr^2\right),$$
$$\chi_2(r) = 2a(17c^2 + 8cdr^2 + 52d^2r^4) - b(15c^2r^2 + 172cdr^4 + 140d^2r^6) + 4kr^4$$
$$(17c^2 + 268cdr^2 + 274d^2r^4),$$
$$\chi_3(r) = 2a(63c^3 + 275c^2dr^2 + 692cd^2r^4 + 572d^3r^6) - b(3c^3r^2 + 205c^2dr^4$$
$$+ 250cd^2r^6 - 20d^3r^8) + 4kr^4(23c^3 + 499c^2dr^2$$
$$+ 946cd^2r^4 + 426d^3r^6),$$
$$\chi_4(r) = 2a(63c^4 + 406c^3dr^2 + 1295c^2d^2r^4 + 1808cd^3r^6 + 860d^4r^8) + br^2(15c^4$$
$$- 30c^3dr^2 + 95c^2d^2r^4 + 508cd^3r^6 + 380d^4r^8)$$
$$+ 4dkr^6(294c^3 + 775c^2dr^2 + 516cd^2r^4 + 15d^3r^6),$$
$$\chi_5(r) = -2a(9c^5 + 63c^4dr^2 + 267c^3d^2r^4 + 525c^2d^3r^6 + 420cd^4r^8 +$$
$$100d^5r^{10}) + bcdr^4(45c^3 + 119c^2dr^2 + 67cd^2r^4 - 15d^3r^6)$$
$$- 4dkr^6(96c^4 + 363c^3dr^2 + 485c^2d^2r^4 + 285cd^3r^6 + 75d^4r^8),$$
$$\chi_6(r) = A^2(20ad + 5bc + 28bdr^2 + 16ckr^2 - 96dkr^4) - A\big[2a(15c^2$$
$$+ 64cdr^2 + 120d^2r^4) + b(-3c^2r^2 - 30cdr^4 + 20d^2r^6)$$
$$+ 4kr^4(-9c^2 + 32cdr^2 + 10d^2r^4)\big] - 2a(9c^3r^2 + 45c^2dr^4 + 100cd^2r^6$$
$$+ 50d^3r^8) + 8A^3k + cr^6(3c + dr^2)(5bd + 12ck).$$

The presented solution also satisfy the causality condition (see Fig. 6.15). Since there is no radial sound speed, the Herrera's cracking method of analyzing stability is not applicable in Einstein's clusters.

6.6.3 Stability analysis using relativistic adiabatic index

Given the significance of the above results in the cluster solution, it would be of interest if some comment regarding stable/instable criterion of the solution can be made. For this purpose one may consider the dynamical stability based on the vari-
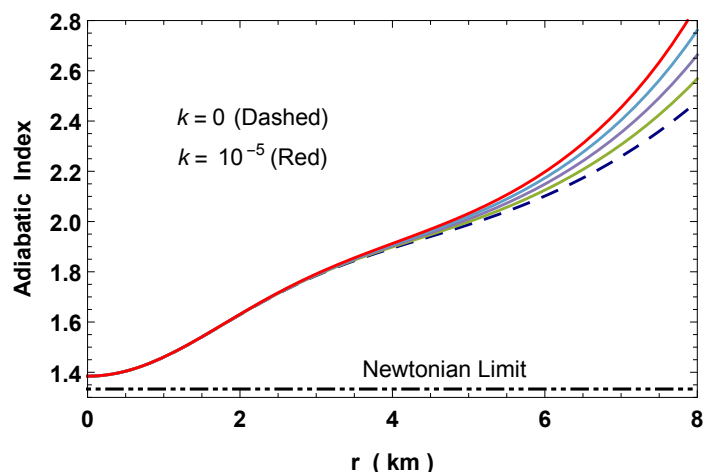
Figure 6.16: Variation of adiabatic index with radial coordinate ($f(\mathbb{T}) = a\mathbb{T} + b$ and T1).
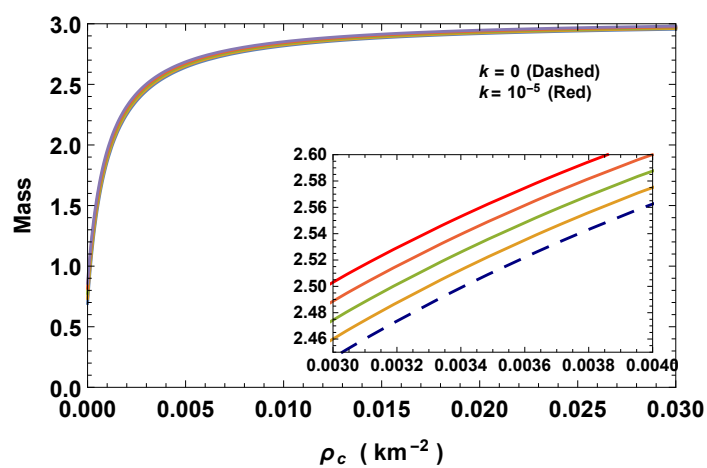
Figure 6.17: Variation of mass with central density ($f(\mathbb{T}) = a\mathbb{T} + b$ and T1).

ational method which was introduced by Chandrasekhar [1964]. Now considering an adiabatic perturbation, the adiabatic index Γ, is defined as following Chandrasekhar [1964], Merafina and Ruffini [1989], Chan et al. [1993], by

$$\Gamma = \frac{\rho + p_t}{p_t} \frac{dp_t}{d\rho}, \tag{6.80}$$

where $dp/d\rho$ is the speed of sound in units of speed of light. This approximation leads to a very useful information for compact astrophysical objects and impose some marginal constraints. In view of the above consideration, Bondi [1964] had clearly mentioned that a stable Newtonian sphere has $\Gamma > 4/3$ and $\Gamma = 4/3$ for a neutral equilibrium. Its values vary from 2 to 4 in most of the neutron stars equations of state (Haensel et al. [2007]). For the solution also the adiabatic index is greater than 4/3. In Fig. 6.16 one can see that the central value of the adiabatic index is independent of electric charge and is about 1.386.

6.6.4 Static stability criterion

In order to clarify further the effect of mass-radius and mass-central density relation for the stable stellar configuration, Harrison-Zeldovich-Novikov (Harrison et al. [1965], Zeldovich and Novikov [1971]) argued that an increasing mass profile with increasing central density i.e. $\partial M/\partial \rho_c > 0$ represents stable configurations and vice-versa. In particular stable or unstable region is achieved when the mass remains constant with increase in central density i.e. $\partial M/\partial \rho_c = 0$. For the new solution $M(\rho_c)$ and $\partial M/\partial \rho_c$ is found to be

$$
\begin{aligned}
M(\rho_c) &= \frac{R^3}{30\left(\frac{6ac}{b+8\pi\rho_c} + 3cR^2 + 5dR^4\right)}\left[\frac{6ac\left(24kR^2 - 5b\right)}{b + 8\pi\rho_c} + 30a\left(c + 2dR^2\right)\right. \\
&\quad \left. + R^4(5bd + 12ck)\right], \tag{6.81}
\end{aligned}
$$

$$
\frac{\partial M}{\partial \rho_c} = \frac{24\pi acR^3\left(c + 2dR^2\right)\left(2a + bR^2 - 4kR^4\right)}{\left(6ac + R^2(b + 8\pi\rho_c)\left(3c + 5dR^2\right)\right)^2}. \tag{6.82}
$$

Here, we can clearly see that $\partial M/\partial \rho_c > 0$ i.e. mass is increasing function of its central density (Fig. 6.17) and therefore can represents static stable configuration.
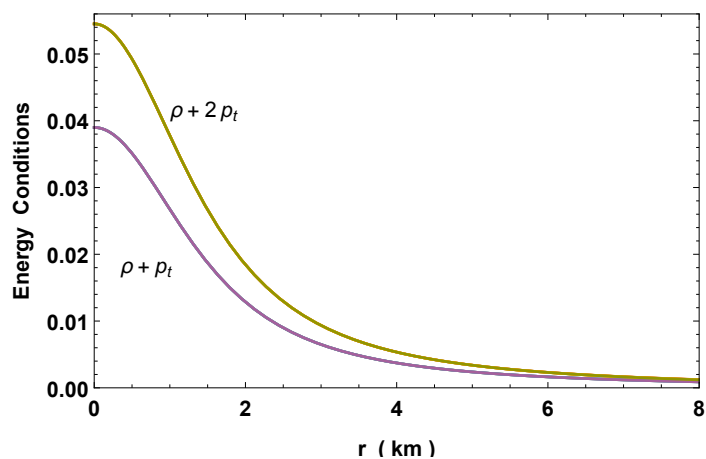
Figure 6.18: Variation of energy conditions with radial coordinate ($f(\mathbb{T}) = a\mathbb{T} + b$ and T1).
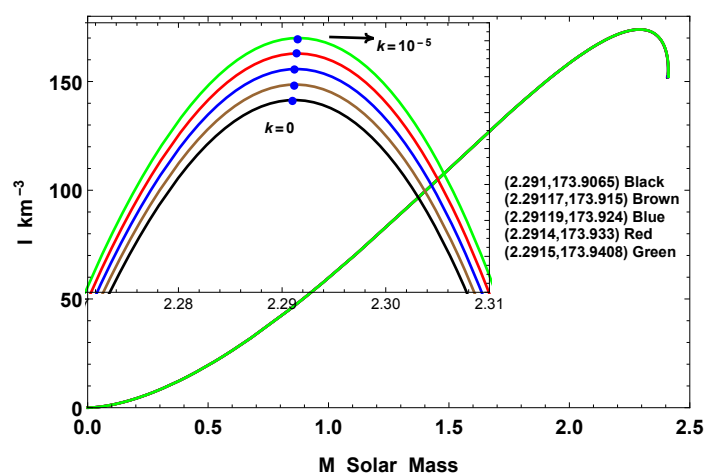
Figure 6.19: Variation of moment of inertia with mass for $a = 1$, $b = 0.01$, $c = 0.01$, $d = 0.0001$ and $A = 0.1$ ($f(\mathbb{T}) = a\mathbb{T} + b$ and T1).
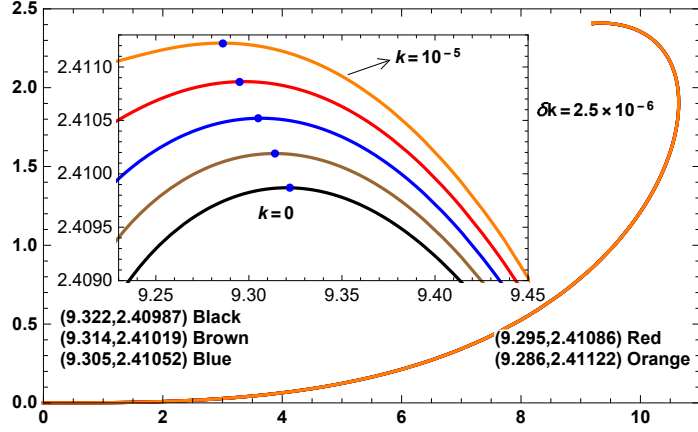
Figure 6.20: Variation of mass with radius for $a = 1$, $b = 0.01$, $c = 0.01$, $d = 0.0001$ and $A = 0.1$ ($f(\mathbb{T}) = a\mathbb{T} + b$ and T1).
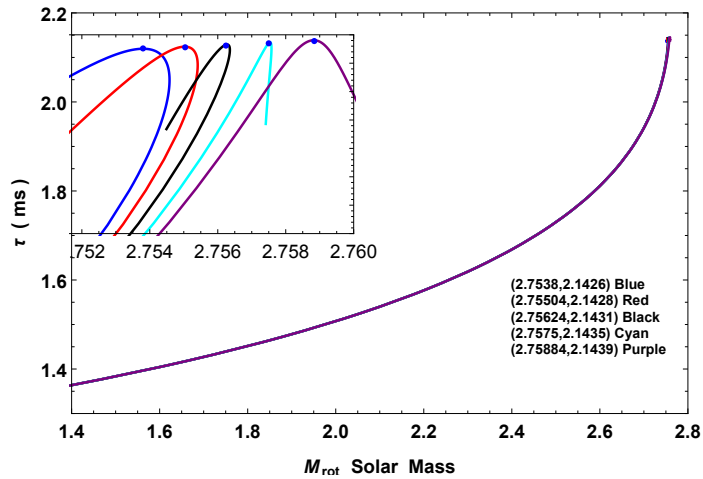
Figure 6.21: Variation of time period of rotation with mass for $a = 1$, $b = 0.01$, $c = 0.01$, $d = 0.0001$ and $A = 0.1$ ($f(\mathbb{T}) = a\mathbb{T} + b$ and T1).

154

6.7   Energy conditions

It is reasonable to expect that models of charged perfect fluids satisfy the energy conditions and such condition depends on the relation between matter density and pressure obeying certain restrictions. In view of the above situation, we examine Strong (SEC), Weak (WEC), Dominant (DEC) and Null (NEC) energy conditions, which are defined as

$$\text{WEC} \quad : \quad \rho \geq 0, \; \rho + p_t \geq 0, \tag{6.83}$$

$$\text{NEC} \quad : \quad \rho + p_t \geq 0, \tag{6.84}$$

$$\text{DEC} \quad : \quad \rho \geq |p_t|, \tag{6.85}$$

$$\text{SEC} \quad : \quad \rho + 2p_t \geq 0. \tag{6.86}$$

Using the above expression, one can easily justify the nature of energy conditions. The presented model also fulfill these energy conditions (Fig. 6.18). Since the allowed values of the electric charge parameter k is very small i.e. $0 \leq k \leq 1.3 \times 10^{-5}$, the graphs of the above energy conditions are very closed to each other.

6.8   Slow rotation model, moment of inertia and time period

For a uniformly rotating star with angular velocity Ω, the moment of inertia is given by Lattimer and Prakash [2000]

$$I = \frac{8\pi}{3} \int_0^R r^4 (\rho + p_r) e^{(\lambda - \nu)/2} \, \frac{\omega}{\Omega} \, dr, \tag{6.87}$$

where, the rotational drag ω satisfy the Hartle's equation (Hartle [1978])

$$\frac{d}{dr} \left(r^4 j \, \frac{d\omega}{dr} \right) = -4r^3 \omega \, \frac{dj}{dr}. \tag{6.88}$$

with $j = e^{-(\lambda + \nu)/2}$ which has boundary value $j(R) = 1$. The approximate solution of moment of inertia I up to the maximum mass M_{max} was given by Bejger and Haensel

as

$$I = \frac{2}{5} \left(1 + \frac{(M/R) \cdot km}{M_\odot} \right) MR^2, \tag{6.89}$$

The $M - I$ graph is shown in Fig. 6.19. The corresponding $M - R$ graph is also shown in Fig. 6.20. From these two graphs we can see that the maximum moment of inertia and maximum mass increases with increase in electric charge. However, the mass corresponding to I_{max} from $M - I$ graph is less by about 5% as compare to M_{max} from $M - R$ graph. This suggest that the corresponding equation of state is free from softening due to hyperonization or phase transition to an exotic state (Bejger et al. [2005]).

The minimum time-periods of any rotating compact stars can be expressed with good precision in terms of the masses and radii of the non-rotating configurations. So long as the equation of states obeyed subluminal sound speeds one can expressed the most accurate minimum time period as (Haensel et al. [1995])

$$\tau \approx 0.82 \left(\frac{M_\odot}{M} \right)^{1/2} \left(\frac{R}{10 \ km} \right)^{3/2} \ ms. \tag{6.90}$$

The maximum values of each minimum time periods are almost equal and are negligibly affected by the presence of electric charge (Fig. 6.21).

6.9   Results and discussions

In this chapter, we present a model of Einstein's cluster mimicking compact star in the context of TEGR, the Teleparallel Equivalent of General Relativity, as a gauge theory of translations with the torsion tensor being non-zero but with a vanishing curvature tensor, hence, the manifold is globally flat. Considering Einstein's clusters in GR realm arises many un-physical outcomes, such as pressure increases outward, imaginary sound speed, negative adiabatic index and therefore can't mimic compact star model. We have developed the TEGR field equations having a diagonal and off-diagonal tetrad with a specific function of $f(\mathbb{T})$. More specifically, considering the field equations with a diagonal (T1) and off-diagonal (T2) tetrads with linear functional form of $f(\mathbb{T}) = a\mathbb{T} + b$, we found Einstein cluster solutions that behaves like a compact star. Thus, it seems interesting that relativistic star solutions are possible only in the case of teleparallel equivalent of general relativity. In connection with

this, we have other solutions for particular power-law of $f(\mathbb{T})$ model with diagonal and off-diagonal tetrad. However, most of the attempts are unsuccessful because the resulting solutions yield negative pressures. Indeed, we found a very compact cluster solution in the case of $f(\mathbb{T}) = a\mathbb{T}^2$ using a off-diagonal tetrad. In this case we found the decreasing and positive energy density and pressure, however, both blows up at $r = 0$ i.e. it contain a central singularity which is unstable under gravitational collapse. This may be because of the fact that the constraint on the field equations i.e. $f_{,\mathbb{T}\mathbb{T}} = 0$ puts a strict restriction on the choice of $f(\mathbb{T})$ function to a linear one. As a result, only if $f(\mathbb{T})$ is a linear function of the torsion scalar $\mathbb{T}$, one can leads to the existence of neutron star solution (Deliduman and Yapiskan [2011]). In a recent paper, Boehmer et al. [2011], Deliduman and Yapiskan [2011] suggested that, instead of choosing $f_{,\mathbb{T}\mathbb{T}} = 0$, if one consider $\mathbb{T}' = 0$ or $\mathbb{T} = \mathbb{T}_0$, the solution yields a constant energy density and pressure, obeying the dark energy equation of state or the pressure which blows up at $r \to 0$. This result is similar to our solution for $f(\mathbb{T}) = a\mathbb{T}^2$ in T2. Therefore, such solutions can't be used to model neutron star alike cluster solution.

For the case of $f(\mathbb{T}) = a\mathbb{T} + b$ in T1 two solutions of clusters were found. As per the rigorous analysis and figures, presented model satisfy causality, energy condition, TOV-equation, Bondi criterion and stable static criterion. This means that the solution has the ability to mimic compact star models. The $M - I$ and $M - R$ graphs suggested that the I_{max} and M_{max} increases with increase in charge parameter k. The $M - \rho_c$ graph signifies that the solution gain its stability with increase in electric charge. However, the maximum time-period of rotation τ_{max} is negligibly affected by the presence of electric charge. The stiffness in the equation of state seems to be same and independent of electric charge from center till upto about 3.5 km, however, beyond 3.5 km till the surface, the stiffness increases with increase in electric charge. This may be because of the central region ($0 \leq r \leq 3.5$ km) is extremely dense thus neutralizing the electric charge through $e + p \to n + \nu_e$, which may also the source of neutrinos as described in Hogan [1973]. As the density decreases outward, the gravity becomes slightly weaker and the repulsive electric field starts affecting the stiffness. The solution favor physical solution for the range $0 \leq k \leq 1.3 \times 10^{-5}$, beyond which the solution doesn't satisfy causality and trigger a gravitational collapse once crossed the Buchdahl limit if $k > 1.3 \times 10^{-5}$. Similarly, for the case of linear $f(\mathbb{T})$ in T2, we have also found cluster solution which mimic the nature of compact star. The solution gives physical cluster solution for a very narrow range of charge parameter k which must be in the range $0 < k \leq 10^{-6}$ or otherwise the solution violates the

causality condition or physically unacceptable. Overall, the presented solution with vanishing radial pressure and/or Einstein's cluster model is fit for mimicking compact star models.

Chapter 7

Physical properties of class I compact star model for linear and Starobinsky$-f(\mathcal{R}, \mathcal{T})$ functions [1]

7.1 Introduction

One of the recent major challenges in modern physics at the present time is to clarify the dynamics of the Universe, specifically the phenomenon of accelerating Universe expansion. Concerning this wonderful phenomenon of accelerating Universe expansion, there are some freethinking perceptions in the background of astrophysics that give proves about the accelerated expanding type of space. These astrophysical perceptions incorporate the results procured from different cosmic sources viz., the Supernova type Ia (SNe Ia)(Perlmutter et al. [1997, 1998, 1999], Riess et al. [2004, 2007]), Cosmic Microwave Radiation Background (CMRB)(Bennett et al. [2003], Spergel et al. [2003, 2007]), Large Scale Structure (LSS)(Hawkins et al. [2003], Tegmark et al. [2004], Cole et al. [2005]), Baryon Acoustic Oscillations (BAO) (Eisenstein et al. [2005], Beutler et al. [2011], Percival et al. [2010], Anderson et al. [2012]) and Weak Lensing (WL) (Jain and Taylor [2003]). This occurrence of accelerating expansion comportment of the Universe is viewed as an extraordinary basic issues of modern physics. The latest experimental datum effectively illustrates that our cosmic is ruled by an element with strongly negative pressure, named as dark energy, which comprises

---

[1]Content of this chapter has been published in *Physics of Dark universe* (Elsevier), 30 (2020) 100620.

with 3/4 of the critical density. So as to clarify the nature of this dominant mysterious component and the accelerated expansion, there are some selections of the hypothetical models, in particular, the quintessence scalar field models (Wetterich [1988], Ratra and Peebles [1988]), the ghost field (Caldwell [2002], Nojiri and Odintsov [2003c,a]), tachyon field (Sen [2002], Padmanabhan and Choudhury [2002]), K-essence (Chiba et al. [2000], Armendariz-Picon et al. [2000, 2001]), quintom (Elizalde et al. [2004], Anisimov et al. [2005]), etc., additionally, the $\Lambda-$CDM model (Bahcall et al. [1999], Frieman et al. [2008]) clarifies this energy by incorporating a cosmological constant into Einstein's field equations (EFEs). However, some cosmological problems are noted in this process (Binétruy [2013], Burgess [2015]) and several models in alternative theories of gravitation have been progressed (Luongo and Quevedo [2014b,a], Luongo and Muccino [2018]). In the present period, many alternative theories of gravitation have been presented, however some theories of gravity such as $f(\mathcal{R})$, $f(\mathcal{T})$ and $f(\mathcal{R}, \mathcal{T})$ have become more important than all other theories of gravitation. Regarding all these theories, the geometric area has been substituted by a specialized functional shape alternatively to modifying the source of the EFEs. This revelation has now become the most significant progression in modern physics, specifically cosmology and astrophysics due to Einstein's theory of general relativity that our Universe is loaded with normal (baryonic, hadronic etc.) or exotic (dark matter (DM), dark energy (DE) etc.) matter and convincing proof that the extension of the Universe is accelerating. In view of these alternative theories, numerous other notable generalised alternative theories are additionally accessible, which help to investigate different cosmic attributes effectively. These all alternative theories have adopted various astrophysical and necessity planetary system requirements and are viewed as feasible candidates.

After the basic mathematical formulation of Einsteins well-known theory of gravity, some alterations in gravitational part of the general relativity action have been included with the time passage in which the sleekest alteration of general relativity is $f(\mathcal{R})$ gravity (Capozziello [2002], Nojiri and Odintsov [2003b], Carroll et al. [2004], Bertolami et al. [2007]) developed by taking a self-assertive function $f(\mathcal{R})$ instead of scalar curvature $\mathcal{R}$ in the action of Einstein-Hilbert. As can be seen, numerous altered gravity theories have been examined in literature and different problems in astrophysics and cosmology have been investigated with the assistance of these wonderful theories, which upgrade the importance of these prolonged theories. Qadir and his co-workers (Qadir et al. [2017]) fortified the prerequisite of the altered relativis-

tic components and showed that this alteration may assist with settling down the issues identified with DM and quantum gravity. Bhatti and his colleagues (Bhatti et al. [2017]) investigate compact stellar structures development by picking inside spherically symmetric line element and dark dynamical effect in the arena of this theory. Numerous investigators Cognola et al. [2005], Abdalla et al. [2005], De la Cruz-Dombriz and Dobado [2006], Bergliaffa [2006], Song et al. [2007], Akbar and Cai [2007], Starobinsky [2007] have used various methods to analyze the stability as well as consistency of this gravity theory. In this respect, to verify the consistency of $f(\mathcal{R})$ gravity theory, we can consider the hydrostatic equilibrium of stellar structures as a test instrument. Nevertheless, there are certain forms of $f(\mathcal{R})$ algebraic function which eliminate the presence of stable astrophysical structures and are reported unrealistic. In recent years, much research has been conducted on the existence, steadiness and dynamical unsteadiness of celestial stellar systems in the context of this theory of gravity (Cooney et al. [2010], Arapoğlu et al. [2011], Ganguly et al. [2014], Goswami et al. [2014], Sharif and Yousaf [2014], Astashenok et al. [2014]).

Altered theories of gravity have provided the theorists with various celestial procedures to survey the purposes behind the phenomenon of accelerating Universe expansion. Harko and his teammates (Harko et al. [2011]) were the first to propose the concept of curvature couplings and matter by representing a new version of altered gravity theory, so-called $f(\mathcal{R}, \mathcal{T})$ gravity. The same authors also determined the relating field equation by using the gravitational potentials mechanism and examined the importance of this alternative gravity theory. Moreover, they have introduced various models for $f(\mathcal{R}, \mathcal{T})$ algebraic functional in detachable compose viz., $f(\mathcal{R}, \mathcal{T}) = f_1(\mathcal{R}) + f_2(\mathcal{T})$. It is accounted as an intriguing alteration in light of the fact that the appearing field equations have not greatly complex structure or not managed order. $f(\mathcal{R}, \mathcal{T})$ gravity models are generally examined in the literature because of its dynamism in determining numerous astrophysical as well as cosmological issues. In $f(\mathcal{R}, \mathcal{T})$ altered gravity the matter Lagrangian density $\mathcal{L}_m$ fluctuates concerning the line element which is appeared by the existence of a source term. The source term expression is acquired as a function of the trace of the stress-energy tensor, $\mathcal{T}$, henceforth various opportunities of $\mathcal{T}$ would provide diverse ensemble of EFEs. Subsequently, numerous researchers did investigate with different stellar systems of Universe by taking diverse matter structures.

With the help of $f(\mathcal{R}, \mathcal{T})-$gravity, Houndjo [2012] investigated matter commanded age of our accelerating cosmic. Baffou and his co-workers (Baffou et al. [2015]) investi-

gated the problem of Universe unsteadiness subsequent to implementing perturbation method on the mathematical power-law systems and determined feasibility conditions. Sahoo and his collaborators (Sahoo et al. [2017]) studied spatially uniform cosmic in the arena of $f(\mathcal{R}, \mathcal{T})-$gravity. Lately, Moraes and his partners (Moraes and Sahoo [2017a]) examined the existence astrophysical structures and got a few reasonability conditions in the background of $f(\mathcal{R}, \mathcal{T})-$gravity. Several authors Yousaf et al. [2016], Ilyas et al. [2017], Yousaf et al. [2017], Maurya and Tello-Ortiz [2020a,b] also worked in the domain of $f(\mathcal{R}, \mathcal{T})-$ gravity with various stellar systems. Generally, anisotropic fluids i.e. unequal radial and tangential pressure ($p_r \neq p_t$) are affected to analyze developmental regime of stellar structure in mathematical physics. In survey of stellar compact systems, term anisotropy is established at an immense area, which has capability to influence and configuration of stellar objects as well as transform stability. It is notable that anisotropic uids portray a more realistic system form the astrophysical perspective. Surrender the isotropy condition raises an interesting event interior the astrophysical object for instance at the point when $p_t > p_r$ the framework encounters an repulsive force that checks the gravitational gradient (attractive if $p_t < p_r$), which permits the building of progressively compact and massive structures (Gokhroo and Mehra [1994]), expanding value of the gravitational surface red-shift (Bowers and Liang [1974], Ivanov [2002b]) which is a significant amount that connects the mass and the radius of the stellar configuration and amelioration of astrophysical system steadiness.

Presently, various works accessible in the literature deal the investigation of compact stellar structures representing the distributions of anisotropic matter; see e.g. Maurya et al. [2018, 2019], Errehymy et al. [2019], Errehymy and Daoud [2020] and references contained in that. Recently, a significant methodology for determining the exact EFEs solutions, describing the compact stellar structures, has been suggested by the theorists specifically the Karmarkar condition. The requisite and adequate condition for a spherically symmetric space-time to be of implanting class one was earliest inferred by Karmarkar [1948]. It is fundamentally a mathematical implement which encourages us to get accurate EFEs solutions. In this respect, several authors have been used this beautiful condition (Eisenhart [1966], Singh et al. [2017c], Bhar et al. [2016a], Maurya et al. [2018, 2019]), for examining the compact stellar systems. So, In this article, we will adopt the Karmarkar condition to build up the analytical and graphical solutions describing compact stellar configurations in the arena of an alternative theory of gravity, specifically $f(\mathcal{R}, \mathcal{T})-$gravity.

7.1. Introduction

Drawing on the above works of literature, in the present article, we will examine the existence of compact stellar models portraying anisotropic matter distributions in the field of altered gravity theory, so-called $f(\mathcal{R},\mathcal{T})-$gravity, by considering a compact stellar structure, namely a low-mass X-ray binary 4U 1820-30. In this regard, we choose two different functional forms of $f(\mathcal{R},\mathcal{T})-$gravity specifically, $f(\mathcal{R},\mathcal{T})$ $= \mathcal{R} + 2\chi\mathcal{T}$ and $f(\mathcal{R},\mathcal{T}) = \mathcal{R} + \xi\mathcal{R}^2 + 2\chi\mathcal{T}$ to address the physical features as well as astronomical impacts of curvature and matter coupling of compact stars. We also use the frame of embedding class one approaches to implant a 4-dimensional space-time into a 5-dimensional pseudo- Euclidean space, in order to acquire a full space-time portrayal within the relativistic astrophysical system in the arena of $f(\mathcal{R},\mathcal{T})-$gravity theory. So, in class one approach which proposed the opportunity of arriving at the well-comported solution, we have ansatz one of the gravitational potentials, in particular, the time-time component (e^{ν}) and we have obtained the second gravitational potential i.e, the radius-radius component (e^{λ}), from the Karmarkar condition. For two viable $f(\mathcal{R},\mathcal{T})$ models, we have investigated the behavior of energy density, radial as well as transverse pressures in the interior geometry of compact stars. Besides, for exploring physical accessibility of the obtained solutions, we have analyzed the new solutions through different physical tests such as hydrostatic equilibrium, causality condition, stability factor, adiabatic index and stability, static stability criterion and energy conditions with the help of the three compact stellar structures, in particular, PSR J1614-2230 ($M = 1.97 \pm 0.04 \ M_{\odot} \ , \ R = 9.69 \pm 0.2 \ km$), Vela X-1 ($M = 1.77 \pm 0.08 \ M_{\odot} \ , \ R = 9.56 \pm 0.08 \ km$) and 4U 1820-30 ($M = 1.58 \pm 0.06 \ M_{\odot} \ , \ R = 9.1 \pm 0.4 \ km$) associate with physical parameters analytically and graphically. Moreover, we have matched the obtained astrophysical configuration with the exterior space-time specified by Schwarzschild line element, in order to acquire the constant parameters. On the other hand, the resulting $M - R$ curve and the appropriate moment of inertia ($M - I$ curve) from our solution are well-adapted with observed data of the mentioned compact stellar structures.

The outline of this chapter is as follows: In Sect. 7.2, we briefly review the fundamental attributes of the altered gravity theory viz., $f(\mathcal{R},\mathcal{T})-$gravity. In Sect. 7.3, we express the fundamental EFEs for anisotropic matter distributions in linear $f(\mathcal{R},\mathcal{T})-$gravity, and we will show the essential formalization of class one space-time and the spherical symmetric line element in Sect. 7.4. In Sect. 7.5, we represent the total astrophysical system under embedding class one method in linear $f(\mathcal{R},\mathcal{T})-$gravity and its thermodynamic portrayal is also specified. In Sect. 7.6, we

have establishing arbitrary constants of the obtained astrophysical system with the exterior spacetime specified by Schwarzschild line element. In Sect. 7.7 we have analyzed the new solutions by means of several physical attempts viz., hydrostatic equilibrium, causality condition, stability factor, Adiabatic index, static stability criterion and energy conditions, as well as the stiffness of EoS, $M-R$ and $I-M$ diagram are represented in subsections 7.7.1–7.7.6. In Sect. 7.8, we present the non-linear model for Starobinsky $f(\mathcal{R}, \mathcal{T})-$ and corresponding field equation with its thermodynamic representation for anisotropic matter distributions in subsection 7.8.1. In subsection 7.8.2, we represent the full stellar system under embedding class one method in Starobinsky $f(\mathcal{R}, \mathcal{T})$ model as well as constant parameters are additionally determined. Finally, the discussion and conclusion are suggested in Sect. 7.9.

7.2   Formalism of $f(\mathcal{R}, \mathcal{T})-$gravity

In this section, we briefly survey the feasible modified gravity theory, as on account of $f(\mathcal{R}, \mathcal{T})-$gravity with $\mathcal{T}$ being the trace of the energy-momentum tensor, $T_{\mu\nu}$. The complete action is

$$S = \frac{1}{16\pi} \int f(\mathcal{R}, \mathcal{T})\sqrt{-g} \; d^4x + \int \mathcal{L}_m \sqrt{-g} \; d^4x \tag{7.1}$$

where $f(\mathcal{R}, \mathcal{T})$ is the algebraic function of scalar curvature $\mathcal{R}$, and g stand the determinant of the metric tensor $g_{\mu\nu}$. We describe the matter Lagrangian density $\mathcal{L}_m$ identified with the stress-energy tensor as

$$T_{\mu\nu} = -\frac{2}{\sqrt{-g}} \frac{\delta(\sqrt{-g}\,\mathcal{L}_m)}{\delta g^{\mu\nu}}, \tag{7.2}$$

with the trace $\mathcal{T} = g^{\mu\nu}T_{\mu\nu}$. According to Harko et al. [2011], we take into account the case of matter Lagrangian density $\mathcal{L}_m$ relies just upon the metric tensor elements $g_{\mu\nu}$. Shrinking Eq. (7.2) yields

$$T_{\mu\nu} = g_{\mu\nu}\mathcal{L}_m - \frac{2\,\partial\mathcal{L}_m}{\partial g^{\mu\nu}}. \tag{7.3}$$

By varying the action, (7.1) as a function of the metric $g^{\mu\nu}$, we obtain the master equations of movement

7.2. Formalism of $f(\mathcal{R}, \mathcal{T})-$gravity

$$
\left(R_{\mu\nu} - \nabla_\mu \nabla_\nu\right) f_{\mathcal{R}}(\mathcal{R}, \mathcal{T}) + g_{\mu\nu} \Box f_{\mathcal{R}}(\mathcal{R}, \mathcal{T}) - \frac{1}{2} f(\mathcal{R}, \mathcal{T}) g_{\mu\nu}
$$
$$
= 8\pi \ T_{\mu\nu} - f_{\mathcal{T}}(\mathcal{R}, \mathcal{T}) \left(T_{\mu\nu} + \Theta_{\mu\nu}\right), \tag{7.4}
$$

where $f_{\mathcal{R}}(\mathcal{R}, \mathcal{T}) = \partial f(\mathcal{R}, \mathcal{T})/\partial \mathcal{R}$ and $f_{\mathcal{T}}(\mathcal{R}, \mathcal{T}) = \partial f(\mathcal{R}, \mathcal{T})/\partial \mathcal{T}$. The ∇_μ indicates covariant derivative which is related to the Levi-Civita association of metric tensor $g_{\mu\nu}$ and box operator $\Box$ is characterized by

$$
\Box \equiv \frac{1}{\sqrt{-g}} \frac{\partial}{\partial x^\mu} \left(\sqrt{-g} \ g^{\mu\nu} \frac{\partial}{\partial x^\nu}\right) \quad \text{and} \quad \Theta_{\mu\nu} = g^{\alpha\beta} \frac{\delta T_{\alpha\beta}}{\delta g^{\mu\nu}}.
$$

In order to arrive at the formula of the covariant derivative of the stress-energy tensor and draw the one of the generic function, we implement the covariant derivative of Eq. (7.4) (Alvarenga et al. [2013]), as

$$
\nabla^\mu T_{\mu\nu} = \frac{f_{\mathcal{T}}(\mathcal{R}, \mathcal{T})}{8\pi - f_{\mathcal{T}}(\mathcal{R}, \mathcal{T})} \left[(T_{\mu\nu} + \Theta_{\mu\nu})\nabla^\mu \ln f_{\mathcal{T}}(\mathcal{R}, \mathcal{T}) + \nabla^\mu \Theta_{\mu\nu} - \frac{1}{2} g_{\mu\nu} \nabla^\mu \mathcal{T}\right] \tag{7.5}
$$

So from this Eq. (7.5), it is clear to see that the stress-energy tensor $T_{\mu\nu}$ in the context of $f(\mathcal{R}, \mathcal{T})-$gravity isn't preserved as a view purpose of Einstein general relativity (GR) because of the presence of nonminimal matter-geometry coupling in the system.

By employing Eq. (7.3), the tensor $\Theta_{\mu\nu}$ is characterized as

$$
\Theta_{\mu\nu} = -2T_{\mu\nu} + g_{\mu\nu}\mathcal{L}_m - 2g^{\alpha\beta} \frac{\partial^2 \mathcal{L}_m}{\partial g^{\mu\nu} \partial g^{\alpha\beta}}. \tag{7.6}
$$

Subsequently, so as to make easy an immediate comparison with the pioneering work of Buchdahl [1959], we pursue his conventions. For star structures, one can assumes a spherically symmetric metric with coordinates (t, r, θ, ϕ) in the accompanying shape

$$
ds^2 = e^{\nu(r)} \ dt^2 - e^{\lambda(r)} dr^2 - r^2(d\theta^2 + \sin^2 \theta \ d\phi^2), \tag{7.7}
$$

where $\nu(r)$ and $\lambda(r)$ are arbitrary functions of the radial coordinate r only. The system of units here adopted is such that $G = c = 1$. We suppose that the inside of stellar configuration is replete of a perfect fluid source and stress-energy tensor of the

shape

$$T_{\mu\nu} = (\rho + p_t)u_\mu u_\nu - p_t g_{\mu\nu} + (p_r - p_t)g_{\mu\nu}, \tag{7.8}$$

where u_ν is the 4-velocity, satisfying $u_\mu u^\mu = -1$ and $u_\nu \nabla^\mu u_\mu = 0$. Here, ρ is the matter density, p_r and p_t are the radial and transverse pressure. Since, we choose another hypothesis, specifically, $\mathcal{L}_m = -\mathcal{P} = (p_r + 2p_t)/3$, as per the definition recommended by Harko and his co-workers in Harko et al. [2011], the tensor (7.6) gives

$$\Theta_{\mu\nu} = -2T_{\mu\nu} - \mathcal{P}\, g_{\mu\nu}. \tag{7.9}$$

Generally, the field equations depend through the stress-energy tensor, on the physical nature of the matter field. Thus on account of $f(\mathcal{R},\mathcal{T})$ gravity relying upon the nature of the matter source, we get several theoretical models corresponding to different matter contributions for $f(\mathcal{R},\mathcal{T})$ gravity are conceivable, where the generalized Einstein-Hilbert Lagrangian is given by

$$f(\mathcal{R},\mathcal{T}) = f_1(\mathcal{R}) + f_2(\mathcal{T}), \tag{7.10}$$

with $f_1(\mathcal{R})$ and $f_2(\mathcal{T})$ being functions purely dependent upon $\mathcal{R}$ and $\mathcal{T}$, respectively. This class of separable models offers a significant opportunities for solving or evading some issues one countenances when regarding GR as the background theory of gravity and can give a reasonable extension of $f(\mathcal{R})$ gravity. On this respect, the $f(\mathcal{R},\mathcal{T})$ gravity has been applied to astrophysics of compact structures and cosmology, among other areas, yielding interesting and testable outcomes. In this regard, the gravitational coupling is again given by an effective, matter dependent coupling, which is proportional to the derivative of the function $f_2(\mathcal{T})$ with respect to $\mathcal{T}$. The gravitational field equations can be reevaluated in such a form that the higher-order corrections, coming both from the geometry and from the matter-geometry coupling, give a stress-energy tensor of geometrical and matter origin, portraying an effective source term on the standard Einstein field equations. In the $f(\mathcal{R},\mathcal{T})$ domain, the cosmic acceleration may result not only from a geometrical contribution to the total cosmic energy density but it is also dependent on the matter content of the universe, which provides new corrections to the Hilbert-Einstein Lagrangian via the matter-geometry coupling. Therefore, depending upon the choice of $f_1(\mathcal{R})$ and $f_2(\mathcal{T})$, we can formulate different $f(\mathcal{R},\mathcal{T})$ models which has consistently with astrophysical restraints

and local gravity test. Being aware of this situation, we choose the two different functional forms of $f(\mathcal{R}, \mathcal{T})-$gravity corresponding linear and Starobinsky $f(\mathcal{R}, \mathcal{T})$ models specifically, $f(\mathcal{R}, \mathcal{T}) = \mathcal{R} + 2\chi\mathcal{T}$ where $f_1(\mathcal{R}) = \mathcal{R}$ and $f(\mathcal{R}, \mathcal{T}) = \mathcal{R} + \xi\mathcal{R}^2 + 2\chi\mathcal{T}$ where $f_1(\mathcal{R}) = \mathcal{R} + \xi\mathcal{R}^2$ along with the linear combination of $f_2(\mathcal{T})$ such as $f_2(\mathcal{T}) = 2\chi\mathcal{T}$ to determine the effective stress-energy tensor (Harko et al. [2011]), where ξ and χ are two coupling constants. We would like to mention here that we can recover GR from our selections of algebraic functions $f(\mathcal{R}, \mathcal{T})$ by setting the coupling parameters ξ and χ to zero. As a general remark, we can say that the astrophysical model related to the existence of the matter-geometry coupling is consistent with the stable stellar configuration, as well as its consequences yield new features and the emergence of corrections and extensions as compared to GR. In this regard, we discuss the physical nature of the two different algebraic functions $f(\mathcal{R}, \mathcal{T}) = \mathcal{R} + 2\chi\mathcal{T}$ and $f(\mathcal{R}, \mathcal{T}) = \mathcal{R} + \xi\mathcal{R}^2 + 2\chi\mathcal{T}$ to address the study of compact astrophysical structures during the framework of $f(\mathcal{R})$ gravity theory examining the admissibility of the astrophysical system, where the coefficient of $\mathcal{R}$ must be one to yield conventional gravity in low curvature environments and χ is a single parameter describing the modification of gravity. Note there is no question of Ostrogradsky instability in this theory. Obtaining strong limits on χ could severely effect the possible contributions of this term in astrophysical situations. The simplest and most trivial choice for the $\mathcal{R}$ dependence corresponds to the Einstein-Hilbert term. This is the way to study how the material corrections given by $2\chi\mathcal{T}$ promote deviations from GR and $f(\mathcal{R})$ gravity. Also, this modification makes change in standard Einstein field equations and exhibits presence of the new matter type interior the compact stellar structure. This type of matter being discovered by a significant interaction of matter curvature coupling. However, the effect of matter curvature coupling present in $f(\mathcal{R}, \mathcal{T})$ gravity on the relativistic structures leads to a source term which may yield interesting results. It can produce a matter-dependent deviation from geodesic motion and also helps to study dark energy, dark matter interactions as well as late-time acceleration. For this purpose, we discuss the models corresponding to linear and non-linear $f(\mathcal{R}, \mathcal{T})$ function in two different sections as follows:

7.3   Field equations in linear $f(\mathcal{R}, \mathcal{T})-$model

By involving of the linear $f(\mathcal{R}, \mathcal{T})$ function in Eq. (7.4), the Einstein tensor be-

comes

$$G_{\mu\nu} = 8\pi \; T_{\mu\nu} + \chi\mathcal{T} \; g_{\mu\nu} + 2\chi(T_{\mu\nu} + \mathcal{P} \; g_{\mu\nu}). \tag{7.11}$$

Note that field equations (7.4) are reduced to EFEs when $f(\mathcal{R}, \mathcal{T}) \equiv \mathcal{R}$. Studying such a particular linear assumption has generally admitted addressing astrophysical as well as cosmological solutions. By substituting the value of $f(\mathcal{R}, \mathcal{T}) = \mathcal{R} + 2\chi\mathcal{T}$ in Eq. (7.5), we find

$$\nabla^\mu T_{\mu\nu} = -\frac{\chi}{2(4\pi + \chi)} \left[g_{\mu\nu}\nabla^\mu\mathcal{T} + 2\,\nabla^\mu\left(\mathcal{P} \; g_{\mu\nu}\right) \right]. \tag{7.12}$$

For the spacetime (7.7), the field equations (7.11) when $f(\mathcal{R}, \mathcal{T}) = \mathcal{R} + 2\chi\mathcal{T}$ reduce to

$$8\pi\rho_{eff} = e^{-\lambda}\left(\frac{\lambda'}{r} - \frac{1}{r^2}\right) + \frac{1}{r^2}, \tag{7.13}$$

$$8\pi p_{reff} = e^{-\lambda}\left(\frac{\nu'}{r} + \frac{1}{r^2}\right) - \frac{1}{r^2}, \tag{7.14}$$

$$8\pi p_{teff} = \frac{e^{-\lambda}}{4}\left(2\nu'' + \nu'^2 + \frac{2(\nu' - \lambda')}{r} - \nu'\lambda'\right). \tag{7.15}$$

where,

$$\rho_{eff} = \rho + \frac{\chi}{24\pi}\left(9\rho - p_r - 2p_t\right)$$
$$p_{reff} = p_r - \frac{\chi}{24\pi}\left(3\rho - 7p_r - 2p_t\right)$$
$$p_{teff} = p_t - \frac{\chi}{24\pi}\left(3\rho - p_r - 8p_t\right).$$

On using the above definitions, the field equations (7.13)-(7.15) becomes

$$
\begin{aligned}
\rho \;\; = \;\; & \frac{e^{-\lambda}}{48r^2(\chi + 2\pi)(\chi + 4\pi)}\Big[r\lambda'\left\{16(\chi + 3\pi) - r\chi\nu'\right\} + 16(\chi + 3\pi) \\
& (e^\lambda - 1) + r\chi\left\{2r\nu'' + \nu'\left(r\nu' + 4\right)\right\}\Big],
\end{aligned}
\tag{7.16}
$$

$$
\begin{aligned}
p_r &= \frac{e^{-\lambda}}{48r^2(\chi+2\pi)(\chi+4\pi)}\Big[r\big\{\chi\lambda'(r\nu'+8)-2r\chi\nu''+\nu'\left(20\chi-r\chi\nu'+48\pi\right)\big\} \\
&\quad -16(\chi+3\pi)(e^{\lambda}-1)\Big], \tag{7.17}
\end{aligned}
$$

$$
\begin{aligned}
p_t &= \frac{e^{-\lambda}}{48r^2(\chi+2\pi)(\chi+4\pi)}\Big[r\big\{-\lambda'\{r(5\chi+12\pi)\nu'+4(\chi+6\pi)\}+2r \\
&\quad (5\chi+12\pi)\nu''+r(5\chi+12\pi)\nu'^{\,2}+8(\chi+3\pi)\nu'\big\}+8\chi\left(e^{\lambda}-1\right)\Big]. \tag{7.18}
\end{aligned}
$$

Solving the above field equations exactly is a difficult task. Many authors have adopted several methods to obtained the solution. In this article, we will adopt the embedding class one approach to solve the field equations.

7.4   Method of embedding class one

Then again, Eisenhart [1966] was showed that an embedding class one space $(n+1)$ dimensional space V^{n+1} can be implemented into a $(n+2)$ dimensional pseudo-Euclidean space E^{n+2} can be represented by a $(n+1)$ dimensional space V^{n+1} if there subsists a symmetric tensor a_{mn} which fulfills the accompanying Gauss-Codazzi equations:

$$
\begin{aligned}
R_{mnpq} &= 2e\, a_{m[p}a_{q]n} \\
0 &= a_{m[n;p]}-\Gamma^q_{[np]}a_{mq}+\Gamma^q_{m[n}a_{p]q},
\end{aligned}
$$

where $e=\pm 1$, R_{mnpq} is the Riemann curvature tensor, while a_{mn} are the coefficients of the 2nd order differential shape.

Kasner [1921] shown that the Schwarzschild's vacuum can be embedded into six dimensional psuedo-Euclidean space by a series of coordinate transformations. This means that the Schwarzschild exterior is of class 2. Similarly, Gupta and Goel [1975] adopted a different coordinate transformations:

$$
z_1 = ke^{\nu/2}\cosh\left(\frac{t}{k}\right),\; z_2 = ke^{\nu/2}\sinh\left(\frac{t}{k}\right),\; z_3 = f(r),
$$

$$
z^4 = r\sin\theta\cos\phi,\; z_5 = r\sin\theta\sin\phi,\; z_6 = r\cos\theta,
$$

to transform a generalized four dimensional spacetime (7.7) into six dimensional pseudo-Euclidean space i.e.

$$
ds^2 = (dz_1)^2-(dz_2)^2\mp(dz_3)^2-(dz_4)^2-(dz_5)^2-(dz_6)^2, \tag{7.19}
$$

with $[f'(r)]^2 = \mp\big[-\big(e^\lambda - 1\big) + k^2 e^\nu \nu'^2/4\big]$. This again involves that the 4-D line element (7.7) can be implemented in 6-D Euclidean space, nevertheless, there exist a conceivable case where $(dz_3)^2 = [f'(r)]^2 = 0$, than the six dimensional Euclidean space (7.19) can be reduces to 5-D pseudo-Euclidean space. This is conceivable only if

$$f'(r)]^2 = \mp\big[-\big(e^\lambda - 1\big) + k^2 e^\nu \nu'^2/4\big] = 0, \tag{7.20}$$

or

$$e^\lambda = 1 + \frac{k^2}{4}\, \nu'^2 e^\nu. \tag{7.21}$$

The same condition (7.21) was originally derived by Karmarkar [1948] in the shape of components of Riemann tensor as

$$R_{1010}R_{2323} = R_{1212}R_{3030} + R_{1220}R_{1330}. \tag{7.22}$$

Pandey and Sharma [1982] drew attention to the fact that Karmarkar condition is just the important condition to turn into a class one, they found the adequate condition as $R_{2323} \neq 0$. Henceforth, the requisite and adequate condition to be a class one is to fulfill both Karmarkar and Pandey-Sharma conditions. In terms of the metric components, (7.22) can be composed as

$$\frac{\lambda'\nu'}{1 - e^\lambda} = \lambda'\nu' - 2(\nu'' + \nu'^2) + \nu'^2 \tag{7.23}$$

which on integration one gets the $g_{tt}-$metric function as

$$e^\nu = \left(A + B\int \sqrt{e^\lambda - 1}\, dr\right)^2. \tag{7.24}$$

where A and B are two constants of integration. One must always keeps in mind that there is no class one vacuum exterior as the static Schwarzschild's vacuum is already a class two solution.

7.5 Embedding class one background in linear $f(\mathcal{R}, \mathcal{T})$ $-$gravity

Solving the field equations in $f(\mathcal{R}, \mathcal{T})-$gravity exactly is a challenging task because of the highly coupled non-linear differential equations. To simplify the problem, we

have adopted the embedding class one approach, which is application to all four dimensional spacetime. Here, we propose a new metric function

$$e^\lambda = 1 + ar^2 \log\left(br^2 + 2\right). \tag{7.25}$$

When ansatz e^λ, one must keep in minds that it must be increasing function of radial coordinate and unity at the center which ensure that the gravitational potential $e^{\lambda(r)}$ must keep the form $e^{\lambda(r)} = 1 + O(r^2)$ near at $r = 0$ as well as it should be not same as Kohlar-Chao solution or Schwarzschild solution otherwise anisotropy will vanishes throughout the model (Maurya et al. [2015a, 2016c]). Using (7.25) in (7.24), we get

$$e^\nu = \left[A + \frac{\sqrt{a}B(br^2 + 2)}{2b}\left\{\sqrt{\log(br^2 + 2)} - F\left(\sqrt{\log(br^2 + 2)}\right)\right\}\right]^2 \tag{7.26}$$

where $F(x)$ is the Dawson's integral defined by

$$F(x) = e^{-x^2}\int_0^x e^{\tau^2}\, d\tau = \frac{\sqrt{\pi}}{2}\, e^{-x^2}\, \text{erfi}(x).$$

Here erfi(x) is the usual imaginary error function. In order to test physical validity of the obtained gravitational potential (7.26), it was proved by the researchers Lake [2003, 2004], Herrera et al. [2008], Maurya et al. [2017a] that any realistic models should preserve the monotonic increasing behaviour of $\nu(r)$ throughout inside the compact object and attains its regular minimum at centre. The said fetures of the $\lambda(r)$ and $\nu(r)$ can be observed from Fig. 7.1.
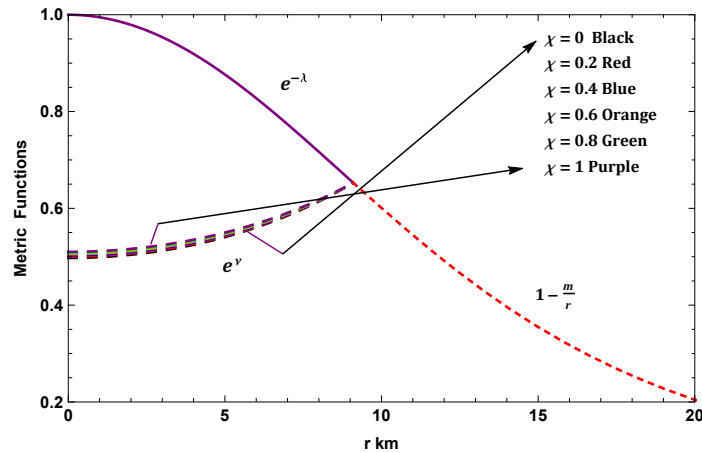
Figure 7.1: Variation of metric functions with radial coordinate for 4U 1820-30 ($M = 1.58 \pm 0.06\ M_\odot$, $R = 9.1 \pm 0.4\ km$) with $b = 0.004$.

Plugging the metric functions into the field equations (7.16)-(7.18), one can write

$$\rho(r) = \frac{a\left[f_1(r) + f_2(r) + f_3(r) - f_4(r)\right]}{6(\chi + 2\pi)(\chi + 4\pi)\left(br^2 + 2\right)f_5(r)[h(r) + 1]^2} \tag{7.27}$$

$$p_r(r) = \frac{a}{6(\chi + 2\pi)(\chi + 4\pi)\left(br^2 + 2\right)g_5(r)[h(r) + 1]^2}\left[b^2 r^2 \chi \left(4A\sqrt{h(r)} - Br\right)\right.$$
$$\left. + g_1(r) + g_2(r) + g_3(r) + g_4(r)\right], \tag{7.28}$$

$$\Delta(r) = \frac{ar^2 k_1(r)\left[a\left(br^2 + 2\right)\log^2\left(br^2 + 2\right) - b\right]}{2(\chi + 4\pi)\left(br^2 + 2\right)[h(r) + 1]^2 k_2(r)}, \tag{7.29}$$
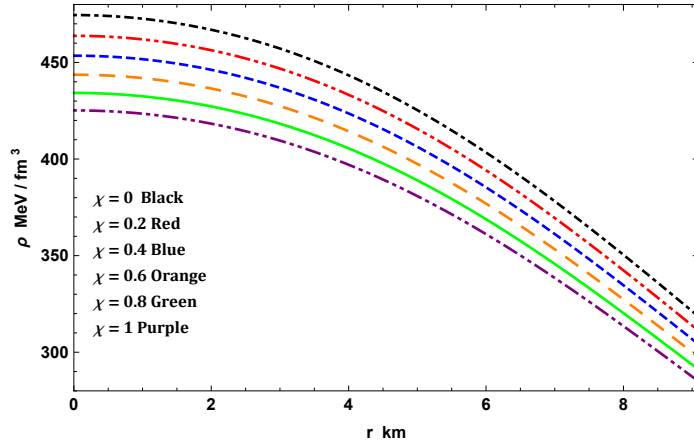
Figure 7.2: Variation of energy density with radial coordinate for 4U 1820-30 ($M = 1.58 \pm 0.06\ M_\odot$, $R = 9.1 \pm 0.4\ km$) with $b = 0.004$.
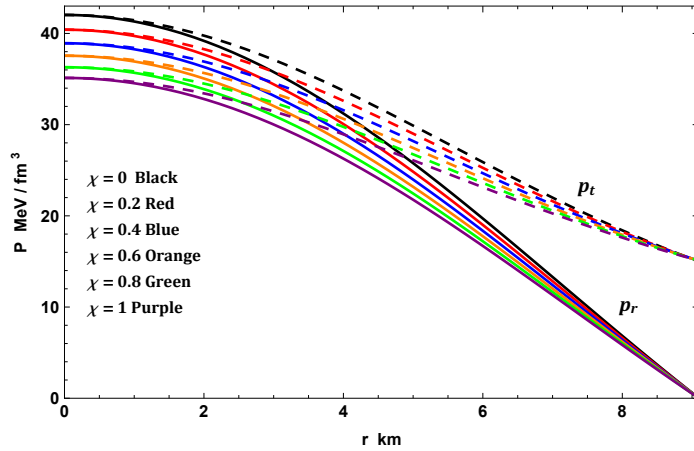
Figure 7.3: Variation of pressures with radial coordinate for 4U 1820-30 ($M = 1.58 \pm 0.06\ M_\odot$, $R = 9.1 \pm 0.4\ km$) with $b = 0.004$.
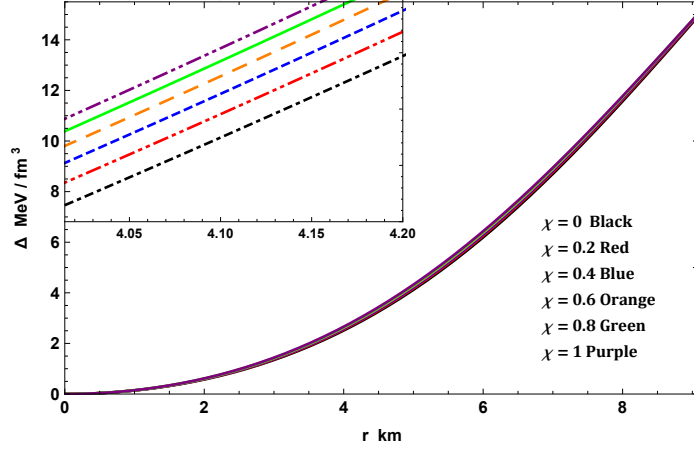
Figure 7.4: Variation of anisotropy with radial coordinate for 4U 1820-30 ($M = 1.58 \pm 0.06\ M_\odot$, $R = 9.1 \pm 0.4\ km$) with $b = 0.004$.

where,

$$
\begin{aligned}
f_1(r) &= 2a^2 Br^3(\chi + 3\pi)\left(br^2 + 2\right)^2 \log^3\left(br^2 + 2\right) + b^2 r^2 \Big[8A(\chi + 3\pi) \\
&\quad \sqrt{ar^2 \log\left(br^2 + 2\right)} + Br\chi\Big] \\
f_2(r) &= b\left(br^2 + 2\right)\log\left(br^2 + 2\right)\Big[12A(\chi + 3\pi)\sqrt{h(r)} + \\
&\quad 4aBr^3(\chi + 3\pi) + 3Br\chi\Big] \\
f_3(r) &= 2ar\left(br^2 + 2\right)\log^2\left(br^2 + 2\right)\Big[2Abr(\chi + 3\pi)\sqrt{h(r)} \\
&\quad + B\left\{4br^2\chi + 9\pi\left(br^2 + 2\right) + 6\chi\right\}\Big], \\
f_4(r) &= \sqrt{\pi}aBr(\chi + 3\pi)\sqrt{\log\left(br^2 + 2\right)}\Big[\left(br^2 + 2\right)\log(br^2 + 2)\big\{ar^2 \\
&\quad \log(br^2 + 2) + 3\big\} + 2br^2\Big]\mathrm{erfi}\left(\sqrt{\log\left(br^2 + 2\right)}\right), \\
f_5(r) &= 2Ab\sqrt{h(r)} - \frac{a}{2}\sqrt{\pi}Br\sqrt{\log\left(br^2 + 2\right)}\mathrm{erfi}\left(\sqrt{\log\left(br^2 + 2\right)}\right) \\
&\quad + aBr\left(br^2 + 2\right)\log\left(br^2 + 2\right) \\
g_1(r) &= -2a^2 Br^3(\chi + 3\pi)\left(br^2 + 2\right)^2 \log^3\left(br^2 + 2\right), \\
g_2(r) &= 2aBr\left(br^2 + 2\right)\sqrt{\log\left(br^2 + 2\right)}\Big[ar^2(\chi + 3\pi)(br^2 + 2)\log^2(br^2 + 2) \\
&\quad - br^2\chi + 3\pi(br^2 + 2)\log(br^2 + 2)\Big]F\left(\sqrt{\log(br^2 + 2)}\right), \\
g_3(r) &= b\left(br^2 + 2\right)\log\left(br^2 + 2\right)\Big[Br\{\chi(2ar^2 + 9) + 24\pi\} - 12\pi A\sqrt{h(r)}\Big], \\
g_4(r) &= 2ar\left(br^2 + 2\right)\log^2\left(br^2 + 2\right)\Big[-2Abr(\chi + 3\pi)\sqrt{h(r)} + 5bBr^2\chi \\
&\quad + \pi B\left(9br^2 - 6\right)\Big],
\end{aligned}
$$

$$
\begin{aligned}
g_5(r) &= aBr\left(br^2 + 2\right)\log\left(br^2 + 2\right) + 2Ab\sqrt{h(r)} - aBr\left(br^2 + 2\right) \\
&\quad \sqrt{\log\left(br^2 + 2\right)}\, F\left(\sqrt{\log\left(br^2 + 2\right)}\right), \\
k_1(r) &= -\sqrt{\pi}aBr\sqrt{\log\left(br^2 + 2\right)}\,\mathrm{erfi}\left(\sqrt{\log\left(br^2 + 2\right)}\right) + 2aBr\left(br^2 + 2\right) \\
&\quad \log\left(br^2 + 2\right) + 4Ab\sqrt{h(r)} - 4bBr, \\
k_2(r) &= 2aBr\left(br^2 + 2\right)\log\left(br^2 + 2\right) + 4Ab\sqrt{h(r)} - \sqrt{\pi} \\
&\quad aBr\sqrt{\log\left(br^2 + 2\right)}\,\mathrm{erfi}\left(\sqrt{\log\left(br^2 + 2\right)}\right).
\end{aligned}
$$

with $h(r) = ar^2\log\left(br^2 + 2\right)$.
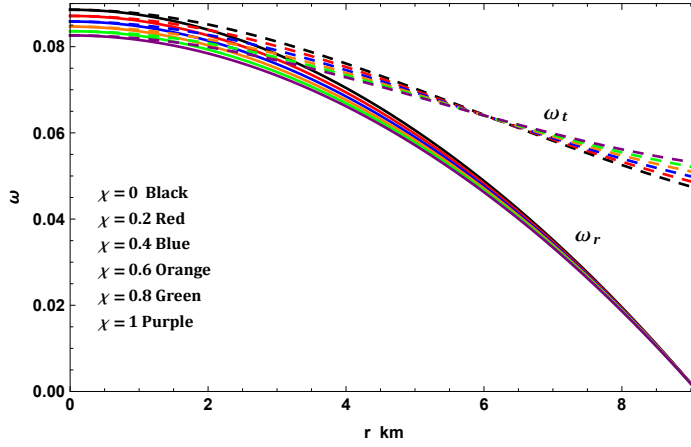
Figure 7.5: Variation of ω_r and ω_t with radial coordinate for 4U 1820-30 ($M = 1.58 \pm 0.06\ M_\odot$, $R = 9.1 \pm 0.4\ km$) with $b = 0.004$.

The remaining physical variables can be calculated from the above physical quantities. The EoS parameter and interior redshift can be found as

$$
\omega_r = \frac{p_r}{\rho} \quad , \quad \omega_t = \frac{p_t}{\rho} \tag{7.30}
$$

$$
z(r) = e^{-\nu/2} - 1. \tag{7.31}
$$

For physical matters one must always satisfy $\omega_i \leq 1$.

7.6 Boundary conditions

It is well-important to matching the inward geometry $\mathcal{M}^-$ at the surface $\Sigma = r = R$ with the outside space-time $\mathcal{M}^+$ encompassing the configuration in order to ensure a confined and limited matter distribution with well-specified mass M and radius R

i.e., a well-behaved compact stellar configuration. In this regard, on account of GR background, the external manifold is notable, exactly it compares to Schwarzschild vacuum space-time by taking into account a compact stellar structure which is static, non-radiating, and uncharged. Nonetheless, with regards to $f(\mathcal{R}, \mathcal{T})$ gravity the external manifold encompassing the fluid sphere doesn't really correspond with the Schwarzschild solution, what is more this outside space-time could on a basic level get contributions from the material area given by the trace of the energy momentum tensor because of the breakdown of the minimal coupling matter standard between the material area and the gravitational. Subsequently, the well-known Israel-Darmois (ID) (Israel [1966a], Darmois [1927]) formalism corresponding to the usual joining conditions applicable in GR, could not work in $f(\mathcal{R}, \mathcal{T})$ gravity anymore. So, in order to obtain the usual junction conditions to be applicable in this theory, we can redefine it appropriately. In this respect, a straightforward method to perceive how the contributions originating from the $f(\mathcal{R}, \mathcal{T})$ function could affect the outside space-time is re-composed the field equations (7.4) as follows,

$$
\begin{aligned}
G_{\mu\nu} \equiv R_{\mu\nu} - \frac{1}{2}\mathcal{R}\,g_{\mu\nu} = \frac{1}{f_{\mathcal{R}}}\bigg[& 8\pi T_{\mu\nu} + \frac{f}{2}g_{\mu\nu} - \frac{\mathcal{R}}{2}f_{\mathcal{R}}\,g_{\mu\nu} \\
& - \left(T_{\mu\nu} + \Theta_{\mu\nu}\right)f_{\mathcal{T}} - \left(g_{\mu\nu}\Box - \nabla_{\mu}\nabla_{\nu}\right)f_{\mathcal{R}}\bigg],
\end{aligned}
\tag{7.32}
$$

afterward by considering the trace of this expression (Eq.(7.32)) one gets

$$
\mathcal{R} = \frac{1}{f_{\mathcal{R}}}\left[8\pi\mathcal{T} + 2f - \left(\mathcal{T} + \Theta\right)f_{\mathcal{T}} - 3\Box f_{\mathcal{R}}\right].
\tag{7.33}
$$

Consequently, by taking into consideration a matter field under vacuum i.e, $T_{\mu\nu} = 0 \rightarrow \mathcal{T} = 0$ Eq. (7.33) gives

$$
\mathcal{R} = \frac{1}{f_{R}}\left[2f_1 - 3\Box f_{\mathcal{R}}\right],
\tag{7.34}
$$

where f_1 stands the geometrical part of the $f(\mathcal{R}, \mathcal{T})$ function that is $f_1 \equiv f_1(\mathcal{R})$. Indeed, the $f(\mathcal{R}, \mathcal{T})$ function can be viewed as $f(\mathcal{R}, \mathcal{T}) = f_1(\mathcal{R}) + f_2(\mathcal{T})$. In this manner, it is easy to see that a disappearing stress-energy tensor in the context of $f(\mathcal{R}, \mathcal{T})$ theory of gravity doesn't mean a null Ricci scalar as we have seen in GR where for $T_{\mu\nu} = 0 \rightarrow \mathcal{R} = 0 \rightarrow R_{\mu\nu} = 0$ which describes a vacuum space-time. Additionally, $T_{\mu\nu} = 0$ doesn't suggest $f_2 = 0$ at all obviously this term could contributes with

a constant term. At this stage, the usual junction conditions proposed by Israel-Darmois are well redefined, well-applicable, and will work as they do in usual gravity, if and only if we make sure that the external solution corresponds to Schwarzschild solution. Clearly it's not a simple task to accomplish it, since the function $f(\mathcal{R}, \mathcal{T})$ can be as complex as one wants. However, in the current circumstance, the linear $f(\mathcal{R}, \mathcal{T})$ function i.e. $f(\mathcal{R}, \mathcal{T}) = \mathcal{R} + 2\chi\mathcal{T}$ guarantees that the contributions of the material and geometric area stay limited to the range $0 \leq r \leq R$. Besides, the reality that the function $f(\mathcal{R}, \mathcal{T})$ is linear in $\mathcal{R}$, in addition to a linear coupling in $\mathcal{T}$ via a flexible parameter χ, can be viewed as a usual gravity model coupled to a variable cosmological constant which likewise breaks the minimal coupling matter with the gravitational area. More precisely, by substituting the linear functional form $f(\mathcal{R}, \mathcal{T}) = \mathcal{R} + 2\chi\mathcal{T}$ into Eq. (7.34) and solving for $\mathcal{R}$ gives $\mathcal{R} = 0$ and subsequently $R_{\mu\nu} = 0$ (in Eq (7.32)) which describes the Schwarzschild geometry encompassing the fluid sphere i.e, a vacuum outside space-time. Then again, if $f(\mathcal{R}, \mathcal{T})$ function takes another more complex form like f_1 includes the $\mathcal{R}^2$, $\mathcal{R}^3$ and so on terms. For this purpose, if $T_{\mu\nu} = 0$ prompts $f_2 = 0$, the external variety can be influenced by the geometric terms encoded in f_1 and $f_{\mathcal{R}}$. These terms $\mathcal{R}^2$, $\mathcal{R}^3$ etc. may alter the interface between the internal geometry and the outside one (Capozziello [2002]). In this regard, Cooney et al. [2010] have exhibited that in the presence of cosmological constant Λ, the outside metric for $f(\mathcal{R})$ gravity is like to Schwarzschild-de Sitter metric which recognizes the constant cosmological, and which can be re-scaled by the chosen $f(\mathcal{R})$ function. Therefore, this claim was also supported by Ganguly et al. [2014] which clarify in detail by taking into account Birkhoff's theorem, i.e. for static spherically symmetric stellar structure, the inside stellar systems can be matched with Schwarzschild vacuum gave that the Ricci scalar and its normal derivative disappears at the boundary surface of the stellar configuration. Therefore, the compatible outer spacetime is only Schwarzschild vacuum solution. Now this exterior spacetime i.e. Schwarzschild vacuum solution is given as

$$ds_+^2 \;=\; \left(1 - \frac{2m}{r}\right)dt^2 - \left(1 - \frac{2m}{r}\right)^{-1}dr^2 - r^2(d\theta^2 + \sin^2\theta\; d\phi^2). \quad (7.35)$$
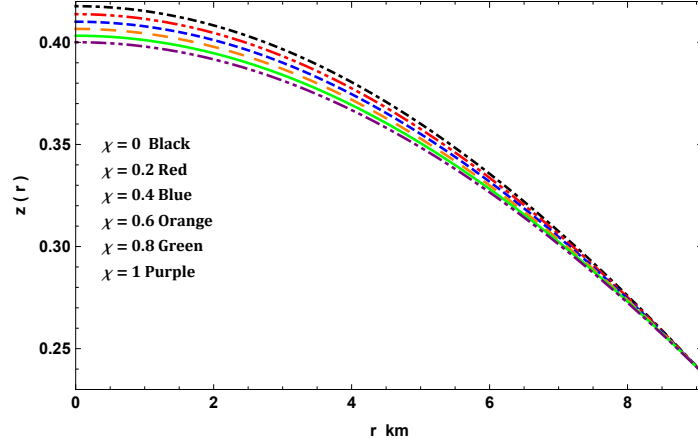
Figure 7.6: Variation of redshift with radial coordinate for 4U 1820-30 ($M = 1.58 \pm 0.06\ M_\odot$, $R = 9.1 \pm 0.4\ km$) with $b = 0.004$.

However, we must keep in mind that to avoid singularity, one must satisfy $r > 2m$.

At the surface $r = R$, we get $ds^2_-|_{r=R} = ds^2_+|_{r=R}$ which imply

$$e^{-\lambda(R)} = 1 - \frac{2M}{R} = e^{\nu(R)}. \tag{7.36}$$

On using (7.36), we get

$$a = \frac{2M}{R^2(R - 2M)\log(bR^2 + 2)} \tag{7.37}$$

$$A = \sqrt{1 - \frac{2M}{R}} + \frac{\sqrt{a}B(bR^2 + 2)}{2b}\left[F\left(\sqrt{\log(bR^2 + 2)}\right) - \sqrt{\log(bR^2 + 2)}\right] \tag{7.38}$$

Generally, in modeling compact stars the pressure at the surface needs to vanish i.e. $p_r(R) = 0$. This condition allow us to determine one more constant as

$$
\begin{aligned}
B = {} & 4b\sqrt{h(R)}\ \sqrt{1 - \frac{2M}{R}}\left[aR^2(\chi + 3\pi)(bR^2 + 2)\log^2\left(bR^2 + 2\right) - bR^2\chi\right. \\
& \left. + 3\pi\left(bR^2 + 2\right)\log\left(bR^2 + 2\right)\right]\left[w_3(R) + w_4(R) - \right. \\
& \frac{2(\chi + 3\pi)h(R)^{5/2}w_1(R)}{\sqrt{a}R^2\left(bR^2 + 2\right)^{-2}} - \frac{6\pi\left(bR^2 + 2\right)^2 h(R)^{3/2}w_1(R)}{\sqrt{a}R^2} \\
& \left. + 2aR\left(bR^2 + 2\right)w_2(R)\sqrt{\log(bR^2 + 2)}F\left(\sqrt{\log(bR^2 + 2)}\right)\right]^{-1}, \tag{7.39}
\end{aligned}
$$

where,

$$
\begin{aligned}
w_1(R) &= F\left(\sqrt{\log\left(bR^2+2\right)}\right) - \sqrt{\log\left(bR^2+2\right)} \\
w_2(R) &= aR^2(\chi+3\pi)\left(bR^2+2\right)\log^2\left(bR^2+2\right) - bR^2\chi + \\
&\quad 3\pi\left(bR^2+2\right)\log\left(bR^2+2\right) \\
w_3(R) &= bR\left(bR^2+2\right)\left(\chi\left(2aR^2+9\right)+24\pi\right)\log\left(bR^2+2\right) + 6\pi aR \\
&\quad \left(bR^2+2\right)\left(3bR^2-2\right)\log^2\left(bR^2+2\right) - b^2R^3\chi \\
w_4(R) &= 2\sqrt{a}bR^2\chi\left(bR^2+2\right)\sqrt{h(R)}w_1(R) + 10abR^3\chi\left(bR^2+2\right)\log^2\left(bR^2+2\right) \\
&\quad -2(\chi+3\pi)a^2R^3\left(bR^2+2\right)^2\log^3\left(bR^2+2\right).
\end{aligned}
$$

The parameter b will be treated as free whereas M and R will be taken from the observational evidences.

7.7 Physical Analysis on the new solution

Any new solutions must be analyze through various physical tests. After satisfying all the physical constraints one can proceed further for modeling physical systems as follows:

7.7.1 Hydrostatc equilibrium

All the physical compact stars are believed to be in equilibrium state. Such equilibrium state can be tested by using equation of hydrostatic equilibrium or the modified TOV-equation which is given by

$$
\frac{\nu'}{2}(\rho+p_r) + \frac{dp_r}{dr} - \frac{2\Delta}{r} - \frac{\chi}{3(8\pi+2\chi)}\frac{d}{dr}\left(3\rho-p_r-2p_t\right) = 0. \tag{7.40}
$$

Here, the first term is gravity (F_g), second term is pressure gradient (F_h), third term is the anisotropic force (F_a) and the last term is the additional force (F_m) in $f(\mathcal{R}, \mathcal{T})-$gravity. The fulfillment of the modified TOV-equation is exhibited in Fig. 7.7. It shows that the forces due to gravity and pressure gradient are highest in GR case i.e. $\chi = 0$, however, anisotropic force is lowest and F_m vanishes. This will enable to hold more mass than other cases. As $\chi > 0$ increases the F_g and F_h decreases although the F_a and F_m slightly increase. Hence the maximum mass that the hold by the system will also reduces with increase in χ.

**Figure 7.7:** Variation of different forces in modified TOV-equation with radial coordinate for 4U 1820-30 ($M = 1.58 \pm 0.06\ M_\odot$, $R = 9.1 \pm 0.4\ km$) with $b = 0.004$.

7.7.2 Causality condition and stability factor

We all aware of $f(\mathcal{R}, \mathcal{T})-$gravity as an prolongation of GR, which provides a constraint on maximum speed limit. All the particle with non-zero rest mass much travel at subluminal speeds i.e. less than the speed of light (causality condition). The velocity of sound in a medium must also satisfy the causality condition and it determines the stiffness of the related EoS. Therefore, one can determine the sound speed in stellar medium to relate its stiffness. The most stiff EoS is the Zeldovich's fluid ($p_z = \rho_z$) where the sound travels exactly at light speed. The sound speed can be determine as

$$v_r^2 = \frac{dp_r}{d\rho} \quad , \quad v_t^2 = \frac{dp_t}{d\rho}. \tag{7.41}$$

In Fig. 7.8, we plot the velocity of sound with the radial coordinate. It can be seen that the velocity of sound is maximum in GR ($\chi = 0$) and decreases with increase in χ. This imply that the solution leads to an stiffer EoS in GR than in $f(\mathcal{R}, \mathcal{T})$.

The speed of sound can also related to the stability of the configuration. As per Abreu et al. [2007], the stability factor can be defined as $v_t^2 - v_r^2$. So long as $v_r > v_t$, the system is generally considered stable, or in other form $-1 \leq v_t^2 - v_r^2 \leq 0$, otherwise unstable. The variation of stability factor is also shown in Fig. 7.9 which clearly indicates the solution is stable.
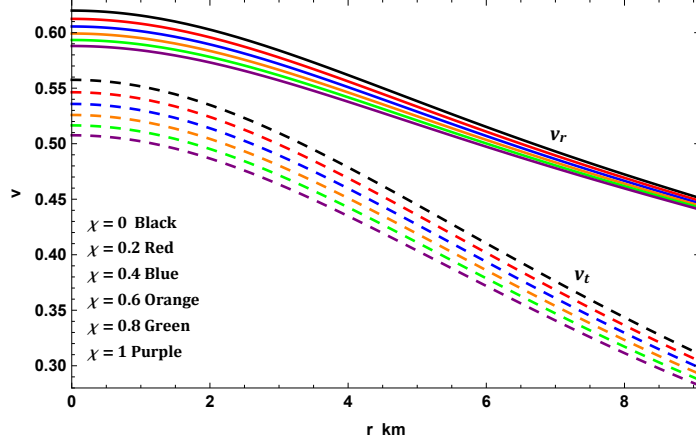
Figure 7.8: Variation of sound speeds with radial coordinate for 4U 1820-30 ($M = 1.58 \pm 0.06 \ M_\odot$, $R = 9.1 \pm 0.4 \ km$) with $b = 0.004$.
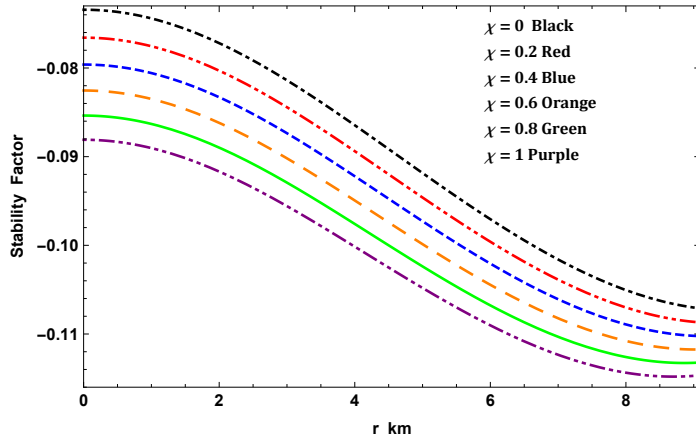
**Figure 7.9:** Variation of stability factor with radial coordinate for 4U 1820-30 ($M = 1.58 \pm 0.06 \ M_\odot$, $R = 9.1 \pm 0.4 \ km$) with $b = 0.004$.

7.7.3   Adiabatic index and stability

Another parameter that determines the stability and stiffness of EoS is the adiabatic index which is defined as the ratio of identifies heat at constant pressure to the identifies heat at constant volume. For any fluid distribution the adiabatic index can be determine as (Bondi [1964])

$$\gamma = \frac{p_r + \rho}{p_r} v_r^2. \tag{7.42}$$

As per Bondi's perceptions, the stellar fluid distribution is stable if $\gamma > 4/3$ in Newtonian limit. If $\gamma \leq 1$ contraction is possible and catastrophic if $\gamma < 1$. This is no longer valid for anisotropic fluids. This was extended by Chan et al. [1993] to anisotropic fluid. For anisotropic fluids, the stable limit of γ depends in the nature of anisotropy and its initial configuration. If anisotropy $\Delta > 0$, the stable limit will be still $\gamma > 4/3$, however, if $\Delta < 0$ stability is still possible even if $\gamma < 4/3$.
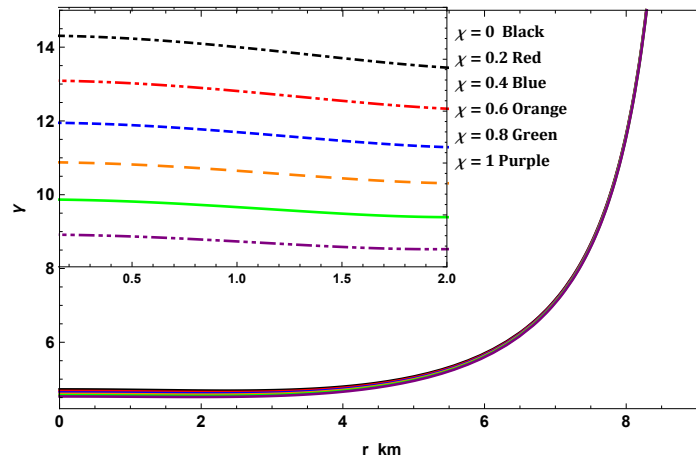
Figure 7.10: Variation of adiabatic index with radial coordinate for 4U 1820-30 ($M = 1.58 \pm 0.06 \ M_\odot$, $R = 9.1 \pm 0.4 \ km$) with $b = 0.004$.

The variation of adiabatic index is shown in Fig. 7.10. Once again we have higher adiabatic index in GR than $f(\mathcal{R}, \mathcal{T})$. This also implies the EoS is more stiff in GR and the solution is stable as $\gamma > 4/3$.

7.7.4   Static stability criterion

This criterion analyze the stability of stellar configurations under radial perturbations originally established by Chandrasekhar [1964]. Further, Harrison et al. [1965] and

Zeldovich and Novikov [1971] simplifies this method. The static stability criterion imposed the condition that if $\partial M/\partial \rho_c$ is greater than zero, the system is stable otherwise unstable. To see it, we have calculate the mass as a function of ρ_c given as

$$M\left(\rho_0\right) = \frac{R}{2}\left[1 - \frac{\log 8}{\rho_0 R^2(3\chi + 8\pi)\log\left(bR^2 + 2\right) + \log 8}\right]. \qquad (7.43)$$
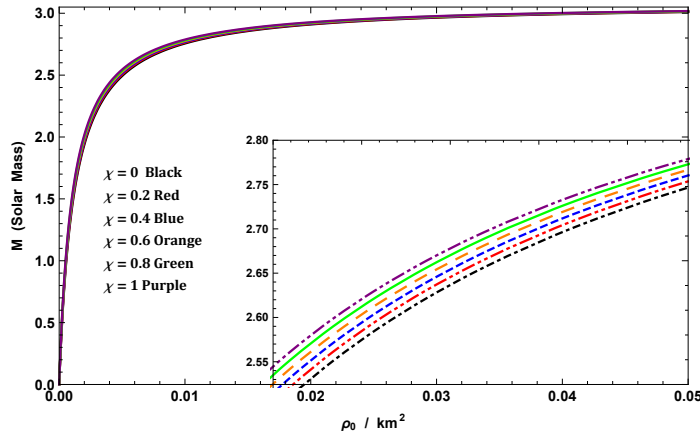
Figure 7.11: Variation of total mass with central density for 4U 1820-30 ($M = 1.58 \pm 0.06\ M_\odot$, $R = 9.1 \pm 0.4\ km$) with $b = 0.004$.

The variation of mass with respect to the central density is shown in Fig. 7.11. From this, one can conclude that the stability is enhance with increase in χ. This is because the range of mass is saturated slightly fast in GR than in $f(\mathcal{R}, \mathcal{T})$. This implies that the stable range of density during radial oscillation is more for higher values of χ. This can conclude that that solution is stable under radial perturbations.

7.7.5   Energy conditions

After confirming all the stability tests, the nature of matter content i.e. either normal (baryonic, hadronic etc.) or exotic (dark matter, dark energy etc.) can be identified by using energy conditions. Satisfaction or violation of certain energy conditions will imply the nature of the matter. These energy conditions are given as

$$
\begin{aligned}
\text{Null} \quad &: \quad \rho + p_r \geq 0,\ \rho + p_t \geq 0, \\
\text{Weak} \quad &: \quad \rho + p_r \geq 0,\ \rho + p_t \geq 0,\ \rho \geq 0, \\
\text{Strong} \quad &: \quad \rho + p_r \geq 0,\ \rho + p_t \geq 0,\ \rho + p_r + 2p_t \geq 0, \\
\text{Dominant} \quad &: \quad \rho \geq |p_r|,\ \rho \geq |p_t|.
\end{aligned}
$$
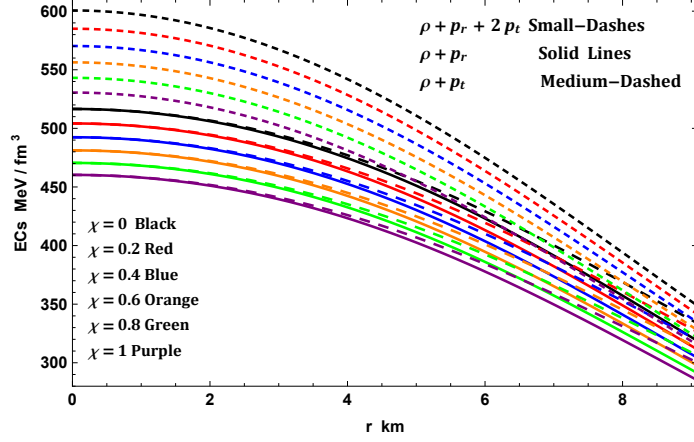
Figure 7.12: Variation of energy conditions (ECs) with radial density for 4U 1820-30 ($M = 1.58 \pm 0.06~M_{\odot}$, $R = 9.1 \pm 0.4~km$) with $b = 0.004$.

From Fig. 7.12, it is found that all the energy conditions are satisfied by the solution and therefore, the matter content is normal.

7.7.6 Stiffness of EoS, $M - R$ and $I - M$ curve

There are several ways of determining the stiffness of an EoS e.g. by determining adiabatic index, sound speed etc. However, the sensitivity to stiffness is found to be very sharp in $M - R$ and $I - M$ graphs. In fact, $I - M$ graph is the most effective and sensitive to the stiffness of an EoS. In Fig. 7.13 we shown the variation of mass with respect to the radius. Since, from the above sections we have already noted that the EoS is stiffest in GR case and as χ increases the stiffness reduces. Due to this, the mass that can hold by the corresponding EoS will also be maximum in GR and reduces as χ increases. The same nature can be seen from the $M - R$ curve in Fig. 7.13. To compare with the $I - M$ curve, one must establish how to determine the moment of inertia (I). Adopting the Bejger and Haensel [2002] formula one can determine the I corresponding to a static solution. It is given by

$$I = \frac{2}{5}\left(1 + \frac{(M/R) \cdot km}{M_{\odot}}\right)~MR^2. \tag{7.44}$$

The change in mass with respective to I is shown in Fig. 7.14. Again, we can verify that the EoS is most stiff in GR regime. The transition at the peak in $I - M$ curve is sharper than in $M - R$ curve. Therefore, one can conclude that the sensitivity in

EoS is better in $I - M$ curve.
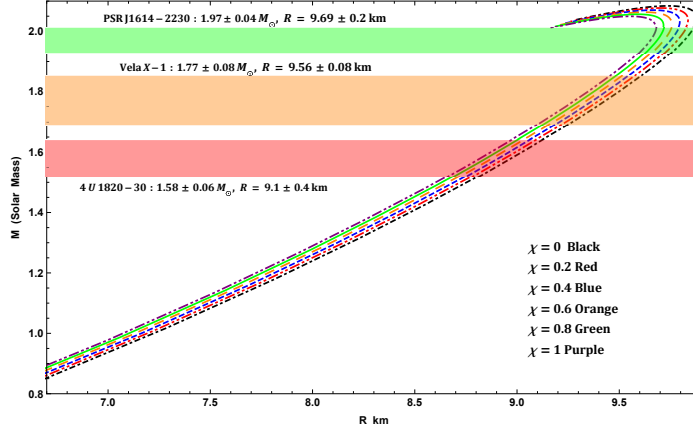
Figure 7.13: $M - R$ curves for $b = 0.004$.
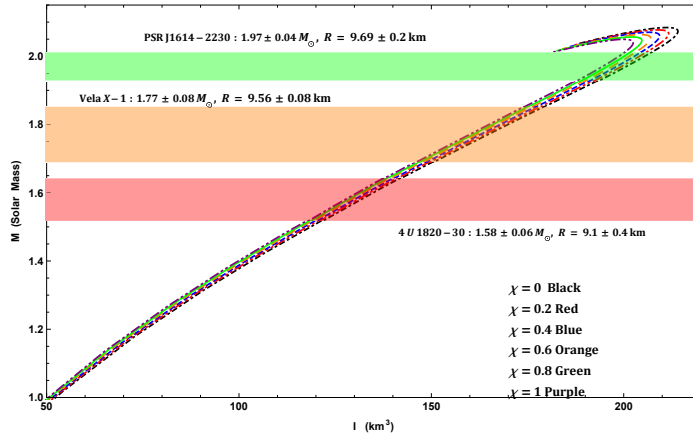
Figure 7.14: $M - I$ curves for $b = 0.004$.

Further, our generated $M - R$ curve is also fit with observational results for few well-known compact stars. As examples, we have matched for PSR J1614$-$2230, Vela X$-$1 and 4U 1820$-$30. Since the $M - R$ curve fit with these compact stars, one possibility arises from $I - M$ graphs to predict the possible range of I for the above mentioned objects.

7.8 Nonlinear model for Starobinsky-$f(\mathcal{R}, \mathcal{T})$ function

7.8.1 Field equations for $f(\mathcal{R}, \mathcal{T}) = \mathcal{R} + \xi\mathcal{R}^2 + 2\chi\mathcal{T}$ function

Taking the $f(\mathcal{R})$ function to be of the form Starobinsky model while keeping $f(\mathcal{T})$ function the same as above i.e. $f(\mathcal{R}, \mathcal{T}) = \mathcal{R} + \xi\mathcal{R}^2 + 2\chi\mathcal{T}$, the general field equations becomes (7.4) reduces to

$$
\begin{aligned}
(1 + 2\xi\mathcal{R})G_{\mu\nu} &+ \frac{\xi}{2}\,\mathcal{R}^2 g_{\mu\nu} + 2\xi(g_{\mu\nu}\Box - \nabla_\mu\nabla_\nu)\mathcal{R} \\
&= 8\pi T_{\mu\nu} + \chi\,\mathcal{T}g_{\mu\nu} + 2\chi(T_{\mu\nu} + \mathcal{P}g_{\mu\nu}),
\end{aligned}
\tag{7.45}
$$

where the RHS can be treated as effective energy-momentum tensor $T_{\mu\nu}^{eff}$. Now, with the interior spacetime (7.7) the decoupled field equations become

$$
\begin{aligned}
\rho = \frac{-e^{-\lambda}}{96r^2(\chi + \pi)(\chi + 4\pi)}\Big[&52r^2\chi F'' + 48\pi r^2 F'' - 10r^2 \\
&\chi F'\lambda' - 24\pi r^2 F'\lambda' - 12r^2\chi F'\nu' + 40r\chi F' + 96\pi r F' - \\
&16Fe^\lambda\chi + 7Fr^2\chi\lambda'\nu' + 12\pi Fr^2\lambda'\nu' - 14Fr^2\chi\nu'' - 24\pi \\
&Fr^2\nu'' - 7Fr^2\chi\nu'^2 - 12\pi Fr^2\nu'^2 - 16Fr\chi\lambda' - 28Fr\chi\nu' \\
&-48\pi Fr\nu' + 16F\chi + 6e^\lambda\xi r^2\mathcal{R}^2\chi + 24\pi e^\lambda\xi r^2\mathcal{R}^2 + 6e^\lambda r^2 \\
&\mathcal{R}\chi + 24\pi e^\lambda r^2\mathcal{R}\Big]
\end{aligned}
\tag{7.46}
$$

$$
\begin{aligned}
p_r = \frac{e^{-\lambda}}{96r^2(\chi + \pi)(\chi + 4\pi)}\Big[&-4r^2\chi F'' - 14r^2\chi F'\lambda' - \\
&12r^2\chi F'\nu' - 24\pi r^2 F'\nu' - 40r\chi F' - 96\pi r F' + 16Fe^\lambda\chi \\
&-7Fr^2\chi\lambda'\nu' - 12\pi Fr^2\lambda'\nu' + 14Fr^2\chi\nu'' + 24\pi Fr^2\nu'' + \\
&7Fr^2\chi\left(\nu'\right)^2 + 12\pi Fr^2\left(\nu'\right)^2 - 32Fr\chi\lambda' - 48\pi Fr\lambda' - \\
&20Fr\chi\nu' - 16F\chi - 6e^\lambda\xi r^2\mathcal{R}^2\chi - 24\pi e^\lambda\xi r^2\mathcal{R}^2 - 6e^\lambda r^2 \\
&\mathcal{R}\chi - 24\pi e^\lambda r^2\mathcal{R}\Big]
\end{aligned}
\tag{7.47}
$$

$$
\begin{aligned}
\Delta = \frac{e^{-\lambda}}{8r^2(\chi + 4\pi)}\Big[&4r^2 F'' + 2rF'\left(r\lambda' + 2\right) - 4Fe^\lambda - \\
&2Fr^2\nu'' - Fr^2\nu'^2 + Fr\lambda'\left(r\nu' + 2\right) + 2Fr\nu' + 4F\Big],
\end{aligned}
\tag{7.48}
$$

and $p_t = \Delta + p_r$. Here $F = \partial f(\mathcal{R}, \mathcal{T})/\partial \mathcal{R} = 1 + 2\xi\mathcal{R}$ and prime "$\prime$" represents the differentiation w.r.t. r. Therefore, it is clear that $F' = 2\xi d\mathcal{R}/dr$ and $F'' = 2\xi d^2\mathcal{R}/dr^2$ with Ricci scalar $\mathcal{R}$ is given by

$$\mathcal{R} = \frac{2}{r^2} - \frac{e^{-\lambda}}{2r^2}\left(2r^2\nu'' + r^2\nu'^2 - r\lambda'\left(r\nu' + 4\right) + 4r\nu' + 4\right).$$

7.8.2 Embedding class one solution in Starobinsky$-f(\mathcal{R}, \mathcal{T})$ model

Since the expression for the field equations (7.46)-(7.48) are very lengthy, we intentionally chosen a simpler class one solution. As a consequence, we are assumed Finch-Skea g_{11} and using (7.24) we get Adler [1974] g_{00} form i.e.

$$e^\lambda = 1 + ar^2 \quad \text{and} \quad e^\nu = \left(\frac{\sqrt{a}}{2}Br^2 + A\right)^2. \qquad (7.49)$$

Then corresponding interior spacetime can written as,

$$ds^2 = \left(\frac{\sqrt{a}}{2}Br^2 + A\right)^2 dt^2 - r^2(d\theta^2 + \sin^2\theta\, d\phi^2) - (1 + ar^2)dr^2, \qquad (7.50)$$

Since the Schwarzschild exterior solution is compatible with the matching of interior solution at the pressure free boundary for this Starobinsy $-f(\mathcal{R}, \mathcal{T})$ model as discussed in Sect. 7.8. Then by joining of interior spactime (7.35) to exterior solution, we determine the constant parameters a and A as

$$a = \frac{1}{R^2}\left[\left(1 - \frac{2M}{R}\right)^{-1} - 1\right] \qquad (7.51)$$

$$A = \sqrt{1 - \frac{2M}{R}} - \frac{\sqrt{a}}{2}BR^2 \qquad (7.52)$$

where, M and R are gravitational mass and radius of the stellar object, respectively. Due to extremely lengthy expressions for density and pressures, we are unable to include in the paper, however, their nature will be discuss in graphical forms.

Here we are comparing four different cases i.e. pure GR $[\xi = \chi = 0]$, linear $f_L(\mathcal{R}, \mathcal{T}) = \mathcal{R} + 2\chi\mathcal{T}$ $[\chi = 0.5,\ \xi = 0]$, Starobinsky $f_S(\mathcal{R}) = \mathcal{R} + \xi\mathcal{R}^2$ $[\chi = 0,\ \xi = 0.5]$ and Starobinsky$-f_{S+L}(\mathcal{R}, \mathcal{T}) = \mathcal{R} + \xi\mathcal{R}^2 + 2\chi\mathcal{T}$ $[\chi = \xi = 0.5]$. From Fig. 7.19,

it can be seen that the central density is highest in pure GR case while lowest in $f_{S+L}(\mathcal{R}, \mathcal{T})$, however, the linear $f_L(\mathcal{R}, \mathcal{T})$ has slightly higher central density than Starobinsky $f_S(\mathcal{R}, \mathcal{T})$ model. Indeed, all these cases has significant difference in central density, although the surface density is almost the same. Further, the central pressure is also highest in pure GR and lowest in $f_{S+L}(\mathcal{R}, \mathcal{T})$ gravity while $f_L(\mathcal{R}, \mathcal{T})$ has slightly low than $f_S(\mathcal{R})$. As a result, the surface radius decreases in the trend $R_{GR} > R_S > R_L > R_{S+L}$, Fig. 7.20. Similar trends can also be observed in transverse pressure as well (Fig. 7.15). In the case of pressure anisotropy Δ, the pure GR and linear $f_L(\mathcal{R}, \mathcal{T})$ has vanishing anisotropy at center and increases outside with same trends and almost equal while the central anisotropy in $f_S(\mathcal{R})$ and $f_{S+L}(\mathcal{R}, \mathcal{T})$ are non-vanishing. And for the last two case, anisotropy decreases towards surface in similar trend exactly equal at the surface, Fig. 7.16. All the four cases also fulfilled all energy conditions (Figs. 7.17, 7.18) and therefore physically viable.
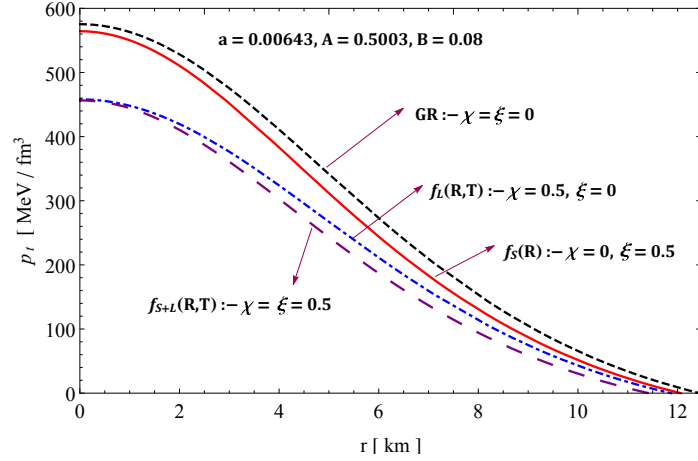
Figure 7.15: Variation of transverse pressure in Starobinsky-$f(\mathcal{R}, \mathcal{T})$ theory.

7.9   Discussion and conclusion

In this chapter, we have investigated the existence of the embedding class one methodology in the arena of $f(\mathcal{R}, \mathcal{T})$ gravity theory. We adopted the embedding class one methodology where a four-dimensional interior spacetime is implanted into the five-dimensional pseudo-Euclidean space throughout the area of $f(\mathcal{R}, \mathcal{T})$ gravity theory, so as to acquire general solutions of the altered EFEs. On the other hand, this methodology not only improve in investigating new accurate solutions throughout
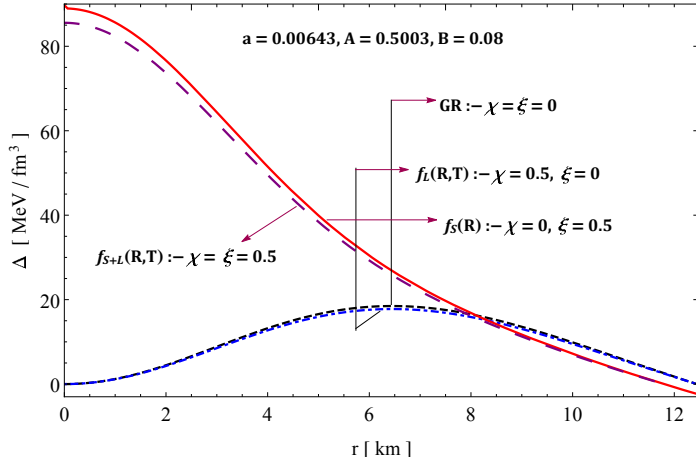
Figure 7.16: Variation of anisotropy in Starobinsky-$f(\mathcal{R}, \mathcal{T})$ theory.
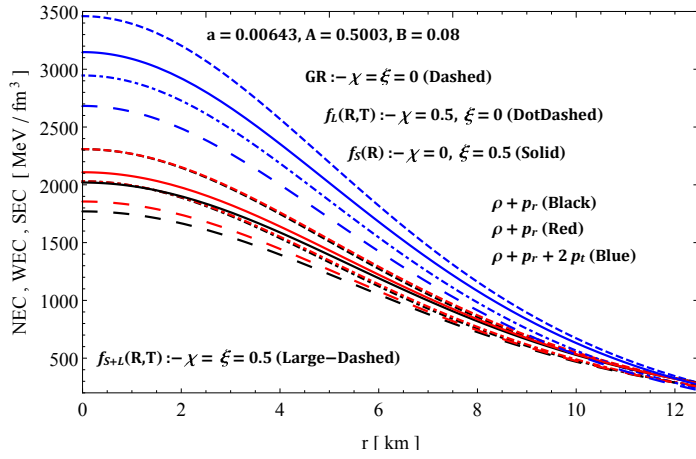
Figure 7.17: Variation of WEC, NEC and SEC in Starobinsky-$f(\mathcal{R}, \mathcal{T})$ theory.
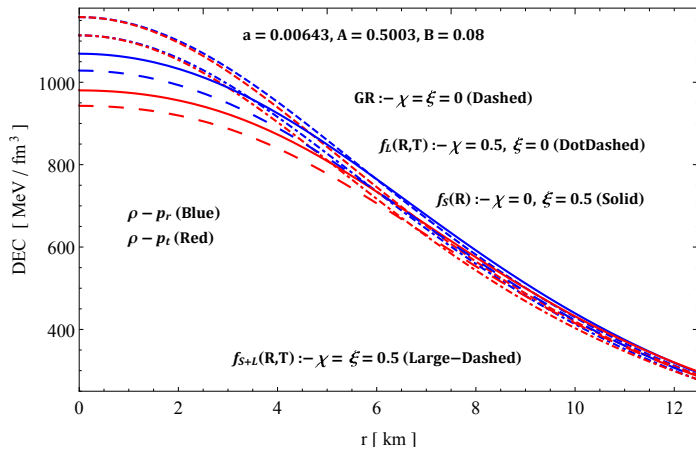
Figure 7.18: Variation of DEC in Starobinsky-$f(\mathcal{R}, \mathcal{T})$ theory.

Figure 7.19: Variation of energy density in Starobinsky-$f(\mathcal{R}, \mathcal{T})$ theory.
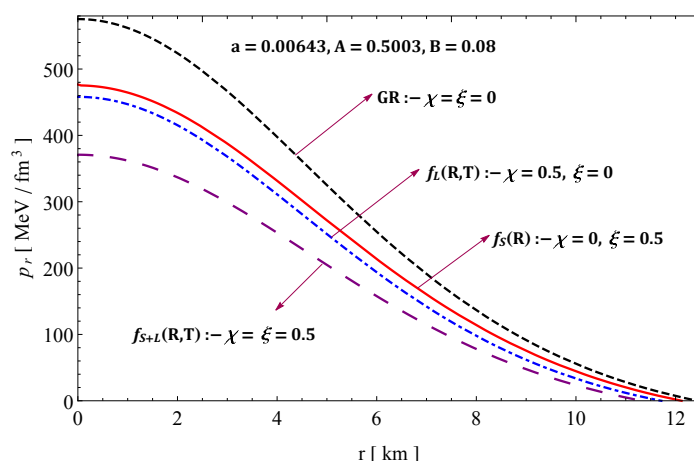
Figure 7.20: Variation of radial pressure in Starobinsky-$f(\mathcal{R}, \mathcal{T})$ theory.

7. Physical properties of class I compact star model for linear and Starobinsky$-f(\mathcal{R}, \mathcal{T})$ functions

$f(\mathcal{R}, \mathcal{T})$ gravity theory, yet additionally to explore the theory of compact stellar structures in the same domain. Using this beautiful methodology notable as Karmarkar condition, we have found a new class of generalised solutions for the anisotropic spherically symmetric relativistic stellar structures. In this regard, we have generalised the portrayal of the compact stellar structures in the background of $f(\mathcal{R}, \mathcal{T})$ gravity by exploring the modified shape of the EFEs. We got the metric potentials from the set of EFEs under the Karmarkar condition and easily coordinated them with outside Schwarzschild solution. It can be observed from the Eqs. (7.25) and (7.26) that $e^\lambda(r = 0) = 1$ and $e^\nu(r = 0) \neq 0$ which shows that our stellar model is physically achievable and agreeable. So, we can also see from Fig. 7.1 that the comportment of the gravitational potentials i.e, the time-time component (e^ν) and the radius-radius component (e^λ), which are finite at the center of the stellar configuration and monotonically increasing with increasing radius towards the surface, as well as the solutions are free from any physical and geometric singularities. Moreover, all the thermodynamic observables, namely energy density (ρ), radial pressure (p_r) and tangential pressure (p_t) are represented in Figs. 7.2 and 7.3 respectively. It is clear from this two figures that all the important conditions for a physical stellar model via the comportment of energy density quantity as well as the two pressure elements via radial and tangential behaviors are positive and well-defined inside the stellar system. Additionally, all these quantities having their maximal values at the center of the stellar configuration and afterward progressively decreasing with increasing radial coordinate to arrive at their minimum value at the boundary surface, which approves the physical availability of the accomplished solutions. The anisotropic stress is described in Fig. 7.4 and expressed in Eq. (7.29). The magnificence of this quantity is that the anisotropy will be directed outward when $\Delta > 0$, i.e. $p_t > p_r$ whereas, $\Delta < 0$ i.e., $p_t < p_r$ involves that direction of the anisotropy will be inward. Besides, from the graph corresponding to the anisotropy stress versus radial coordinates r, it is easy to observe that at the center anisotropy disappears, i.e., at the origin, the radial pressure and tangential pressure are equal ($p_t = p_r$). Moreover, the anisotropy stress is positive and reaches maximum value at the boundary surface of the stellar structure, which provides an intrinsic property and helps to build a more compact and massive stellar body. The profile of the radial (ω_r) and tangential (ω_t) EOS parameters with radial coordinate for 4U 1820-30 is shown in Fig. 7.5. In this respect, the curve shows that the EoS parameters are less than one i.e., $\omega_r, \omega_t < 1$, which establishes that the Zeldovich condition is well-respected everywhere inside the astrophysical system for

all the chosen values of $\chi-$coupling parameter of the $f(\mathcal{R}, \mathcal{T})-$gravity. Concerning the gravitational redshift Z_s, for an isotropic stellar structure without a cosmological constant, Buchdahl [1959] and Straumann [2012] have exhibited that $Z_s \leq 2$. Böhmer and Harko [2006] showed that for an anisotropic stellar structure within the sight of a cosmological constant, the gravitational redshift can take significantly higher value $Z_s \leq 5$. This last constraint was thusly altered by Ivanov [2002b] who exhibited that the most extraordinary acceptable value could be as high as $Z_s = 5.211$. Along these lines, the accomplishment of the gravitational redshift with radial coordinate for 4U 1820-30 is represented in Fig. 7.6. From this figure, it can observe that the gravitational redshift within representative value showing by the investigators Buchdahl [1959], Straumann [2012], Böhmer and Harko [2006], Ivanov [2002b] which strongly proves the agreement of our compact astrophysical system in the arena of $f(\mathcal{R}, \mathcal{T})-$gravity.

To reveal stability of the stellar model as far as the equilibrium state of the forces, we have examined the equation of hydrostatic equilibrium or the modified TOV-equation in the arena of $f(\mathcal{R}, \mathcal{T})-$gravity theory. The behavior of the four forces, namely, gravity (F_g), pressure gradient (F_h), the anisotropic force (F_a) and the additional force (F_m) in $f(\mathcal{R}, \mathcal{T})$ -gravity are expressed in Eq. 7.40 and featured in Fig. 7.7, which affirms that our stellar model is completely stable in terms of the equilibrium state of forces. The curve corresponding to the different forces also presents an intriguing phenomenon: an additional force F_m is generated because of the effect of matter-geometry coupling. We presented this additional force as an altered force and we noticed that this force is repulsive in kind as well as proceeds alongside the external direction in the astrophysical system. On the other hand, concerning the effect of $\chi-$ coupling constant of the $f(\mathcal{R}, \mathcal{T})-$gravity, the forces F_g and F_h are highest in GR case i.e. $\chi = 0$, however, F_a is lowest and F_m vanishes, as well as in this case can hold more mass than the other cases. As a consequence, when χ goes from 0 to 1 the F_g and F_h decrease despite the fact that the F_a and F_m lightly increase, which also reduces the maximum mass that the stellar system can contain. So, after the fulfillment of the equation of hydrostatic equilibrium or the modified TOV-equation, the stability was also analyzed through different physically stringent conditions such as causality condition, stability criteria via Bondi's condition, Abreu et al. condition and static stability criterion. In this connection, it is obvious to see from Fig. 7.8 the behavior of sound velocities against radial coordinate for different values of the coupling parameter χ. The figure shows that the sound velocities along a radial as

well as transverse direction are well in the range between 0 and 1, and demonstrate that the stellar system is totally well-behaved and keeps up the causality condition within the source. Additionally, it can be seen from Fig. 7.8 that the sound velocity is greatest in GR ($\chi = 0$) and decreases with increase in χ. This infers that the solution prompts a stiffer EoS in GR i.e., the case $\chi = 0$ than in $f(\mathcal{R}, \mathcal{T})$ i.e., the case $\chi \neq 0$. The sound velocity can evenly be linked to the stability of the stellar structure. According to Abreu et al. condition, the stability factor can be characterized as $v_t^2 - v_r^2$. Since $v_r > v_t$, the stellar system is completely viewed as stable, or in another form $-1 \leq v_t^2 - v_r^2 \leq 0$, otherwise unstable. The behavior of stability factor has additionally appeared in Fig. 7.9 which plainly demonstrates the solution is stable. Fig. 7.10 highlights that in all the choices of the $\chi-$coupling constant of the $f(\mathcal{R}, \mathcal{T})-$gravity, our anisotropic stellar system is perfectly stable versus an infinitesimal radial adiabatic oscillation according to Bondi's perceptions, as γ is greater than 4/3 in all inside points of the stellar structure and also confirms that the EoS is more stiff in GR case. We too presented the behavior of mass as function the central density in Fig. 7.11, which also validates the stability of our stellar system under radial perturbations, and provides improvements with the increase in the values of $\chi-$coupling parameter.

It is intriguing to mention here that after affirming all the stability tests talked about above, we have identified the nature of matter content by employing the ECs. Along these lines, it is easy to see from Fig. 7.12 that all the ECs viz., null, weak, strong and dominant in $f(\mathcal{R}, \mathcal{T})-$ gravity for all the chosen values of $\chi-$ coupling parameter are fulfilled by the solution and thusly, the matter content is normal (baryonic, hadronic, etc.).

The magnificence of our investigation isn't just to have generated a new class of generalized solutions for the anisotropic spherically symmetric stellar structures under embedding class one space-time using Karmarkar's condition in the arena of $f(\mathcal{R}, \mathcal{T})-$gravity, but also the sensitivity to stiffness which is very clear in $M - R$ and $M - I$ diagrams. In this regards, the behavior of mass M with respect to the total radius R appeared in Fig. 7.13 show that the EoS is stiffest in GR case i.e., $\chi = 0$ and as χ increases the stiffness diminishes which also infer that the mass can hold by the corresponding EoS will likewise be most extreme in GR and diminishes as χ increases. On the other hand, Fig. 7.14 shows the behavior of mass versus the moment of inertia with different values of $\chi-$coupling parameter. Also, it can be easily observed from this figure that the EoS is most stiff in GR case. So the comparison between these both beautiful results viz., $M - R$ and $M - I$ curves concluded that the sensitivity

in EoS is better in $I - M$ curve than in $M - R$ curve. Moreover, the resulting $M - R$ and $M - I$ curves are also well-adapted with observational data for some compact stellar structures namely, PSR J1614-2230, Vela X-1 and 4U 1820-30, and also we have predicted the corresponding possible range and their respective moment of inertia from the well-behaved solution i.e, $M - I$ curve.

Let us now discuss the impact of nonlinear $f(\mathcal{R}, \mathcal{T})$ functional form expressed as $f(\mathcal{R}, \mathcal{T}) = \mathcal{R} + \xi \mathcal{R}^2 + 2\chi \mathcal{T}$ on the physical features and astronomical effects of curvature and matter coupling of compact stellar structures. It is worthwhile to mention here that the dynamics present in $f(\mathcal{R}, \mathcal{T})$ gravity involves extra terms of $\mathcal{T}$ that describes more generalized modification of GR as compared to $f(\mathcal{R})$ gravity. So depending on the parameters of the stellar model ξ and χ, we have analyzed the stellar configuration from $[\xi = 0, \chi = 0]$, $[\xi = 0.5, \chi = 0]$, $[\xi = 0, \chi = 0.5]$ and $[\xi = 0.5, \chi = 0.5]$ corresponding pure GR, linear$-f_L(\mathcal{R}, \mathcal{T})$, Starobinsky- $f_S(\mathcal{R})$ and Starobinsky$-f_{S+L}(\mathcal{R}, \mathcal{T})$, respectively. To present a realistic modeling of compact stellar structures, we have applied Finch-Skea g_{rr} potential and we obtain the other potential using the Karmarkar condition which corresponds to Adler g_{tt} form as given in (7.49), in which the unknown constant parameters a and A are determined through a smooth link of inside and outside geometries of compact stellar structures. We have examined graphically the physical behavior of transverse pressure, anisotropy, energy conditions via WEC, NEC, SEC and DEC, energy density, and radial pressure corresponding to specific choice of stellar model parameters, i.e., ξ and χ. All these physical amounts can be observed in Figs. 7.15, 7.16, 7.17, 7.18, 7.19 and 7.20, respectively. We have established that all energy conditions are fulfilled for all cases considered by the choice of stellar model parameters which affirm the presence of normal matter in the inside regime of compact stellar structures. The impact of anisotropic parameter is additionally examined, i.e., $\Delta > 0$ which prompts the presence of a repulsive anisotropic force that allows the building of more massive structure. It is also found that the physical amounts viz., ρ, p_r, p_t exhibit regular as well as finite comportment in the inside of compact stellar structures and the values of these amounts decrease towards the surface of compact stellar objects.

In conclusion, our system of compact stellar spherical structures well-respected all the critical physical tests carried out and mathematical point of view necessary under embedding class one via Karmarkar condition in the arena of $f(\mathcal{R}, \mathcal{T})-$gravity, as well as their $M - R$ and $M - I$ diagrams, are well-fitted with observational data. In this regard, we have successfully describes the effects of all the physical requirements in

the framework of $f(\mathcal{R}, \mathcal{T})-$gravity and we compared them with the standard theory of GR. Accordingly, this new class of generalised solutions might have astrophysical importance in future works.

Chapter 8

Color-flavor locked quark stars in energymomentum squared gravity [1]

8.1 Introduction

Einsteins General Relativity agrees with all tests in the solar system to a precision of 10^{-5} (Will [2006]). Cosmic acceleration led to two possibilities: exotic matter fields called dark energy, or a cosmological constant (Λ). However, some issues are still unresolved which keep open the way to frameworks which try to extend GR. These issues have led to another possibility by assuming that Einstein's GR has to be modified in some way. Hence, the search for modified gravity theories which may describe accelerating universe has become very popular due to their ability to provide an alternative framework to understand dark energy. Some of these modified theories are Lovelocks' theory of gravitation (Lovelock [1971, 1972]), EinsteinGaussBonnet theory (Lanczos [1938]), $f(\mathcal{R})$ gravity (Sotiriou and Faraoni [2010], De Felice and Tsujikawa [2010]), etc. For a brief review of modified gravity theories, see Ref. De Felice and Tsujikawa [2010].

In addition to the theories mentioned above, energy-mom-entum-squared gravity (EMSG) (Katirci and Kavuk [2014], Roshan and Shojai [2016]) has been proposed to encode the non-minimal coupling between geometry and matter. According to

---

[1]Content of this chapter has been published in *Physics of Dark universe* (Elsevier), 31 (2021) 100774.

8. Color-flavor locked quark stars in energy-momentum squared gravity

Ref. Katirci and Kavuk [2014], Roshan and Shojai [2016], the Lagrangian contains an arbitrary functional of the Ricci scalar $\mathcal{R}$ and the square of the energy-momentum tensor i.e. $f(\mathcal{R}, T^{\mu\nu}T_{\mu\nu})$ gravity. Interestingly, it has been found that the non-linear matter contributions in the field equations would affect the right-hand side of the EFEs without invoking some new forms of fluid stress, such as bulk viscosity or scalar fields. Concerning this approach, several interesting consequences have been reported, such as cosmological solutions (Akarsu et al. [2018b, 2017], Faria et al. [2019], Barbar et al. [2020]), dynamical system analysis (Bahamonde et al. [2019]), charged black hole (Chen and Chen [2020]), wormhole solutions (Moraes and Sahoo [2018]), and so on. In addition to these studies, mass-radius relations of neutron stars have been studied for four different realistic EoS (Akarsu et al. [2018a]). In fact, authors have used recent observational measurements for the masses and radii of neutron stars to constrain the coupling constant α. Further, in Maulana and Sulaksono [2019] polytropic EoS have been used to find mass-radius relation for neutron stars.

Neutron stars are dense, compact astrophysical objects with masses up to $2M_\odot$ (Demorest et al. [2010], Antoniadis et al. [2013]). On the other hand, the radio pulsar PSR J1614-2230 (Demorest et al. [2010]) around 1.97 ± 0.04 $M_\odot$ mass has set rigid constraints on various matter EoS for neutron stars at high densities. Initially, it was assumed that neutron stars were composed of pure neutron matter described as a non-interacting relativistic Fermi gas. Current sensitivities put up constraints in the internal composition of neutron stars i.e. the composition and behaviour of equations of state (EoS) of the dense nuclear matter. In addition to this measurements on the radii of neutron stars provide additional constraints on the EoS (Steiner et al. [2013], Lattimer and Steiner [2014]). However, in the aftermath of a core-collapse supernova explosion, several compact objects can sustain densities above a few times the nuclear saturation density in its interior. Thus, the composition and the properties of dense and strongly interacting matter is still an open question, and of the greatest importance for compact astrophysical objects. In spite of many efforts to explore the EoS, dense matter in the core of compact stars may consist of quark matter which is widely expected. On the other hand, several authors have considered an even more extreme possibility in the formation of a degenerate Fermi gas of quarks in which the quark Cooper pairs with very high binding energy condense near the Fermi surface. And their prediction is the Color-Flavor Locking (CFL) phase is the real ground state of Quantum Chromodynamics (QCD) at asymptotically large densities.

In this chapter, we focus on the CFL phase where all three flavors as well as

three colors undergo pairing near the Fermi surface due to the attractive one-gluon exchange potential. In fact, the color neutrality constraint is to be imposed in the CFL quark matter because a macroscopic chunk of quark matter must be color singlet (see Alford and Rajagopal [2002], Steiner et al. [2002] for a review). According to Ref. Rajagopal and Wilczek [2001], Alford et al. [2008] quarks in the cores of neutron stars are likely to be in a paired phase. Depending on the previous results one may consider that the CFL matter gives 'absolute stability' for sufficiently high densities (Alford [2004]). The CFL phase has several remarkable properties, such as CFL is more stable than SQM as long as $\mu \gtrsim m_s^2/4\Delta$, with m_s being the strange quark mass and Δ the pairing gap (Alford et al. [2001]); at asymptotically large densities the CFL phase is the energetically favored phase; at extremely high densities, where the QCD gauge coupling is small, quark matter is always in the CFL phase with broken chiral symmetry and so on. As it was mentioned earlier in Ref. Flores and Lugones [2017, 2010], Banerjee and Singh [2021], Lugones and Horvath [2003] that CFL matter could be adequate candidate to explain stable neutron stars or strange stars.

From the above handful of literature it is clear that the structure of compact stars with CFL quark matter could represent a testbed for EMSG theory. The outline of the chapter is the following: In Sec. 8.2 we briefly introduce EMSG and its field equations. In Sec. 8.3 we discuss the EoS for CFL strange matter. In Sec. 8.4 we give a detailed analysis of the numerical methods employed to determine the mass-radius relations. Sec. 8.5 and 8.6, is devoted to reporting the general properties of the spheres in terms of the CFL strange quark matter. We finally draw our conclusion in Sec. 8.7.

8.2 Field equations in energy-momentum squared gravity (EMSG)

The main feature of EMSG theory is that the non-linear contributions of EM tensor, to encode the non-minimal matter-geometry coupling. The Lagrangian contains an arbitrary functional of the Ricci scalar and the square of the EM tensor, and the action for EMSG theory is (Katirci and Kavuk [2014], Roshan and Shojai [2016])

$$S = \int \left(\frac{1}{8\pi} \mathcal{R} + \alpha T_{\mu\nu} T^{\mu\nu} + \mathcal{L}_m \right) \sqrt{-g} \ d^4x, \qquad (8.1)$$

8. Color-flavor locked quark stars in energy-momentum squared gravity

where $\mathcal{R}$ is the Ricci scalar and $T_{\mu\nu}$ is the energy-momentum tensor (EMT) with the coupling paramter α. The $\mathcal{L}_m$ denotes the matter Lagragian density.

The EMT, $T_{\mu\nu}$, is defined via the matter Lagrangian density as follows

$$T_{\mu\nu} = -\frac{2}{\sqrt{-g}}\frac{\delta(\sqrt{-g}\mathcal{L}_m)}{\delta g^{\mu\nu}} = \mathcal{L}_m\, g_{\mu\nu} - 2\frac{\partial\mathcal{L}_m}{\partial g^{\mu\nu}}, \tag{8.2}$$

which depends only on the metric tensor components, and not on its derivatives. If we vary the action (8.1) with respect to $g^{\mu\nu}$, gives us the equation of motion for metric functions:

$$R_{\mu\nu} - \frac{1}{2}\mathcal{R}g_{\mu\nu} = 8\pi T_{\mu\nu} + 8\pi\alpha\left(g_{\mu\nu}T_{\beta\gamma}T^{\beta\gamma} - 2\Theta_{\mu\nu}\right), \tag{8.3}$$

where,

$$\begin{aligned}
\Theta_{\mu\nu} &= T^{\beta\gamma}\frac{\delta T_{\beta\gamma}}{\delta g^{\mu\nu}} + T_{\beta\gamma}\frac{\delta T^{\beta\gamma}}{\delta g^{\mu\nu}} \\
&= -2\mathcal{L}_m\left(T_{\mu\nu} - \frac{1}{2}g_{\mu\nu}\mathfrak{T}\right) - \mathfrak{T}T_{\mu\nu} + 2T_\mu^\gamma T_{\nu\gamma} - 4T^{\beta\gamma}\frac{\partial^2\mathcal{L}_m}{\partial g^{\mu\nu}\partial g^{\beta\gamma}}
\end{aligned} \tag{8.4}$$

with $\mathfrak{T} = g^{\mu\nu}T_{\mu\nu}$, the trace of EMT.

Throughout this work we assume a perfect fluid EMT for the compact object. For that we assume $\mathcal{L}_m = P$ and using (8.2) the perfect fluid form is given by

$$T_{\mu\nu} = (\rho + P)u_\mu u_\nu + Pg_{\mu\nu}, \tag{8.5}$$

where ρ is the enrgy density, P is the isotropic pressure with $u_\mu u^\mu = -1$ & $u_\mu\nabla_\nu u^\nu = 0$, respectively. The conservation equation can be found by covariant derivative of Eq. (8.3), which yield

$$\nabla^\mu T_{\mu\nu} = -\alpha g_{\mu\nu}\nabla^\mu(T_{\beta\gamma}T^{\beta\gamma}) + 2\alpha\nabla^\mu\Theta_{\mu\nu}. \tag{8.6}$$

Note that the standard conservation equation of the energy-momentum tensor does not hold for this theory i.e., $\nabla^\mu T_{\mu\nu}$ is not identically zero.

8.2. Field equations in energy-momentum squared gravity (EMSG)

After some algebra, one obtains the following field equations

$$
\begin{aligned}
R_{\mu\nu} - \frac{1}{2}\mathcal{R}g_{\mu\nu} \;=\; & 8\pi\rho\left[\left(1 + \frac{P}{\rho}\right)u_\mu u_\nu + \frac{P}{\rho}g_{\mu\nu}\right] + 8\pi\alpha\rho^2 \\
& \left[2\left(1 + \frac{4P}{\rho} + \frac{3P^3}{\rho^2}\right)u_\mu u_\nu + \left(1 + \frac{3P^2}{\rho^2}\right)g_{\mu\nu}\right].
\end{aligned}
\tag{8.7}
$$

The Eq. (8.7) can further reduce to coupled differential equations by consider a specific spacetime geometry. For the stellar configurations, it is generally assume a spherically symmetric spacetime of the form

$$
ds^2 \;=\; e^{2\nu}dt^2 - e^{2\lambda}dr^2 - r^2(d\theta^2 + \sin^2\theta\; d\phi^2),
\tag{8.8}
$$

with two independent functions $\nu(r)$ and $\lambda(r)$. Using the metric given in Eq. (8.8) in Eq. (8.7), we reach the following set of equations (see Ref. Akarsu et al. [2018a])

$$
\frac{e^{-2\lambda}}{r^2}\left(2r\lambda' - 1\right) + \frac{1}{r^2} = \rho_{\text{eff}}(r),
\tag{8.9}
$$

$$
\frac{e^{-2\lambda}}{r^2}\left(2r\nu' + 1\right) - \frac{1}{r^2} = P_{\text{eff}}(r),
\tag{8.10}
$$

where prime represent derivative with respect to r. Also, the effective density and pressure $\rho_{\text{eff}}(r)$ and $P_{\text{eff}}(r)$ respectively, are given as

$$
\begin{aligned}
\rho_{\text{eff}}(r) \;&=\; 8\pi\rho + 8\pi\alpha\rho^2\left(1 + \frac{8P}{\rho} + \frac{3P^2}{\rho^2}\right), \\
P_{\text{eff}}(r) \;&=\; 8\pi P + 8\pi\alpha\rho^2\left(1 + \frac{3P^2}{\rho^2}\right).
\end{aligned}
$$

To recast the Eq. (8.10) to a more familiar form we input the gravitational mass function within the sphere of radius r, such that

$$
e^{-2\lambda} = 1 - \frac{2m(r)}{r}.
\tag{8.11}
$$

The other metric function, $\nu(r)$, is related to the pressure via

$$
\begin{aligned}
\frac{d\nu}{dr} \;=\; & -\left[\rho\left(1 + \frac{P}{\rho}\right)\left\{1 + 2\alpha\rho\left(1 + \frac{3P}{\rho}\right)\right\}\right]^{-1} \\
& \left[(1 + 6\alpha P)P'(r) + 2\alpha\rho\rho'(r)\right],
\end{aligned}
\tag{8.12}
$$

which is the radial component of the divergence of the field. It is straightforward to use (8.11) into (8.9), we have

$$m'(r) = 4\pi\rho r^2 \left[1 + \alpha\rho \left(\frac{3P^2}{\rho^2} + \frac{8P}{\rho} + 1 \right) \right]. \tag{8.13}$$

Finally, using the expressions (8.9)-(8.12), the modified TOV equation takes the following convenient form (Akarsu et al. [2018b])

$$
\begin{aligned}
P'(r) &= -\frac{m\rho}{r^2} \left(1 + \frac{P}{\rho} \right) \left(1 - \frac{2m}{r} \right)^{-1} \left[1 + \frac{4\pi P r^3}{m} + \alpha \frac{4\pi r^3 \rho^2}{m} \left(\frac{3P^2}{\rho^2} + 1 \right) \right] \\
&\quad \left[1 + 2\alpha\rho \left(1 + \frac{3P}{\rho} \right) \right] \left[1 + 2\alpha\rho \left(\frac{d\rho}{dP} + \frac{3P}{\rho} \right) \right]^{-1}.
\end{aligned}
\tag{8.14}
$$

The system of Eqs. (8.9)-(8.14) are not enough to solve for the four variables, since there are one degrees of freedom. To complete this set of equations, we need now to specify the EoS relating the pressure and energy density of the fluid.

8.3 Color-flavor locked equations of state

Here, we outline the equation of state (EoS) for CFL quark matter that can be obtained in the framework of the MIT bag model. In the CFL phase, the thermodynamic potential for electric and color charge neutral CFL quark matter is given by (Alford et al. [2001])

$$\Omega_{CFL} = \frac{6}{\pi^2} \int_0^{\gamma_F} p^2 (p - \mu)\, dp + \frac{3}{\pi^2} \int_0^{\gamma_F} p^2 \left(\sqrt{p^2 + m_s^2} - \mu \right)\, dp - \frac{3\Delta^2\mu^2}{\pi^2} + B, \tag{8.15}$$

to the order of Δ^2, where μ is the quark chemical potential and Δ denotes the color superconducting gap parameter of CFL phase of quark matter. The first term is the contribution of the CFL condensate to Ω_{CFL}, while the second and third terms of (8.15) gives the thermodynamic potential of (fictional) unpaired quark matter in which all quarks that are going to pair have a common Fermi momentum γ_F which minimizes the thermodynamic potential of the fictional unpaired quark matter (Alford and Reddy [2003]). The final term is the bag constant.

The common Fermi momentum is given by

$$\gamma_F = \left[\left(2\mu - \sqrt{\mu^2 + \frac{m_s^2 - m_u^2}{3}} \right)^2 - m_u^2 \right]^{1/2} \tag{8.16}$$

8.3. Color-flavor locked equations of state

where $\mu = (\mu_s + \mu_u + \mu_d)/3$ i.e. the average quark chemical potential, m_s & m_u are strange and up quark masses respectively. For massless up and down quarks we get

$$\gamma_F = 2\mu - \sqrt{\mu^2 + \frac{m_s^2}{3}} \sim \mu - \frac{m_s^2}{6\mu}. \tag{8.17}$$

By following the pairing ansatz in the CFL phase (Steiner et al. [2002])

$$n_u = n_r, \qquad n_d = n_g, \qquad \text{and} \qquad n_s = n_b \tag{8.18}$$

where n_r, n_g, n_b and n_u, n_d, n_s are color and flavor number densities respectively. In the discussion that follows, color neutrality automatically enforces electric charge neutrality in the CFL phase, and the quark number densities are $n_u = n_d = n_s = \frac{\gamma_F^3 + 2\Delta^2\mu}{\pi^2}$. It is to be noted that the color neutral CFL quark matter is electric charge neutral, the corresponding electric charge chemical potential is $\mu_e = 0$. In our discussion we consider the values of the CFL gap parameter in the range of $\Delta \sim 50 - 100\ MeV$ (see Ref. Alford and Spicer [2002], Rapp et al. [1998]). As the necessary condition for MIT based EoS the bag constant B to be always greater than $57\ MeV/fm^3$ (Farhi and Jaffe [1984]). In fact, the free energy contributed from CFL pairing is more than the free energy consumes to maintain equal number of quark densities (Alford et al. [2001]). Thus, CFL paired quarks are more stable than unpaired.

Since it is always difficult to obtain an exact expression for an EoS when $m_s \neq 0$. However, a simple EoS similar to the MIT-bag model can be obtained for $m_s = 0$, with an extra term from CFL contribution as $\rho = 3p + 4B - 6\Delta^2\mu^2/\pi^2$. Considering the series upto the order Δ^2 and m_s^2, the expression for pressure and energy density in the CFL phase can be obtained as (Lugones and Horvath [2002])

$$P = \frac{3\mu^4}{4\pi^2} + \frac{9\beta\mu^2}{2\pi^2} - B \ , \ \text{and} \ \rho = \frac{9\mu^4}{4\pi^2} + \frac{9\beta\mu^2}{2\pi^2} + B, \tag{8.19}$$

where $\beta = -m_s^2/6 + 2\Delta^2/3$. Finally, an explicit function of the energy density ρ in the form

$$\rho = 3P + 4B - \frac{9\beta}{\pi^2}\left\{ \left[\frac{4\pi^2(B + P)}{3} + 9\beta^2 \right]^{1/2} - 3\beta \right\}. \tag{8.20}$$

8.4   Numerical Approach

Since the field equations (8.9) and (8.10) are highly non-linear, so we adopt numerical integration in Mathematica. For solving the field equations we will be directly use the TOV-equation (8.14) along with equation of mass function (8.13). Since the two equations include three unknown quantities i.e. $\rho(r)$, $P(r)$ and $m(r)$, we need an additional information. Therefore, we will consider an EoS for color-flavor locked (CFL) quark matter given in (8.20) that generalizes the MIT bag model. As a first step we convert the units in EoS, TOV and mass function equations so that the mass will be measured in solar mass, radius in km, pressure, density & bag constant B in MeV/fm^3, strange quark mass m_s & color-superconducting gap Δ in MeV.

Next we use "`NDSolve`" package in Mathematica defining a coupled differential equations (8.13) and (8.14) with initial ($\mathcal{I}$) and boundary ($\mathcal{B}$) conditions given below:

$$
\begin{aligned}
\mathcal{I} \;\; : \;\; & P(r_0) = p_0, \quad r_0 = 10^{-10}\,km \\
& m(r_0) = \frac{4\pi r_0^3}{3}\rho_0\left[1 + \alpha\rho_0\left(\frac{3p_0^2}{\rho_0^2} + \frac{8p_0}{\rho_0} + 1\right)\right]
\end{aligned}
\tag{8.21}
$$

$$
\mathcal{B} \;\; : \;\; P(R) = 0, \qquad m(R) = M,
\tag{8.22}
$$

and solve for pressure and mass functions. Here $P(r_0) = p_0$, $\rho(r_0) = \rho_0$, R is the radius of the star and M is the total gravitational mass. To proceed we start by supplying the values of the constant parameters i.e. (B, m_s, Δ, α). Solving the TOV equation by choosing a central pressure e.g. $P(r_0) = 60\ MeV/fm^3$ until the pressure vanishes i.e. $P(R) = 0$, which defines the surface of the star generating the Figs. 8.1-8.3. The Figs. 8.4-8.7 were generated by integrating the TOV-equation for different values of $P(r_0)$. In the following, we will focus on the four cases: (i) [60 MeV/fm^3, 0, $100MeV$], (ii) [60 MeV/fm^3, $150MeV$, $100MeV$], (iii) [70 MeV/fm^3, $150MeV$, $100MeV$], and (iv) [70 MeV/fm^3, $150MeV$, $150MeV$], respectively. Further, we analyse the resulting mass and radius for the central pressure allowed by the EoS under consideration, and each cases have been examined carefully which are valid from a physical point of view.

8.5   Physical acceptability of the model

To check the numerical solution for its acceptability through physical constraints,

we need to analyze thoroughly and how it behaves when changing the constant parameters.
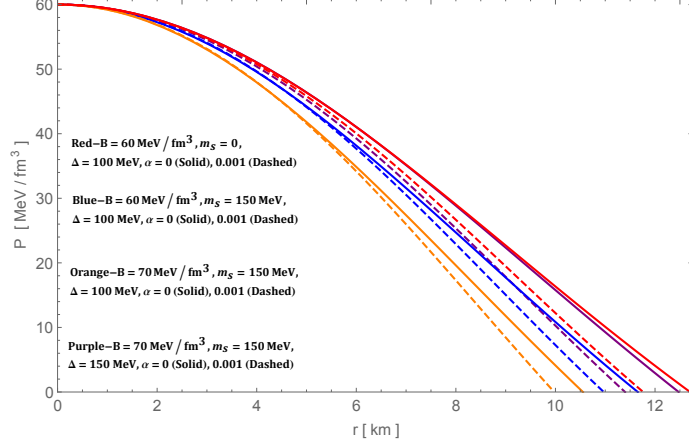
Figure 8.1: Variation of pressure with radius for different (B, m_s, Δ, α) and $P(r_0) = 60 \ MeV/fm^3$.
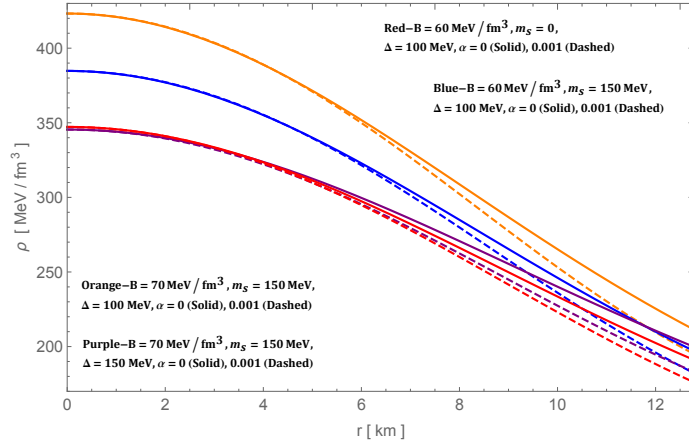
Figure 8.2: Variation of energy density with radius for different (B, m_s, Δ, α) and $P(r_0) = 60 \ MeV/fm^3$.

8.5.1 Non-singular central density and pressure

In order to check the EoS behavior and viability of a compact star model, the central values of density and pressure must be finite. Since the central pressure is one of the initial input parameters for the numerical integration, it is clearly finite. Figure 8.1 shows the variation of pressure for different physical inputs in the interior of compact objects. Then solving the pressure from TOV-equation, the density can be calculated

203

using EoS. From the Fig. 8.2, we can also see that the central densities for 4 cases are finite and thereby both the central density and pressure are non-singular.

It can also be seen that as the strange quark mass increases ($0 \rightarrow 150\ MeV$), the radius of the star decreases while the central density increases, see Red & Blue curves in Figs. 8.1 and 8.2, respectively. Further, when bag constant increases ($60 \rightarrow 70\ MeV/fm^3$), the radius of the star reduces significantly while the density increases very much (Figs. 8.1, 8.2, Blue & Orange). Again, if the color superconducting gap increases ($100 \rightarrow 150\ MeV$), the radius of the star increases as compared to the case III but still lesser than case I while almost equivalent with case II. However, the density is lower than case III but slightly higher than case II. Finally, the comparison of GR ($\alpha = 0$) and EMSG ($\alpha = 0.001$) is that GR has larger surface boundary than EMSG counterpart while the density is the same for both gravity till about 6 km than start lesser value in EMSG than GR i.e. EMSG has lower surface density than GR counterpart.
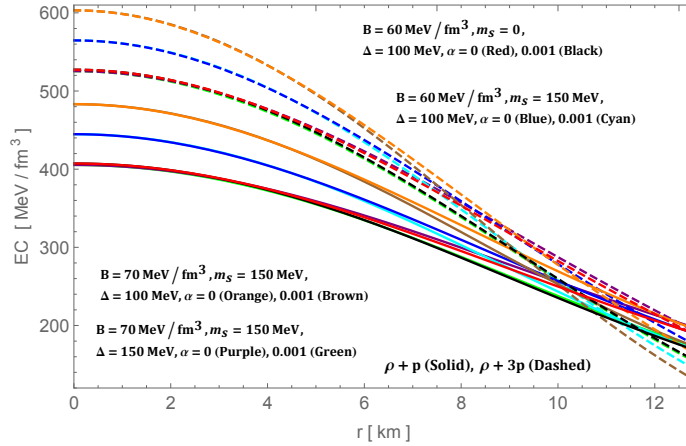
Figure 8.3: Variation of energy conditions with radius for different (B, m_s, Δ, α) and $P(r_0) = 60\ MeV/fm^3$.

8.5.2   Energy conditions

For any physically plausible fluid, physical constraint demands strict energy conditions namely strong, weak, null and dominant conditions or mathematically

$$\text{SEC} \quad : \quad \left(T_{\mu\nu} - \frac{1}{2}Tg_{\mu\nu}\right)u^{\mu}u^{\nu} \geq 0 \quad \text{or} \quad \rho + P \geq 0, \quad \rho + 3P \geq 0, \quad (8.23)$$

$$\text{WEC} \quad : \quad T_{\mu\nu}u^{\mu}u^{\nu} \geq 0, \quad \text{or} \quad \rho \geq 0, \quad \rho + P \geq 0, \quad (8.24)$$

$$\text{NEC} \quad : \quad T_{\mu\nu}k^{\mu}k^{\nu} \geq 0 \quad \text{or} \quad \rho + P \geq 0, \quad (8.25)$$

$$\text{DEC} \quad : \quad T_{\mu\nu}v^{\mu}v^{\nu} \geq 0 \quad \text{or} \quad \rho \geq |P|, \quad (8.26)$$

where u^{μ} is time-like vector, k^{μ} is the null-vector and v^{μ} is any future directed causal vector. All these energy conditions is fulfilled by the solution from Figs. 8.1, 8.2 and 8.3.
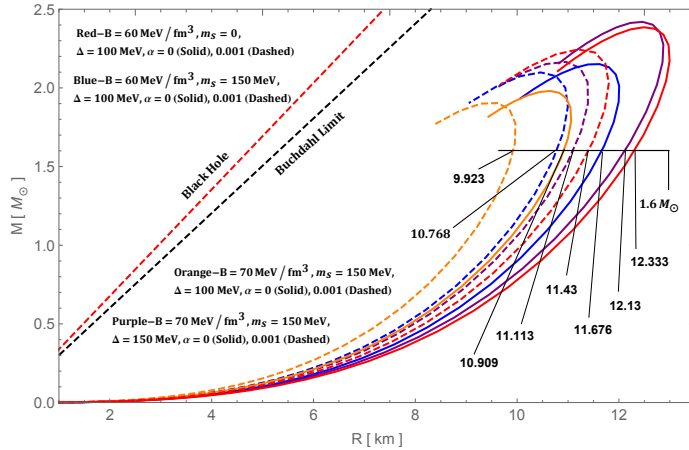
Figure 8.4: $M - R$ for different (B, m_s, Δ, α) by varying $P(r_0)$.

8.5.3 $M - R$ and $M - I$ curves

The $M - R$ curve was directly generated from the TOV-equation via the numerical solution. This only means that EMSG, increasing B and m_s soften the EoS while increasing Δ stiffens it. This graph was generated by varying the central pressure $P(r_0)$ and measuring the mass with the corresponding radius at the boundary $P(R) = 0$. For the cases, introducing EMSG soften the EoS thereby reducing the maximum mass (Solid & Dashed lines). From Fig. 8.4, one can observed that increasing strange quark mass reduces the M_{max} (Red & Blue) and further M_{max} reduces when increas-
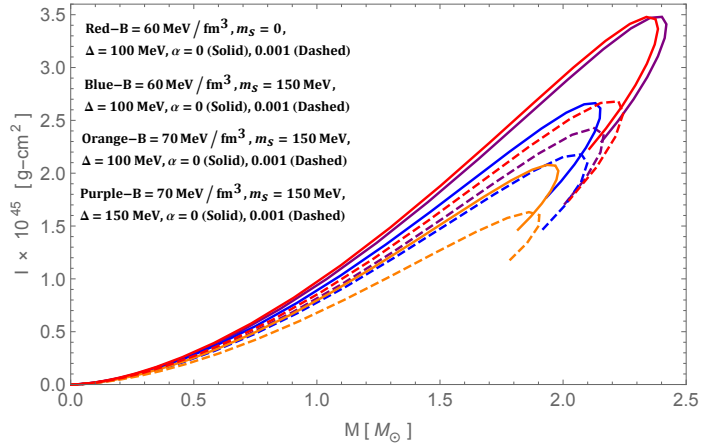
Figure 8.5: $M - I$ for different (B, m_s, Δ, α) by varying $P(r_0)$.

ing bag constant (Blue & Orange) however, for the same bag constant when color superconducting gap increases the M_{max} significantly increases. In the $M - R$ curve Fig. 8.4, we have also included the Buchdahl condition where the collapse of the star may proceed beyond it and finally forming a black hole once the $r = 2m$ is fulfilled.

The $M - I$ curve is obtain by using the approximate relationship which is defined as (Bejger and Haensel [2002])

$$I = \frac{2}{5} \left(1 + \frac{M}{R} \frac{km}{M_\odot} \right). \tag{8.27}$$

Equation (8.27) has the accuracy of 5% and less and on using this equation we have generated the $M - I$ curve (Fig. 8.5).
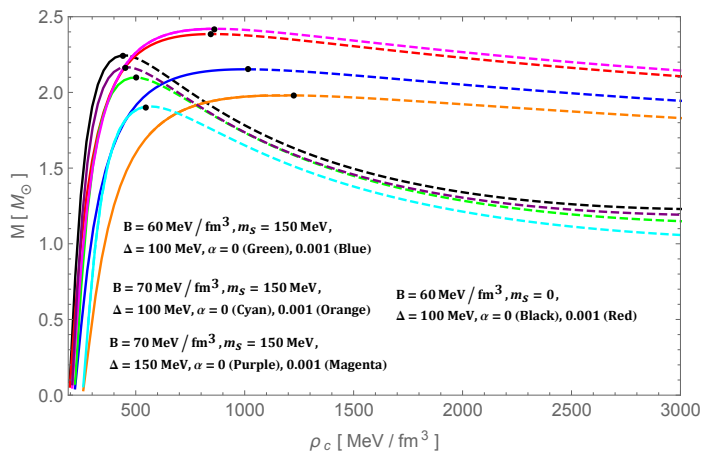
Figure 8.6: $M - \rho_c$ for different (B, m_s, Δ, α) for different values of $P(r_0)$.

Figure 8.7: $M - 2M/R$ for different (B, m_s, Δ, α) for different values of $P(r_0)$.

8.6 Static stability criterion

For completeness, we would also like to check the stability of compact stars constructed in EMSG and explore the physical properties in the interior of the fluid sphere. In the following, we discuss the mass with central energy density, compactness, and the stability of stars.

8.6.1 Mass with the central energy density

Once the TOV stationary configuration has been determined, one can probe its stability towards collapse. A necessary (but not sufficient) condition for stability of a compact star is that the total mass is an increasing function of the central density, $dM/d\rho_c > 0$ (Zeldovich and Novikov [1971], Harrison et al. [1965]); this is the *static stability criterion*. Therefore, it is interesting to ask what would happen to our constraints on $M_{\max}$ if we measured a quark star with $\sim 2M_\odot$. Our mass-central density diagram is reported in Fig. 8.6 for the stellar configuration obtained by solving the TOV equations and changing the value of central density. Here, we want to stress that while performing the calculation we have chosen different values of central pressure while the corresponding central density is found to be in the range $340 < \rho_c < 450 \ MeV/fm^3$ for different values of constant parameters, see Fig. 8.2. From Fig. 8.6, one can immediately see that the mass initially increases with central density until it attains a maximum value. Then the mass decreases with the increasing central density. The most interesting part is that in EMSG (i.e. $\alpha \neq 0$), all curves having positive slops i.e. $dM/d\rho_c > 0$ in the regime, $340 < \rho_c < 450 \ MeV/fm^3$. But

outside this range most of them correspond to the unstable configuration. Therefore, this solution presents a very dense stable star upto certain range depending on the values of central density and pressure. Obviously, this is a necessary condition for a stable equilibrium configuration. Interestingly, the solid curves corresponding to GR (i.e. $\alpha = 0$) are quite satisfactory and consequently leads to a stable configuration. Of course, a careful and detailed analysis of stability conditions in EMSG, would help to clarify this issue. We leave this point as a subject of study for future works.

8.6.2 Compactness

It is useful to explore extremities of compactness for compact star structure. Thus, we introduce the dimensionless compactness parameter $r_g/R = 2M/R$, where r_g is the Schwarzschild radius. This situation is illustrated in Fig. 8.7 for different values of parameters (B, m_s, Δ, α). Regarding the stars with the same M and coupling constant α, it is noticed that the compactness increases when the bag constant increases. Here we define the Schwarzschild radius $r_g = 2M$. The detailed behavior of compactness is shown in Fig. 8.7 which lies in the range $0.54 < r_g/R < 0.62$ for QSs corresponding their respective EoS.

8.7 Results and discussions

In the present chapter we have tested energy-momentum squared gravity (EMSG) model in the strong gravity field regime using quark stars. We have successfully presented a quark star model that quite accurately meets the observed constraints on the mass-radius relation and corresponding maximal mass. Moreover, the recent observations of gravitational waves (GW) from binary NS mergers GW 170817 (Abbott et al. [2017]) by the LIGO-Virgo Collaboration (LVC) has opened up a new avenue to constrain the EOS at high densities. Here, we assumed the equation of state for CFL quark matter that can be obtained in the framework of the MIT bag model. Using this EoS we solved the system of equations and derived the mass-central density and mass-radius profile for quark stars numerically.

Our main motivation is to discuss the features of the EMSG model and the affects of (B, m_s, Δ, α) on the physical properties of the CFL star in these theories. Then, we discuss the physical implications of such compact object by analyzing the trends of pressure, energy density and mass-radius relation (Figs. 8.1,8.2,8.4), respectively.

The decreasing nature of the pressure and energy density are one of the important requirements for realistic compact star models. Moreover, the fulfilment of energy conditions makes CFL star composed of non-exotic matters.

We further extend our chapter by discussing the hydrostatic equilibrium equations in spherical symmetry from the field equations within the EMSG context. We discussed the static stability criterion which is required to satisfy by all stellar configurations (see Fig. 8.6). We also examined the mass-radius relation depends on the choice of the value for the coupling constant α. Interestingly, the CFL quark matters can support maximum mass when the strange quark mass m_s is negligible in GR case. When the EMS coupling is introduced the CFL matter get softer thereby reducing the maximum mass. Further, if m_s increases the stiffness of CFL matter gets more softer, again the M_{max} is reduced further. However, when the bag constant increases the stiffness of the CLF matters significantly reduces. Although, with the increase in color superconducting gap Δ the stiffness also increases significantly. These effects due to changes in (B, m_s, Δ) are similar to Lugones & Horvath predictions (Lugones and Horvath [2003]) however, the coupling constant α modification in EMSG action makes the physical properties changes drastically. In all the cases, the radius for a particular mass is always lesser in EMSG than GR thereby more compactness factor. Due to more compactness factor the surface redshift $z_s = (1 - 2M/R)^{-1/2} - 1$ will be more in EMSG than GR. Also in Fig. 8.6, it is clear that the mass saturate faster with smaller range of central density in EMSG (Dahsed Lines) and saturate at larger ρ_c range in GR (Solid Lines). These means that the stellar system will be more stable in GR than EMSG when changing the central density due to radial perturbations.

On the other hand, we have seen in Ref. Bauswein et al. [2017] that using the data from GW 170817 the radius of a neutron star $1.6M_\odot$ must be above $10.68^{+0.15}_{-0.03}$ km. Followed by this, we see that the radius corresponding to $1.6M_\odot$ in $M - R$ curve (Fig. 8.4) is in agreement with this constraints except for a case with $B = 70 MeV/fm^3$, $m_s = 150 MeV$, $\Delta = 100 MeV$, $\alpha = 0.001$, whose radius is 9.923 km. This means that our model is physically realistic and might have astrophysical applications in future.

Chapter 9

Conformally symmetric traversable wormholes in modified teleparallel gravity [1]

9.1   Introduction

Wormholes are popular tools in science fiction which act as a tunnel-like structure connecting different universes or widely separated regions lie in the same universe. These geometrical model can be considered as a way for rapid interstellar travel, time machines and warp drives. In this direction investigation led by Einstein and Rosen [1935] in the middle of the 1935s, where they constructed an elementary particle model represented by a *bridge* linking two identical sheets: Einstein-Rosen bridge (ERB). This mathematical representation of physical space was an unsuccessful particle model. Twenty years later Wheeler [1955] interested in topological issues in GR, which he denoted "gravitational-electromagnetic entity" in short geons. These were considered as a configuration of the gravitational field, possibly coupled to other zero-mass fields such as massless neutrinos (Brill and Wheeler [1957]) or the electromagnetic field (Brill and Hartle [1964]). Dubbing Einstein-Rosen bridges, Wheeler [1962] sought a way that particles would emerge from a kind of spacetime foam connecting different regions of spacetime at the Planck scale. However, the terminology of "wormhole" was first coined by Wheeler [1957] in 1957. In the late 1962s, Fuller and Wheeler [1962] were able to prove that ERB would collapse instantly upon formation.

---

[1] Content of this chapter has been published in *Physical Review D* (APS), 101 (2020) 084012.

9. Conformally symmetric traversable wormholes in modified teleparallel gravity

In fact, ERB is a non-traversable wormhole, even by a photon.

Modern interest in wormholes are mainly based on the seminal work by Morris and Thorne [1988] and subsequently Morris, Thorne and Yurtsever (Morris et al. [1988]). This issue was investigated after introducing a static spherically symmetric metric with the desired structures and then recovered the matter fields through Einstein's equation. The character of wormhole is asymptotically flat with a constant or variable radius which depends on its configuration. These authors have showed that wormholes can be traversable provided that they are supported by "exotic" matter with a minimal surface area linked to satisfy flare-out condition, which is called throat of the wormhole. It turns out that the energy-momentum tensor to violate the null energy conditions (NEC) called exotic matter; in fact wormhole solutions violate all of the standard energy conditions (Visser [1995]). However, this type of matter sounds to be unusual in general relativity (GR), but from a quantum gravitational perspective, they are seen as a natural consequence if the topology of spacetime fluctuates in time (Wheeler [1955]). As a consequence, it is important and useful to minimize the violation of the energy conditions or reduce the encounter of exotic matter at the throat. The energy conditions of dynamical wormholes in general relativity was explored in Ref. Ori [1993], Ori and Soen [1994], Wang and Letelier [1995].

A notable result was the 'volume integral quantifier' proposed by Visser et al. [2003]. They showed that the amount of exotic matter can be made infinitesimally small by choosing the geometry of the wormhole in a very specific and appropriate way. In the same direction another interesting proposal came from Kuhfittig [2002, 1999] by imposing a condition on $b'(r)$ to be close to one at the throat. It has been demonstrated that evolving wormhole without violation of the weak energy condition (WEC) could exist within classical GR (Kar and Sahdev [1996], Kar [1994]). They consider a metric with a conformal time-dependent factor, whose spacelike sections are $\tilde{R} \times \tilde{S}^2$ with a wormhole metric. The thin-shell formalism is another approach to minimize the exotic matter, where the exotic matter is concentrated at the throat (Visser [1989a,b]).

It goes without saying that violation of NEC is an unavoidable consequence within GR. However, in the context of modified gravity and higher dimensional theories, it was shown that the normal matter threading the wormhole satisfies all of the energy conditions. In this regard, the study of wormhole solutions in modified theories of gravity enchanted researchers in avoiding the presence of these non standard fluids. More precisely, all known modifications to Einstein gravity introduce new degrees of

freedom in the gravitational sector. In particular, it was shown that wormhole throats can be constructed without the presence of exotic matter in $f(\mathcal{R})$ gravity (Lobo and Oliveira [2009]). In this context, wormhole geometries have been studied assuming different fluids with specific shape functions and examined the validity of energy conditions in Mazharimousavi and Halilsoy [2016], Pavlovic and Sossich [2015], Sharif and Nawazish [2018], DeBenedictis and Horvat [2012]. Author of Ref. Garcia and Lobo [2011] studied the wormhole geometries supported by a non-minimal curvature-matter coupling. It turns out that the matter threading the solution satisfies the null energy condition. This type of solutions were also found in Einstein-Gauss-Bonnet theory (Bhawal and Kar [1992], Mehdizadeh et al. [2015], Kanti et al. [2012], Maeda and Nozawa [2008]), Born-Infeld gravity (Shaikh [2018]) and Lovelock gravity (Dehghani and Dayyani [2009], Zangeneh et al. [2015], Matulich and Troncoso [2011]). In the curvature-matter coupled theory, $f(\mathcal{R}, \mathcal{T})$ gravity, exact solutions were found (Moraes and Sahoo [2017b], Elizalde and Khurshudyan [2018, 2019], Banerjee et al. [2020]).

Motivated by the above discussion, our aim is to find wormhole solutions in $f(\mathbb{T})$ gravity. Inspired by the formulation of higher-order gravity theories, such as $f(\mathcal{R})$ theories, 'Teleparallel Equivalent of General Relativity' (TEGR) has been generalized to $f(\mathbb{T})$ gravity. Interestingly, TEGR (Unzicker and Case [2005], Shirafuji et al. [1996], Maluf [2013], Okołów [2014]) is a gravity theory based on spacetime torsion, replacing a zero torsion Levi-Civita connection by a zero curvature Weitzenböck connection with the vierbein as a fundamental tool. The Weitzenböck linear connection furnishes a null Riemann curvature tensor, and characterize a globally flat space-time endowed with a non-zero torsion tensor. It is important to mention that this connection is metric-compatible, and the dynamics of the theory is based only on the torsion. This is one of the main differences between GR and TEGR, and comparing with GR, TEGR has some advantages (Ortín [2004]) over the conventional formulation.

In analogy to the above theory, the so-called $f(\mathbb{T})$ gravity has been introduced as a straight forward modification of Teleparallel gravity by changing in the TEGR action. These $f(\mathbb{T})$ gravity models, where $\mathbb{T}$ is the torsion scalar, the Lagrangian is taken to be a non-linear function of the TEGR Lagrangian $\mathbb{T}$ (Ferraro and Fiorini [2007, 2008], Cai et al. [2016]). This construction crucially depended on an appropriate ansatz for the tetrad field. In contrast to this, the equations of motion of the torsion-based $f(\mathbb{T})$ theory involve only the usual second order derivatives of the tetrad fields. However, the curvature-based $f(\mathcal{R})$ gravity leads to fourth order derivative of the metric in the

9. Conformally symmetric traversable wormholes in modified teleparallel gravity

resulting equations of motion. Subsequently, in the pure tetrad formalism (absence of the spin connection), $f(\mathbb{T})$ gravity exhibits violation of the local Lorentz invariance (Cai et al. [2016]) (for more review see Ferraro and Fiorini [2007]). Other potentially helpful approaches in this respect must be explored, as the proposals of *covariant* formulation of teleparallel gravities where the spin connection is taken different from zero (Krššák and Saridakis [2016], Golovnev et al. [2017], Bejarano et al. [2019]). Thus, the choice of the tetrad always a sensitive issue in $f(\mathbb{T})$ theory and different tetrads might give rise to different solutions. The good and bad tetrads in $f(\mathbb{T})$ gravity has been widely studied in Tamanini and Boehmer [2012]. In this context, $f(\mathbb{T})$ theories can potentially be used to explain the late-time cosmic accelerating expansion without invoking dark energy (Wu and Yu [2010a,b], Myrzakulov [2011], Karami and Abdolmaleki [2013]), cosmological perturbations (Chen et al. [2011], Dent et al. [2011]), spherically symmetric solutions (Wang [2011]), solar system constraints (Iorio and Saridakis [2012]), and so on.

Additionally, the application of $f(\mathbb{T})$ gravity are not restricted only for cosmological solutions, but there are wide range of application in astrophysics also. In this theory, static and spherically symmetric solutions were considered (Deliduman and Yapiskan [2011], Wu and Yu [2011], Nashed [2013]). By analyzing different tetrads in detail, Boehmer et al. [2011] proved the existence of relativistic stars in $f(\mathbb{T})$ gravity and explicitly constructed several classes of static perfect fluid solutions. Furthermore, in a recent paper Singh et al. [2019], we proposed a new approach to find Einstein's cluster solution that mimicking the behaviors of compact star. In fact compact stars have been theoretically modelled within the frame work of $f(\mathbb{T})$ gravity (for reviews see Ref. Das et al. [2015], Chanda et al. [2019], Abbas et al. [2015b]).

The main aim of this chapter is to present a class of wormhole solutions with a diagonal tetrad and assuming different hypotheses for their matter content in both TEGR and $f(\mathbb{T})$ gravity. In Boehmer et al. [2012] an off-diagonal tetrad has considered to explore traversable wormhole geometries are supported by $f(\mathbb{T})$ gravity. It was demonstrated that obtained solution satisfies the weak and the null energy conditions at the throat and its vicinity. In this line of direction several solutions have been thoroughly analyzed for wormholes (Jamil et al. [2013], Lin et al. [2019], Sharif and Rani [2013b]). It should be stressed that, dynamical wormhole in $f(\mathbb{T})$ gravity was found in Sharif and Rani [2013a].

Here, we focus on a new class of traversable wormholes where the spacetime is assumed to be spherically symmetric and to possess a conformal symmetry. Never-

theless, an exact solutions of traversable wormholes were found under the assumption of *non-static* conformal symmetry (Böhmer et al. [2008]). To be more precise, conformal symmetry gives a natural link between geometry and matter through the Einstein field equations. Our work reveals the feature of conformal Killing operator $\mathcal{L}$ associate with the metric g is a linear mapping from the space $\mathcal{J}(\xi)$ of vector fields on ξ, which yield

$$\mathcal{L}_\xi g_{ik} = \psi g_{ik}, \quad \text{where} \quad \xi \in \mathcal{J}(\xi), \tag{9.1}$$

where ψ is the conformal factor and the metric g is conformally mapped onto itself along ξ. Note that for ψ is zero, we refer to this as a *true* Killing vector and the metric is completely invariant as it is dragged along the curves with that true Killing vector as their tangent vector. In favor of this mathematical technique was applied by Herrera et al. [1984], Herrera and de León [1985] and in Maartens and Maharaj [1990] to show that for a one-parameter group of conformal motions, the EoS is uniquely determined by the Einstein equations. Further, strange quark stars with respect to one class of admissible transformations was explored in Ref Mak and Harko [2004].

Meanwhile, this approach has been utilized very successfully in wormhole geometry (Kuhfittig [2015b], Rahaman et al. [2015b], Bhar et al. [2016b], Sharif and Fatima [2016]). The main motivation comes from a recent article by us (Banerjee et al. [2020]), where wormholes were found under the assumption of spherically symmetric and to possess a conformal symmetry in $f(\mathcal{R}, \mathcal{T})$ gravity. This chapter is outlined in the following manner: After the introduction in Section 9.1, we briefly review the basics of the $f(\mathbb{T})$ gravity model in Section 9.2. In Section 9.3, we give an overview about the general geometries and constraints of traversable wormholes. Section 9.4 and 9.5, is devoted to study the field equations of the $f(\mathbb{T})$ theory with a linear and power-law model of $f(\mathbb{T})$ functions, respectively. In Section 9.6 and 9.7, exact general solutions are deduced using static conformal symmetries for both TEGR and $f(\mathbb{T})$ gravity. In Section 9.6, we explore the wormhole geometries in TEGR by assuming suitable conditions. In the case of TEGR wormholes matter violates the null and weak energy conditions at the throat and its vicinity. While, in Section 9.7, we devoted to explore the wormhole solutions by assuming a power-law $f(\mathbb{T})$ model as well as different shape functions. Summary and conclusions are reported in Section 9.8.

9.2 Teleparallel gravity and its modifications: Basic equations and action

Before starting our considerations on $f(\mathbb{T})$ gravity and its astrophysical realization, it is useful to briefly review the $f(\mathbb{T})$ gravitational paradigm. The notation is as follows: Greek indices μ, ν, run over the coordinate space-time and lower case Latin indices i, j,... run over the tangent space-time. We begin by recalling that the dynamical variables in teleparallel gravity are the vierbein or tetrad fields, e^i_μ, which satisfy

$$e^i_\mu e^\nu_i = \delta^\mu_\nu \ \ \text{and} \ \ e^i_\mu e^\mu_j = \delta^j_i, \tag{9.2}$$

where δ is the Kronecker tensor. Thus, the spacetime metric tensor and the tetrads are related by

$$g_{\mu\nu}(x) = \eta_{ij} e^i_\mu(x) e^j_\nu(x), \tag{9.3}$$

where η_{ij} is the Minkowski metric of the tangent space with the form of $\eta_{ij} = $ diag $(1, -1, -1, -1)$. The metric g is used to raise and lower coordinate indices and η raises and lowers frame indices.

Since, Teleparallel gravity carries a fundamental distinction from curvature based descriptions of gravity. Instead of using the torsionless Levi-Civita connection in GR, one uses the Weitzenböck connection, which is given by

$$\widetilde{T}^\sigma_{\mu\nu} = e^\sigma_i \partial_\nu e^i_\mu = -e^i_\mu \partial_\nu e^\sigma_i. \tag{9.4}$$

With the above consideration, the covariant derivative, D_μ, of the tetrad fields

$$D_\mu e^i_\nu \equiv \partial_\mu e^i_\nu - \widetilde{T}^\sigma_{\mu\nu} e^i_\sigma, \tag{9.5}$$

vanishes identically, leads to a vanishing scalar curvature but non-zero torsion.

Now, introducing the torsion and contorsion tensors, to clarify the interrelations between Weitzenböck and Levi-Civita connections, which are

$$T^\sigma_{\mu\nu} = \widetilde{T}^\sigma_{\nu\mu} - \widetilde{T}^\sigma_{\mu\nu} = e^\sigma_i \left(\partial_\nu e^i_\mu - \partial_\mu e^i_\nu \right), \tag{9.6}$$

$$K^{\mu\nu}_\sigma \equiv T^\sigma_{\mu\nu} - \widetilde{T}^\sigma_{\mu\nu} = \frac{1}{2} \left(T^{\mu\nu}_\sigma + T^{\nu\mu}_\sigma - T^{\mu\nu}_\sigma \right), \tag{9.7}$$

9.2. Teleparallel gravity and its modifications: Basic equations and action

respectively. Furthermore, the super-potential tensor relates the torsion and contorsion tensors, as follows

$$S^{\mu\nu}_{\sigma} = K^{\mu\nu}_{\sigma} - \delta^{\nu}_{\sigma} T^{\alpha\mu}_{\alpha} + \delta^{\mu}_{\sigma} T^{\alpha\nu}_{\alpha}, \qquad (9.8)$$

Finally, we define the torsion scalar $\mathbb{T}$, as

$$\mathbb{T} \equiv T^{\sigma}_{\mu\nu} S^{\mu\nu}_{\sigma}, \qquad (9.9)$$

which used in the action and varied in terms of the vierbeins give rise to the same equations with GR. Thus, the torsion-based variant of the theory is known as the teleparallel equivalent of General Relativity (TEGR). Analogous to $f(\mathcal{R})$ gravity, Teleparallel gravity has been extended by constructing gravitational Lagrangians to a function $f(\mathbb{T})$ of a torsion scalar $\mathbb{T}$.

Therefore, the corresponding action of $f(\mathbb{T})$ gravity reads as (with geometrized units $c = G = 1$)

$$S = \frac{1}{16\pi} \int e f(\mathbb{T}) \, d^4x + \int e\mathcal{L} \, d^4x, \qquad (9.10)$$

where e is the determinant of e^i_μ and $\mathcal{L}$ is the matter Lagrangian.

Now, varying the resultant action with respect to the tetrads e^i_μ, one obtains the following field equation for $f(\mathbb{T})$ gravity:

$$S^{\mu\nu}_i f_{\mathbb{TT}} \, \partial_\mu \mathbb{T} + e^{-1}\partial_\mu(eS^{\mu\nu}_i) \, f_{\mathbb{T}} - T^{\sigma}_{\mu i}S^{\nu\mu}_{\sigma}f_{\mathbb{T}} - \frac{1}{4}e^{\nu}_i f = -4\pi \mathcal{T}^{\nu}_i. \qquad (9.11)$$

where $f_{\mathbb{T}} = df(\mathbb{T})/d\mathbb{T}$ and $f_{\mathbb{TT}} = d^2f(\mathbb{T})/d\mathbb{T}^2$, and the tensor $\mathcal{T}^{\nu}_i$ represents the energy-momentum tensor of the matter source $\mathcal{L}$. When $f(\mathbb{T}) = \mathbb{T}$, the action is the same as in TEGR, and $f(\mathbb{T}) = \mathbb{T} - 2\Lambda$, the equations of motion (9.11) are the same as that of the Teleparallel theory with a cosmological constant, and this is dynamically equivalent to the GR.

Since, the field equation (9.11) appears very different from Einstein's equations

due to partial derivatives and tetrad components.

9.3 Traversability conditions and general remarks for wormholes

The spacetime ansatz for seeking traversable wormholes are described by a static and spherically symmetric metric which is in the usual spherical (t, r, θ, ϕ) coordinates, and the corresponding line element can be written as (Morris and Thorne [1988]),

$$ds^2 = e^{\nu(r)}dt^2 - \left(1 - \frac{b(r)}{r}\right)^{-1} dr^2 - r^2 \left(d\theta^2 + \sin^2\theta \ d\phi^2\right), \qquad (9.12)$$

where $\nu(r)$ and $b(r)$ are the redshift and the shape functions, respectively. The function $b(r)$ in Eq. (9.12) is called the shape function, since it represents the spatial shape of the wormhole. The shape function $b(r)$ should obey the boundary condition $b(r = r_0) = r_0$ at the throat r_0 where $r_0 \leq r \leq \infty$. In order to describe the wormhole solution, the shape function must satisfy the *flaring-out* condition that can be obtained from the embedding calculation, and reads

$$\frac{b(r) - rb'(r)}{b^2(r)} > 0. \qquad (9.13)$$

Mathematically the above condition can be also written in a short way, namely, $b'(r_0) < 1$ at the throat $r = r_0$. Since, the geometry is static and spherically symmetric, we assume that $\nu(r)$ should be finite everywhere in order to avoid the presence of an event horizon (Morris and Thorne [1988]). The condition $1 - b(r)/r \geq 0$ is also imposed. Another important criterion is the proper radial distance $\ell(r)$, defined as

$$\ell(r) = \pm \int_{r_0}^{r} \frac{dr}{\sqrt{1 - \frac{b(r)}{r}}}, \qquad (9.14)$$

is required to be finite everywhere. Thus, the proper distance decreases from the upper universe $\ell = +\infty$ to the throat of the wormhole ℓ and then from $\ell = 0$ to $\ell = -\infty$ in the lower universe. Moreover, 'ℓ' should greater than or equal to the coordinate distance, i.e. $\mid \ell(r) \mid \geq r - r_0$; the $\pm$ signs denote the upper and lower parts of the wormhole which are connected by the wormhole throat. The embedding surface of the wormhole can be observed by determining the embedding surface $z(r)$

at a fixed time $t = \text{const}$ and $\theta = \pi/2$. With this constraint the metric of Eq. (9.12) becomes,

$$z'(r) = \pm \frac{1}{\sqrt{r/b(r) - 1}}. \tag{9.15}$$

Considering the conformal symmetry, the above equation turns out to be

$$z(r) = \pm \int \frac{c_3}{\psi} \left(1 - \frac{\psi^2}{c_3^2}\right) dr. \tag{9.16}$$

In the present situation, we consider the matter is described by an anisotropic stress-energy tensor of the form

$$\mathcal{T}_i^\nu = (\rho + p_t)u^\nu u_i + p_t g_i^\nu + (p_r - p_t)\chi_i \chi^\nu, \tag{9.17}$$

where u_ν is the four-velocity and χ_ν is the unit spacelike vector in the radial direction. In the following expression $\rho(r)$ is the energy density, $p_r = p_r(r)$ and $p_t = p_r(r)$ are the radial and transverse pressures, respectively. If matter is considered to be isotropic then $p_r = p_t$. Throughout the discussion prime denotes the derivative with respect to the radial coordinate r.

9.4 Wormhole solutions in different forms of $f(\mathbb{T})$

Since, by considering different forms of $f(\mathbb{T})$'s we arrive at different field equations with the choice of a set of diagonal tetrads. Here, we will consider two classes of solution, (i) linear function in $f(\mathbb{T})$ i.e. TEGR, and (ii) a viable power-law form of the $f(\mathbb{T})$ model.

9.4.1 Field equations in teleparallel gravity $f(\mathbb{T}) = a\mathbb{T} + B$

In order to compute the field equations, we employ the following diagonal tetrad (Momeni et al. [2018], Abbas et al. [2015b]),

$$[e_\mu^i] = \text{diag}(e^{\nu/2}, \ (1 - b/r)^{-1/2}, \ r, \ r\sin\theta), \tag{9.18}$$

and its determinant is $|e_i^i| = r^2 \sin\theta \ e^{\nu/2}(1 - b/r)^{-1/2}$. As a consequence, the torsion scalar becomes

$$\mathbb{T}(r) = \frac{2}{r}\left(1 - \frac{b(r)}{r}\right)\left(\nu'(r) + \frac{1}{r}\right), \tag{9.19}$$

where the prime denotes the derivative with respect to r.

Since we know that the off diagonal components of the field equations vanish in the static case of GR, whereas for $f(\mathbb{T})$ gravity there exists a (r, θ) component which gives an extra equation $\mathbb{T}' f_{,\mathbb{TT}} = 0$. But this equation does not appear in the corresponding curvature-based equations of motion. It rises from the specific choice of tetrad in spite of that they are diagonal. According to the Ref. Tamanini and Boehmer [2012], this equation leads to satisfy either $f_{,\mathbb{TT}} = 0$ or $\mathbb{T}' = 0$, where the former reduces the theory to TEGR. In what follows, the choice of $f_{,\mathbb{TT}} = 0$ leads to the following linear model $f(\mathbb{T}) = a\mathbb{T} + B$ (Abbas et al. [2015b]), which are of physical interest in this context.

Now, inserting the vierbein choice (9.18) into the field equations (9.11) we obtain the set of equations for an anisotropic fluid as

$$4\pi\rho = \frac{1}{4}\left(\frac{2ab'}{r^2} + B\right), \tag{9.20}$$

$$4\pi p_r = \frac{r^2\left(2a\nu' - Br\right) - 2b\left(ar\nu' + a\right)}{4r^3}, \tag{9.21}$$

$$4\pi p_t = \frac{1}{8r^3}\Big[r\big(ab'(a\nu' + 2) + r\{2ar\nu'' + a\nu'(r\nu' + 2) - 2Br\}\big) \\ - ab\left\{\nu'(a + r^2\nu' + 2r) + 2r^2\nu'' + 2\right\}\Big], \tag{9.22}$$

where ρ is the energy density with p_r and p_t are the radial and tangential pressure of the matter sector, respectively.

9.4.2 Field equations in $f(\mathbb{T}) = a\mathbb{T}^2 + B$

Here, we will study for the choice of a set of diagonal tetrads with a particular power-law form of $f(\mathbb{T})$ model i.e. $f(\mathbb{T}) = a\mathbb{T}^2 + B$, where a and B are constants. It has been shown that the power-law inflation model can easily accommodate with the regular thermal expanding history including the radiation and cold dark matter dominated phases. Utilizing the model along with Eq. (9.12), we obtain the following expression

$$4\pi\rho = \frac{1}{4r^6}\Big[r^2\left(24ab' - 36a + Br^4\right) - 24arb\left(b' - 3\right) - 36ab^2\Big], \tag{9.23}$$

$$4\pi p_r = \frac{27ab^2}{r^6} - \frac{48ab}{r^5} + \frac{21a}{r^4} - \frac{B}{4}, \tag{9.24}$$

$$4\pi p_t = \frac{1}{4r^6}\Big[r^2\left(60a - 24ab' - Br^4\right) + 24arb\left(b' - 4\right) + 36ab^2\Big]. \tag{9.25}$$

Since, the choice of $f(\mathbb{T})$ in this case do not satisfy $f_{,\mathbb{T}\mathbb{T}} = 0$ and $\mathbb{T}' = 0$. So, the field equations are not corresponding to TEGR.

Notice that above field equations for both models give three independent equations with five unknown quantities i.e. $\rho(r)$, $p_r(r)$, $p_t(r)$, $\nu(r)$ and $b(r)$. Therefore, system of equations is under-determined, and we shall reduce the number of unknown functions by assuming suitable conditions.

9.5   Conformal killing vectors

Despite the success of numerical computation, exact solutions are still important in GR as well as modified gravity, because they allow a *global* acceptance without specifying the choice of parameters and initial conditions. In this sprite conformal symmetries provide important insight and information into the general properties of self-gravitating matter configurations. Guided by the above motivations we assume that the static and spherically symmetric spacetime admit a Conformal Motion. According to Ref. Herrera et al. [1984], Maartens and Maharaj [1990], we simplify the problem and build up its basic mathematical structure.

In general, Conformal Motion (CM) is a map $\mathcal{M} \to \tilde{\mathcal{M}}$ such that the metric g of the spacetime transforms under the rule

$$g \to \tilde{g} = 2e^{\psi}g, \quad \text{with} \quad \psi = \psi(x^a),$$

which can be expressed as

$$\mathcal{L}_{\xi}g_{ab} = \xi_{a;b} + \xi_{b;a} = \psi g_{ab}, \tag{9.26}$$

where $\mathcal{L}$ signifies the Lie derivative along ξ^a and $\psi(x^a)$ is the conformal factor. In Herrera et al. [1984], authors assumed that the vector field generating the conformal symmetry is static and spherically symmetric within the framework of GR, which yield

$$\xi = \xi^0 r \frac{\partial}{\partial t} + \xi^1 r \frac{\partial}{\partial r}. \tag{9.27}$$

Using this form of the conformal vector in Eq. (9.26), one obtains

$$\xi^r \nu' = \psi(r), \ \xi^t = \text{const.}, \ \xi^r = \frac{\psi r}{2}, \ \xi^r \lambda' + 2\xi^{r'} = \psi(r).$$

These vectors are of physical significance as (i) $\psi = 0$ then Eq. (9.26) gives the Killing vector, (ii) $\psi = $ constant gives homothetic vector, and (iii) when $\psi = \psi(\mathbf{x}, t)$ having a conformal motion.

Thus, conformal equation (9.26) for the metric (9.12) provides the following set of equations

$$e^\nu = c_2^2 r^2, \tag{9.28}$$

$$1 - \frac{b(r)}{r} = \left[\frac{\psi}{c_3}\right]^2, \tag{9.29}$$

$$\xi^i = c_1 \delta_4^i + \left[\frac{\psi r}{2}\right]\delta_r^i, \tag{9.30}$$

where c_1, c_2 and c_3 are constants of integration. Interestingly, if we rearrange the Eq. (9.29) in terms of the shape function, then the conformal factor is zero at the throat, i.e. $\psi(r_0) = 0$.
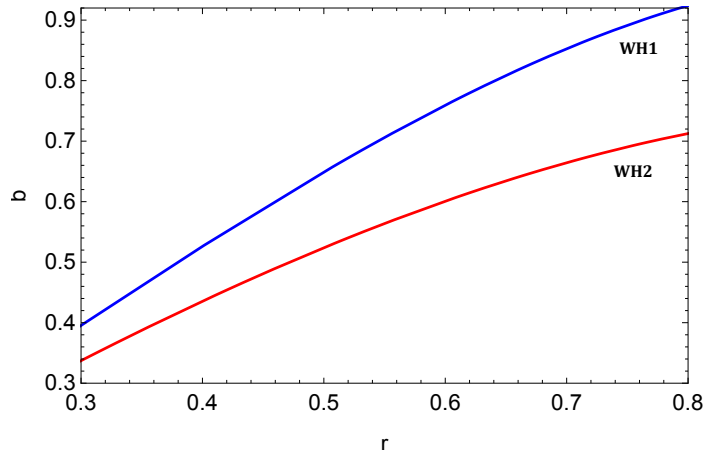
Figure 9.1: Variation of shape functions with radial coordinate for $a = 0.1, A = -2, B = 0.5, \omega = -1.4, c_3 = 1.88$ (WH1) and $a = 0.2, d = -0.014, B = 0.5, n = 0.14, c_3 = 0.13$ (WH2).

9.5.1 Field equations with conformal symmetry in teleparallel gravity

With the assumption (9.1) the gravitational field equations describing the interior of a wormhole geometry will be imposed by the existence of conformal killing vector, so that the components of stress-energy tensor are written solely in terms of the
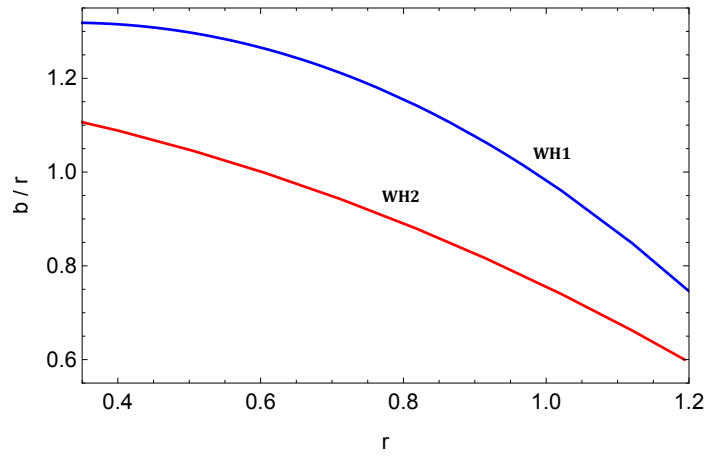
Figure 9.2: Variation of b/r with radial coordinate.
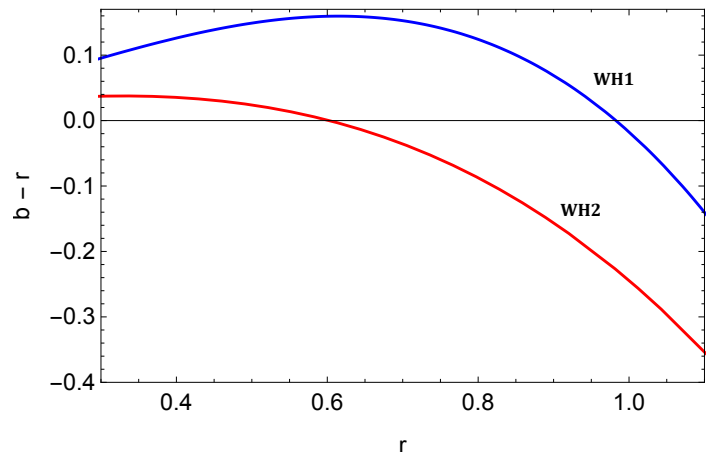
Figure 9.3: Variation of $b - r$ with radial coordinate.
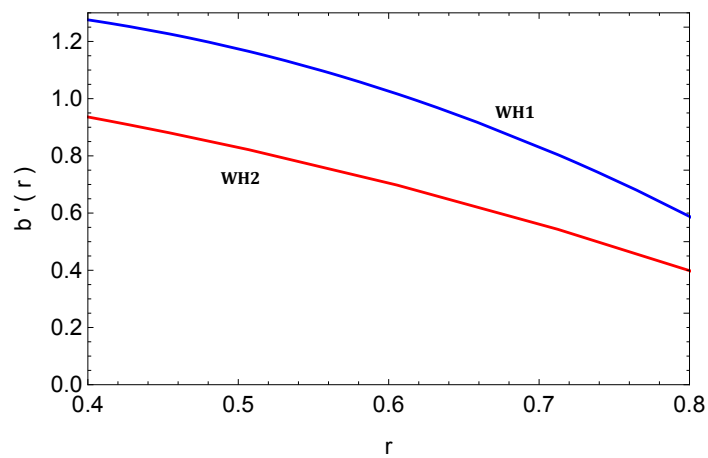
Figure 9.4: Variation of $b'(r)$ with radial coordinate.

conformal factor. Substituting Eqs. (9.28)-(9.29) into the field Eqs. (9.20)-(9.22), we obtain

$$4\pi\rho = \frac{1}{4}\left[B - \frac{2a\psi\left(2r\psi' + \psi\right)}{c_3^2 r^2} + \frac{2a}{r^2}\right], \tag{9.31}$$

$$4\pi p_r = \frac{1}{4}\left(\frac{6a\psi^2}{c_3^2 r^2} - \frac{2a}{r^2} - B\right), \tag{9.32}$$

$$4\pi p_t = \frac{a\psi\left[\psi - (a + r)\psi'\right]}{2c_3^2 r^2} - \frac{B}{4}. \tag{9.33}$$

It becomes clear from Eq. (9.29) that we impose the following condition $(\psi^2)' > 0$ when evaluated at the throat. The NEC asserts that for any null vector k^μ, we have $T_{\mu\nu}k^\mu k^\nu \geq 0$. Using the Einstein field equations (9.31) and (9.32) provide the following relation

$$4\pi\left(\rho + p_r\right) = \frac{a\psi\left(\psi - r\psi'\right)}{c_3^2 r^2}. \tag{9.34}$$

The NEC at the throat is given by

$$4\pi\left(\rho + p_r\right)\big|_{r_0} = -\frac{a^2}{2r_0^4}\left(1 - b'(r_0)\right) < 0. \tag{9.35}$$

Taking into account the condition $b'_0 < 1$, one verifies the general condition $(\rho + p_r)\big|_{r_0} < 0$. Therefore, the flaring-out condition entails the violation of the NEC.

9.5.2 Field equations with conformal symmetry in $f(\mathbb{T}) = a\mathbb{T}^2 + B$

Proceeding the same, the field Eqs. (9.23)-(9.25) are written solely in terms of the conformal factor, and the stress energy-momentum components are the following form

$$4\pi\rho = \frac{1}{4}\left(B - \frac{2a\psi\left[2r\psi' + \psi\right]}{c_3^2 r^2} + \frac{2a}{r^2}\right), \tag{9.36}$$

$$4\pi p_r = \frac{1}{4}\left(\frac{6a\psi^2}{c_3^2 r^2} - \frac{2a}{r^2} - B\right), \tag{9.37}$$

$$4\pi p_t = \frac{a\psi\left(\psi - (a + r)\psi'\right)}{2c_3^2 r^2} - \frac{B}{4}. \tag{9.38}$$

Now the NEC condition can be determine from the addition of density and pressure as

$$4\pi(\rho + p_r) = \frac{a\psi\,(\psi - r\psi')}{C_3^2 r^2}.$$

(9.39)

and the violation of NEC requires $(\psi^2)' > 0$. The NEC at the throat is given by

$$4\pi(\rho + p_r)|_{r_0} = \frac{a(r_0 - b_0)\,(r_0 b_0' - 2b_0 + r_0)}{r_0^4},$$

(9.40)

Note that the NEC, evaluated at the throat, r_0, is identically zero for arbitrary r i.e. $(\rho + p_r)|_{r_0} = 0$. The same situation was found in Ref. Arellano and Lobo [2006] due to violation of flaring-out condition of the throat when axisymmetric traversable wormholes coupled to nonlinear electrodynamics. But, the main aim in our wormhole construction is that throughout the wormhole solution the matter obeying the NEC or not. This needs some explanation, and we will discuss later.
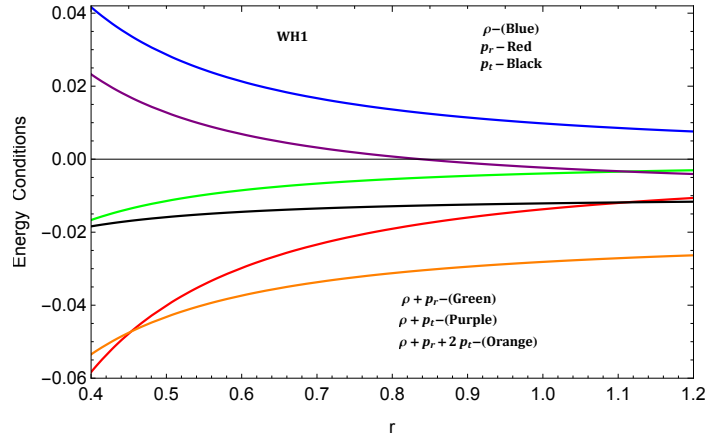
Figure 9.5: Variation of energy conditions for WH1 with radial coordinate.

Since the solutions analyzed in this work are not asymptotically flat, so that one needs to match these interior geometries to an exterior vacuum spacetime in the asymptotic limit by taking into account thin shells, using the cut-and-paste technique (Poisson and Visser [1995]). The appropriate framework to match the interior to the exterior solution we need the junction conditions across a timelike hypersurface for the $f(\mathbb{T})$ gravity. In particular, the junction conditions for $f(\mathbb{T})$ gravity has been performed in Velay-Vitow and DeBenedictis [2017] via the variational principle. It is known that the conditions for matching of two spacetime in a region given by
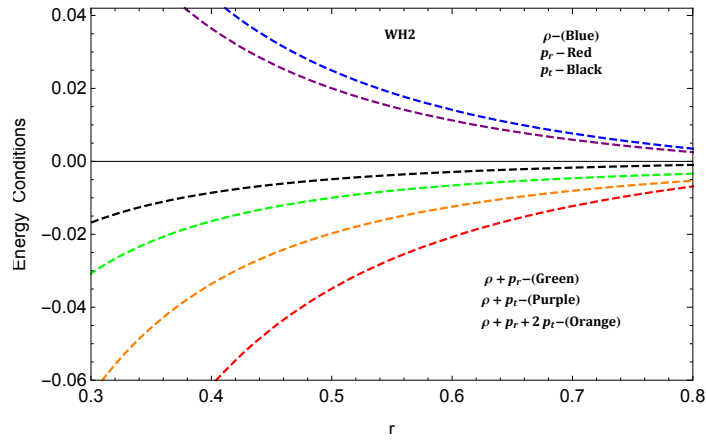
Figure 9.6: Variation of energy conditions for WH2 with radial coordinate.
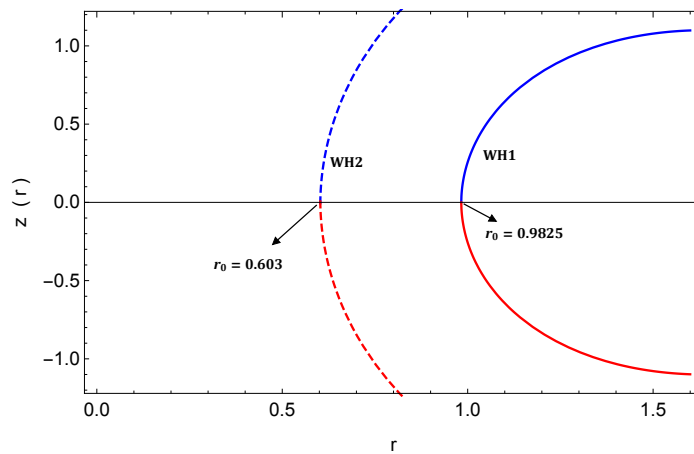
Figure 9.7: Embedding surfaces of the two wormholes in two dimensional space slices in R^3.

$r > R$, if the interior metric is matched to this vacuum spacetime at $r = R > r_0$. In contradistinction for regular geometry with an interior wormhole spacetime, $r_0 \leq r \leq R$, and a Schwarzschildlike vacuum, $r_h < R \leq r < \infty$, at a junction interface. In addition, the junction conditions in this theory have been worked out (de la Cruz-Dombriz et al. [2016]).

9.6 TEGR Wormholes

For the simplest linear function $f(\mathbb{T}) = a\mathbb{T} + b$, we will discuss some particular wormhole solutions. To start with, we shall first consider the isotropic case and then various choices for the form function.

9.6.1 Isotropic wormhole solution

First, we shall restrict our investigation in isotropic condition i.e. $p_r = p_t$, which on imposing to the field equations (9.32) and (9.33), one can get the following solution:

$$\psi = \frac{\sqrt{c_3^2(a+r)^4 + e}}{\sqrt{2}(a+r)^2},$$ (9.41)

thus substituting this value into (9.29), we have

$$b(r) = \frac{r}{2}\left[1 - \frac{e}{c_3^2(a+r)^4}\right],$$ (9.42)

where e is the constant of integration.

It becomes clear that this form of the shape function gives non asymptotically flat geometries, i.e. $b(r)/r \to 1/2$ as $r \to \infty$ and $b'(r_0) \not< 1$. This implies that there are no wormhole solutions sustained for isotropic pressure in TEGR.

9.6.2 Wormhole (WH1) solution with $p_r = \omega\rho$:

To solve the field equations (9.31)-(9.33), we assume an additional information as a linear equation of state (EoS) $p_r = \omega\rho$, and the corresponding solutions can be written as

$$\psi(r) = \frac{1}{\sqrt{6a(\omega+3)}}\left[6aA(\omega+3)r^{-\frac{\omega+3}{\omega}} + c_3^2\{6a(\omega+1) + Br^2(\omega+3)\}\right]^{1/2},$$ (9.43)

where A is an integrating constant. Note that the solution given by (9.42) holds for $\omega \neq -3$ only.

Immediately, one can write down the corresponding shape function as

$$b(r) = \frac{2r}{\omega + 3} - \frac{Br^3}{6a} - \frac{Ar^{-3/\omega}}{c_3^2}. \tag{9.44}$$

It is clear that the solutions are asymptotically flat, i.e. $b(r)/r \to 0$ as $r \to \infty$. Note that from Eq. (9.44) when $\omega = 0$, one obtains $b(r) = \frac{2}{3}r - \frac{Br^3}{a}$ which presents a non-asymptotically flat wormhole geometry. Further, to be a wormhole solution, we deduce $b'(r) = \frac{2}{\omega+3} - \frac{Br^2}{2a} + \frac{3Ar^{-3/\omega-1}}{C_3^2\omega}$, and impose the the condition $b'(r_0) < 1$. In fact, we fix the range of parameters from the criterion.

We now discuss the possibility of sustaining a traversable wormhole in spacetime via exotic matter made out of phantom energy EoS, $p_r = \omega\rho$ with $\omega < -1$, and the stress-energy tensor components are given by

$$\rho = \frac{a}{8\pi r^3}\left(\frac{3Ar^{-3/\omega}}{c_3^2\omega} + \frac{2r}{\omega + 3}\right), \tag{9.45}$$

$$\rho + p_r = \frac{a(\omega + 1)}{8\pi r^3}\left(\frac{3Ar^{-3/\omega}}{c_3^2\omega} + \frac{2r}{\omega + 3}\right), \tag{9.46}$$

$$\rho + p_t = \frac{1}{48\pi r^4}\left[\frac{3aA(\omega + 3)(a + 3r)r^{-3/\omega}}{c_3^2\omega} + ar^2(6 - Br) - 3Br^4\right] \tag{9.47}$$

$$\rho + p_r + 2p_t = \frac{1}{24\pi r^4}\left[\frac{3aAr^{-3/\omega}(a(\omega + 3) + 6r(\omega + 1))}{c_3^2\omega}\right.$$
$$\left. + r^2\left(\frac{12a(\omega + 1)}{\omega + 3} - aBr - 3Br^2\right)\right]. \tag{9.48}$$

To check the NEC evaluated at the throat is given by

$$(\rho + p_r)|_{r_0} = \frac{a(\omega + 1)}{8\pi r_0^3}\left(\frac{3Ar^{-3/\omega}}{c_3^2\omega} + \frac{2r_0}{\omega + 3}\right). \tag{9.49}$$

Clearly, in this case for $\omega \neq -1$ and $\omega \neq -3$, we consider the interval $-3 < \omega < -1$, implying the violation of the NEC at the throat i.e. the throat needs to open with phantom energy.

In Figs. 9.1-9.4, we plot $b(r)$, $b(r)/r$, $b(r) - r$ and $b'(r)$ respectively, for $a = 0.1, A = -2, B = 0.5, \omega = -1.4, c_3 = 1.88$ (WH1). Note that, $b(r) - r$ cuts r-axis at $r_0 = 0.9825$ corresponds to the throat radius of WH1. This situation is shown

graphically in Fig. 9.7. In fact, wormhole geometries fulfilling the required condition $b'(0.9825) \approx 0.843 < 1$, that can see directly from Fig. 9.4.

On the other hand, Fig. 9.5 depicts the behavior of the energy conditions using the field Eqs. (9.45)-(9.43). One may also see that a matter content with a radial pressure having a phantom EoS i.e $\omega < -1$ and everywhere positive energy density $\rho > 0$. Note that it will be valid far from the throat. More specifically, NEC is violated due to $\rho + p_r < 0$. The embedded surface can be evaluated from Eq. (9.16). The Eq. (9.16) is strongly dependent on numerical values of the model parameters and thereby adopting the numerical approach using "Mathematica" command we plot the embedding surface Fig. 9.7.

Since the redshift function $\nu(r)$ does not tend to zero when $r \to \infty$ due to the conformal symmetry. Thus, a constant limit for $\nu(r)$ would also allow us to obtain asymptotically at solutions under time reparametrization. Leading to Ref. Böhmer et al. [2008], the conditions for matching of two spacetime in a region given by $r > R$, if the interior metric is matched to the vacuum spacetime at $r = R > r_0$. Several examples of conformal symmetry have been found mainly in wormhole physics Rahaman et al. [2015a], Kuhfittig [2015a,b], Rahaman et al. [2015b].

9.6.3 Wormhole (WH2) solution with $p_t = np_r$:

Another closed-form solution is derived by taking $p_t = np_r$ (see Ref. Rahaman et al. [2007], Moraes and Sahoo [2017b] for more details) and then deduce the following relationship:

$$
\begin{aligned}
\psi(r) \;=\; & (a+b)\left[\frac{c_3^2}{a}\left(\frac{a^2 B(n-1)+2an}{2(3n-1)(a+r)^2} - \frac{2aB(n-1)}{(6n-1)(a+r)} + \frac{B(n-1)}{6n}\right)\right. \\
& \left.+d(a+r)^{-6n}\right]^{1/2},
\end{aligned}
\tag{9.50}
$$

where the state parameter n is a constant. We obtain from Eq. (9.50) yielding for the shape function

$$
\begin{aligned}
b(r) \;=\; & \frac{r}{6}\left[-\frac{B(n-1)(a+r)^2}{an} + \frac{12B(n-1)(a+r)}{6n-1} - \right. \\
& \left.\frac{3[aB(n-1)+2n]}{3n-1} - \frac{6d(a+r)^{2-6n}}{c_3^2} + 6\right].
\end{aligned}
\tag{9.51}
$$

9. Conformally symmetric traversable wormholes in modified teleparallel gravity

In this case for $n < 1$ implies $b(r)/r \to 0$ as $r \to \infty$ i.e. asymptotically flat spacetimes.

Using the Einstein field equations (9.31)-(9.33) with the following shape function, one obtains

$$\rho = \frac{1}{48\pi r^2}\left[\frac{f_1(r)/(3n-1)}{n(6n-1)} - \frac{6ad(a - 6nr + 3r)}{c_3^2(a + r)^{6n-1}}\right], \tag{9.52}$$

$$\rho + p_r = \frac{a}{24\pi r^2}\left[\frac{6d(a + 3nr)(a + r)^{1-6n}}{c_3^2} + \right.$$
$$\left.\frac{aB(n-1) - B(n-1)(3n-1)r + 6(6n-1)n^2}{n(3n-1)(6n-1)}\right], \tag{9.53}$$

$$\rho + p_t = \frac{(a+r)^{-6n}}{48\pi c_3^2 n(6n-1)r^2}\left[c_3^2(a+r)^{6n}\Big\{a^2 B(n-1) - 2aB(n-1)(3n-2)r\right.$$
$$+ 6an(6n-1) - 3B(n-1)(6n-1)r^2\Big\} + 6adn\{9n(2n-1) + 1\}$$
$$\left.(a + 3r)(a + r)\right]. \tag{9.54}$$

$$\rho + p_r + 2p_t = \frac{(a+r)^{-6n}}{24\pi c_3^2 n(3n-1)(6n-1)r^2}\left[c_3^2 f_3(r)(a + r)^{6n}\right.$$
$$\left.+ 6adn\{9n(2n-1) + 1\}(a + r)(3an + a + 6nr)\right]. \tag{9.55}$$

Note we have used the notations

$$f_1(r) = a^2(B - Bn) + 4aB(n-1)(3n-1)r + 6an$$
$$(2n-1)(6n-1) + 3B(9n(2n-1) + 1)r^2$$
$$f_2(r) = a^2 B(n-1) - 2a[n\{B(3n-4)r - 6n + 1\} + Br]$$
$$+ B\{9(1-2n)n - 1\}r^2$$
$$f_3(r) = a^2 B(n-1)(3n+1) - aB(n-1)(3n-1)(6n+1)$$
$$r + 12an^2(6n-1) - 3Bn\{9n(2n-1) + 1\}r^2.$$

The above expression must be investigated at the throat r_0 to check the NEC, which is given by

$$(\rho + p_r)|_{r_0} = \frac{a}{24\pi r_0^2}\left[\frac{6d(a + 3nr_0)(a + r_0)^{1-6n}}{c_3^2} + \right.$$
$$\left.\frac{aB(n-1) - B(n-1)(3n-1)r_0 + 6(6n-1)n^2}{n(3n-1)(6n-1)}\right]. \tag{9.56}$$

We plot the quantities $b(r)$, $b(r)/r$, $b(r) - r$ and $b'(r)$ in Figs. 9.1-9.4. For the figures we consider $a = 0.2, d = -0.014, B = 0.5, n = 0.14, c_3 = 0.13$ (WH2). We can see from Fig. 9.3 and Fig. 9.7 that $b(r) - r$ cuts r-axis at $r_0 = 0.603$, which is the throat of WH2. One verifies, $b'(0.603) \approx 0.534 < 1$ is shown in Fig. 9.4.

Let us emphasize again the energy conditions. This situation differs from the above discussion that $\rho + p_r$ and $\rho + p_t$ both are negative, whereas ρ is positive throughout the spacetime. As shown in Fig. 9.6, for some fixed parametric values, the NEC is violated in a small region around r_0. The embedding surface $z(r)$ in 3-D Euclidean space can be obtained from Eq. (9.16). In Fig. 9.7 we show the wormhole embedding diagrams for the values of WH2. However, for this solution as well it is not integrable and therefore adopting the numerical approach using "NIntegrate" command within the limits $r_0 \leq r \leq R$. It becomes clear that all embedding surfaces flare outward.
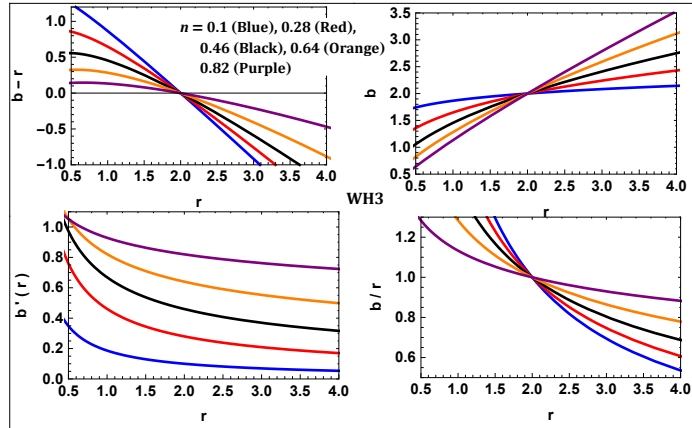
Figure 9.8: Characteristics of the shape function of WH3 for $a = 0.6, R = 2, B = 0.5, c_3 = 1.165$.

9.6.4 Wormhole (WH3) solution with $b(r) = r_0 \left(r/r_0\right)^n$:

To proceed further we ansatz the shape function as $b(r) = r_0 \left(r/r_0\right)^n$. In this case, we need to impose $0 < n < 1$, and corresponding conformal factor takes the form

$$\psi = c_3 \sqrt{1 - \frac{r_0}{r} \left(\frac{r}{r_0}\right)^n}. \tag{9.57}$$

Our aim here is to explore the local energy conditions, and we examine the WEC. Taking into account the diagonal energy momentum tensor, the the WEC implies
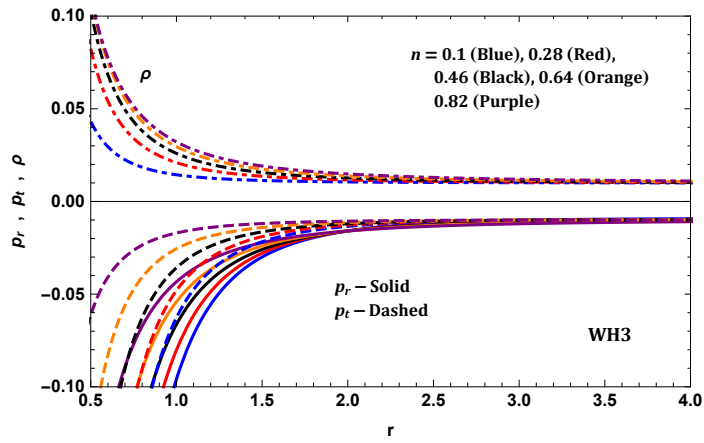
Figure 9.9: Trends of density and pressures for WH3.
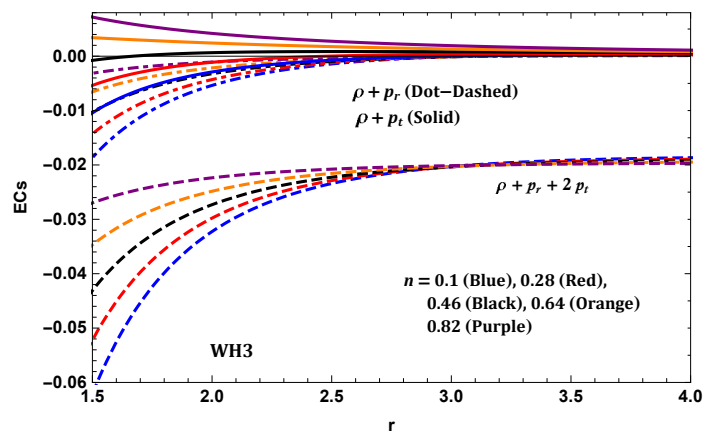
Figure 9.10 Variations of energy conditions for WH3.

$\rho \geq 0$, $\rho + p_r \geq 0$ and $\rho + p_t \geq 0$. Note that last two inequalities reduce to the null energy condition (NEC). The components of the energy-momentum tensor (9.31)-(9.33) then take the form

$$\rho = \frac{2anr_0\left(r/r_0\right)^n + Br^3}{16\pi r^3}, \tag{9.58}$$

$$\rho + p_r = \frac{a\left[(n-3)r_0\left(\frac{r}{r_0}\right)^n + 2r\right]}{8\pi r^3}, \tag{9.59}$$

$$\rho + p_t = \frac{a(n-1)r_0(a+3r),\left(\frac{r}{r_0}\right)^n + 2ar^2}{16\pi r^4} \tag{9.60}$$

$$\rho + p_r + 2p_t = \frac{1}{8\pi r^4}\left[ar_0[a(n-1) + 2(n-3)r]\left(\frac{r}{r_0}\right)^n + 4ar^2 - Br^4\right]. \tag{9.61}$$

Note that at the throat, Eq. (9.52) reduces to

$$(\rho + p_r)|_{r_0} = \frac{a(n-1)}{8\pi r_0^2}. \tag{9.62}$$

Taking into account the condition $b'(r_0) < 1$, and for $0 < n < 1$, one may verify that $(\rho + p_r)|_{r_0} < 0$. Fig. 9.8 shows the behaviour of $b(r)$, $b(r) - r$, $b'(r)$ and $b(r)/r$, respectively. In this case, $b(r) - r$ cuts the r-axis at $r_0 = 2$, which is the throat radius for WH3 (see Fig. 9.13).

From the graphical behavior of the energy conditions in terms of (9.58)-(9.61) are presented in Fig. 9.9-9.10. From Fig. 9.9 , we see that the energy density is positive throughout the whole spacetime, while the radial and transverse pressures are negative, and both tend to zero in the asymptotic limit by construction. Moreover, we observe that for fixed values of the parameters $a = 0.6, R = 2, B = 0.5, c_3 = 1.165$ the NEC is violated due $\rho + p_r < 0$; note also that $\rho > 0$ for different values of n. The embedding surface $z(r)$ in 3-D Euclidean space obtained by using Eq. (9.16) through "NIntegrate" in Mathematica and shown in Fig. 9.13.

9.6.5 Wormhole (WH5) solution with $b(r) = \alpha\left(1 - r_0/r\right) + r_0$:

Now, we will consider the wormhole solution generated by imposing the shape function in the form $b(r) = \alpha\left(1 - r_0/r\right) + r_0$. For this specific case, $b'(r_0) = \alpha/r_0 < 1$ when
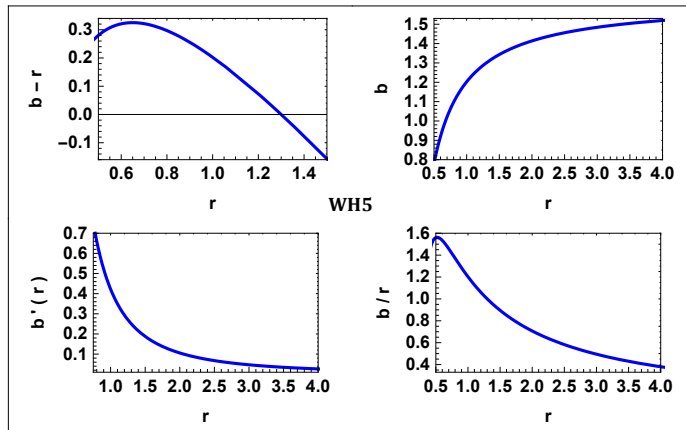
Figure 9.11: Characteristics of the shape function of WH5 for $a = 0.2, R = 1.3, \alpha = 0.25, B = 0.3, c_3 = 1.165$.
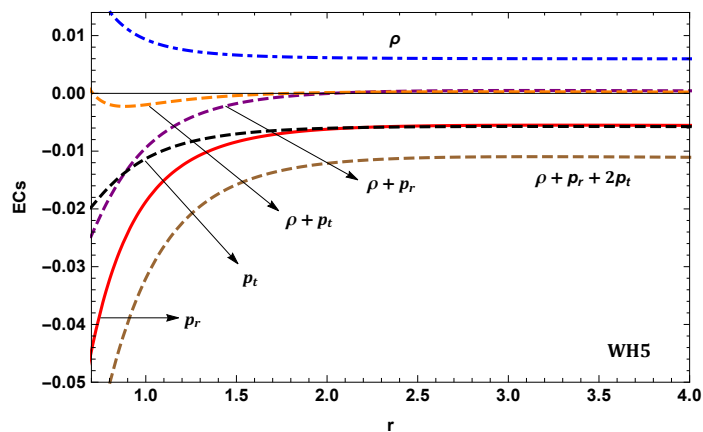
Figure 9.12: Trends of energy conditions for WH5.

$\alpha < 1$, and Eq. (9.29) provides the following solution

$$\psi = c_3 \sqrt{1 - \frac{\alpha R \left(1 - \frac{R}{r}\right) + R}{r}}.$$
(9.63)

In this case the tress energy components are given by

$$\rho = \frac{2a\alpha r_0^2 + Br^4}{16\pi r^4},$$
(9.64)

$$\rho + p_r = \frac{a\left(2r^2 - 3(\alpha+1)rr_0 + 4\alpha r_0^2\right)}{8\pi r^4},$$
(9.65)

$$\rho + p_t = \frac{a}{16\pi r^5}\left[2r^3 - \alpha r_0(a+3r)(r-2r_0) - rr_0(a+3r)\right],$$
(9.66)

$$\rho + p_r + 2p_t = -\frac{1}{8\pi r^5}\left[a^2 r_0(\alpha r + r - 2\alpha r_0) + 2ar\left\{-2r^2\right.\right.$$

$$\left.\left. +3(\alpha+1)rr_0 - 4\alpha r_0^2\right\} + Br^5\right].$$
(9.67)

We now check the energy condition at the throat of the wormhole, which is

$$(\rho + p_r)|_{r_0} = \frac{a(\alpha - 1)}{8\pi r_0{}^2},$$
(9.68)

One can easily check that for $0 < \alpha < 1$ the condition $(\rho + p_r)|_{r_0} < 0$. Fig. 9.11 depicts $b(r)$, $b(r)-r$, $b'(r)$ and $b(r)/r$, in terms of r for $a = 0.2, r_0 = 1.3, \alpha = 0.25, B = 0.3$ and $c_3 = 1.165$, respectively. It can be noted that $b(r)$ cuts the r-axis at $r_0 = 1.3$ for WH5 (see Fig. 9.13). Moreover, from the Fig. 9.12, we see that $\rho + p_r < 0$ and $\rho + p_t < 0$, while $\rho > 0$ throughout the spacetime lead to the violation of WEC, and consequently NEC also. The embedding surface can be determine using (9.16), and found to

$$z(r) = 2r_0\left[(\alpha+1)\log\left(\sqrt{r-\alpha r_0} + \sqrt{r-r_0}\right) - \sqrt{\alpha}\tanh^{-1}\left(\frac{\sqrt{\alpha}\sqrt{r-r_0}}{\sqrt{r-\alpha r_0}}\right)\right]$$
(9.69)

The embedding surface are shown in Fig. 9.13. For a full visualization of the surface sweep through a 2π rotation around the $z$axis, as depicted in Fig. 9.23.

9.7 $f(\mathbb{T})$ **Wormholes**

In this section we proceed in an attempt to analytically solve the basic equations
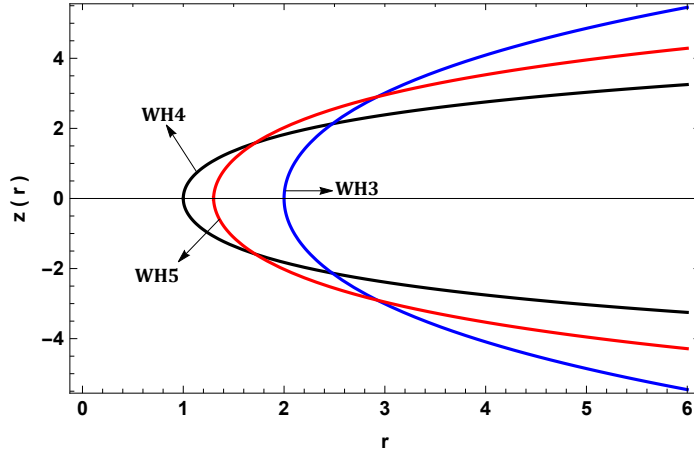
Figure 9.13: The figure shows three dimensional wormhole embedding diagrams for WH3, WH4 and WH5.

by considering a power-law $f(\mathbb{T}) = a\mathbb{T}^2 + B$ function, and for the anisotropic fluid. Here we assume different shape function in finding wormhole solutions. Since solving the differential equations (9.36-9.38) in general, are too complicated for the choices of $p_r = \omega\rho$ or $p_t = np_r$. Therefore, in order to simplify the analysis, we will consider restrictions on the choice of shape functions.
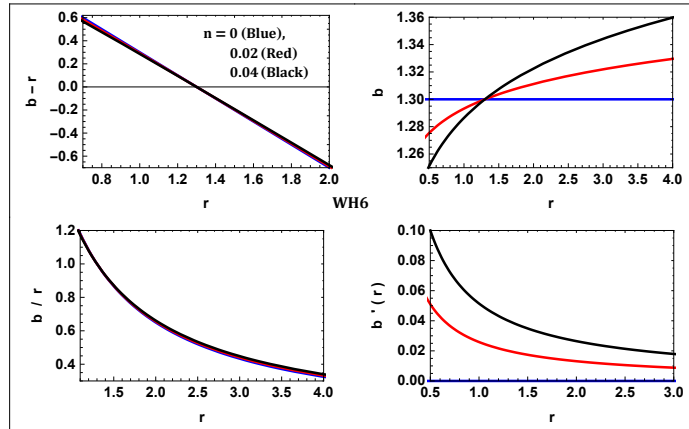
Figure 9.14: Characteristics of shape functions for WH6 with $a = 0.5, R = 1.3, c_3 = 1.165$ and $B = 0.2$.

9.7.1   Wormhole (WH6) with $b(r) = r_0 \left(r/r_0 \right)^n$:

Here, we assume the simplest and viable power-law form of the $f(\mathbb{T}) = a\mathbb{T}^2 + B$ model with a and B are constants. Consider the specific shape function given by
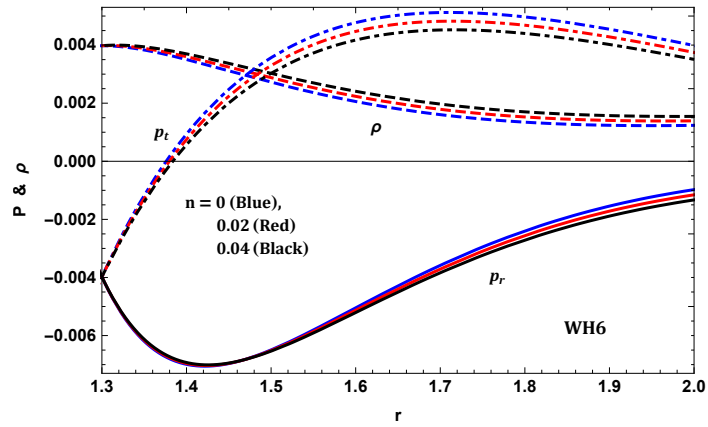
Figure 9.15: Variations of density and pressures for WH6.
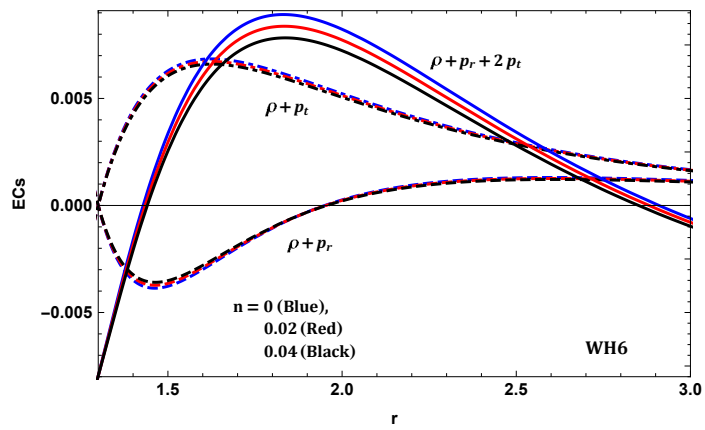
Figure 9.16: Variations of energy conditions for WH6.

$b(r) = r_0 \left(r/r_0 \right)^n$, we obtain the conformal factor as follows:

$$\psi(r) = c_3 \sqrt{1 - \frac{r_0 \left(r/r_0 \right)^n}{r}}, \tag{9.70}$$

Inserting these functions into the stress-energy tensor profile, Eqs. (9.36)-(9.38), provides the following expressions

$$\rho = \frac{Br^6 - 12a}{16\pi r^6} \left[3r - (2n+3)r_0 \left(\frac{r}{r_0} \right)^n \right] \left[r - r_0 \left(\frac{r}{r_0} \right)^n \right], \tag{9.71}$$

$$\rho + p_r = \frac{3a}{2\pi r^6} \left[(n-3)r_0 \left(\frac{r}{r_0} \right)^n + 2r \right] \left[r - r_0 \left(\frac{r}{r_0} \right)^n \right], \tag{9.72}$$

$$\rho + p_t = \frac{3a \left[r - r_0 \left(\frac{r}{r_0} \right)^n \right]}{2\pi r^5}, \tag{9.73}$$

$$\rho + p_r + 2p_t = \frac{r^{-6}}{8\pi} \left[12a \left\{ r - r_0 \frac{r^n}{r_0^n} \right\} \left\{ 7r - (n+6)r_0 \frac{r^n}{r_0^n} \right\} - Br^6 \right]. \tag{9.74}$$

The geometrical properties and characteristics for these shape function is depicted in Fig. 9.14. In this case, $b(r) - r$ cuts the r-axis at $r_0 = 1.3$, which is the throat radius for WH6 when $n < 1$ (see Fig. 9.23 also).

Let us focus the case when $n < 1$ to visualise better the behaviour of the energy conditions. Indeed, one may see that $(\rho + p_r)|_{r_0} = 0$ at the throat of the wormhole, however Fig. 9.15 shows the validity of $\rho > 0$. Thus, one can in principle construct wormhole solutions that satisfy the NEC at the wormhole throat.

In Figs. 9.14 and 9.15 we plot the quantities ρ, $\rho + p_r$, $\rho + p_t$ and $\rho + p_r + 2p_t$. For the figures we have considered $a = 0.5, r_0 = 1.3, c_3 = 1.165$ and $B = 0.2$, respectively. For these choices, the quantities outside the throat $\rho + p_r < 0$ but $\rho + p_t > 0$, which in principle violation of the NEC implying that the WEC is also violated. Therefore, the range of $0 < r < r_0$, the solution obeys the NEC, whereas for any value of $r > r_0$, violation of the NEC outside the throat radius and goes up to the radius R as we need to match at some $r \leq R$, so that we can use the junction conditions to match the interior wormhole solution to the exterior vacuum spherically symmetric solution for finite redshit function. The embedding surface $z(r)$ is calculated numerically in Mathematica using "NIntegrate" package for $r \geq r_0$, and shown in Fig. 9.23.

9.7.2 Wormhole (WH7) with $b(r) = \alpha\, r_0^3 \log{(r_0/r)} + r_0$:

Consider the specific shape function $b(r) = \alpha r_0^3 \log{(r_0/r)} + r_0$. For this choice, the conformal factor becomes

$$\psi = c_3\sqrt{1 - \frac{\alpha r_0^3 \log{(r_0/r)} + r_0}{r}}, \tag{9.75}$$

and corresponding the stress energy components are
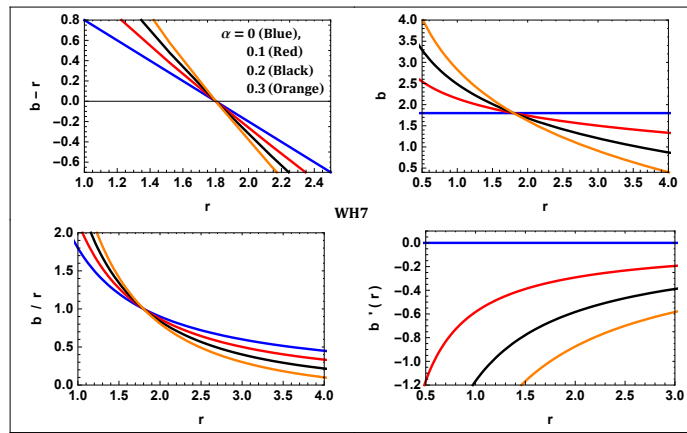
Figure 9.17: Characteristics of shape function for WH7 with $a = 0.5, R = 1.8, c_3 = 1.165, B = 0.2$.
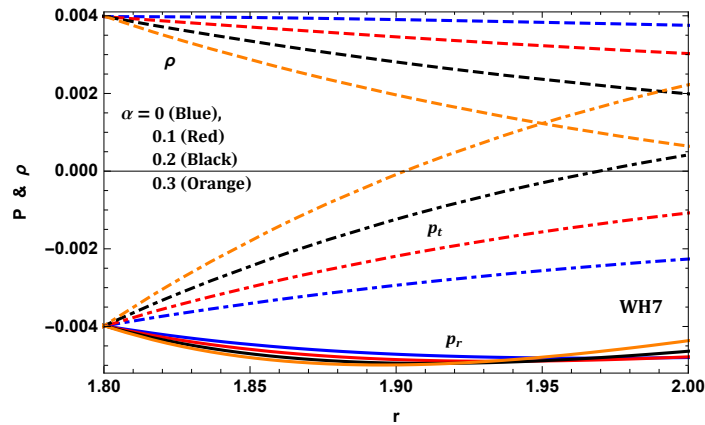
Figure 9.18: Variation of density and pressures for WH7.
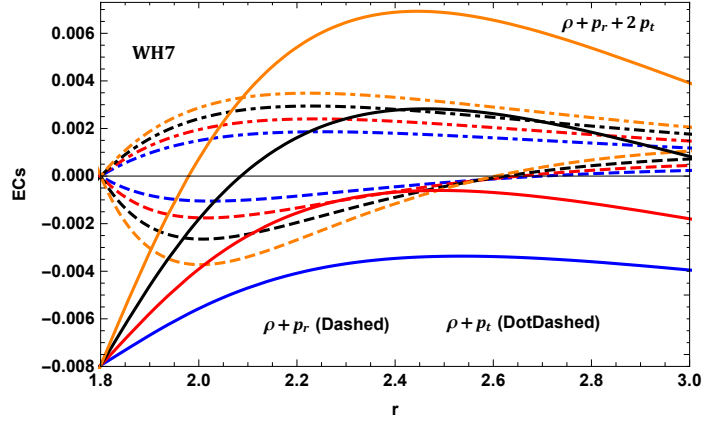
Figure 9.19: Variation of energy conditions for WH7.

$$\rho = \frac{1}{16\pi r^6}\left[Br^6 - 36a\alpha^2 r_0^6 \log^2\left(\frac{r_0}{r}\right) - 12a(r - r_0)(3r\right.$$
$$\left. + 2\alpha r_0^3 - 3r_0) + 24a\alpha r_0^3\left(3r + \alpha r_0^3 - 3r_0\right)\log\left(\frac{r_0}{r}\right)\right] \quad (9.76)$$

$$\rho + p_r = \frac{3a}{2\pi r^6}\left[3\alpha^2 r_0^6 \log^2\left(\frac{r_0}{r}\right) + \alpha r_0^3(6r_0 - 5r + \alpha r_0^3)\right.$$
$$\left. \log\left(\frac{r_0}{r}\right) + (r - r_0)\left\{2r - r_0\left(\alpha r_0^2 + 3\right)\right\}\right] \quad (9.77)$$

$$\rho + p_t = \frac{3a\left(r - \alpha r_0^3 \log\left(\frac{r_0}{r}\right) - r_0\right)}{2\pi r^5}, \quad (9.78)$$

$$\rho + p_r + 2p_t = \frac{1}{8\pi r^6}\left[72a\alpha^2 r_0^6 \log^2\left(\frac{r_0}{r}\right) - Br^6 + 12a(r - r_0)\left(7r + \right.\right.$$
$$\left.\left. \alpha r_0^3 - 6r_0\right) - 12a\alpha r_0^3(13r + \alpha r_0^3 - 12r_0)\log\left(\frac{r_0}{r}\right)\right]. \quad (9.79)$$

In light of the flaring-out condition at the wormhole throat $b_0' < 1$, the parameters α have to meet the requirement $\alpha < 1$. With $a = 0.5, R = 1.8, c_3 = 1.165$, and $B = 0.2$, we plot $b(r)$, $b(r) - r$, $b'(r)$ and $b(r)/r$ in Fig. 9.17. In addition to this, the wormhole throat located at $r_0 = 1.8$.

Here also the situation is same as in the previous discussion i.e. at the throat $(\rho + p_r)|_{r_0} = 0$ and $(\rho + p_t)|_{r_0} = 0$, however $\rho > 0$ inside and outside the throat for the specific value of $a = 0.5, R = 1.8, c_3 = 1.165$, and $B = 0.2$ with different values of α. Moreover, in Fig. 9.18, we plot ρ, p_r and p_t, while in Fig. 9.19 the behavior of the energy conditions are shown outside the throat radius. The fundamental wormhole

conditions, namely, NEC is violated outside the throat, as can be readily verified from Fig. 9.18. We explore the geometrical properties of these solutions via the embedding diagram which is calculated numerically in Mathematica using "NIntegrate" package for $r \geq r_0$ and shown in Fig. 9.23.

9.7.3 Wormhole (WH8) with $b(r) = \alpha r_0 \left(1 - r_0/r\right) + r_0$:

We consider wormhole with the following shape function $b(r) = \alpha r_0 \left(1 - r_0/r\right) + r_0$. Thus, the conformal factor becomes

$$\psi = c_3 \sqrt{1 - \frac{\alpha r_0 \left(1 - r_0/r\right) + r_0}{r}}, \qquad (9.80)$$
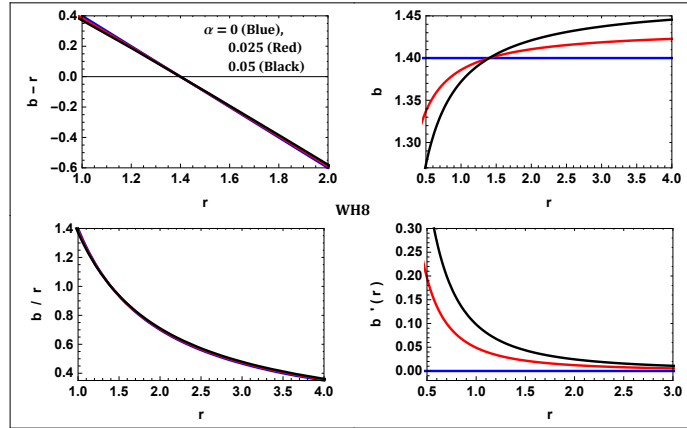
Figure 9.20: Characteristics of shape function for WH8 with $a = 0.5, R = 1.4, c_3 = 1.165, B = 0.2$.

Using Eqs. (9.80) and (9.36)-(9.38), we can obtain the energy density and pressure
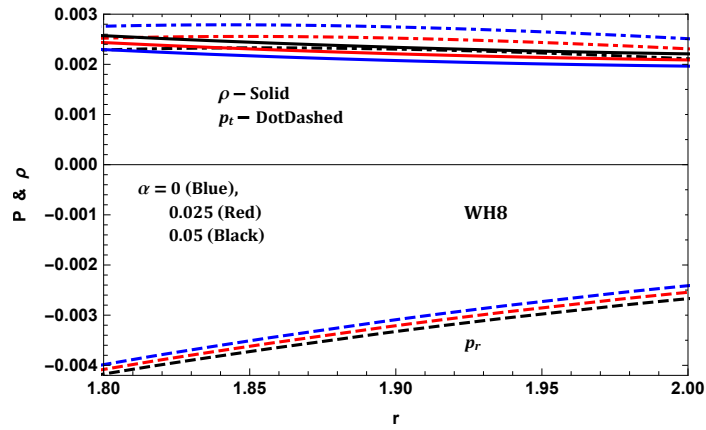
Figure 9.21: Variation of density and pressures for WH8.
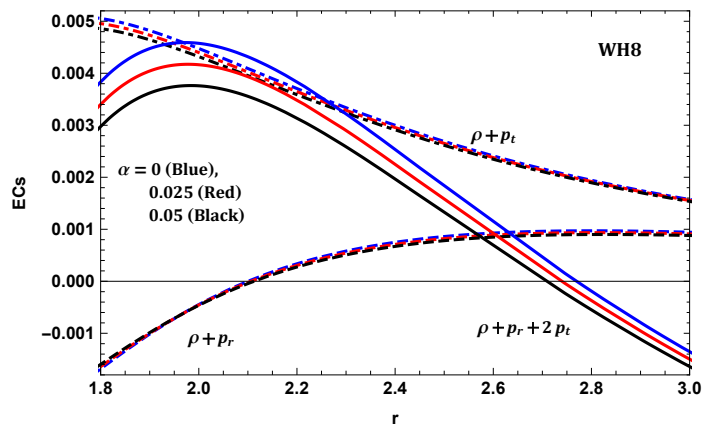
Figure 9.22: Variation of energy conditions for WH8.

components as

$$\rho = \frac{1}{16\pi r^8}\Big[Br^8 - 12a(r - r_0)\Big\{3r^3 - 3r^2(2\alpha r_0 + r_0) \\ + \alpha(3\alpha + 4)rr_0^2 - \alpha^2 r_0^3\Big\}\Big], \qquad (9.81)$$

$$\rho + p_r = \frac{3a(r - r_0)}{2\pi r^8}\Big[2r^3 - (5\alpha + 3)r^2 r_0 + \alpha(3\alpha + 7)rr_0^2 - 4\alpha^2 r_0^3\Big], (9.82)$$

$$\rho + p_t = \frac{3a(r - r_0)(r - \alpha r_0)}{2\pi r^6}, \qquad (9.83)$$

$$\rho + p_r + 2p_t = \frac{1}{8\pi r^8}\Big[12a(r - r_0)\Big\{7r^3 - (13\alpha + 6)r^2 r_0 + \\ \alpha(6\alpha + 11)rr_0^2 - 5\alpha^2 R^3\Big\} - Br^8\Big]. \qquad (9.84)$$
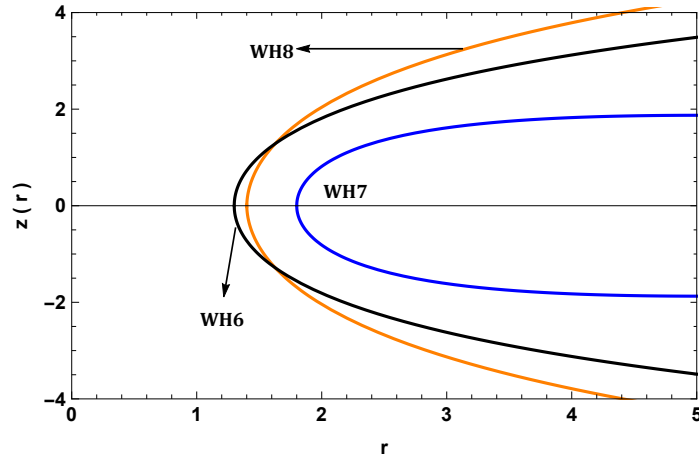
Figure 9.23: Plots of the embedded surface $z(r)$ for WH6, WH7 and WH8.
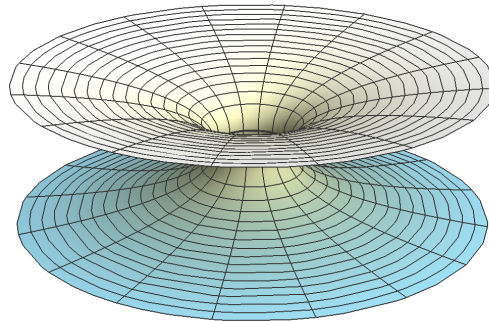
Figure 9.24: The embedding diagram for WH5.
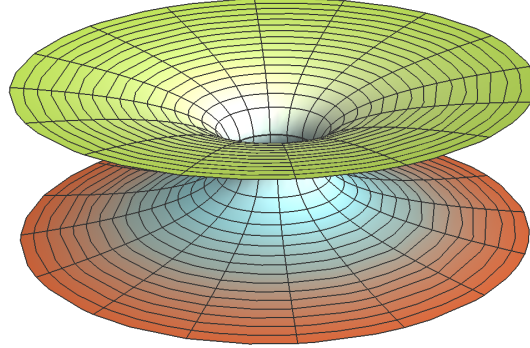
Figure 9.25: The wormhole embedding for WH8.

Based on Eq. (9.80) and (9.29), the behaviors of $b(r)$, $b(r) - r$, $b'(r)$ and $b(r)/r$ are displayed in Fig. 9.19. The $b(r) - r$ cuts the r-axis at $r_0 = 1.4$, which is the throat of the wormhole WH8.

According to Eqs. (9.81)-(9.84) we discuss about the energy conditions. The corresponding results for the pressure and density profile are shown in Figs. 9.21 and 9.22, respectively. As mentioned in the above discussion, one can find that $\rho > 0$ inside and outside the throat for the specific value of $a = 0.5, r_0 = 1.4, c_3 = 1.165$, $B = 0.2$ and for different values of α. In this analogy, the energy density has regions of positive magnitude near the throat, and regions with negative radial pressure which tend to zero from above in the asymptotic region. Our results show that NEC is violated when $r \geq r_0$ and hence the WEC is violated also. The other embedding surface $z(r)$ requires numerical integration, and for that purpose we use "NIntegrate" package which is depicted in Fig. 9.23. Fig. 9.25 shows the revolution surface.

9.8 Results and discussions

In this chapter, we have discussed wormhole geometries in the context of teleparallel equivalent of general relativity (TEGR) and its straightforward extension of $f(\mathbb{T})$ gravity. Since the teleparallel models of gravity are based on the torsion tensor while GR is formulated using the curvature. Motivated by the attempts to explain the observed late time accelerated expansion of the universe, $f(\mathbb{T})$ theories of gravity have been extensively applied to cosmology without invoking the dark energy. An important argument is that when $f(\mathbb{T}) = \mathbb{T}$ we recover the well-known conservation

equation of TEGR. However, in the pure tetrad formalism, $f(\mathbb{T})$ gravity exhibits violation of the local Lorentz invariance.

Further, we have discussed wormhole configuration in TEGR and $f(\mathbb{T})$ context. In particular, wormhole physics possess a peculiar property, namely *exotic matter*, involving a stress-energy tensor that violates the null energy condition. We have developed the wormhole solution under the assumption of spherical symmetry and the existence of a conformal symmetries. Since, we know that if a spacetime admits conformal symmetry then there exists a conformal killing vector field in the spacetime, which reduces the number unknown quantities also. We have studied various type of solutions with the exotic matter restricted at the throat neighborhood applying the cut-and-paste approach of the stress-energy tensor at a junction interface. This approach is motivated for finding asymptotically flat geometries.

For this purpose, we explore wormhole solutions in TEGR gravity, and shows that stress-energy tensor violates the null energy condition (see Eq. (9.35)) to maintain the flaring out condition. Furthermore, we also consider phantom energy EoS, which violates the null energy condition. In this manner, in TEGR, exact solution was found for the case of $\omega \neq -1, -3$, and the interval $-3 < \omega < -1$. An interesting feature of the phantom regime is that $\rho > 0$ throughout the spacetime. More specifically, for the case of phantom wormholes, it was found that infinitesimal amounts of phantom energy may support traversable wormholes. By carefully constructing specific and different shape functions, we have analysed the wormhole geometries and discussed some of the properties of the resulting spacetime.

In the second part of this article, is based on the power-law of $f(\mathbb{T})$ model. Considering the field equations with a diagonal tetrad and the anisotropic fluid matter distribution, a plethora of asymptotically flat exact solutions were found for different shape functions. This analysis shows that NEC is identically zero at the throat r_0 i.e. $(\rho + p_r)|_{r_0} = 0$ (see Eq. 9.40). However, the energy density is positive inside and outside the throat radius. One important property of the solutions is that the matter obeys the NEC at the throat, but outside the throat radius NEC is violated and goes upto to the radius $r \leq R$. This situation is quite different from TEGR solution, but not new in wormhole physics. Since, the redshift function is not finite when $r \rightarrow \infty$ due to the conformal symmetry. Therefore, one needs a cut-off of the stress-energy by matching the interior solution to an exterior vacuum spacetime, at a junction interface.

Thus, it is safe to conclude that for the choice of diagonal tetrad, we found sev-

eral solutions of wormhole geometries that violate the NEC at the throat and its neighbourhood in both TEGR and $f(\mathbb{T})$ gravity theories. However, the wormhole geometries in teleparallel gravity is more appealing than the $f(\mathbb{T})$ gravity.

Chapter 10

Summary and Future Scopes

10.1 Summary

The propose of this thesis to study about spherically symmetric astrophysical structure like compact stars, black holes, wormholes and Einstein cluster in general relativity as well as its extended gravity theories like $f(\mathcal{R}, \mathcal{T})$, $f(\mathbb{T})$, 4-D Einstein-Gauss-Bonnet and Energy Momentum Squared gravity. The overall picture of thesis is as given below:

In **Chapter 1**, we highlights the preliminary concepts of the general relativity and its observational verification. We have also included some physics of compact star, wormholes, Einstein cluster and theories of modified gravity.

Minimal geometric deformation technique has been adopted to decouple the Einstein field equations in **Chapter 2**. Further, we have presented an anisotropic compact star solution which was also analyzed via several physical constraints. We have also compared the $M - R$ curves with and without rotation (in Keplerian frequency $\Omega_K = \sqrt{GM_{NR}/R_{NR}^2}$). For the first time in an exact solution, we have also included the compression modulus K_e to analyze the stiffness of the equation of state.

We have presented a compact star model with exotic matters content using Tolman VII interior solution in **Chapter 3**. The chosen equation of is in the form $p_r = A\rho - B\rho^{1/n}$, where A and B are constants. For a proper choices of A, B and n, we can have Zeldovich's fluid, radiation, polytropic maatters, MIT bag model of quarks, dark energy, Chaplygin gas etc. An interesting fact about this equation of

state is the exotic matter contribution is minimum when the density is highest i.e. at the center of the compact star. Further, we have used to model few well-known compact stars i.e. PSR J1614+2230, 4U 1820-30, 4U 1608-52 and EXO 1785-248 by fitting in the $M - R$ curve. We have also estimated their possible moment of inertia by fitting in the $M - I$ curve using their observed masses. Finally, we come to concluded that the mass of the compact star increases if one increases the exotic matter contribution.

In **Chapter 4**, we have used the embedding class one technique via Karmarkar condition to explore new solutions. I have ansatz a g_{rr} metric potential and used the Karmarkar condition to determine the g_{tt} metric potential. Then the solution was tested with various physical conditions. Further, we generate the $M - R$ curves with and without rotation and the rotational frequency for different values of the parameter n. As a result, we get if n decreases from -2 to -5 the maximum mass increases, indicating that the stiffness of the EoS increases.

Chapter 5 also generalized Finch-Skea g_{rr} metric potential by adding a higher order correction term $b^{n-1}r^n$ with n as free parameter. The g_{tt} component of the metric tensor is then determined via the Karmarkar condition. The physical acceptability of the new solution is than tested through many physical constraints. Most importantly, we have generated the $M - R$ and $M - I$ curves by varying the n parameter from 7 to 12. It has been found that when n increases, the maximum mass of the compact star M_{max} increases indicating that the corresponding EoS increases its stiffness.

The stability of Einstein cluster in $f(\mathbb{T})$ gravity with zero net charge as well a small net charge $\approx 10^{-5}$ has been discussed in **Chapter 6**. We have used diagonal and off-diagonal tetrads and compare the results. Further, we have also chosen two functional forms of $f(\mathbb{T})$ as $a\mathbb{T}+b$ and $a\mathbb{T}^2$. Interestingly, we have found that Einstein cluster solution exists only for diagonal tetrad in both TEGR and $f(\mathbb{T}) = a\mathbb{T}^2$ gravity. The off-diagonal tetrad in both the $f(\mathbb{T})$ functions do yield solutions with vanishing radial pressure however, the transverse pressure either goes to negative or blows up at $r = 0$. The stability of the Einstein cluster is found to be enhanced when the net electric charge increase from 0 till 1.3×10^{-5} and 10^{-6}, however if the charge goes beyond this limit, it crosses the Buchdahl limit that will leads to a gravitational collapse.

Chapter 7 discussed compact star model in $f(\mathcal{R}, \mathcal{T})$ gravity with linear and

Starobinsky$-f(\mathcal{R}, \mathcal{T})$ function. Again, we employed embedding class one spacetime to present new solutions. The quadratic contribution $\mathcal{R}^2$ is scaled by the parameter ξ and the $\mathcal{T}$ contribution by χ. Hence, $\xi = 0 = \chi$ gives the general relativistic (GR) limit. The presented solutions are well-behaved in all aspect of physical conditions. Hence, we have fitting three well-knonw compact stars PSR J1614-2230, Vela X-1 and 4U 1820-30 in the $M - R$ and $M - I$ curves so that one can determines their radii and the moment of inertia. Finally, we have also compared are results with GR limits.

We considered color-flavor locked equation of state in energy-monetum-squared gravity to model quark stars in **Chapter 8**. We solved the modified TOV-equation via numerical technique using Mathematica. To generate the solution, we have employed boundary condition and generate the $M - R$ curve. We have considered different values of B, m_s, Δ and α to analyzed how the model changes. We found that when the bag constant, strange quark mass and EMSG parameter increases the stiffness of the CFL equation of state decreases leading to less M_{max}. However, when the color-superconducting gap increases the M_{max} increase due to the increase in stiffness. Finally, we have supported our results by fitting with the observational evidences found from the first neutron stars merger GW 170817.

In the last chaper (**Chapter 9**), we have again used the $f(\mathbb{T})-$gravity in diagonal and off-diagonal tetrads to model wormhole solutions admitting conformal motion. We first obtained an isotropic solution in linear $f(\mathbb{T})$ function, however the solution was not physically inspired as it violates the flared-our condition. Next we took linear EoS $p_r = \omega\rho$, an specific anisotropic form $p_r = np_r$ and different functional forms of the shape function $b(r)$ to generate the wormhole solutions. Further, we have also obtained two wormhole solutions in $f(\mathbb{T}) = a\mathbb{T}^2 + B$ gravity for two different $b(r)$ functions. All the solutions tested with flared-out condition, asymptotic flatness, energy conditions etc. We have also generated the embedded surface off all the wormholes with analytic and numerical methods. At the end, we have found that all the wormholes presented are supported by phantom field as the equation of state parameter $\omega < -1$.

10.2   Future Scopes

The minimal geometric deformation technique adopted in chapter two can be applied to complete geometric deformation where both the g_{tt} and g_{rr} metric functions are deformed. Also one can applied to other extended theories of gravity.

The exotic equation we have used in chapter three can be used in other modified gravity or one can also include some net electric charge in the stellar system.

The Karmarkar condition adopted in chapters four and five can also be used in any other four dimensional extended gravity and explore new solution. This is because the embedding class one approach is the simplest method and yet generally physically reliable.

We have seen for the first time that Einstein cluster mimicking compact star in $f(\mathbb{T})$ gravity discussed in chapter six, can be further investigate in any other extended gravity.

In chapter seven we have again used the Karmarkar condition in $f(\mathcal{R}, \mathcal{T})$ gravity. In future, one can also employ this method in other functional form the $f(\mathcal{R}, \mathcal{T})$ like exponential etc.

In chapter eight a color-flavor locked quark star model has been presented in energy-momentum squared gravity. As a future scope, one can use the same equation of state in other modified gravity and see how the quark star behaves under several parameters.

We have used the conformal Killing symmetry in $f(\mathbb{T})$ gravity to generate physically inspired wormhole solution in chapter nine. The same method can be extended to other modified gravity theories.

References

Abbas, G., Kanwal, A., and Zubair, M. (2015a). Anisotropic compact stars in $f(\mathbb{T})$ gravity. *Astrophysics and Space Science*, 357(2), 109.

Abbas, G., Qaisar, S., Javed, W., and Meraj, M. (2018). Compact stars of emending class one in $f(\mathbb{T})$ gravity. *Iranian Journal of Science and Technology, Transactions A: Science*, 42(3), 1659–1668.

Abbas, G., Qaisar, S., and Jawad, A. (2015b). Strange stars in $f(\mathbb{T})$ gravity with MIT bag model. *Astrophysics and Space Science*, 359(2), 57.

Abbas, G., Qaisar, S., and Jawad, A. (2015c). Strange stars in $f(\mathbb{T})$ gravity with MIT bag model. *Astrophysics and Space Science*, 359(2), 156.

Abbott, B.P., Abbott, R., Abbott, T., Acernese, F., Ackley, K., Adams, C., Adams, T., Addesso, P., Adhikari, R., Adya, V.B., et al. (2017). GW170817: observation of gravitational waves from a binary neutron star inspiral. *Physical Review Letters*, 119(16), 161101.

Abdalla, M.C.B., Nojiri, S., and Odintsov, S.D. (2005). Consistent modified gravity: dark energy, acceleration and the absence of cosmic doomsday. *Classical and Quantum Gravity*, 22(5), L35.

Abreu, H., Hernandez, H., and Nunez, L. (2007). Sound speeds, cracking and the stability of self-gravitating anisotropic compact objects. *Classical and Quantum Gravity*, 24(18), 4631.

Adler, R.J. (1974). A fluid sphere in general relativity. *Journal of Mathematical Physics*, 15(6), 727–729.

Aguilar, M., Alberti, G., Alpat, B., Alvino, A., Ambrosi, G., Andeen, K., Anderhub, H., Arruda, L., Azzarello, P., Bachlechner, A., et al. (2013). First result from the

Alpha Magnetic Spectrometer on the International Space Station: precision measurement of the positron fraction in primary cosmic rays of 0.5–350 GeV. *Physical Review Letters*, 110(14), 141102.

Akarsu, Ö., Barrow, J.D., Çıkıntoğlu, S., Ekşi, K.Y., and Katırcı, N. (2018a). Constraint on energy-momentum squared gravity from neutron stars and its cosmological implications. *Physical Review D*, 97(12), 124017.

Akarsu, Ö., Katırcı, N., and Kumar, S. (2017). Energy-momentum powered gravity and cosmic acceleration. *Elementary Particle Physics and Gravity*, 105.

Akarsu, Ö., Katırcı, N., and Kumar, S. (2018b). Cosmic acceleration in a dust only universe via energy-momentum powered gravity. *Physical Review D*, 97(2), 024011.

Akbar, M. and Cai, R.G. (2007). Thermodynamic behavior of field equations for $f(\mathcal{R})$ gravity. *Physics Letters B*, 648(2-3), 243–248.

Akbar, M. (2017). Embedding flrw geometries in pseudo-Euclidean and anti–de Sitter spaces. *Physical Review D*, 95(6), 064058.

Alcock, C., Farhi, E., and Olinto, A. (1986). Strange stars. *The Astrophysical Journal*, 310, 261–272.

Alford, M. (2004). Dense quark matter in nature. *Progress of Theoretical Physics Supplement*, 153, 1–14.

Alford, M. and Rajagopal, K. (2002). Absence of two-flavor color-superconductivity in compact stars. *Journal of High Energy Physics*, 2002(06), 031.

Alford, M., Rajagopal, K., Reddy, S., and Wilczek, F. (2001). Minimal color-flavor-locked–nuclear interface. *Physical Review D*, 64(7), 074017.

Alford, M. and Reddy, S. (2003). Compact stars with color superconducting quark matter. *Physical Review D*, 67(7), 074024.

Alford, M.G., Schmitt, A., Rajagopal, K., and Schäfer, T. (2008). Color superconductivity in dense quark matter. *Reviews of Modern Physics*, 80(4), 1455.

Alford, W. and Spicer, B. (2002). Nucleon charge-exchange reactions at intermediate energy. In *Advances in Nuclear Physics*, 1–82. Springer.

References

Alvarenga, F., Houndjo, M., Monwanou, A., and Orou, J. (2013). Testing some $f(\mathcal{R}, \mathcal{T})$ gravity models from energy conditions. *Journal of Modern Physics*, 4(1), 130–139.

Anderson, L., Aubourg, E., Bailey, S., Bizyaev, D., Blanton, M., Bolton, A.S., Brinkmann, J., Brownstein, J.R., Burden, A., Cuesta, A.J., et al. (2012). The clustering of galaxies in the SDSS-III Baryon Oscillation Spectroscopic Survey: baryon acoustic oscillations in the data release 9 spectroscopic galaxy sample. *Monthly Notices of the Royal Astronomical Society*, 427(4), 3435–3467.

Andréasson, H. and Böhmer, C.G. (2009). Bounds on M/R for static objects with a positive cosmological constant. *Classical and Quantum Gravity*, 26(19), 195007.

Anisimov, A., Babichev, E., and Vikman, A. (2005). $b-$inflation. *Journal of Cosmology and Astroparticle Physics*, 2005(06), 006.

Antoniadis, J., Freire, P.C., Wex, N., Tauris, T.M., Lynch, R.S., Van Kerkwijk, M.H., Kramer, M., Bassa, C., Dhillon, V.S., Driebe, T., et al. (2013). A massive pulsar in a compact relativistic binary. *Science*, 340(6131), 1233232.

Arapoğlu, S., Deliduman, C., and Ekşi, K.Y. (2011). Constraints on perturbative $f(\mathcal{R})$ gravity via neutron stars. *Journal of Cosmology and Astroparticle Physics*, 2011(07), 020.

Arellano, A.V. and Lobo, F.S. (2006). Non-existence of static, spherically symmetric and stationary, axisymmetric traversable wormholes coupled to nonlinear electrodynamics. *Classical and Quantum Gravity*, 23(24), 7229.

Armendariz-Picon, C., Mukhanov, V., and Steinhardt, P.J. (2000). Dynamical solution to the problem of a small cosmological constant and late-time cosmic acceleration. *Physical Review Letters*, 85(21), 4438.

Armendariz-Picon, C., Mukhanov, V., and Steinhardt, P.J. (2001). Essentials of $k-$essence. *Physical Review D*, 63(10), 103510.

Astashenok, A.V., Capozziello, S., and Odintsov, S.D. (2013). Further stable neutron star models from $f(\mathcal{R})$ gravity. *Journal of Cosmology and Astroparticle Physics*, 2013(12), 040.

Astashenok, A.V., Capozziello, S., and Odintsov, S.D. (2014). Maximal neutron star mass and the resolution of the hyperon puzzle in modified gravity. *Physical Review D*, 89(10), 103509.

Astashenok, A.V., Capozziello, S., and Odintsov, S.D. (2015). Magnetic neutron stars in $f(\mathcal{R})$ gravity. *Astrophysics and Space Science*, 355(2), 333–341.

Baffou, E., Kpadonou, A., Rodrigues, M., Houndjo, M., and Tossa, J. (2015). Cosmological viable $f(\mathcal{R}, \mathcal{T})$ dark energy model: dynamics and stability. *Astrophysics and Space Science*, 356(1), 173–180.

Bahamonde, S., Böhmer, C.G., and Wright, M. (2015). Modified teleparallel theories of gravity. *Physical Review D*, 92(10), 104042.

Bahamonde, S., Marciu, M., and Rudra, P. (2019). Dynamical system analysis of generalized energy-momentum-squared gravity. *Physical Review D*, 100(8), 083511.

Bahamonde, S. and Wright, M. (2015). Teleparallel quintessence with a nonminimal coupling to a boundary term. *Physical Review D*, 92(8), 084034.

Bahamonde, S. and Wright, M. (2016). Erratum: Teleparallel quintessence with a nonminimal coupling to a boundary term [phys. rev. d 92, 084034 (2015)]. *Physical Review D*, 93(10), 109901.

Bahcall, N.A., Ostriker, J.P., Perlmutter, S., and Steinhardt, P.J. (1999). The cosmic triangle: Revealing the state of the universe. *Science*, 284(5419), 1481–1488.

Bamba, K., Capozziello, S., Nojiri, S., and Odintsov, S.D. (2012). Dark energy cosmology: the equivalent description via different theoretical models and cosmography tests. *Astrophysics and Space Science*, 342(1), 155–228.

Bamba, K., Nojiri, S., and Odintsov, S.D. (2014). Trace-anomaly driven inflation in $f(\mathbb{T})$ gravity and in minimal massive bigravity. *Physics Letters B*, 731, 257–264.

Bamba, K., Odintsov, S.D., and Saridakis, E.N. (2017). Inflationary cosmology in unimodular $f(\mathbb{T})$ gravity. *Modern Physics Letters A*, 32(21), 1750114.

Banerjee, A. and Som, M. (1981). Einstein cluster of charged particles. *Progress of Theoretical Physics*, 65(4), 1281–1289.

References

Banerjee, A., Bandyopadhyay, T., and Chakraborty, S. (2007). Emergent universe in brane world scenario. *arXiv preprint arXiv:0705.3933*.

Banerjee, A. and Singh, K.N. (2021). Color-flavor locked strange stars in 4D Einstein-Gauss-Bonnet gravity. *Physics of the Dark Universe*, 31, 100792.

Banerjee, A., Singh, K.N., Jasim, M., and Rahaman, F. (2020). Conformally symmetric traversable wormholes in $f(\mathcal{R}, \mathcal{T})$ gravity. *Annals of Physics*, 422, 168295.

Banik, S. and Bandyopadhyay, D. (2003). Color superconducting quark matter core in the third family of compact stars. *Physical Review D*, 67(12), 123003.

Barbar, A.H., Awad, A.M., and Al Fiky, M.T. (2020). Viability of bouncing cosmology in energy-momentum-squared gravity. *Physical Review D*, 101(4), 044058.

Barnes, A. (1974). Space times of embedding class one in general relativity. *General Relativity and Gravitation*, 5(2), 147–162.

Barnes, A. (2011). Vacuum spacetimes of embedding class two. In *Journal of Physics: Conference Series*, volume 314, 012091. IOP Publishing.

Barreto, W. and Rojas, S. (1992). An equation of state for radiating dissipative spheres in general relativity. *Astrophysics and space science*, 193(2), 201–215.

Bauswein, A., Just, O., Janka, H.T., and Stergioulas, N. (2017). Neutron-star radius constraints from GW170817 and future detections. *The Astrophysical Journal Letters*, 850, L34.

Baym, G., Pethick, C., and Pines, D. (1969). Superfluidity in neutron stars. *Nature*, 224, 673674.

Bedran, M. and Som, M. (1982). Conformally flat solution of a static dust sphere in Einstein-Cartan theory. *Journal of Physics A: Mathematical and General*, 15(11), 3539.

Bejarano, C., Ferraro, R., Fiorini, F., and Guzmán, M.J. (2019). Reflections on the covariance of modified teleparallel theories of gravity. *Universe*, 5(6), 158.

Bejger, M., Bulik, T., and Haensel, P. (2005). Constraints on the dense matter equation of state from the measurements of PSR J0737-3039A moment of inertia

and PSR J0751+1807 mass. *Monthly Notices of the Royal Astronomical Society*, 364(2), 635–639.

Bejger, M. and Haensel, P. (2002). Moments of inertia for neutron and strange stars: Limits derived for the crab pulsar. *Astronomy & Astrophysics*, 396(3), 917–921.

Bennett, C.L., Halpern, M., Hinshaw, G., Jarosik, N., Kogut, A., Limon, M., Meyer, S.S., Page, L., Spergel, D.N., Tucker, G.S., Wollack, E., Wright, E.L., Barnes, C., Greason, M.R., Hill, R.S., Komatsu, E., Nolta, M.R., Odegard, N., Peiris, H.V., Verde, L., and Weiland, J.L. (2003). First-Year Wilkinson Microwave Anisotropy Probe (WMAP) Observations: Preliminary Maps and Basic Results. *The Astrophysical Journal Supplement Series*, 148(1), 1–27.

Bennett, C.L., Larson, D., Weiland, J.L., Jarosik, N., Hinshaw, G., Odegard, N., Smith, K., Hill, R., Gold, B., Halpern, M., et al. (2013). Nine-year Wilkinson Microwave Anisotropy Probe (WMAP) Observations: Final Maps and Results. *The Astrophysical Journal Supplement Series*, 208(2), 20.

Bergliaffa, S.P. (2006). Constraining $f(\mathcal{R})$ theories with the energy conditions. *Physics Letters B*, 642(4), 311–314.

Bertolami, O., Boehmer, C.G., Harko, T., and Lobo, F.S. (2007). Extra force in $f(\mathcal{R})$ modified theories of gravity. *Physical Review D*, 75(10), 104016.

Beutler, F., Blake, C., Colless, M., Jones, D.H., Staveley-Smith, L., Campbell, L., Parker, Q., Saunders, W., and Watson, F. (2011). The 6dF galaxy survey: baryon acoustic oscillations and the local hubble constant. *Monthly Notices of the Royal Astronomical Society*, 416(4), 3017–3032.

Bhaduri, R.K. (1988). Models of the nucleon - from quarks to soliton. *Addison Wesley Publishing*.

Bhar, P., Maurya, S., Gupta, Y., and Manna, T. (2016a). Modelling of anisotropic compact stars of embedding class one. *The European Physical Journal A*, 52(10), 1–10.

Bhar, P., Rahaman, F., Manna, T., and Banerjee, A. (2016b). Wormhole supported by dark energy admitting conformal motion. *The European Physical Journal C*, 76(12), 1–9.

References

Bhar, P., Singh, K.N., Rahaman, F., Pant, N., and Banerjee, S. (2017). A charged anisotropic well-behaved Adler-Finch-Skea solution satisfying karmarkar condition. *International Journal of Modern Physics D*, 26(08), 1750078.

Bhatti, M., Yousaf, Z., and Ilyas, M. (2017). Evolution of compact stars and dark dynamical variables. *The European Physical Journal C*, 77(10), 1–9.

Bhawal, B. and Kar, S. (1992). Lorentzian wormholes in Einstein-Gauss-Bonnet theory. *Physical Review D*, 46(6), 2464.

Binétruy, P. (2013). Dark energy and fundamental physics. *The Astronomy and Astrophysics Review*, 21(1), 67.

Boehmer, C. and Harko, T. (2007). On Einstein clusters as galactic dark matter haloes. *Monthly Notices of the Royal Astronomical Society*, 379(1), 393–398.

Boehmer, C.G., Harko, T., and Lobo, F.S. (2012). Wormhole geometries in modified teleparallel gravity and the energy conditions. *Physical Review D*, 85(4), 044033.

Boehmer, C.G., Mussa, A., and Tamanini, N. (2011). Existence of relativistic stars in $f(\mathbb{T})$ gravity. *Classical and Quantum Gravity*, 28(24), 245020.

Böhmer, C. and Harko, T. (2006). Bounds on the basic physical parameters for anisotropic compact general relativistic objects. *Classical and Quantum Gravity*, 23(22), 6479.

Böhmer, C.G., Harko, T., and Lobo, F.S. (2008). Wormhole geometries with conformal motions. *Classical and Quantum Gravity*, 25(7), 075016.

Bondi, H. (1964). The contraction of gravitating spheres. *Proceedings of the Royal Society of London. Series A. Mathematical and Physical Sciences*, 281(1384), 39–48.

Bowers, R.L. and Liang, E. (1974). Anisotropic spheres in general relativity. *The Astrophysical Journal*, 188, 657.

Brill, D.R. and Hartle, J.B. (1964). Method of the self-consistent field in general relativity and its application to the gravitational geon. *Physical Review*, 135(1B), B271.

Brill, D.R. and Wheeler, J.A. (1957). Interaction of neutrinos and gravitational fields. *Reviews of Modern Physics*, 29(3), 465.

Buchdahl, H. (1967). General-relativistic fluid spheres. III. a static gaseous model. *The Astrophysical Journal*, 147, 310.

Buchdahl, H.A. (1959). General relativistic fluid spheres. *Physical Review*, 116(4), 1027.

Burgess, C. (2015). The cosmological constant problem: Why it's hard to get dark energy from micro-physics. *100e Ecole dEte de Physique: Post-Planck Cosmology*, 149–197.

Burstin, C. (1931). A contribution to the problem of embedding Riemannian spaces in Euclidean spaces. , 38(3-4), 74–85.

Cai, Y.F., Capozziello, S., De Laurentis, M., and Saridakis, E.N. (2016). $f(\mathbb{T})$ teleparallel gravity and cosmology. *Reports on Progress in Physics*, 79(10), 106901.

Caldwell, R.R. (2002). A phantom menace? Cosmological consequences of a dark energy component with super-negative equation of state. *Physics Letters B*, 545(1-2), 23–29.

Campbell, J.E. (1926). *A course of differential geometry.* Oxford Claredon.

Capano, C.D., Tews, I., and Brown, Stephanie, M.e. (2020). Stringent constraints on neutron-star radii from multimessenger observations and nuclear theory. *Nature Astronomy*, 4, 625–632.

Capozziello, S. (2002). Curvature quintessence. *International Journal of Modern Physics D*, 11(04), 483–491.

Capozziello, S., Luongo, O., Pincak, R., and Ravanpak, A. (2018a). Cosmic acceleration in non-flat $f(\mathbb{T})$ cosmology. *General Relativity and Gravitation*, 50(5), 1–21.

Capozziello, S., Nojiri, S., and Odintsov, S.D. (2018b). The role of energy conditions in $f(\mathcal{R})$ cosmology. *Physics Letters B*, 781, 99–106.

Carroll, S.M., Duvvuri, V., Trodden, M., and Turner, M.S. (2004). Is cosmic speed-up due to new gravitational physics? *Physical Review D*, 70(4), 043528.

References

Cartan, E. (1927). Sur la possibilité de plonger un espace riemannien donné dans un espace euclidien. *Ann. Soc. Polon. Math.*, 6, 1–7.

Casadio, R., Ovalle, J., and Da Rocha, R. (2015). The minimal geometric deformation approach extended. *Classical and Quantum Gravity*, 32(21), 215020.

Chaisi, M. and Maharaj, S. (2005). Compact anisotropic spheres with prescribed energy density. *General relativity and gravitation*, 37(7), 1177–1189.

Chan, R., Herrera, L., and Santos, N. (1993). Dynamical instability for radiating anisotropic collapse. *Monthly Notices of the Royal Astronomical Society*, 265(3), 533–544.

Chanda, A., Dey, S., and Paul, B. (2019). Anisotropic compact objects in $f(\mathbb{T})$ gravity with Finch–Skea geometry. *The European Physical Journal C*, 79(6), 1–12.

Chandrasekhar, S. (1931). The maximum mass of ideal white dwarfs. *The Astrophysical Journal*, 74, 81–82.

Chandrasekhar, S. (1964). Dynamical instability of gaseous masses approaching the schwarzschild limit in general relativity. *Physical Review Letters*, 12(4), 114.

Chen, C.Y. and Chen, P. (2020). Eikonal black hole ringings in generalized energy-momentum squared gravity. *Physical Review D*, 101(6), 064021.

Chen, S.H., Dent, J.B., Dutta, S., and Saridakis, E.N. (2011). Cosmological perturbations in $f(\mathbb{T})$ gravity. *Physical Review D*, 83(2), 023508.

Chen, X., Gong, Y., and Saridakis, E.N. (2009). Phase-space analysis of interacting phantom cosmology. *Journal of Cosmology and Astroparticle Physics*, 2009(04), 001.

Cheng, K. and Harko, T. (2000). Approximate mass and radius formulas for static and rotating strange stars. *Physical Review D*, 62(8), 083001.

Chiba, T., Okabe, T., and Yamaguchi, M. (2000). Kinetically driven quintessence. *Physical Review D*, 62(2), 023511.

Chodos, A., Jaffe, R., Johnson, K., Thorn, C.B., and Weisskopf, V. (1974). New extended model of hadrons. *Physical Review D*, 9(12), 3471.

Chu, P.C., Zhou, Y., Qi, X., Li, X.H., Zhang, Z., and Zhou, Y. (2019). Isospin properties in quark matter and quark stars within isospin-dependent quark mass models. *Physical Review C*, 99(3), 035802.

Cocco, V. and Ruffini, R. (1997). On metastable Einstein's clusters. *Nuovo Cimento B Serie*, 112(2), 271–287.

Cognola, G., Elizalde, E., Nojiri, S., Odintsov, S.D., and Zerbini, S. (2005). One-loop $f(\mathcal{R})$ gravity in de sitter universe. *Journal of Cosmology and Astroparticle Physics*, 2005(02), 010.

Cole, S., Percival, W.J., Peacock, J.A., Norberg, P., Baugh, C.M., Frenk, C.S., Baldry, I., Bland-Hawthorn, J., Bridges, T., Cannon, R., et al. (2005). The 2dF galaxy redshift survey: power-spectrum analysis of the final data set and cosmological implications. *Monthly Notices of the Royal Astronomical Society*, 362(2), 505–534.

Collaboration, A. (2013). Silicon Detector Dark Matter Results from the Final Exposure of CDMS II. *Physical Review Letters*, 111, 251301.

Collaboration, L.S. and Collaboration, V. (2016). Observation of gravitational waves from a binary black hole merger. *Physical Review Letters*, 116, 061102.

Collaboration, L.S. and Collaboration, V. (2017). Multi-messenger observations of a binary neutron star merger. *The Astrophysical Journal Letters*, 848, L12.

Collaboration, P. (2014). Planck 2013 results. I. Overview of products and scientific results. *Atronomy and Astrophysics*, 571, A1.

Collaboration, T.E.H.T. (2019). First M87 event horizon telescope results. I. the shadow of the supermassive black hole. *The Astrophysical Journal Letters*,, 875, L1.

Collins, J.C. and Perry, M.J. (1975). Superdense matter: neutrons or asymptotically free quarks? *Physical Review Letters*, 34(21), 1353.

Comer, G. and Katz, J. (1993). Thick einstein shells and their mechanical stability. *Classical and Quantum Gravity*, 10(9), 1751.

Comer, G., Langlois, D., and Peter, P. (1993). A brief comment on thick Einstein shells. *Classical and Quantum Gravity*, 10(9), L127.

References

Contreras, E. (2018). Minimal geometric deformation: the inverse problem. *The European Physical Journal C*, 78(8), 678.

Contreras, E. (2019). Gravitational decoupling in $2+1$ dimensional space-times with cosmological term. *Classical and Quantum Gravity*, 36(9), 095004.

Contreras, E. and Bargueño, P. (2018). Minimal geometric deformation decoupling in $2+1$ dimensional space–times. *The European Physical Journal C*, 78(7), 558.

Contreras, E., Rincón, Á., and Bargueño, P. (2019). A general interior anisotropic solution for a BTZ vacuum in the context of the minimal geometric deformation decoupling approach. *The European Physical Journal C*, 79(3), 216.

Cooney, A., DeDeo, S., and Psaltis, D. (2010). Neutron stars in $f(\mathcal{R})$ gravity with perturbative constraints. *Physical Review D*, 82(6), 064033.

Cosenza, M., Herrera, L., Esculpi, M., and Witten, L. (1981). Some models of anisotropic spheres in general relativity. *Journal of Mathematical Physics*, 22(1), 118–125.

Cottam, J., Paerels, F., and Mendez, M. (2002). Gravitationally redshifted absorption lines in the X-ray burst spectra of a neutron star. *Nature*, 420(6911), 51–54.

Cromartie, H.T., Fonseca, E., Ransom, S.M., Demorest, P.B., Arzoumanian, Z., Blumer, H., Brook, P.R., DeCesar, M.E., Dolch, T., Ellis, J.A., et al. (2020a). Relativistic Shapiro delay measurements of an extremely massive millisecond pulsar. *Nature Astronomy*, 4(1), 72–76.

Cromartie, H., Fonseca, E., and Ransom, S.e. (2020b). Relativistic shapiro delay measurements of an extremely massive millisecond pulsar. *Nature Astronomy*, 4, 7276.

Dai, D.C., Lue, A., Starkman, G., and Stojkovic, D. (2010). Electroweak stars: How nature may capitalize on the standard model's ultimate fuel. *Journal of Cosmology and Astroparticle Physics*, 2010(12), 004.

Darmois, G. (1927). Mémorial des sciences mathématiques. *Fascicule XXV (Gauthier-Villars, Paris, 1927)*.

Das, A., Rahaman, F., Guha, B., and Ray, S. (2015). Relativistic compact stars in $f(\mathbb{T})$ gravity admitting conformal motion. *Astrophysics and Space Science*, 358(2), 36.

de Andrade, V.C., Guillen, L.C.T., and Pereira, J.G. (2000). Teleparallel Gravity: An Overview. *arXiv:gr-qc/0011087v1*.

De Felice, A. and Tsujikawa, S. (2010). $f(\mathcal{R})$ theories. *Living Reviews in Relativity*, 13(1), 1–161.

de Felice, F., Siming, L., and Yunqiang, Y. (1999). Relativistic charged spheres: II. regularity and stability. *Classical and Quantum Gravity*, 16(8), 2669.

De la Cruz-Dombriz, A. and Dobado, A. (2006). $f(\mathcal{R})$ gravity without a cosmological constant. *Physical Review D*, 74(8), 087501.

de la Cruz-Dombriz, Á., Dunsby, P.K., Luongo, O., and Reverberi, L. (2016). Model-independent limits and constraints on extended theories of gravity from cosmic reconstruction techniques. *Journal of Cosmology and Astroparticle Physics*, 2016(12), 042.

de la Fuente, M.M. (2009). Análisis comparativo de algunos modelos analíticos para estrellas de quarks. 27, 125–133.

de Leon, J.P. (2015). Embeddings for general relativity. *Classical and Quantum Gravity*, 32(19), 195018.

Deb, D., Chowdhury, S.R., Ray, S., Rahaman, F., and Guha, B. (2017). Relativistic model for anisotropic strange stars. *Annals of Physics*, 387, 239–252.

Deb, D., Khlopov, M., Rahaman, F., Ray, S., and Guha, B. (2018). Anisotropic strange stars in the Einstein–Maxwell spacetime. *The European Physical Journal C*, 78(6), 465.

DeBenedictis, A. and Horvat, D. (2012). On wormhole throats in $f(\mathcal{R})$ gravity theory. *General Relativity and Gravitation*, 44(11), 2711–2744.

Dehghani, M. and Dayyani, Z. (2009). Lorentzian wormholes in Lovelock gravity. *Physical Review D*, 79(6), 064010.

References

Delgaty, M. and Lake, K. (1998). Physical acceptability of isolated, static, spherically symmetric, perfect fluid solutions of einstein's equations. *Computer Physics Communications*, 115(2-3), 395–415.

Deliduman, C. and Yapiskan, B. (2011). Absence of relativistic stars in $f(\mathbb{T})$ gravity. *arXiv preprint arXiv:1103.2225*.

Demorest, P.B., Pennucci, T., Ransom, S., Roberts, M., and Hessels, J. (2010). A two-solar-mass neutron star measured using shapiro delay. *Nature*, 467(7319), 1081–1083.

Dent, J.B., Dutta, S., and Saridakis, E.N. (2011). $f(\mathbb{T})$ gravity mimicking dynamical dark energy. background and perturbation analysis. *Journal of Cosmology and Astroparticle Physics*, 2011(01), 009.

Dev, K. and Gleiser, M. (2002). Anisotropic stars: exact solutions. *General relativity and gravitation*, 34(11), 1793–1818.

Dev, K. and Gleiser, M. (2003). Anisotropic stars II: stability. *General relativity and gravitation*, 35(8), 1435–1457.

Drake, J.J., Marshall, H.L., Dreizler, S., Freeman, P.E., Fruscione, A., Juda, M., Kashyap, V., Nicastro, F., Pease, D.O., Wargelin, B.J., et al. (2002). Is RX J1856.5–3754 a quark star? *The Astrophysical Journal*, 572(2), 996.

Duorah, H. and Ray, R. (1987). An analytical stellar model. *Classical and Quantum Gravity*, 4(6), 1691.

Easson, I. and Pethick, C. (1977). Stress tensor of cosmic and laboratory type-II superconductors. *Physical Review D*, 16(2), 275.

Einstein, A. (1907). On the relativity principle and the conclusions drawn from it. *Jahr. Radioaktivititat Elektron*, 4, 411–462.

Einstein, A. (1915a). —. *Sitzungsberichte der K´oniglich Preuischen Akademie der Wissenschaften (Berlin)*, 1915, 3115.

Einstein, A. (1915b). Explanation of the perihelion motion of mercury from the general theory of relativity. *Sitzungsberichte der K´oniglich Preuischen Akademie der Wissenschaften (Berlin)*, 1915, 831–839.

Einstein, A. (1915c). The field equations of gravitation. *Sitzungsberichte der K$^{'}$oniglich Preuischen Akademie der Wissenschaften (Berlin)*, 1915, 844–847.

Einstein, A. (1915d). Zur Allgemeinen Relativit$^{'}$atstheorie. *Sitzungsberichte der K$^{'}$oniglich Preuischen Akademie der Wissenschaften (Berlin)*, 1915, 778–786.

Einstein, A. (1928). Riemannian geometry with maintaining the notion of distant parallelism. *Session Report of the Prussian Academy of Sciences*, 217–221.

Einstein, A. (1930). A unified field theory based on the Riemannian metric and distant parallelism. *Mathematische Annalen*, 102, 685–697.

Einstein, A. (1939). On a stationary system with spherical symmetry consisting of many gravitating masses. *Annals of Mathematics*, 922–936.

Einstein, A. and Rosen, N. (1935). The particle problem in the general theory of relativity. *Physical Review*, 48(1), 73.

Eisenhart, L.P. (1966). *Riemannian geometry*. Princeton university press.

Eisenstein, D.J., Zehavi, I., Hogg, D.W., Scoccimarro, R., Blanton, M.R., Nichol, R.C., Scranton, R., Seo, H.J., Tegmark, M., Zheng, Z., et al. (2005). Detection of the baryon acoustic peak in the large-scale correlation function of sdss luminous red galaxies. *The Astrophysical Journal*, 633(2), 560.

Elizalde, E. and Khurshudyan, M. (2018). Wormhole formation in $f(\mathcal{R}, \mathcal{T})$ gravity: Varying Chaplygin gas and barotropic fluid. *Physical Review D*, 98(12), 123525.

Elizalde, E. and Khurshudyan, M. (2019). Wormholes with $\rho(\mathcal{R}, \mathcal{R})$ matter in $f(\mathcal{R}, \mathcal{T})$ gravity. *Physical Review D*, 99(2), 024051.

Elizalde, E., Nojiri, S., and Odintsov, S.D. (2004). Late-time cosmology in a (phantom) scalar-tensor theory: dark energy and the cosmic speed-up. *Physical Review D*, 70(4), 043539.

Ellis, G.F., Murugan, J., and Tsagas, C.G. (2003). The emergent universe: an explicit construction. *Classical and Quantum Gravity*, 21(1), 233.

Errehymy, A. and Daoud, M. (2020). Studies an analytic model of a spherically symmetric compact object in Einsteinian gravity. *The European Physical Journal C*, 80(3), 1–12.

References

Errehymy, A., Daoud, M., and Sayouty, E.H. (2019). A spherically symmetric model of anisotropic fluid for strange quark spheres. *The European Physical Journal C*, 79(4), 346.

Esculpi, M. and Aloma, E. (2010). Conformal anisotropic relativistic charged fluid spheres with a linear equation of state. *The European Physical Journal C*, 67(3), 521–532.

Esculpi, M. and Herrera, L. (1986). Conformally symmetric radiating spheres in general relativity. *Journal of mathematical physics*, 27(8), 2087–2096.

Estrada, M. and Prado, R. (2019). The gravitational decoupling method: the higher-dimensional case to find new analytic solutions. *The European Physical Journal Plus*, 134(4), 168.

Faraji, M., Rashidi, N., and Nozari, K. (2021). Inflation in energy-momentum squared gravity in light of Planck 2018. *arXiv:2107.13547v1 [gr-qc]*.

Farhi, E. and Jaffe, R.L. (1984). Strange matter. *Physical Review D*, 30(11), 2379.

Faria, M., Martins, C., Chiti, F., and Silva, B. (2019). Low redshift constraints on energy-momentum-powered gravity models. *Astronomy & Astrophysics*, 625, A127.

Ferraro, R. and Fiorini, F. (2007). Modified teleparallel gravity: inflation without an inflaton. *Physical Review D*, 75, 084031.

Ferraro, R. and Fiorini, F. (2008). Born-infeld gravity in Weitzenböck spacetime. *Physical Review D*, 78(12), 124019.

Finch, M.R. and Skea, J.E. (1989). A realistic stellar model based on an ansatz of Duorah and Ray. *Classical and Quantum Gravity*, 6(4), 467.

Fiorini, F. and Ferraro, R. (2009). A type of Born-Infeld regular gravity and its cosmological consequences. *International Journal of Modern Physics A*, 24, 1686–1689.

Flamm, L. (1916). Beitŕage zur einsteinschen gravitationstheorie. *Phys. Z.*, 17, 448.

Flores, C.V. and Lugones, G. (2010). Radial oscillations of color superconducting self-bound quark stars. *Physical Review D*, 82(6), 063006.

Flores, C.V. and Lugones, G. (2017). Constraining color flavor locked strange stars in the gravitational wave era. *Physical Review C*, 95(2), 025808.

Florides, P.S. (1974). A new interior Schwarzschild solution. *Proceedings of the Royal Society of London. A. Mathematical and Physical Sciences*, 337(1611), 529–535.

Folomeev, V. and Dzhunushaliev, V. (2015). Magnetic fields in anisotropic relativistic stars. *Physical Review D*, 91(4), 044040.

Friedman, A. (1922). Über die krümmung des raumes. *Zeitschrift für Physik*, 10(1), 377–386.

Frieman, J.A., Turner, M.S., and Huterer, D. (2008). Dark energy and the accelerating universe. *Annu. Rev. Astron. Astrophys.*, 46, 385–432.

Fuller, R.W. and Wheeler, J.A. (1962). Causality and multiply connected space-time. *Physical Review*, 128(2), 919.

Gabbanelli, L., Ovalle, J., Sotomayor, A., Stuchlik, Z., and Casadio, R. (2019). A causal schwarzschild-de sitter interior solution by gravitational decoupling. *The European Physical Journal C*, 79(6), 486.

Gabbanelli, L., Rincón, A., and Rubio, C. (2018). Gravitational decoupled anisotropies in compact stars. *The European Physical Journal C*, 78, 370.

Gangopadhyay, T., Ray, S., Li, X.D., Dey, J., and Dey, M. (2013). Strange star equation of state fits the refined mass measurement of 12 pulsars and predicts their radii. *Monthly Notices of the Royal Astronomical Society*, 431(4), 3216–3221.

Ganguly, A., Gannouji, R., Goswami, R., and Ray, S. (2014). Neutron stars in the Starobinsky model. *Physical Review D*, 89(6), 064019.

Garcia, N.M. and Lobo, F.S. (2011). Nonminimal curvature–matter coupled wormholes with matter satisfying the null energy condition. *Classical and Quantum Gravity*, 28(8), 085018.

Geralico, A., Pompi, F., and Ruffini, R. (2012). On Einstein clusters. *International Journal of Modern Physics: Conference Series*, 12, 146–173.

Ghosh, P. (2007). *Rotation and accretion powered pulsars*, volume 7. World Scientific.

References

Gilhert, C. (1954). The stability of a spherically symmetric cluster of stars describing circular orbits. *Monthly Notices of the Royal Astronomical Society*, 114(6), 628–634.

Ginzburg, V.L. and Kirzhnits, D.A. (1964). On the superconductivity of neutron stars. *Zh. Teor. Eksper. Fiz.*, 47, 2006–2007.

Glendenning, N.K. (1982). The hyperon composition of neutron stars. *Physics Letters B*, 114, 392–396.

Glendenning, N.K. (1985). Neutron stars are giant hypernuclei? *The Astrophysical Journal*, 293, 470–493.

Glendenning, N.K. and Schaffner-Bielich, J. (1998). Kaon condensation and dynamical nucleons in neutron stars. *Physical Review Letters*, 81(21), 4564.

Gokhroo, M. and Mehra, A. (1994). Anisotropic spheres with variable energy density in general relativity. *General relativity and gravitation*, 26(1), 75–84.

Golovnev, A., Koivisto, T., and Sandstad, M. (2017). On the covariance of teleparallel gravity theories. *Classical and quantum gravity*, 34(14), 145013.

Goswami, R., Nzioki, A.M., Maharaj, S.D., and Ghosh, S.G. (2014). Collapsing spherical stars in $f(\mathcal{R})$ gravity. *Physical Review D*, 90(8), 084011.

Gupta, Y. and Goel, P. (1975). Class two analogue of TY Thomas's theorem and different types of embeddings of static spherically symmetric space-times. *General Relativity and Gravitation*, 6, 499.

Gupta, Y. and Maurya, S.K. (2011). A class of regular and well behaved charge analogue of Kuchowicz's relativistic super-dense star model. *Astrophysics and Space Science*, 332(2), 415–421.

Güver, T., Özel, F., Cabrera-Lavers, A., and Wroblewski, P. (2010a). The distance, mass, and radius of the neutron star in 4U 1608-52. *The Astrophysical Journal*, 712(2), 964.

Güver, T., Wroblewski, P., Camarota, L., and Özel, F. (2010b). The mass and radius of the neutron star in 4U 1820-30. *The Astrophysical Journal*, 719(2), 1807.

Haensel, P., Potekhin, A.Y., and Yakovlev, D. (2007). Neutron Stars 1: Equation of State and Structure. *Springer.*

Haensel, P., Salgado, M., and Bonazzola, S. (1995). Equation of state of dense matter and maximum rotation frequency of neutron stars. *Astronomy and Astrophysics*, 296, 745.

Harko, T. (2008). Modified gravity with arbitrary coupling between matter and geometry. *Physics Letters B*, 669(5), 376–379.

Harko, T., Lobo, F.S.N., and Nojiri, S.e.a. (2011). $f(\mathcal{R}, \mathcal{T})-$gravity. *Physical Review D*, 84, 024020.

Harrison, B.K., Thorne, K.S., Wakano, M., and Wheeler, J.A. (1965). *Gravitation theory and gravitational collapse.* University of Chicago.

Hartle, J.B. (1978). Bounds on the mass and moment of inertia of non-rotating neutron stars. *Physics Reports*, 46(6), 201–247.

Hartle, J., Sawyer, R., and Scalapino, D. (1975). Pion condensed matter at high densities-equation of state and stellar models. *The Astrophysical Journal*, 199, 471–481.

Hawkins, E., Maddox, S., Cole, S., Lahav, O., Madgwick, D.S., Norberg, P., Peacock, J.A., Baldry, I.K., Baugh, C.M., Bland-Hawthorn, J., et al. (2003). The 2dF galaxy redshift survey: correlation functions, peculiar velocities and the matter density of the universe. *Monthly Notices of the Royal Astronomical Society*, 346(1), 78–96.

Hayashi, K. (1977). The gauge theory of the translation group and underlying geometry. *Physics Letters B*, 69(4), 441–444.

Hayashi, K. and Shirafuji, T. (1979). New general relativity. *Physical Review D*, 19(12), 3524.

Hayashi, K. and Shirafuji, T. (1981). Addendum to "New general relativity". *Physical Review D*, 24(12), 3312.

Hehl, F.W., Von der Heyde, P., Kerlick, G.D., and Nester, J.M. (1976). General relativity with spin and torsion: Foundations and prospects. *Reviews of Modern Physics*, 48(3), 393.

References

Herrera, L. (1992). Cracking of self-gravitating compact objects. *Physics Letters A*, 165(3), 206–210.

Herrera, L. and de León, J.P. (1985). Isotropic and anisotropic charged spheres admitting a oneparameter group of conformal motions. *Journal of Mathematical Physics*, 26, 2302.

Herrera, L., Di Prisco, A., Martin, J., Ospino, J., Santos, N., and Troconis, O. (2004). Spherically symmetric dissipative anisotropic fluids: A general study. *Physical Review D*, 69(8), 084026.

Herrera, L., Jiménez, J., Leal, L., and de León, J.P. (1984). Anisotropic fluids and conformal motions in general relativity. *Journal of Mathematical Physics*, 25, 3274.

Herrera, L., Martin, J., and Ospino, J. (2002). Anisotropic geodesic fluid spheres in general relativity. *Journal of Mathematical Physics*, 43(10), 4889–4897.

Herrera, L., Ospino, J., and Di Prisco, A. (2008). All static spherically symmetric anisotropic solutions of Einsteins equations. *Physical Review D*, 77(2), 027502.

Herrera, L. and Ponce de Leon, J. (1985). Anisotropic spheres admitting a one-parameter group of conformal motions. *Journal of Mathematical Physics*, 26(8), 2018–2023.

Herrera, L., Prisco, A.D., Ospino, J., and Fuenmayor, E. (2001). Conformally flat anisotropic spheres in general relativity. *Journal of Mathematical Physics*, 42(5), 2129–2143.

Herrera, L. and Santos, N.O. (1997). Local anisotropy in self-gravitating systems. *Physics Reports*, 286(2), 53–130.

Hogan, P.A. (1973). A note on the escape of neutrinos from within einstein's spherical cluster of gravitating masses. In *Proceedings of the Royal Irish Academy. Section A: Mathematical and Physical Sciences*, volume 73, 91–97. JSTOR.

Hohmann, M., Järv, L., and Ualikhanova, U. (2017). Dynamical systems approach and generic properties of $f(\mathbb{T})$ cosmology. *Physical Review D*, 96(4), 043508.

Houndjo, M. (2012). Reconstruction of $f(\mathcal{R}, \mathcal{T})$ gravity describing matter dominated and accelerated phases. *International Journal of Modern Physics D*, 21(01), 1250003.

Ilijić, S. and Sossich, M. (2018). Compact stars in $f(\mathbb{T})$ extended theory of gravity. *Physical Review D*, 98(6), 064047.

Ilyas, M., Yousaf, Z., Bhatti, M., and Masud, B. (2017). Existence of relativistic structures in $f(\mathcal{R}, \mathcal{T})$ gravity. *Astrophysics and Space Science*, 362(12), 237.

Iorio, L. and Saridakis, E.N. (2012). Solar system constraints on $f(\mathbb{T})$ gravity. *Monthly Notices of the Royal Astronomical Society*, 427(2), 1555–1561.

Israel, W. (1966a). Singular hypersurfaces and thin shells in general relativity. *Il Nuovo Cimento B (1965-1970)*, 44(1), 1–14.

Israel, W. (1966b). Singular hypersurfaces and thin shells in general relativity. *Il Nuovo Cimento B (1965-1970)*, 44(1), 1–14.

Itoh, N. (1970). Hydrostatic equilibrium of hypothetical quark stars. *Progress of Theoretical Physics*, 44(1), 291–292.

Ivanov, B.V. (2002a). Maximum bounds on the surface redshift of anisotropic stars. *Physical Review D*, 65(10), 104011.

Ivanov, B. (2002b). Static charged perfect fluid spheres in general relativity. *Physical Review D*, 65(10), 104001.

Jain, B. and Taylor, A. (2003). Cross-correlation tomography: measuring dark energy evolution with weak lensing. *Physical Review Letters*, 91(14), 141302.

Jamil, M., Momeni, D., and Myrzakulov, R. (2013). Wormholes in a viable $f(\mathbb{T})$ gravity. *The European Physical Journal C*, 73(1), 1–13.

Jamil, M., Momeni, D., and Myrzakulov, R. (2015). Warm intermediate inflation in $f(\mathbb{T})$ gravity. *International Journal of Theoretical Physics*, 54(4), 1098–1112.

Janet, M. (1927). Sur la possibilité de plonger un espace riemannien donné dans un espace euclidien. *Annales de la Société Polonaise de Mathématique T. 5 (1926)*.

Jasim, M., Maurya, S., Gupta, Y., and Dayanandan, B. (2016). Well behaved anisotropic compact star models in general relativity. *Astrophysics and Space Science*, 361(11), 352.

References

Jeans, J.H. (1922). The motions of stars in a Kapteyn universe. *Monthly Notices of the Royal Astronomical Society*, 82, 122–132.

Jones, P. (1975). The alignment of the crab pulsar magnetic axis. *Astrophysics and Space Science*, 33(1), 215–230.

Josset, T., Perez, A., and Sudarsky, D. (2017). Dark energy from violation of energy conservation. *Physical Review Letters*, 118, 021102.

Joyce, A., Jain, B., Khoury, J., and Trodden, M. (2015). Beyond the cosmological standard model. *Physics Reports*, 568, 1–98.

Kalam, M., Rahaman, F., Ray, S., Hossein, S., Karar, I., Naskar, J., et al. (2012). Anisotropic strange star with de sitter spacetime. *The European Physical Journal C*, 72(12), 2248.

Kalam, M., Usmani, A.A., Rahaman, F., Hossein, S.M., Karar, I., and Sharma, R. (2013). A relativistic model for strange quark star. *International Journal of Theoretical Physics*, 52(9), 3319–3328.

Kanti, P., Kleihaus, B., and Kunz, J. (2012). Stable Lorentzian wormholes in dilatonic Einstein-Gauss-Bonnet theory. *Physical Review D*, 85(4), 044007.

Kaplan, D. and Nelson, A. (1986). Strange goings on in dense nucleonic matter. *Physics Letters B*, 175(1), 57–63.

Kar, S. (1994). Evolving wormholes and the weak energy condition. *Physical Review D*, 49(2), 862.

Kar, S. and Sahdev, D. (1996). Evolving lorentzian wormholes. *Physical Review D*, 53(2), 722.

Karami, K. and Abdolmaleki, A. (2013). $f(\mathbb{T})$ modified teleparallel gravity as an alternative for holographic and new agegraphic dark energy models. *Research in Astronomy and Astrophysics*, 13(7), 757.

Karmarkar, K.R. (1948). Gravitational metrics of spherical symmetry and class one. *Proceedings of the Indian Academy of Sciences - Section A*, 27, 56.

Kasner, E. (1921). Finite representation of the solar gravitational field in flat space of six dimensions. *American Journal of Mathematics*, 43(2), 130–133.

Katirci, N. and Kavuk, M. (2014). $f(\mathcal{R}, T_{\mu\nu}T^{\mu\nu})$ gravity and cardassian-like expansion as one of its consequences. *The European Physical Journal Plus*, 129, 163.

Kippenhahn, R., Weigert, A., and Weiss, A. (1990). *Stellar structure and evolution*, volume 192. Springer.

Kohler, M.. and Chao, K.L. (1965). Zentralsymmetrische statische Schwerefelder mit R´aumen der Klasse 1. *Zeitschrift f´ur Naturforschung*, 20, 1537–1543.

Komathiraj, K. and Maharaj, S. (2007). Analytical models for quark stars. *International Journal of Modern Physics D*, 16(11), 1803–1811.

Krššák, M. and Saridakis, E.N. (2016). The covariant formulation of $f(\mathbb{T})$ gravity. *Classical and Quantum Gravity*, 33(11), 115009.

Kuhfittig, P.K. (1999). A wormhole with a special shape function. *American Journal of Physics*, 67(2), 125–126.

Kuhfittig, P.K. (2002). Static and dynamic traversable wormhole geometries satisfying the Ford-Roman constraints. *Physical Review D*, 66(2), 024015.

Kuhfittig, P.K. (2015a). Wormholes admitting conformal Killing vectors and supported by generalized chaplygin gas. *The European Physical Journal C*, 75(8), 1–4.

Kuhfittig, P.K. (2015b). Wormholes with a barotropic equation of state admitting a one-parameter group of conformal motions. *Annals of Physics*, 355, 115–120.

Kuhfittig, P.K. (2018). Two diverse models of embedding class one. *Annals of Physics*, 392, 63–70.

Kuhfittig, P.K. and Gladney, V.D. (2018). A model for dark energy based on the theory of embedding. *Advanced Studies in Theoretical Physics*, 12, 233–241.

Kumar, S., Pratibha, and Gupta, Y. (2010). Invariant solutions of Einstein field equation for nonconformally flat fluid spheres of embedding class one. *International Journal of Modern Physics A*, 25(20), 3993–4000.

Lake, K. (2003). All static spherically symmetric perfect-fluid solutions of Einsteins equations. *Physical Review D*, 67(10), 104015.

References

Lake, K. (2004). Galactic potentials. *Physical Review Letters*, 92(5), 051101.

Lake, K. (2006). Galactic halos are Einstein clusters of WIMPs. *arXiv preprint gr-qc/0607057*.

Lanczos, C. (1938). A remarkable property of the Riemann-Christoffel tensor in four dimensions. *Annals of Mathematics*, 842–850.

las Heras, C. and León, P. (2018). Using MGD gravitational decoupling to extend the isotropic solutions of Einstein equations to the anisotropical domain. *Fortschritte der Physik*, 66, 1800036.

Lattimer, J.M. and Prakash, M. (2000). Nuclear matter and its role in supernovae, neutron stars and compact object binary mergers. *Physics Reports*, 333, 121–146.

Lattimer, J.M. and Steiner, A.W. (2014). Neutron star masses and radii from quiescent low-mass X-ray binaries. *The Astrophysical Journal*, 784(2), 123.

Lemaître, G. (1933). L'Univers en expansion. In *Annales de la Société scientifique de Bruxelles*, volume 53, 51.

Lemaître, G. (1997). The expanding universe. *General Relativity and Gravitation*, 29, 641–680.

Li, B., Sotiriou, T.P., and Barrow, J.D. (2011). $f(\mathbb{T})$ gravity and local Lorentz invariance. *Physical Review D*, 83(6), 064035.

Lim, Y., Kwak, K., Hyun, C.H., and Lee, C.H. (2014). Kaon condensation in neutron stars with Skyrme-Hartree-Fock models. *Physical Review C*, 89, 055804.

Lin, R.H., Wu, Z.Y., and Zhai, X.H. (2019). Wormholes without exotic matter in nonminimal torsion-matter coupling $f(\mathbb{T})$ gravity. *arXiv preprint arXiv:1906.10323*.

Lobo, F.S. and Oliveira, M.A. (2009). Wormhole geometries in $f(\mathcal{R})$ modified theories of gravity. *Physical Review D*, 80(10), 104012.

Lovelock, D. (1971). The Einstein tensor and its generalizations. *Journal of Mathematical Physics*, 12(3), 498–501.

Lovelock, D. (1972). The four-dimensionality of space and the Einstein tensor. *Journal of Mathematical Physics*, 13(6), 874–876.

Lugones, G. and Horvath, J.E. (2002). Color-flavor locked strange matter. *Physical Review D*, 66, 074017.

Lugones, G. and Horvath, J. (2003). High-density QCD pairing in compact star structure. *Astronomy & Astrophysics*, 403(1), 173–178.

Luongo, O. and Muccino, M. (2018). Speeding up the universe using dust with pressure. *Physical Review D*, 98(10), 103520.

Luongo, O. and Quevedo, H. (2014a). Cosmographic study of the universes specific heat: a landscape for cosmology? *General Relativity and Gravitation*, 46(1), 1649–1661.

Luongo, O. and Quevedo, H. (2014b). A unified dark energy model from a vanishing speed of sound with emergent cosmological constant. *International Journal of Modern Physics D*, 23(02), 1450012.

Maartens, R. and Maharaj, M.S. (1990). Conformally symmetric static fluid spheres. *Journal of Mathematical Physics*, 31, 151.

Maartens, R., Maharaj, S.D., and Tupper, B.O. (1995). General solution and classification of conformal motions in static spherical spacetimes. *Classical and Quantum Gravity*, 12(10), 2577.

Maartens, R., Maharaj, S.D., and Tupper, B.O. (1996). Conformal motions in static spherical spacetimes. *Classical and Quantum Gravity*, 13(2), 317.

Maeda, H. and Nozawa, M. (2008). Static and symmetric wormholes respecting energy conditions in Einstein-Gauss-Bonnet gravity. *Physical Review D*, 78(2), 024005.

Maekawa, M. and Tamagaki, R. (1968). An attempt to explain the origin of magnetic field in superdense stars. *Proceedings of the Symposium on Cosmology (Kyoto: Research Institute for Fundamental Physics)*, 80.

Mafa Takisa, P. and Maharaj, S. (2013). Compact models with regular charge distributions. *Astrophysics and Space Science*, 343(2), 569–577.

Maharaj, S., Maartens, R., and Maharaj, M. (1995). Conformal symmetries in static spherically symmetric spacetimes. *International Journal of Theoretical Physics*, 34(11), 2285–2291.

References

Maharaj, S., Sunzu, J., and Ray, S. (2014). Some simple models for quark stars. *The European Physical Journal Plus*, 129(1), 1–10.

Mak, M., Dobson Jr, P.N., and Harkó, T. (2002). Exact models for anisotropic relativistic stars. *International Journal of Modern Physics D*, 11(02), 207–221.

Mak, M. and Harko, T. (2003). Anisotropic stars in general relativity. *Proceedings of the Royal Society of London. Series A: Mathematical, Physical and Engineering Sciences*, 459(2030), 393–408.

Mak, M. and Harko, T. (2004). Quark stars admitting a one-parameter group of conformal motions. *International Journal of Modern Physics D*, 13(01), 149–156.

Malaver, M. (2014). Strange quark star model with quadratic equation of state. *arXiv preprint arXiv:1407.0760*.

Maluf, J.W. (2013). The teleparallel equivalent of general relativity. *Annalen der Physik*, 525(5), 339–357.

Manjonjo, A., Maharaj, S., and Moopanar, S. (2018). Static models with conformal symmetry. *Classical and Quantum Gravity*, 35(4), 045015.

Matulich, J. and Troncoso, R. (2011). Asymptotically Lifshitz wormholes and black holes for Lovelock gravity in vacuum. *Journal of High Energy Physics*, 2011(10), 1–17.

Maulana, H. and Sulaksono, A. (2019). Impact of energy-momentum nonconservation on radial pulsations of strange stars. *Physical Review D*, 100(12), 124014.

Maurya, S.K. and Tello-Ortiz, F. (2019). Generalized relativistic anisotropic compact star models by gravitational decoupling. *The European Physical Journal C*, 79, 85.

Maurya, S., Banerjee, A., and Hansraj, S. (2018). Role of pressure anisotropy on relativistic compact stars. *Physical Review D*, 97(4), 044022.

Maurya, S., Banerjee, A., Jasim, M., Kumar, J., Prasad, A., and Pradhan, A. (2019). Anisotropic compact stars in the Buchdahl model: A comprehensive study. *Physical Review D*, 99(4), 044029.

Maurya, S., Errehymy, A., Singh, K.N., Tello-Ortiz, F., and Daoud, M. (2020). Gravitational decoupling minimal geometric deformation model in modified $f(\mathcal{R}, \mathcal{T})$ gravity theory. *Physics of the Dark Universe*, 30, 100640.

Maurya, S. and Govender, M. (2017). Generating physically realizable stellar structures via embedding. *The European Physical Journal C*, 77(5), 1–13.

Maurya, S., Gupta, Y., Dayanandan, B., and Ray, S. (2016a). A new model for spherically symmetric anisotropic compact star. *The European Physical Journal C*, 76(5), 1–9.

Maurya, S., Gupta, Y., and Ray, S. (2017a). All spherically symmetric charged anisotropic solutions for compact stars. *The European Physical Journal C*, 77(6), 360.

Maurya, S., Gupta, Y., Ray, S., and Chowdhury, S.R. (2015a). Spherically symmetric charged compact stars. *The European Physical Journal C*, 75(8), 389.

Maurya, S., Gupta, Y., Ray, S., and Deb, D. (2016b). Generalised model for anisotropic compact stars. *The European Physical Journal C*, 76(12), 1–12.

Maurya, S., Gupta, Y., and Ray, S. (2015b). Spherically symmetric electromagnetic mass models of embedding class one. *arXiv:1506.02498v1*.

Maurya, S., Gupta, Y., Smitha, T., and Rahaman, F. (2016c). A new exact anisotropic solution of embedding class one. *The European Physical Journal A*, 52(7), 191.

Maurya, S., Ratanpal, B., and Govender, M. (2017b). Anisotropic stars for spherically symmetric spacetimes satisfying the karmarkar condition. *Annals of Physics*, 382, 36–49.

Maurya, S. and Tello-Ortiz, F. (2020a). Anisotropic fluid spheres in the framework of $f(\mathcal{R}, \mathcal{T})$ gravity theory. *Annals of Physics*, 414, 168070.

Maurya, S. and Tello-Ortiz, F. (2020b). Charged anisotropic compact star in $f(\mathcal{R}, \mathcal{T})$ gravity: A minimal geometric deformation gravitational decoupling approach. *Physics of the Dark Universe*, 27, 100442.

References

Mazharimousavi, S.H. and Halilsoy, M. (2016). Necessary conditions for having wormholes in $f(\mathcal{R})$ gravity. *Modern Physics Letters A*, 31(37), 1650203.

Mehdizadeh, M.R., Zangeneh, M.K., and Lobo, F.S. (2015). Einstein-Gauss-Bonnet traversable wormholes satisfying the weak energy condition. *Physical Review D*, 91(8), 084004.

Merafina, M. and Ruffini, R. (1989). Systems of selfgravitating classical particles with a cutoff in their distribution function. *Astronomy and Astrophysics*, 221, 4–19.

Miller, C. (2002). Twinkle, twinkle, neutron star. *Nature*, 420(6911), 31–33.

Momeni, D., Abbas, G., Qaisar, S., Zaz, Z., and Myrzakulov, R. (2018). Modelling of a compact anisotropic star as an anisotropic fluid sphere in $f(\mathbb{T})$ gravity. *Canadian Journal of Physics*, 96(12), 1295–1303.

Moopanar, S. and Maharaj, S.D. (2010). Conformal symmetries of spherical spacetimes. *International Journal of Theoretical Physics*, 49, 18781885.

Moraes, P.H.R.S. and Sahoo, P.K. (2017a). The simplest non-minimal mattergeometry coupling in the $f(\mathcal{R}, \mathcal{T})$ cosmology. *European Physical Journal C*, 77, 480.

Moraes, P. and Sahoo, P. (2017b). Modeling wormholes in $f(\mathcal{R}, \mathcal{T})$ gravity. *Physical Review D*, 96(4), 044038.

Moraes, P. and Sahoo, P. (2018). Nonexotic matter wormholes in a trace of the energy-momentum tensor squared gravity. *Physical Review D*, 97(2), 024007.

Morales, E. and Tello-Ortiz, F. (2018a). Charged anisotropic compact objects by gravitational decoupling. *The European Physical Journal C*, 78(8), 618.

Morales, E. and Tello-Ortiz, F. (2018b). Compact anisotropic models in general relativity by gravitational decoupling. *The European Physical Journal C*, 78(10), 841.

Morris, M.S. and Thorne, K.S. (1988). Wormholes in space-time and their use for interstellar travel: a tool for teaching general relativity. *American Journal of Physics*, 56, 395–412.

Morris, M.S., Thorne, K.S., and Yurtsever, U. (1988). Wormholes, time machines, and the weak energy condition. *Physical Review Letters*, 61(13), 1446.

Moustakidis, C.C. (2017). The stability of relativistic stars and the role of the adiabatic index. *General Relativity and Gravitation*, 49(5), 68.

Mukherjee, S., Paul, B., Dadhich, N., Maharaj, S., and Beesham, A. (2006). Emergent universe with exotic matter. *Classical and Quantum Gravity*, 23(23), 6927.

Mukherjee, S., Paul, B., Maharaj, S., and Beesham, A. (2005). Emergent universe in Starobinsky model. *arXiv preprint gr-qc/0505103*.

Murad, M.H. and Fatema, S. (2015a). Anisotropic charged stellar models in generalized Tolman iv spacetime. *The European Physical Journal Plus*, 130(1), 1–19.

Murad, M.H. and Fatema, S. (2015b). Some new Wyman–Leibovitz–Adler type static relativistic charged anisotropic fluid spheres compatible to self-bound stellar modeling. *The European Physical Journal C*, 75(11), 533.

Myrzakulov, R. (2011). Accelerating universe from $f(\mathbb{T})$ gravity. *The European Physical Journal C*, 71(9), 1–8.

Nashed, G.G. (2013). A special exact spherically symmetric solution in $f(\mathbb{T})$ gravity theories. *General Relativity and Gravitation*, 45(10), 1887–1899.

Nazari, E., Sarvi, F., and Roshan, M. (2020). Generalized energy-momentum-squared gravity in the Palatini formalism. *Physical Review D*, 102, 064016.

Neary, N., Ishak, M., and Lake, K. (2001). Tolman type VII solution, trapped null orbits, and w-modes. *Physical Review D*, 64(8), 084001.

Negi, P. and Durgapal, M. (1999). Stable ultracompact objects. *General Relativity and Gravitation*, 31(1), 13–20.

Negi, P. and Durgapal, M. (2001). Relativistic supermassive stars. *Astrophysics and Space Science*, 275(3), 185–207.

Negreiros, R.P., Weber, F., Malheiro, M., and Usov, V. (2009). Electrically charged strange quark stars. *Physical Review D*, 80(8), 083006.

Nelson, A.E. and Kaplan, D.B. (1987). Strange condensate realignment in relativistic heavy ion collisions. *Physics Letters B*, 192(1-2), 193–197.

References

Ngubelanga, S.A., Maharaj, S.D., and Ray, S. (2015). Compact stars with quadratic equation of state. *Astrophysics and Space Science*, 357(1), 1–9.

Nishizaki, S., Yamamoto, Y., and Takatsuka, T. (2002). Hyperon-mixed neutron star matter and neutron stars. *Progress of Theoretical Physics*, 108, 703–718.

Nojiri, S., Odintsov, S., and Oikonomou, V. (2017). Modified gravity theories on a nutshell: inflation, bounce and late-time evolution. *Physics Reports*, 692, 1–104.

Nojiri, S. and Odintsov, S.D. (2003a). de Sitter brane universe induced by phantom and quantum effects. *Physics Letters B*, 565, 1–9.

Nojiri, S. and Odintsov, S.D. (2003b). Modified gravity with negative and positive powers of curvature: Unification of inflation and cosmic acceleration. *Physical Review D*, 68(12), 123512.

Nojiri, S. and Odintsov, S.D. (2003c). Quantum de sitter cosmology and phantom matter. *Physics Letters B*, 562(3-4), 147–152.

Nunes, R.C., Alves, M.E., and de Araujo, J.C. (2019). Forecast constraints on $f(\mathbb{T})$ gravity with gravitational waves from compact binary coalescences. *Physical Review D*, 100(6), 064012.

Nunes, R.C., Pan, S., and Saridakis, E.N. (2018). New observational constraints on $f(\mathbb{T})$ gravity through gravitational-wave astronomy. *Physical Review D*, 98(10), 104055.

Okołów, A. (2014). Kinematic quantum states for the teleparallel equivalent of general relativity. *General Relativity and Gravitation*, 46(1), 1–39.

Oppenheimer, J.R. and Volkoff, G.M. (1939). On massive neutron cores. *Physical Review*, 55, 374–381.

Ori, A. (1993). Must time-machine construction violate the weak energy condition? *Physical Review Letters*, 71(16), 2517.

Ori, A. and Soen, Y. (1994). Causality violation and the weak energy condition. *Physical Review D*, 49(8), 3990.

Ortín, T. (2004). *Gravity and strings*. Cambridge University Press.

Ovalle, J. (2010). Braneworld stars: anisotropy minimally projected onto the brane. Gravitation and Astrophysics ed J. Luo. *World Scientific*, 173–182.

Ovalle, J. (2019). Decoupling gravitational sources in general relativity: The extended case. *Physics Letters B*, 788, 213–218.

Ovalle, J., Casadio, R., Da Rocha, R., Sotomayor, A., and Stuchlik, Z. (2018a). Einstein-Klein-Gordon system by gravitational decoupling. *EPL (Europhysics Letters)*, 124(2), 20004.

Ovalle, J., Casadio, R., and da Rocha, R. (2018b). Black holes by gravitational decoupling. *The European Physical Journal C*, 78, 690.

Ovalle, J. (2016). Extending the geometric deformation: New black hole solutions. In *International Journal of Modern Physics: Conference Series*, volume 41, 1660132. World Scientific.

Ovalle, J. (2017). Decoupling gravitational sources in general relativity: from perfect to anisotropic fluids. *Physical Review D*, 95(10), 104019.

Ovalle, J., Casadio, R., da Rocha, R., and Sotomayor, A. (2018c). Anisotropic solutions by gravitational decoupling. *The European Physical Journal C*, 78(2), 122.

Padmanabhan, T. and Choudhury, T.R. (2002). Can the clustered dark matter and the smooth dark energy arise from the same scalar field? *Physical Review D*, 66(8), 081301.

Paliathanasis, A., Barrow, J.D., and Leach, P. (2016). Cosmological solutions of $f(\mathbb{T})$ gravity. *Physical Review D*, 94(2), 023525.

Panahi, H., Monadi, R., and Eghdami, I. (2016). A gaussian model for anisotropic strange quark stars. *Chinese Physics Letters*, 33(7), 072601.

Pandey, S. and Sharma, S. (1982). Insufficiency of Karmarkar's condition. *General Relativity and Gravitation*, 14, 113115.

Panotopoulos, G. and Rincón, Á. (2018). Minimal geometric deformation in a cloud of strings. *The European Physical Journal C*, 78(10), 851.

Parisi, L., Radicella, N., and Vilasi, G. (2012). Stability of the Einstein static universe in massive gravity. *Physical Review D*, 86(2), 024035.

References

Paul, B.C. and Ghose, S. (2010). Emergent universe scenario in the Einstein–Gauss–Bonnet gravity with dilaton. *General Relativity and Gravitation*, 42(4), 795–812.

Pavlovic, P. and Sossich, M. (2015). Wormholes in viable $f(\mathcal{R})$ modified theories of gravity and weak energy condition. *The European Physical Journal C*, 75(3), 1–8.

Percival, W.J., Reid, B.A., Eisenstein, D.J., Bahcall, N.A., Budavari, T., Frieman, J.A., Fukugita, M., Gunn, J.E., Ivezić, Ž., Knapp, G.R., et al. (2010). Baryon acoustic oscillations in the Sloan Digital Sky Survey data release 7 galaxy sample. *Monthly Notices of the Royal Astronomical Society*, 401(4), 2148–2168.

Perlmutter, S., Aldering, G., Goldhaber, G., Knop, R., Nugent, P., Castro, P., Deustua, S., Fabbro, S., Goobar, A., Groom, D., et al. (1999). Measurements of ω and λ from 42 high-redshift supernovae. *The Astrophysical Journal*, 517, 565–586.

Perlmutter, S., Aldering, G., Valle, M.D., Deustua, S., Ellis, R., Fabbro, S., Fruchter, A., Goldhaber, G., Groom, D., Hook, I., et al. (1998). Discovery of a supernova explosion at half the age of the universe. *Nature*, 391(6662), 51–54.

Perlmutter, S., Gabi, S., Goldhaber, G., Goobar, A., Groom, D., Hook, I., Kim, A., Kim, M., Lee, J., Pain, R., et al. (1997). Measurements* of the cosmological parameters Ω and Λ from the first seven supernovae at $z \geq 0.35$. *The astrophysical journal*, 483(2), 565.

Perrotta, F., Baccigalupi, C., and Matarrese, S. (1999). Extended quintessence. *Physical Review D*, 61(2), 023507.

Poisson, E. and Visser, M. (1995). Thin-shell wormholes: Linearization stability. *Physical Review D*, 52(12), 7318.

Ponce de Leon, J. (1987). General relativistic electromagnetic mass models of neutral spherically symmetric systems. *General Relativity and Gravitation*, 19(8), 797–807.

Ponce de Leon, J. (1993). Limiting configurations allowed by the energy conditions. *General Relativity and Gravitation*, 25(11), 1123–1137.

Pons, J.A., Walter, F.M., Lattimer, J.M., Prakash, M., Neuhäuser, R., and An, P. (2002). Toward a mass and radius determination of the nearby isolated neutron star RX J185635–3754. *The Astrophysical Journal*, 564(2), 981.

Pound, R.V. and Rebka, G.A. (1960). Apparent weight of photons. *Physical Review Letters*, 4, 337 – 341.

Prakash, M., Bombaci, I., Prakash, M., Ellis, P.J., Lattimer, J.M., and Knorren, R. (1997). Composition and structure of protoneutron stars. *Physics Reports*, 280(1), 1–77.

Qadir, A., Lee, H.W., and Kim, K.Y. (2017). Modified relativistic dynamics. *International Journal of Modern Physics D*, 26(05), 1741001.

Qiu, T., Tian, K., and Bu, S. (2019). Perturbations of bounce inflation scenario from $f(\mathbb{T})$ modified gravity revisited. *The European Physical Journal C*, 79(3), 1–9.

Radinschi, I., Rahaman, F., Kalam, M., and Chakraborty, K. (2010). Classical electron model with non static conformal symmetry. *Fizika B*, 19, 125–134.

Raghoonundun, A.M. and Hobill, D.W. (2015). Possible physical realizations of the Tolman VII solution. *Physical Review D*, 92(12), 124005.

Rahaman, F., Kalam, M., and Chakraborty, S. (2007). Gravitational lensing by stable $C-$field wormhole. *arXiv preprint arXiv:0705.0740*, 45, 518.

Rahaman, F., Jamil, M., Kalam, M., Chakraborty, K., and Ghosh, A. (2010a). On role of pressure anisotropy for relativistic stars admitting conformal motion. *Astrophysics and Space Science*, 325(1), 137–147.

Rahaman, F., Karmakar, S., Karar, I., and Ray, S. (2015a). Wormhole inspired by non-commutative geometry. *Physics Letters B*, 746, 73–78.

Rahaman, F., Kuhfittig, P., Kalam, M., Usmani, A., and Ray, S. (2011). A comparison of Hořava–Lifshitz gravity and einstein gravity through thin-shell wormhole construction. *Classical and Quantum Gravity*, 28(15), 155021.

Rahaman, F., Maharaj, S.D., Sardar, I.H., and Chakraborty, K. (2017). Conformally symmetric relativistic star. *Modern Physics Letters A*, 32(08), 1750053.

Rahaman, F., Maulick, R., Yadav, A.K., Ray, S., and Sharma, R. (2012a). Singularity-free dark energy star. *General Relativity and Gravitation*, 44(1), 107–124.

References

Rahaman, F., Ray, S., Jafry, A.K., and Chakraborty, K. (2010b). Singularity-free solutions for anisotropic charged fluids with chaplygin equation of state. *Physical Review D*, 82(10), 104055.

Rahaman, F., Ray, S., Khadekar, G., Kuhfittig, P., and Karar, I. (2015b). Non-commutative geometry inspired wormholes with conformal motion. *International Journal of Theoretical Physics*, 54(2), 699–709.

Rahaman, F., Sharma, R., Ray, S., Maulick, R., and Karar, I. (2012b). Strange stars in Krori–Barua space-time. *The European Physical Journal C*, 72(7), 2071.

Rajagopal, K. and Wilczek, F. (2001). The condensed matter physics of QCD. In *At The Frontier of Particle Physics: Handbook of QCD (In 3 Volumes)*, 2061–2151. World Scientific.

Randall, L. and Sundrum, R. (1999a). An alternative to compactification. *Physical Review Letters*, 83(23), 4690.

Randall, L. and Sundrum, R. (1999b). Large mass hierarchy from a small extra dimension. *Physical Review Letters*, 83(17), 3370.

Rani, S., Bilal Amin, M., and Jawad, A. (2016a). Exponential and logarithmic $f(\mathbb{T})$ wormhole solutions in Lorentzian noncommutative background. *The European Physical Journal Plus*, 131(12), 1–15.

Rani, S., Jawad, A., and Amin, M.B. (2016b). Charged noncommutative wormhole solutions via power-law $f(\mathbb{T})$ models. *Communications in Theoretical Physics*, 66(4), 411.

Rapp, R., Schäfer, T., Shuryak, E., and Velkovsky, M. (1998). Diquark Bose condensates in high density matter and instantons. *Physical Review Letters*, 81(1), 53.

Ratra, B. and Peebles, P.J. (1988). Cosmological consequences of a rolling homogeneous scalar field. *Physical Review D*, 37(12), 3406.

Ray, S., Espindola, A.L., Malheiro, M., Lemos, J.P., and Zanchin, V.T. (2003). Electrically charged compact stars and formation of charged black holes. *Physical Review D*, 68(8), 084004.

Rhoades, C.E.J. and Ruffini, R. (1974). Maximum mass of a neutron star. *Physical Review Letters*, 32, 324.

Riess, A.G., Filippenko, A.V., Challis, P., Clocchiatti, A., Diercks, A., Garnavich, P.M., Gilliland, R.L., Hogan, C.J., Jha, S., Kirshner, R.P., et al. (1998a). Observational evidence from supernovae for an accelerating universe and a cosmological constant. *The Astronomical Journal*, 116(3), 1009.

Riess, A.G., Filippenko, A.V., and Challis, P.e.a. (1998b). Observational evidence from supernovae for an accelerating universe and a cosmological constant. *The Astrophysical Journal*, 116, 1009.

Riess, A.G., Strolger, L.G., Casertano, S., Ferguson, H.C., Mobasher, B., Gold, B., Challis, P.J., Filippenko, A.V., Jha, S., Li, W., et al. (2007). New Hubble space telescope discoveries of type Ia supernovae at $z \geq 1$: narrowing constraints on the early behavior of dark energy. *The Astrophysical Journal*, 659(1), 98.

Riess, A.G., Strolger, L.G., Tonry, J., Casertano, S., Ferguson, H.C., Mobasher, B., Challis, P., Filippenko, A.V., Jha, S., Li, W., et al. (2004). Type Ia supernova discoveries at $z > 1$ from the Hubble Space Telescope: Evidence for past deceleration and constraints on dark energy evolution. *The Astrophysical Journal*, 607(2), 665.

Rippl, S., Romero, C., and Tavakol, R. (1995). $D-$dimensional gravity from $(D + 1)$ dimensions. *Classical and Quantum Gravity*, 12(10), 2411.

Robertson, H.P. (1933). Relativistic cosmology. *Reviews of Modern Physics*, 5(1), 62.

Romero, C., Tavakol, R., and Zalaletdinov, R. (1996). The embedding of general relativity in five dimensions. *General Relativity and Gravitation*, 28(3), 365–376.

Roshan, M. and Shojai, F. (2016). Energy-momentum squared gravity. *Physical Review D*, 94, 044002.

Ruderman, M. (1967). Proceedings of the fifth annual eastern theoretical physics conference. 63. Benjamin.

Ruderman, M. (1972). Pulsars: structure and dynamics. *Annual Review of Astronomy and Astrophysics*, 10(1), 427–476.

References

Ruffini, R. and Bonazzola, S. (1969). Systems of self-gravitating particles in general relativity and the concept of an equation of state. *Physical Review*, 187(5), 1767.

Ruiz-Lapuente, P. (2010). *Dark energy: observational and theoretical approaches.* Cambridge University Press.

Sahoo, P., Sahoo, P., Bishi, B.K., and Aygün, S. (2017). Magnetized strange quark model with Big Rip singularity in $f(\mathcal{R}, \mathcal{T})$ gravity. *Modern Physics Letters A*, 32(21), 1750105.

Santos, J., Alcaniz, J., Carvalho, F., and Pires, N. (2008). Latest supernovae constraints on $f(\mathcal{R})$ cosmologies. *Physics Letters B*, 669(1), 14–18.

Santos, N. (1985). Non-adiabatic radiating collapse. *Monthly Notices of the Royal Astronomical Society*, 216, 403–410.

Sawyer, R.F. (1972). Condensed π- phase in neutron-star matter. *Physical Review Letters*, 29(6), 382.

Schaffner-Bielich, J., Hanauske, M., Stöcker, H., and Greiner, W. (2002). Phase transition to hyperon matter in neutron stars. *Physical Review Letters*, 89(17), 171101.

Schertler, K., Greiner, C., Schaffner-Bielich, J., and Thoma, M. (2000). Quark phases in neutron stars and a third family of compact stars as signature for phase transitions. *Nuclear Physics A*, 677(1-4), 463–490.

Schlaefli, L. (1871). *Ann. Mat. Pura Appl.*, 5, 178.

Schunck, F.E. and Mielke, E.W. (2003). General relativistic boson stars. *Classical and Quantum Gravity*, 20(20), R301.

Schwarzschild, K. (1916a). ʹUber das gravitationsfeld einer kugel aus inkompressibler flssigkeit nach der einsteinschen theorie. *Sitzungsberichte der Kʹoniglich Preussischen Akademie der Wissenschaften zu Berlin, Phys.-Math. Klasse*, 424–434.

Schwarzschild, K. (1916b). Über das gravitationsfeld eines massenpunktes nach der einsteinschen theorie. *Sitzungsberichte der Koniglich Preussischen Akademie der Wissenschaften*, 7, 189–196.

Sen, A. (2002). Rolling tachyon. *Journal of High Energy Physics*, 2002(04), 048.

Shaikh, R. (2018). Wormholes with nonexotic matter in Born-Infeld gravity. *Physical Review D*, 98(6), 064033.

Shapiro, S.L. and Teukolsky, S.A. (2008). *Black holes, white dwarfs, and neutron stars: The physics of compact objects*. John Wiley & Sons.

Sharif, M. and Fatima, H.I. (2016). Conformally symmetric traversable wormholes in $f(G)$ gravity. *General Relativity and Gravitation*, 48(11), 1–19.

Sharif, M. and Nawazish, I. (2018). Wormhole geometry and noether symmetry in $f(\mathcal{R})$ gravity. *Annals of Physics*, 389, 283–305.

Sharif, M. and Rani, S. (2013a). Dynamical wormhole solutions in $f(\mathbb{T})$ gravity. *General Relativity and Gravitation*, 45(11), 2389–2402.

Sharif, M. and Rani, S. (2013b). Wormhole solutions in $f(\mathbb{T})$ gravity with noncommutative geometry. *Physical Review D*, 88(12), 123501.

Sharif, M. and Saba, S. (2018). Gravitational decoupled anisotropic solutions in $f(\mathcal{G})$ gravity. *The European Physical Journal C*, 78(11), 921.

Sharif, M. and Sadiq, S. (2018a). Gravitational decoupled anisotropic solutions for cylindrical geometry. *The European Physical Journal Plus*, 133(6), 245.

Sharif, M. and Sadiq, S. (2018b). Gravitational decoupled charged anisotropic spherical solutions. *The European Physical Journal C*, 78(5), 410.

Sharif, M. and Waseem, A. (2019). Anisotropic spherical solutions by gravitational decoupling in $f(\mathcal{R})$ gravity. *Annals of Physics*, 405, 14–28.

Sharif, M. and Yousaf, Z. (2014). Electromagnetic field and dynamical instability of collapse with CDTT model. *Astroparticle Physics*, 56, 19–25.

Sharma, R. and Maharaj, S. (2007). A class of relativistic stars with a linear equation of state. *Monthly Notices of the Royal Astronomical Society*, 375(4), 1265–1268.

Sharma, R. and Ratanpal, B. (2013). Relativistic stellar model admitting a quadratic equation of state. *International Journal of Modern Physics D*, 22(13), 1350074.

References

Shee, D., Rahaman, F., Guha, B., and Ray, S. (2016). Anisotropic stars with non-static conformal symmetry. *Astrophysics and Space Science*, 361(5), 167.

Shirafuji, T., Nashed, G.G., and Hayashi, K. (1996). Energy of general spherically symmetric solution in the tetrad theory of gravitation. *Progress of Theoretical Physics*, 95(3), 665–678.

Singh, K.N., Pant, N., and Govender, M. (2017a). Anisotropic compact stars in Karmarkar spacetime. *Chinese Physics C*, 41(1), 015103.

Singh, K.N., Pant, N., and Govender, M. (2017b). Physical viability of fluid spheres satisfying the Karmarkar condition. *The European Physical Journal C*, 77(2), 1–11.

Singh, K.N., Pant, N., and Troconis, O. (2017c). A new relativistic stellar model with anisotropic fluid in Karmarkar space–time. *Annals of Physics*, 377, 256–267.

Singh, K.N., Rahaman, F., and Banerjee, A. (2019). Einsteins cluster mimicking compact star in the teleparallel equivalent of general relativity. *Physical Review D*, 100(8), 084023.

Sokolov, A. (1980). Phase transformations in a superfluid neutron liquid. *Zhurnal Ehksperimental'noj i Teoreticheskoj Fiziki*, 49(4), 1137–1140.

Song, Y.S., Hu, W., and Sawicki, I. (2007). Large scale structure of $f(\mathcal{R})$ gravity. *Phys. Rev. D*, 75, 044004.

Sotiriou, T.P. and Faraoni, V. (2010). $f(\mathcal{R})$ theories of gravity. *Reviews of Modern Physics*, 82(1), 451.

Sotiriou, T.P., Li, B., and Barrow, J.D. (2011). Generalizations of teleparallel gravity and local Lorentz symmetry. *Physical Review D*, 83(10), 104030.

Spergel, D.N., Bean, R., Doré, O., Nolta, M.R., Bennett, C.L., Dunkley, J., Hinshaw, G., Jarosik, N., Komatsu, E., Page, L., Peiris, H.V., Verde, L., Halpern, M., Hill, R.S., Kogut, A., Limon, M., Meyer, S.S., Odegard, N., Tucker, G.S., Weiland, J.L., Wollack, E., and Wright, E.L. (2007). Three-Year Wilkinson Microwave Anisotropy Probe (WMAP) Observations: Implications for Cosmology. *The Astrophysical Journal Supplement Series*, 170(2), 377–408.

Spergel, D.N., Verde, L., Peiris, H.V., Komatsu, E., Nolta, M.R., Bennett, C.L., Halpern, M., Hinshaw, G., Jarosik, N., Kogut, A., Limon, M., Meyer, S.S., Page, L., Tucker, G.S., Weiland, J.L., Wollack, E., and Wright, E.L. (2003). First-Year Wilkinson Microwave Anisotropy Probe (WMAP) Observations: Determination of Cosmological Parameters. *The Astrophysical Journal Supplement Series*, 148(1), 175–194.

Starobinsky, A.A. (2007). Disappearing cosmological constant in $f(\mathcal{R})$ gravity. *JETP letters*, 86(3), 157–163.

Steiner, A.W., Lattimer, J.M., and Brown, E.F. (2013). The neutron star mass–radius and the equation of state of dense matter. *The Astrophysical Journal Letters*, 765(1), L5.

Steiner, A.W., Reddy, S., and Prakash, M. (2002). Color-neutral superconducting quark matter. *Physical Review D*, 66(9), 094007.

Straumann, N. (2012). *General relativity and relativistic astrophysics*. Springer Science & Business Media.

Takisa, P. and Maharaj, S. (2013). Some charged polytropic models. *General Relativity and Gravitation*, 45(10), 1951–1969.

Tamanini, N. and Boehmer, C.G. (2012). Good and bad tetrads in $f(\mathbb{T})$ gravity. *Physical Review D*, 86(4), 044009.

Tegmark, M., Strauss, M.A., Blanton, M.R., Abazajian, K., Dodelson, S., Sandvik, H., Wang, X., Weinberg, D.H., Zehavi, I., Bahcall, N.A., et al. (2004). Cosmological parameters from SDSS and WMAP. *Physical Review D*, 69(10), 103501.

Tello-Ortiz, F., Maurya, S.K., and Gomez-Leyton, Y. (2020). Class I approach as MGD generator. *The European Physical Journal C*, 80, 324.

Thirukkanesh, S., Govender, M., and Lortan, D.B. (2015). Spherically symmetric static matter configurations with vanishing radial pressure. *International Journal of Modern Physics D*, 24(01), 1550002.

Thirukkanesh, S. and Maharaj, S. (2008). Charged anisotropic matter with a linear equation of state. *Classical and Quantum Gravity*, 25(23), 235001.

References

Tipler, F., Clarke, C., and Ellis, G. (1980). General relativity and gravitation. *ed. Held, A., Plenum*, 97–206.

Tolman, R.C. (1939). Static solutions of Einstein's field equations for spheres of fluid. *Physical Review*, 55(4), 364–673.

Unzicker, A. and Case, T. (2005). Translation of Einstein's attempt of a unified field theory with teleparallelism. *arXiv preprint physics/0503046*.

Usov, V.V. (2004). Electric fields at the quark surface of strange stars in the color-flavor locked phase. *Physical Review D*, 70(6), 067301.

Varela, V., Rahaman, F., Ray, S., Chakraborty, K., and Kalam, M. (2010). Charged anisotropic matter with linear or nonlinear equation of state. *Physical Review D*, 82(4), 044052.

Velay-Vitow, J. and DeBenedictis, A. (2017). Junction conditions for $f(\mathbb{T})$ gravity from a variational principle. *Physical Review D*, 96(2), 024055.

Visser, M. (1989a). Traversable wormholes from surgically modified Schwarzschild spacetimes. *Nuclear Physics B*, 328(1), 203–212.

Visser, M. (1989b). Traversable wormholes: Some simple examples. *Physical Review D*, 39(10), 3182.

Visser, M. (1995). *Lorentzian Wormholes. From Einstein to Hawking.* American Institute of Physics.

Visser, M., Kar, S., and Dadhich, N. (2003). Traversable wormholes with arbitrarily small energy condition violations. *Physical Review Letters*, 90(20), 201102.

Walecka, J. (1975). Equation of state for neutron matter at finite T in a relativistic mean-field theory. *Physics Letters B*, 59(2), 109–112.

Walter, F.M. and Lattimer, J.M. (2002). A revised parallax and its implications for RX J185635–3754. *The Astrophysical Journal*, 576(2), L145.

Wang, A. and Letelier, P.S. (1995). Dynamical wormholes and energy conditions. *Progress of Theoretical Physics*, 94(1), 137–142.

Wang, T. (2011). Static solutions with spherical symmetry in $f(\mathbb{T})$ theories. *Physical Review D*, 84(2), 024042.

Weinberg, S. (1972). *Gravitation and Cosmology: Principles and Applications of the General Theory of Relativity.* John Wiley & Son.

Weisberg, J.M., Nice, D.J., and Taylor, J.H. (2010). Timing measurements of the relativistic binary pulsar PSR B1913+16. *The Astrophysical Journal*, 722, 1030–1034.

Wetterich, C. (1988). Cosmology and the fate of dilatation symmetry. *Nuclear Physics B*, 302(4), 668–696.

Wheeler, J. (1962). *Geometrodynamics.* Academic Press, New York and London.

Wheeler, J.A. (1957). On the nature of quantum geometrodynamics. *Annals of Physics*, 2(6), 604–614.

Wheeler, J.A. (1955). Geons. *Physical Review*, 97(2), 511.

Will, C.M. (2006). The confrontation between general relativity and experiment. *Living reviews in relativity*, 9, 3.

Witten, E. (1984). Cosmic separation of phases. *Physical Review D*, 30, 272.

Wu, P. and Yu, H. (2010a). The dynamical behavior of $f(\mathbb{T})$ theory. *Physics Letters B*, 692(3), 176–179.

Wu, P. and Yu, H. (2010b). Observational constraints on $f(\mathbb{T})$ theory. *Physics Letters B*, 693(4), 415–420.

Wu, P. and Yu, H. (2011). The stability of the Einstein static state in $f(\mathbb{T})$ gravity. *Physics Letters B*, 703(3), 223–227.

Yousaf, Z., Bamba, K., and Bhatti, M.Z.u.H. (2016). Causes of irregular energy density in $f(\mathcal{R}, \mathcal{T})$ gravity. *Physical Review D*, 93(12), 124048.

Yousaf, Z., Ilyas, M., and Zaeem-ul Haq Bhatti, M. (2017). Static spherical wormhole models in $f(\mathcal{R}, \mathcal{T})$ gravity. *The European Physical Journal Plus*, 132(6), 268.

References

Zangeneh, M.K., Lobo, F.S., and Dehghani, M.H. (2015). Traversable wormholes satisfying the weak energy condition in third-order Lovelock gravity. *Physical Review D*, 92(12), 124049.

Zapolsky, H.S. (1968). Can the redshifts of quasi-stellar objects BE gravitational? *The Astrophysical Journal*, 153, L163.

Zeldovich, Y.B. and Novikov, I.D. (1971). *Relativistic Astrophysics Stars and Relativity, Vol. 1.* University of Chicago.

Zel'Dovich, Y.B. and Polnarev, A. (1974). Radiation of gravitational waves by a cluster of superdense stars. *Soviet Astronomy*, 18, 17.

Zhang, K., Wu, P., and Yu, H. (2013). Oscillating universe in massive gravity. *Physical Review D*, 87(6), 063513.

Zhou, E.P., Zhou, X., and Li, A. (2018). Constraints on interquark interaction parameters with GW170817 in a binary strange star scenario. *Physical Review D*, 97(8), 083015.

Zhou, Y., Chen, L.W., and Zhang, Z. (2019). Equation of state of dense matter in the multimessenger era. *Physical Review D*, 99(12), 121301.